HOT GAS DESULPHURISATION USING LIQUID TIN

A Thesis Submitted to

The University of Sheffield

by

Mohd Halim Shah Ismail, B.Eng., MEng.

for the degree of

Doctor of Philosophy (PhD.)

Project Supervisors:

Professor V. N. Sharifi & Professor J. Swithenbank

Department of Chemical and Process Engineering

The University of Sheffield

April 2008

SUMMARY

Present integrated gasification combined cycle (IGCC) systems demonstrate high system efficiency and impressive environmental performance, giving them an edge over conventional pulverised fuel power stations. A key area in the development of IGCC is hot fuel gas clean-up (HGCU). Fuel gas cleaning at elevated temperatures reduces thermal efficiency losses associated with gas quenching in conventional coal gas cleaning methods. The current hot gas clean-up method centres on the use of metal oxide sorbents for sulphur removal and the utilisation of a ceramic barrier filter for particulate cleaning. A fresh and radical approach may provide the key to overcoming the inherent limitations associated with metal oxide sorbents.

A molten tin irrigated packed bed scrubber adopted in this research project is one such innovative way forward in HGCU. The hot scrubber offers the prospect of a multicomponent clean-up device. In this proposed system, high-temperature sulphur removal take place via absorption of H_2S into molten tin whilst discrete molten tin droplets and rivulets on the packing surface act as solid particulate collectors. The main objective of this PhD research programme was to investigate a novel hot flue clean-up system using molten tin as the scrubbing medium for the removal of solid particulates and H_2S. Towards the end of this research work, tin sulphide cleaning tests were performed to investigate the effects of both zinc and no zinc powder on tin sulphide during the cleaning processes.

Major modifications were made to the existing rig in order to investigate the process of particulate cleaning. Various parts of the equipment have been modified including a packing support plate, gas heaters, air seal and gas lift. For particulate removal tests, an additional system was added to the original design i.e. particle feeder. It consisted of a screw feeder and a venturi system. An online filter was also added to the system to determine the total efficiency of particle removal. This modification work represented a major contribution during the research work.

The liquid tin-irrigated packed bed scrubber demonstrated particulate removal performance with total efficiency ranging from 60 to 98%. The total efficiency decreased as the inlet dust loading increased. The results also showed that the temperature had a significant influence on the total efficiency. As the temperature increased from 350℃ and 400℃, the total efficiency decreased. The major reason for this is the temperature difference between the inlet particles and the scrubber, which resulted in the formation of a thicker bed of agglomerates. The resulting grade efficiency curves were not able to demonstrate fully realistic results. This was because at corresponding liquid flow rates and inlet solid loading, the particles collected in the impinger were not a true representation of the total removal efficiency. Thus from the particulate cleaning test, the equipment operation had low efficiency. Nevertheless, the proposed objectives have been met and it is evident that with several important modifications, the particle removal system would be able to operate satisfactorily.

The absorption behavior of H_2S in the novel liquid tin irrigated hot gas scrubber was investigated for various operating parameters in the lab-scale packed bed. Height of a gas film transfer unit values ranged from 0.84 to 0.181 m for tested conditions at 1000 ppm of H_2S concentration, which meant that this system has a very good potential for efficient desulphurisation at industrial scale. This was the most important conclusion from this research. The cleaning of SnS was performed with and without the presence of zinc powder. Addition of zinc powder saw around 20% reduction of sulphur in the sample compared to without zinc.

Fluent modelling work was carried out to model the particulate removal in a packed bed of spheres operating under hot gas conditions. Efficiencies of 98% were predicted for particles of 40 μm and larger. The main conclusion for this CFD study was that high gas velocity would significantly improve the total efficiency of the particle removal. A mathematical model using a Microsoft® Excel spreadsheet was used to simulate the rate of reaction in the packed-bed scrubber. The range of reaction rate constants from this work was between 0.011 to 0.019 m/s for various operating temperatures, which are within the range of values as reported by Hedden (1986).

ACKNOWLEDGEMENTS

The present work was carried out at the Combustion and Incineration Laboratory at the Chemical & Process Engineering Department (CPE) Department, University of Sheffield. I would like to thank all the persons who have through their cooperation contributed to the achievement of my PhD thesis.

First I would like to praise and thank Allah the Almighty, Who have granted me all these graces to complete this thesis. All praises are due to Allah, the Creator of humankind.

I would like to express my gratitude to my supervisors Professor Vida Nasserzadeh Sharifi and Professor Jim Swithenbank for their help, supervision, scientific guidance, valuable discussions, continued support of my work and numerous helpful discussions provided.

I am also very grateful to Dr Changkook Ryu for his invaluable help and suggestions in the research project.

I would also like to thank to PQ Potters Europe GmbH for the supplies of glass powder that made the experimental work possible.

I would like to thank the technical and secretarial staff at the Chemical and Process Engineering Department, University of Sheffield: Mr Chris Wright, Mr. Adrian Lumby, Mr. Andy Patrick, Mr. Oz McFarlane, Mr. Keith Penny for the technical assistance with the experimental work and analytical assistance, and Ms Maria Soto for her secretarial support. Special thanks to Stuart Richards who helped in the construction of the test rig and helped me run the experiments, worked with me from the very early stages of the research. I am also very appreciative to Mr. Alan Cox from the Department of Chemistry for their laboratory help.

All my colleagues of the Laboratory for Combustion and Incineration and other research laboratories at University of Sheffield for their help and the friendly atmosphere at the CPE are also acknowledged.

Finally I would like to wish personal thanks to my wife, Zuraida and my kids Muhammad Azlan Shah, Muhammad Azren Shah and Nur Addina Shah, for their encouragement and support during this study.

CONTENTS

LIST OF FIGURES

LIST OF TABLES

NOMENCLATURE

Symbol	Description	Unit
a	Cross-section area of annular flow	ft^2
a, a_e	Interfacial area per unit volume of column	m^2/m^3
a_p	Packing specific surface area	(1/m)
a	Empirical constant	-
A	Gas lift pipe cross-section area	ft^2
A	Column cross-section area	m^2
c	Concentration in liquid phase	$kmol/m^3$
c*	Concentration in liquid phase in equilibrium with gas phase	$kmol/m^3$
C_D	Discharge coefficient	-
C_D	Drag coefficient	-
C_O	Orifice coefficient	-
C_p	Dust concentration	ppmw
C_s	Capacity factor = $u_g\{\rho_G/(\rho_L-\rho_G)\}^{0.5}$	ft/s
d	Particle diameter; Packing size or characteristic length	m
$d_{contact}$	Contact diameter	m
d_e	Equatorial diameter	m
d_{equiv}	Packing particle equivalent diameter	m
d_o	Orifice diameter	inch
d_s	Diameter measured from distance d_e up from base of drop	m
d_{sv}	Surface-volume diameter of Sauter diameter	m
d_{50}	Median diameter	µm
D	Gas lift riser inside diameter	in, m
D_G	Gas phase diffusion coefficient or diffusivity	m^2/s
D_h	Hydraulic diameter	mm
D_L	Liquid phase diffusion coefficient or diffusivity	m^2/s
D_{col}/ d_{pe}	Column diameter	m
e	Absolute error	-
E_D	Eddy diffusivity	m^2/s
E_T/ E_{total}	Total or overall efficiency	-
f	Moody friction factor	-
F	Packing factor	m^2/m^3
F	Wall frictional pressure gradient in two-phase flow	Pa/m
F_i	Source term in momentum equation	kg/m^2s^2
F_s	Wall frictional pressure gradient in single liquid phase flow	Pa/m
F_x	Source term in force balance	m/s^2
g	Gravitational acceleration	(m/s^2)
G	Gas superficial mass velocity	kg/m^2s

G'	Molar gas flowrate per unit cross-sectional area of column	$kmol/m^2s$
G'	Gas mass flowrate to base of air lift pump (Clark and Dabolt's model)	kg/s
G(x)	Grade efficiency	-
ΔG_R	Gibbs free energy change of reaction	kJ/mol
h_{atm}	Liquid head corresponding to atmospheric pressure	m
h_D	Dynamic (operating or moving) liquid holdup	m^3/m^3
h_E	Effective liquid holdup	m^3/m^3
h_L	Liquid head	ft
h_S	Static liquid holdup	m^3/m^3
$\bar{h}_s$	Average static liquid holdup	m^3/m^3
h_T	Total liquid holdup	m^3/m^3
H	Shape dependent quantity	-
H_{OG}	Height of a gas film transfer unit	m
H_{OL}	Height of a liquid film transfer unit	m
H_T	Total volumetric liquid holdup	ml
H	Henry's Law constant	Pa,
I	Turbulence intensity	%
k	Turbulent kinetic energy	m^2/s^2
K_o	Overall mass transfer coefficient	m/s
k_G	Gas film mass transfer coefficient	$kmol/m^2sPa$
k'_G	Gas film mass transfer coefficient in term of mol fraction	$kmol/m^2s$
k'_Ga	Volumetric gas film mass transfer coefficient in term of mol fraction	$kmol/m^3s$
k_L	Liquid film mass transfer coefficient	m/s
k'_L	Liquid film mass transfer coefficient in term of mol fraction	$kmol/m^2s$
k'_La	Volumetric liquid film mass transfer coefficient in term of mol fraction	$kmol/m^3s$
K	Vapour-liquid equilibrium constant	mol/mol
K_c	Sudden concentration loss coefficient = 0.5	-
K_G	Overall gas phase mass transfer coefficient	$kmol/m^2sPa$
K'_G	Overall gas phase mass transfer coefficient in term of mol fraction	$kmol/m^2s$
K_Ga	Overall volumetric gas phase mass transfer coefficient	$kmol/m^3sPa$
K'_Ga	Overall volumetric gas phase mass transfer coefficient in term of mol fraction	$kmol/m^3s$
K_L	Overall liquid phase mass transfer coefficient	m/s
K'_L	Overall liquid phase mass transfer coefficient in term of mol fraction	$kmol/m^2s$
K_La	Overall volumetric liquid phase mass transfer coefficient	l/s
K'_La	Overall volumetric liquid phase mass transfer coefficient in term of mol fraction	$kmol/m^3s$

K_p	Equilibrium constant in terms of partial pressure	-
K	Vapour-liquid equilibrium constant	-
K_n	Kundsen number	-
k_r	Reaction kinetic effect at the interface	m/s
l	Bed thickness or bed height	m
L	Length/Lift	m
L	Liquid superficial mass velocity	kg/m^2s
L'	Molar liquid flowrate per unit cross-sectional area of column	$kmol/m^2s$
L_v	Liquid superficial volumetric velocity	$m^3/s.m^2$
L_w	Wetting rate	m^2/s
m	Vapour-liquid equilibrium constant	mol/mol
M	Mass of sample	g
m_{in}	Mass of dust fed into scrubber	g
m_{out}	Mass of unseparated dust in exit air retained on filter	g
M	$W_GP = G'P_{atm}/A\rho_G$	kg/s^3
M	Mass flowrate of a sample	kg/s
M	Mean mass flowrate	g/s
M_c	Mass flowrate of coarse (separated) dust in underflow	kg/s
M_f	Mass flowrate of fine (unseparated or penetrating) dust in overflow	kg/s
M_G	Mass flowrate of gas phase	kg/s
M_{in}	Mass flowrate of feed (challenging) dust	kg/s
M_x	Mass flowrate of particles of size x in the sample	kg/s
N	Total molar flux (relative to a fixed plane); Molar rate of absorption per unit area	$kmol/m^2s$
N	Number of data sets	-
N_G	Number of gas film transfer units	-
N_L	Number of liquid film transfer units	-
N_o	Number of orifices	-
N_{OG}	Number of overall gas phase transfer units	-
N_{OL}	Number of overall liquid phase transfer units	-
N_t	Number of transfer units	-
p	Partial pressure in bulk gas phase	Pa
p^*	Partial pressure in gas phase in equilibrium with liquid phase	Pa
p^o	Vapour pressure of pure component	Pa
p_i	Partial pressure at interface	Pa
P	Total pressure	Pa
P_{atm}	Atmospheric pressure	Pa
P_g	Gauge pressure	Pa
P_o	Pressure at air injector level	Pa
P_{op}	Operating pressure	Pa

ΔP	Pressure drop	Pa
ΔP_{dry}	Dry bed pressure drop	Pa
ΔP_A	Accelerative pressure loss	Pa
ΔP_D	Downcomer pressure loss	Pa
$\Delta P/l$	Pressure gradient	Pa/m
Q	Volumetric flowrate	l/min
R	Universal gas constant	J/kmol.K
R^2	Coefficient of determination	-
Re	Reynolds number	-
Re_G	Gas phase Reynolds number	-
Re_L	Liquid phase Reynolds number	-
Re_p	Single particle Reynolds number = $\rho ud/\mu$	-
Re_R	Relative Reynolds number = $\rho_G u_R d/\mu_G$	-
Re*	Reynolds number for packed bed flow	-
S	Specific surface area of particle or packing	m^2/m^3
S	Shape dependent quantity	-
S	Submergence	m, ft
S_m	Source term in continuity equation	kg/m^3s
S_p	External area of a packing particle	m^2
S_B	Specific surface area of packed bed	m^2/m^3
S_R	Submergence ratio	-
S_{sl}	Spreading coefficient	N/m
Sc_G	Gas phase Schmidt number = $\mu_G/\rho_G D_G$	-
Sc_L	Liquid phase Schmidt number = $\mu_L/\rho_L D_L$	-
t	Time	s
T	Temperature	K
u	Superficial velocity	m/s
u'	Actual single phase velocity in two-phase flow	m/s
u'	Root-mean-square of velocity fluctuations in turbulent flow	m/s
u	Mean flow velocity	m/s
U_G	True gas velocity based on irrigated bed porosity = u_G/ε_{eff}	m/s
U_R	Relative velocity of gas and liquid stream	m/s
v	Superficial velocity	m/s
V	Volume	m^3
V_G	Gas volumetric flowrate	m^3/s
V_p	Volume of a packing particle	m^3
x	Mole fraction in liquid phase	mol/mol
x*	Mole fraction in liquid phase in equilibrium with gas phase	mol/mol
x	Distance	m
X	Dust particle size (particle physical diameter)	μm

x_{ae}	Particle aerodynamic diameter	$\mu m(g/cm^3)^{1/2}$
x_{max}	Limit separation	μm
x_{50}	Cut size	μm
x_{98}	Approximate limit of separation	μm
y	Mole fraction in gas phase	mol/mol
y	Distance	m
y_{in}	Inlet gas concentration	ppm
y_{out}	Outlet gas concentration	ppm
y^*	Mole fraction in gas phase in equilibrium with liquid phase	mol/mol
z_G, z_L	Effective gas film thickness and effective liquid film thickness respectively	m
Z	Packed bed height	m
Z_{end}	Equilibrium bed height of end effects	m

Greek Symbol

α	Empirical constant	-
α	Gas voidage fraction in two-phase flow	-
β	Empirical constant	-
Δ	Change in	-
ε	Dry bed voidage or porosity	-
ε	Turbulent dissipation rate	m^2/s^3
ε_{eff}	Effective voidage or porosity	-
η_p	Pumping efficiency	-
φ	Gas density correction factor = $(\rho_G/\rho_{air, 293K})^{0.5}$	-
λ	Mean free path of gas molecules	μm
μ	Absolute viscosity (in centipoises in GPDC)	kg/ms
μ_G, μ_L	Viscosity of gas, Viscosity of liquid	kg/ms
μ_s	Ratio of liquid viscosity to water (20℃) viscosity	-
μ_t	Turbulent viscosity	kg/ms
ν	Kinematic viscosity = μ/ρ	cst, m^2/s
θ	Contact angle	degree
ρ	Density	kg/m^3
ρ_p	Particle density	kg/m^3
ρ_s	Ratio of liquid density to water (20℃) density	-
σ	Surface tension	mN/m
σ_c	Critical surface tension	N/m
σ_g	Geometric standard deviation	-
σ_s	Ratio of liquid surface tension of water (20℃) surface tension	-
τ_{ij}	Stress tensor	kg/ms^2

ω_x	Mass fraction of particles size x in the sample	kg/kg
$\omega_{c,x}$	Mass fraction of coarse (separated) dust at particle size x	kg/kg
$\omega_{f,x}$	Mass fraction of fine (unseparated or penetrating) dust at particle size x	kg/kg
$\omega_{in,x}$	Mass fraction of feed dust at particle size x	kg/kg
$\omega_{out,x}$	Mass fraction of exit dust at particle size x	kg/kg
ψ	Liquid density correction factor = (ρ_{water}/ρ_L)	-
ψ_s	Sphericity	-

Subscript

Atm	Atmospheric pressure
A	Component A
B	Bottom of packed bed
F	Fluid
G	(Bulk) Gas phase
I	Gas-liquid interface
lm	Logarithmic mean
L	(Bulk) Liquid phase
lv	Liquid-vapour
p	Particle
sl	Solid-liquid
sv	Solid-vapour
T	Top of packed bed

ACRONYMS & ABBREVIATIONS

AFBC	Atmospheric Fluidised Bed Combustor
AHPC	Advanced Hybrid Particulate Collector
ASU	Air Separation Unit
ATS	Advanced Turbine Systems
BGL	British Gas Lurgi (gasifier)
CCGT	Combined Cycle Gas Turbine
CCT	Clean Coal Technologies
CFB	Circulating Fluidized Bed
CHP	Combined Heat and Power
COHPAC	Compact Hybrid Particulate Technology
DEFRA	Department for Environment, Food & Rural Affairs
DOE	United States Department of Energy
EEC	European Economic Commission
ESP	Electrostatic Precipitator
FBC	Fluidised Bed Combustor
FGD	Flue Gas Desulphurisation
HGCU	Hot Gas Clean-Up
HGS	Hot Gas Scrubber
HHV	Higher Heating Value
HP	High Pressure
HTHP	High Temperature & High Pressure
HRSG	Heat Recovery Steam Generator
IC	Internal Combustion (Engine)
IEA	International Energy Agency
IGCC	Integrated Gasification Combined Cycle
ICP-AES	Inductively Coupled Plasma-Atomic Emission Spectrometry
IPPC	Integrated Pollution Prevention & Control
LHV	Lower Heating Value
LNG	Liquefied Natural Gas
LP	Low Pressure
LRTAP	Long-Range Transboundary Air Pollution
MEA	Monoethanolamine
MJ	Mega Joule (10^6 Joule)
MWt	Megawatt Thermal
NGCC	Natural Gas Combined Cycle
Nm^3	Normal Cubic Meter
NRA	National Rivers Authority
NRC	National Research Council's
OPOS	Single Particle Optical Sensing
PAH	Polyaromatic Hydrocarbon
PCC	Sub & Supercritical Pulverised Coal Combustion
PF	Pulverised Fuel
PFBC	Pressurised Fluidised Bed Combustor
ppm	Parts Per Million
RDF	Refuse-Derived Fuel
SCR	Selective Catalytic Reduction
SO_x	Oxides of Sulphur
Syngas	Synthesis Gas
STP	Standard Temperature & Pressure
Nm^3	Normal Metre^3
NO_x	Oxides of Nitrogen
PC	Pulverised Coal
UNECE	Nations Economic Commission for Europe
WCI	World Coal Institute

CHAPTER ONE

Introduction

1.1 Background

Natural gas prices are on the rise, environmental requirements are becoming ever more stringent, and there is an urgent need to diversify the world's fuel supply. In addition, energy demand is surging in developing countries, whilst pressure builds to reduce greenhouse-gas emissions worldwide. To meet this need, the world cannot ignore any of the sources of energy available especially coal, which is the most abundant and affordable of all the fossil fuels (Table 1.1). All fuels will have to play their part and coal's role will be a vital one.

Table 1: Important characteristics of energy source (WCI, 2003)

Fuel	Positive points	Negative points
Coal	• Abundant, affordable, safe, secure. • Easy to transport and store. • Widely available.	• The most carbon intensive fuel for electricity. • Poses technological challenges as part of low global CO_2 growth.
Oil	• Convenient. • Easy to transport and store. • No effective substitute in transportation uses.	• Carbon intensive. • Price volatility. • Resource concentration. • Vulnerability to disruption or geopolitical instability. • Transport risks.
Gas	• Efficient and convenient. • Fuel of choice for many uses, such as residential heating.	• Carbon intensive. • Expensive and risky to transport and store. • Requires dedicated, inflexible infrastructure. • Price volatility. • Resource concentration.
Nuclear	• Carbon-free generation. • Few resource constraints.	• Public acceptability. • Waste disposal question marks. • Capital intensive – may be uneconomic in some markets.
Renewables	• Low emissions on a life cycle basis. • Sustainable.	• Generally high cost. • Intermittent sources. • Major expansion will take time. • Potential siting problems.

All forms of energy production have their impacts, negative as well as positive. There is no truly risk-free way of producing energy, whether in terms of human physical safety, security of supply or environmental impact. As the most important fuel for electricity generation, coal will have a major and vital role to play, along with other fossil fuels. At the same time, society is demanding cleaner energy and less pollution.

Forecasts Longwell *et al.* (1995) suggest that coal will continue to be the world's largest source of fuel for electricity generation for the next 30 years. The price of all forms of commercially traded energy also has increased. Recent energy prices have been significantly different from previous experience. The last five years have seen exceptional energy prices (Christof, 2007). The price of oil has gone up each year during this period, despite now rising surplus production capacity. Gas prices have tended to follow, especially in the oil price indexed markets of Europe and Asia Pacific (Figure 1.1).

Christof (2007) also reported that all over the world, static fuels have driven the acceleration of energy consumption growth. Partially because of price effects, partially because of access and location, and partially because of the demands of industrialisation and economic development, coal has become the static fuel of choice. It continues to increase its share in global primary energy consumption. These make studies into the sustainable use of coal to be a paramount importance.

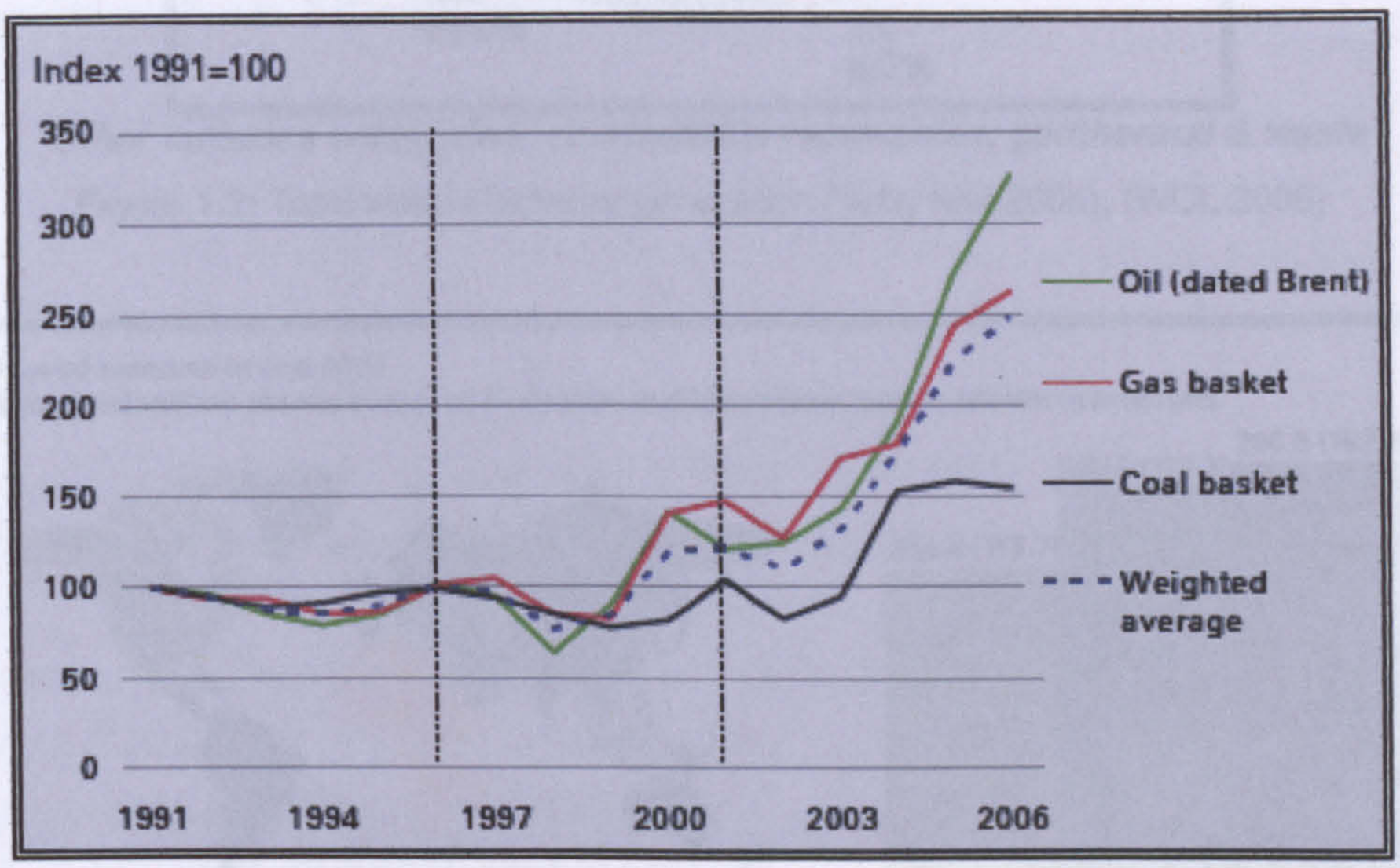

Figure 1.1: Energy prices – BP statistical review of world energy 2007 (Christof, 2007)

Coal is the most plentiful and lowest cost fuel for producing secure and reliable electric power in the world. It fuels almost 40% of electricity worldwide, with even higher percentages in several countries (Figure 1.2). The World Coal Institute (WCI, 2006) reported that coal resources are available in almost every country worldwide (Figure 1.3) with recoverable reserves in around 70 countries.

At current production levels, proven coal reserves are estimated to last 155 years. In contrast, proven oil and gas reserves are equivalent to around 41 and 65 years at current production levels respectively. Accordingly, there is a vast and growing international market for cleaner coal technologies notably for electricity generation.

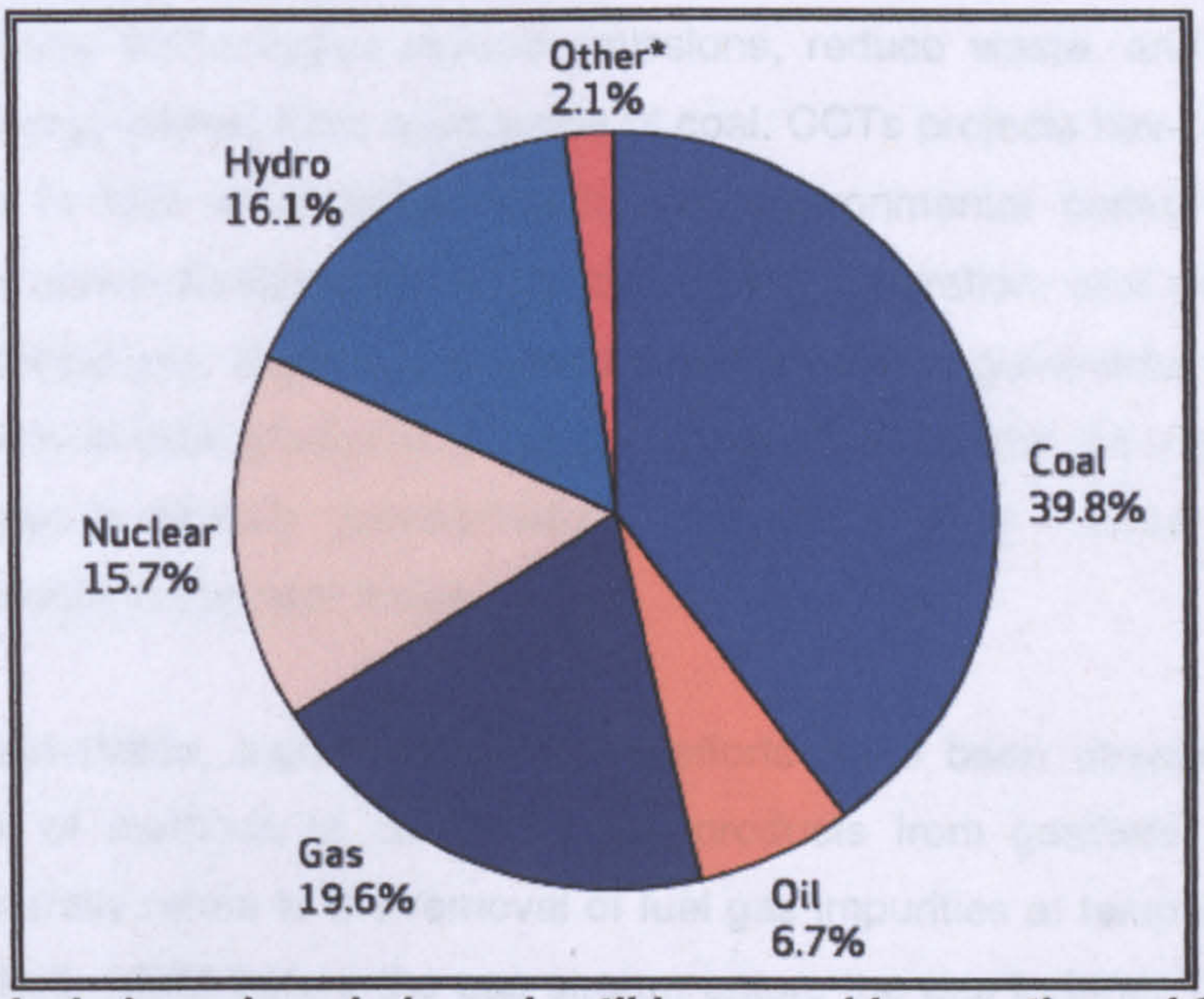

*Other includes solar, wind, combustible renewables, geothermal & waste

Figure 1.2: Total world electricity generation (% by fuel 2004), (WCI, 2006)

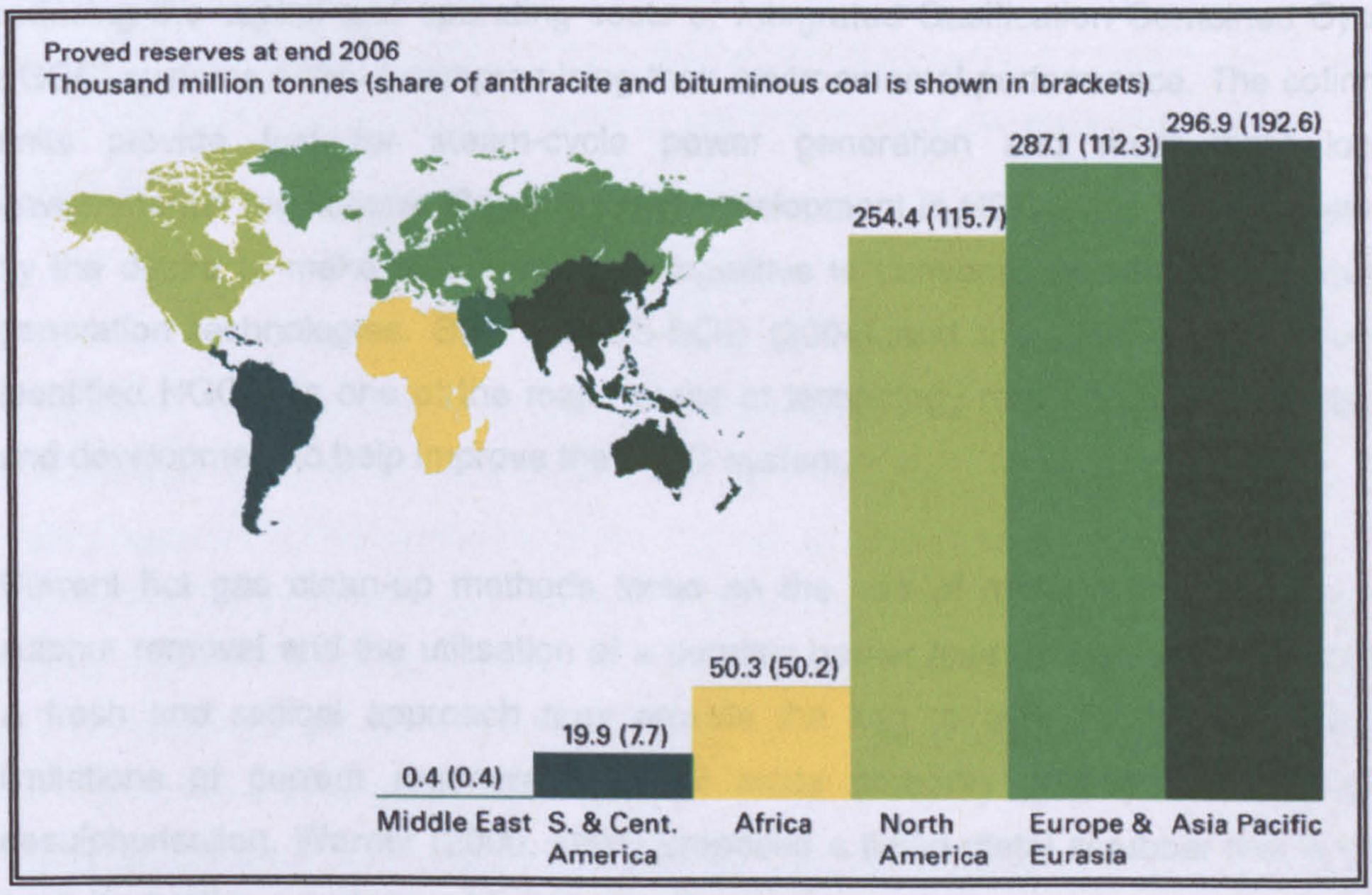

Figure 1.3: Proved coal reserves at the end of 2006 (Christof, 2007)

1.2 Statement of the Problem

Clean Coal Technologies (CCTs) are defined as 'technologies designed to enhance both the efficiency and the environmental acceptability of coal extraction, preparation and use'. These technologies reduce emissions, reduce waste, and increase the amount of energy gained from each tonne of coal. CCTs projects have demonstrated technologies in four main areas which are: environmental control technologies applicable to conventional plants, advanced power generation, coal processing and industrial applications. Most CCTs concentrate on power generation from coal, as more than 50% of coal produced is used to generate electricity. An impressive array of technologies is already commercially viable, and a large number of others will become available in the near future.

Since the mid-1980s, significant research efforts have been directed toward the development of methods to clean the raw products from gasifiers. Hot fuel gas cleaning generally refers to the removal of fuel gas impurities at temperatures above 250℃ (Mitchell, 1998) before the gas stream enters the gas turbine. The integration of hot gas clean-up (HGCU) technology to remove pollutants from coal-derived fuel gas offers the prospect of increasing thermal efficiency whilst simultaneously reducing the capital and operating costs of Integrated Gasification Combined Cycle (IGCC) systems without compromising their environmental performance. The cofiring units provide fuel for steam-cycle power generation and must meet local environmental regulations. Research and development in HGCU has been propelled by the desire to make IGCCs more competitive to conventional coal-based power generation technologies. Both the US-DOE (2004) and the UK-DTI (1998) have identified HGCU as one of the major areas of technology requiring further research and development to help improve the IGCC system.

Current hot gas clean-up methods focus on the use of metal oxide sorbents for sulphur removal and the utilisation of a ceramic barrier filter for particulate cleaning. A fresh and radical approach may provide the key to overcoming the inherent limitations of current regenerable metal oxide sorbents employed in hot gas desulphurisation. Warner (2000, 2001) proposed a liquid metal scrubber that is one such innovative way forward in hot gas cleaning, providing not only sulphur removal capability but the potential for particulate control as well.

The concept of using liquid metals for gas desulphurisation dates back to the late 1970s when Meissner (1976) first patented the concept of removing sulphur from hot reducing gases using liquid lead. However since than, only few others have propounded the use of liquid metals for gas cleaning theoretically and experimentally. They are Meissner and Shora (1981), Schüermann (1984), Hedden et al., (1987) and most recently, Warner (1997, 2000, 2001). However, none of these studies have been able to successfully demonstrate hot gas cleaning by liquid metal. Hence, this thesis in intended to broaden and deepen our knowledge of hot gas cleaning taking place in a packed bed hot gas scrubber. This subject is identified as essential to optimise the operation of hot gas wet scrubber systems and their future development.

1.3 Objective of Research

The present approach to the investigation of the fundamental aspects of hot gas-cleaning is based upon an experimental investigation in a packed bed hot gas scrubber. This research project explores a new approach to hot fuel gas cleaning technology incorporating molten tin as the scrubbing medium for the removal of H_2S and solid particulates, as first put forward by Warner (2001).

In the proposed gas cleaning process, high temperature sulphur removal takes place in a packed bed wet scrubber. Sulphur removal occurs via absorption of H_2S into molten tin:

$$H_2S + Sn \rightarrow SnS + H_2$$

In addition to gas desulphurisation, the packed bed offers the prospect of simultaneous removal of solid particulates from the gas stream, hence acting as a multicomponent clean-up device. Molten tin having high surface energy exhibits non-wetting droplet and rivulet flow on the solid packing surface, potentially giving good inertial capture of solid particulates by the packed bed from the gas stream. The aim of this research project is to perform studies of hot gas cleaning using a pilot unit of the high temperature gas scrubbing by liquid metal constructed by Chang (2003). Liquid tin introduced at the top of the packed bed disintegrates into discrete droplets and rivulets flowing downwards by gravity, countercurrently to an upward nitrogen gas flow.

This hot experiment would concentrate on the H_2S absorption performance and particulate removal of the packed column operation under high temperature conditions. As the hot gas cleaning using molten metal is a relatively new field in gas cleaning, there is limited data available. Findings from the investigation would provide better understanding into the operation and performance of a packed bed hot gas scrubber. A molten tin irrigated packed bed scrubber adopted in this research project is one such innovative way forward in HGCU. The novel liquid tin irrigated packed bed scrubber is thereby a key feature in this research work.

The specific objectives for the research can be summarised as follows:

- To investigate particulates removal and gas absorption performance of the packed bed hot gas scrubber using molten tin.
- To obtain comprehensive data on the liquid and gas flows, height of packing, temperatures and concentrations to determine the optimum running conditions.
- To investigate the possibility of cleaning tin sulphide using zinc powder.
- To perform computational fluid dynamics modelling using FLUENT on particulate removal in a packed bed hot gas scrubber under non-wetting conditions.
- To model the absorption of H_2S in liquid tin with chemical reaction in a packed bed column using Microsoft Excel.
- To evaluate, economically, the feasibility of incorporating such a packed bed hot gas scrubber into a power plant.

1.4 Overview and Scope of the Research

This PhD thesis presents the research work carried out over a period of three years. It consists of eight chapters. These are as follows:

Chapter one introduces the purpose of this research by giving the background of recent world energy developments. A brief background to current hot gas clean-up methods is also presented. This section outlines the aim of this PhD research.

Chapter two of this thesis gives an overview of the combustion technologies used for power generation. The remaining part of the chapter describes the IGCC system with other combined cycle technologies. Discussion includes the legislation covering the environmental and energy policies.

Chapter three reviews existing high temperature gas cleaning technologies for particles and sulphur and also previous work on hot has cleaning by molten metal. First, a short explanation is presented about the need for hot fuel gas cleaning. The remainder of the chapter focuses on the techniques and development of particulate control and desulphurisation processes in hot gas clean-up.

Chapter four explains the theoretical background and previous work on gas-solid separation and gas absorption. Mass transfer with chemical reaction theory is also detailed in this chapter.

Chapter five gives a description of the whole of the experimental rig set-up. Here the materials used in the experiments are described in detail showing how they fit into the research being carried out. The experimental procedure for all the tests is also given.

Chapter six covers the experimental results and discussion of the particulate cleaning and H_2S absorption experiments conducted in the packed bed hot gas scrubber. This chapter also contains the experimental results on the tin recovery using zinc powder.

Chapter seven covers the computational fluid dynamic simulations performed on particulate removal in a packed bed using FLUENT. This section also presents the conditions applied in the mathematical model that was used to simulate the gas absorption in the packed bed. Microsoft Excel was used to illustrate the rate of reaction between molten tin and H_2S. The discussion of the computational modelling results includes comparison with experimental values.

Chapter eight compares the particulate cleaning and gas absorption performance obtained from this study with current apparatus. The limitations of these two processes, affecting the subsequent energy recovery systems and application in 'real' plants are discussed.

Chapter nine completes this thesis with the conclusion derived from this study as well as suggestions for future work in the next stage of this research programme.

CHAPTER TWO

Review of Combustion Technologies for Power Generation

This chapter reviews the gasification technologies for power generation in general, including basic reactions, technical descriptions, type of gasification and comparison with combustion process. IGCC systems demonstrate high system efficiency and impressive environmental performance, emphasis is therefore given to the IGCC system. This is followed by a review on various combined cycle technologies such as the natural gas combined cycle (NGCC), sub and supercritical pulverised coal combustion (PCC), atmospheric and pressurised fluidised bed combustion (AFBC and PFBC). Status of current gasification processes and review of conventional gas cleaning technologies for power generation plant are then discussed. The current energy policies in Europe are discussed at the end of this chapter.

2.1 Overview of Gasification

Gasification-based energy conversion systems are capable of providing a stable, affordable, high-efficiency energy supply with minimal environmental impact. They can provide flexibility in the production of a wide range of products including electricity, fuels, chemicals, hydrogen, and steam, while utilizing low-cost, widely available feedstocks. All carbon-containing feedstocks including hazardous wastes, municipal solid waste and sewage sludge, biomass, etc., can be readily gasified after proper preparation, to produce clean synthesis gas for further processing. Because of its ability to use low-cost feedstocks, gasification is the technology of choice for many industrial applications such as in refineries.

2.1.1 Basic Reactions

Gasification is a thermal chemical conversion process designed to maximise the conversion of the carbonaceous fuel and waste to a synthesis gas (syngas) containing primarily carbon monoxide and hydrogen (over 85%) with lesser amounts of carbon dioxide, water, methane, argon, and nitrogen. The chemical reactions take place in the presence of steam in an oxygen-lean reducing atmosphere, in contrast to combustion where reactions take place in an oxygen-rich, excess air environment. In other words, the ratio of oxygen molecules to carbon molecules is less than one in the gasification reactor.

The following simplified chemical conversion formulas describe the basic gasification process (Neville, 2004)

The following reactions are important in coal gasification:

- $C\ (Fuel) + O_2 \rightarrow CO_2$ (exothermic) (2.1)
- $C + \frac{1}{2} O_2 \rightarrow CO$ (exothermic) (2.2)
- $C + H_2O\ (steam) \rightarrow CO + H_2$ (endothermic) (2.3)
- $C + CO_2 \rightarrow 2CO$ (endothermic) (2.4)
- $CO + H_2O \rightarrow CO_2 + H_2$ (exothermic) (2.5)
- $CO + 3H_2 \rightarrow CH_4 + H_2O$ (exothermic) (2.6)
- $C + 2H_2 \rightarrow CH_4$ (exothermic) (2.7)

2.1.2 Technical Description of the Gasification Process

The heart of any gasification-based system is the gasifier, which can process a wide variety of feedstocks, including coal, biomass, petroleum coke, refinery residues, and other wastes. The gasifier converts carbonaceous feedstock into gaseous products at high temperature and (usually) elevated pressure in the presence of oxygen and steam. Partial oxidation of the feedstock in a reducing (oxygen starved) atmosphere provides the heat. At operating conditions, chemical reactions occur that produce the syngas, a mixture of predominantly CO and H_2. Minerals in the feedstock (ash) separate and leave the bottom of the gasifier as an inert slag (or bottom ash), a potentially marketable solid product. The fraction of the ash entrained with the syngas, which is dependent upon the type of gasifier employed, requires removal downstream in particulate control equipment, such as filtration and water scrubbers. This particulate is typically recycled to the gasifier to ensure high carbon conversion. Some gasifiers also yield devolatilisation or pyrolysis products (coal tars, oils, phenols, etc.) that can and must be controlled. While this is a major issue with moving-bed gasifiers, it is less of a concern for fluidised-bed and multi-stage/single-stage entrained-flow gasifiers. Fig. 2.1 presents a simplified schematic diagram of many of the technology options which could constitute the energy plants for the 21st century.

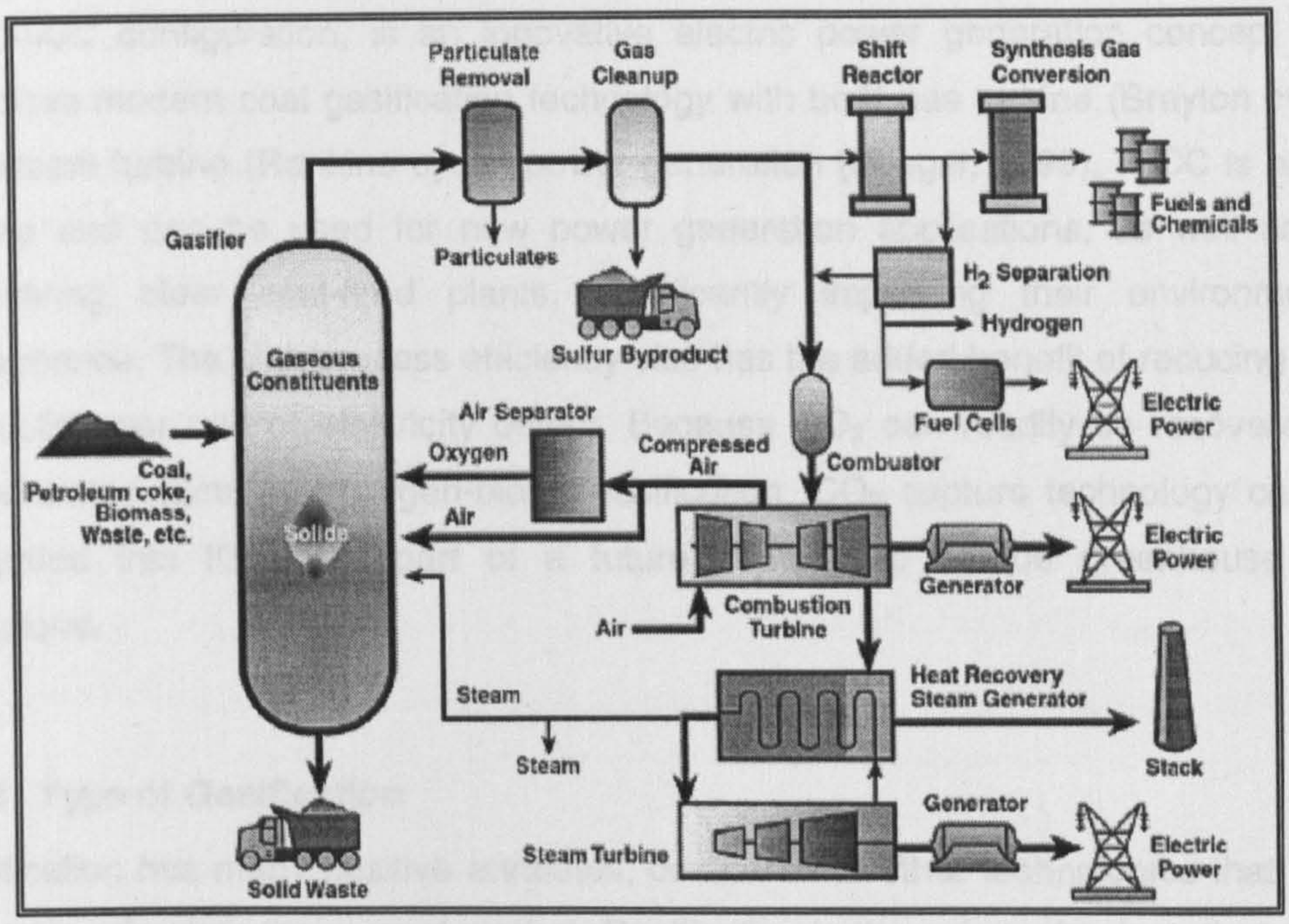

Figure 2.1: Schematic diagram of a typical gasification unit (Ness et al., 1999)

Other potential pollutants, such as sulphur and nitrogen compounds, form species that can be readily extracted. Hydrogen sulphide (H_2S) and carbonyl sulphide (COS), once hydrolysed, are removed by dissolution in, or reaction with, an organic solvent and converted to valuable by-products, such as elemental sulphur or sulphuric acid. Fuel nitrogen is mainly converted to diatomic nitrogen, but a small fraction is converted to ammonia (NH_3) and some cyanide and thiocyanate in the gasifiers reducing environment, which is readily removed via water scrubbing. Most trace pollutants are removed in the slag/bottom ash or in the particulate control equipment. Since some pollutants end up in the wastewater, proper water treatment facilities are quite important for overall environmental performance.

After cleanup, the syngas can:

- Be combusted in a gas turbine, the waste heat from which can be used to generate steam in a combined cycle mode (so-called IGCC configuration);
- Provide hydrogen, through separation, for refinery applications or as a fuel for highly efficient fuel cells, the waste heat from which can be used to generate steam in a combined cycle mode; and
- Produce a broad range of chemicals and clean fuels using established processes.

The IGCC configuration, is an innovative electric power generation concept that combines modern coal gasification technology with both gas turbine (Brayton cycle) and steam turbine (Rankine cycle) power generation (Stiegel, 1999). IGCC is highly flexible and can be used for new power generation applications, as well as for repowering older coal-fired plants, significantly improving their environmental performance. The high process efficiency also has the added benefit of reducing CO_2 production per unit of electricity output. Because CO_2 can readily be recovered in concentrated form with oxygen-blown gasification, CO_2 capture technology can be integrated into IGCC as part of a future strategy to reduce greenhouse gas emissions.

2.1.3 Type of Gasification

Gasification has many positive attributes, compared to other technologies that have helped to stimulate the current market. Gasification is the only technology that offers both upstream (feedstock flexibility) and downstream (product flexibility) advantages (Gary and Russell, 2001). Three major types of gasification are used today (Androutsopoulos and Hatzilyberis, 2001). These are the oxygen-blown fixed bed gasifier or moving-bed reactor (Lurgi, British Gas Lurgi) with conventional cold gas cleaning, the oxygen-blown entrained-flow gasifier (Shell, Texaco, Destec, Prenflo) with conventional cold gas cleaning, and the air-blown fluidised bed gasifier (HTW, U-Gas, KRW, British Coal) with hot gas cleaning (Minchener, 2005).

These processes are illustrated in Figure 2.2, while Table 2.1 shows the feed fuel and operating characteristics for each of the gasification methods. In a moving bed gasifier, gas and solid contact in counter-current flow. Its cold gas efficiency is higher than fluidised bed and entrained bed gasifiers. But its capacity is less and lump, non-caking coal is needed as raw material. Because of lower temperature of the gas outlet, the volatile material in coal is difficult to decompose and there is a greater concentration of methane and tar in the gas. A treatment system for the tar and the phenolic water is needed. In an entrained flow bed, although the contact time of gas and solid is several seconds, the reaction rate and gasification capacity is greater because of higher gasification temperature (1350-1700℃) and the smaller diameter of pulverised coal (<100μm) (Bonk et al., 1996; Smeers et al., 2001).

On the other hand, because of higher operating temperature, part of the coal energy is converted to heat and its cold gasification efficiency is lower. High gas temperature also makes the gas cleaning and waste heat recovery systems more expensive, the coal preparation system is complicated, the electricity consumption is greater and the fire-resistant material used for the gasifier under layer needs to resist higher temperature. The fluidised bed gasifier has the advantages of simpler reactor structure, moderate operating temperature and easy operation, free of tar and phenol. In a conventional fluidised bed coal gasifier, like the Winkler gasifier, absence of a selected ash discharge design results in low temperature operation and higher carbon content in bottom ash, which causes low carbon conversion, limited coal feedstock resources and relatively small gasification capacity. The ICC's ash agglomerating fluidised bed gasifier has a special selected ash separating system.

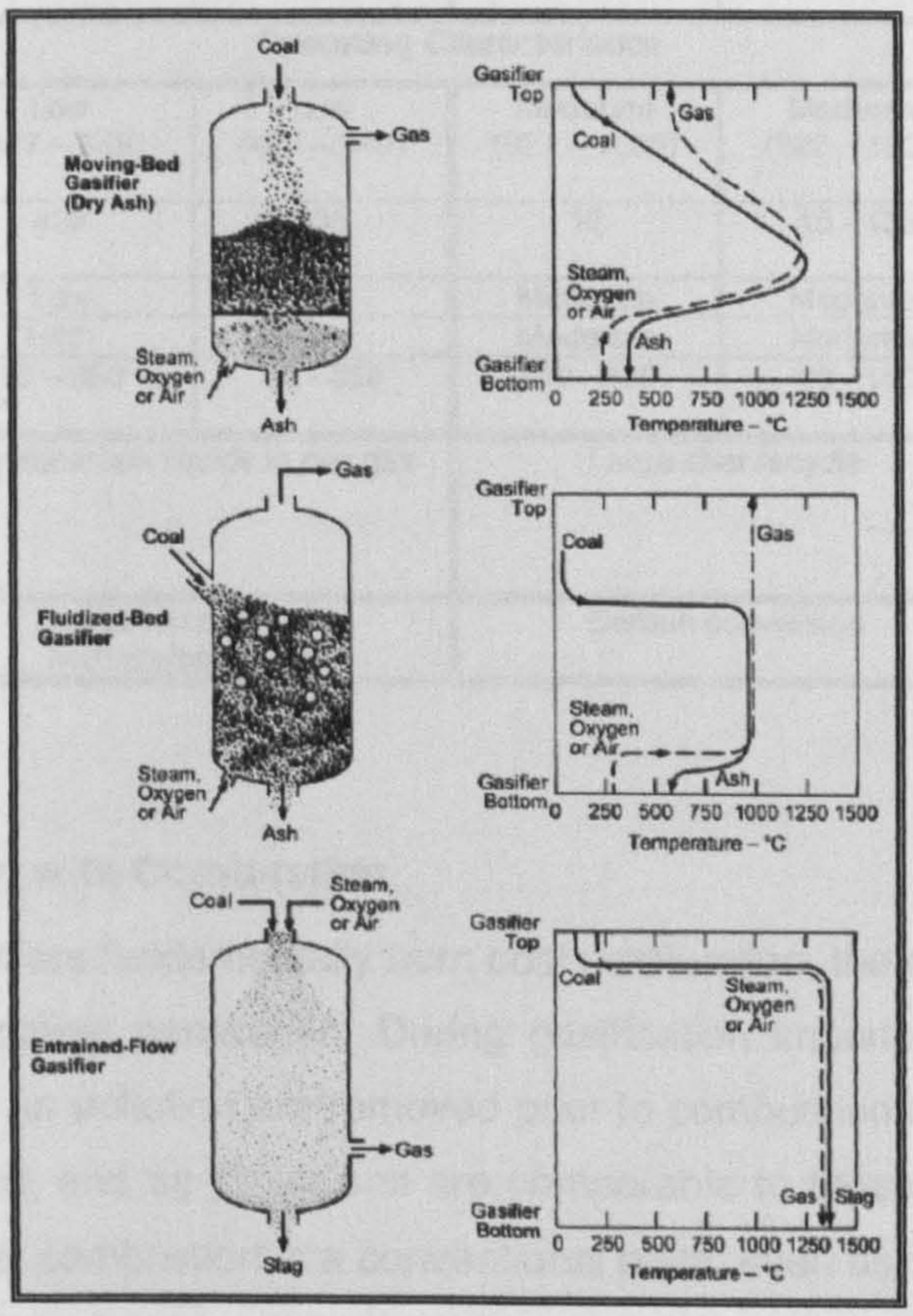

Figure 2.2: The three major types of gasification processes (Ratafia-Brown et al., 2002)

As a result, the carbon content in bottom and upper fly ash can be decreased, thus the carbon conversion and productivity can be improved. In addition, the range of feedstock coal is extensively broadened. However, it has to solve the problem due to magnifying and treatment of upper fly ash.

Table 2.1: Important characteristics of generic types of gasifiers – Performance comparison of different types of coal gasification technology (Ratafia-Brown et al., 2002)

Gasifier Types	**Moving-Bed**		**Fluidised-Bed**		**Entrained-Flow**
Ash Conditions	**Dry Ash**	**Slagging**	**Dry Ash**	**Agglomerating**	**Slagging**
Feed Fuel Characteristics					
Fuel size limits	6 – 50 mm	6 – 50 mm	< 6 mm	< 6 mm	< 0.1 mm
Acceptability of caking coal	Yes (with modifications)	Yes	Possibly	No, Non-caking	Yes
Preferred feedstock	Liguite, reactive bituminous coal, anthracite, waste	Bituminous coal, anthracite, petcoke, wastes	Liguite, reactive bituminous coal, anthracite, waste	Liguite, bituminous coal, anthracite, cokes, biomass, waste	Liguite, reactive bituminous coal, anthracite, waste
Ash content limits	No limitation	< 25% preferred	No limitation	No limitation	< 25% preferred
Preferred ash melting temperature, (℃)	> 1204	< 1299	> 1093	> 1093	< 1300
Operating Characteristics					
Exit gas temperature, (℃)	Low (427 – 649)	Low (427 – 649)	Moderate (927 – 1038)	Moderate (927 – 1038)	High (> 1260)
Gasification Pressure, psi	435	435	15	15 - 435	< 725
Oxidant requirement	Low	Low	Moderate	Moderate	High
Steam requirement	High	Low	Moderate	Moderate	Low
Unit Capacities, MWth	10 – 350	10 - 350	100 - 700	20 - 150	Up to 700
Key Distinguishing Characteristics	Hydrocarbon liquids in raw gas		Large char recycle		Large amount of sensible heat energy in the hot raw gas
Key Technical Issue	Utilisation of fines & hydrocarbon liquids		Carbon conversion		Raw gas cooling

2.1.4 Comparison with Combustion

Coal gasification differs fundamentally from coal combustion, the conventional means of using coal for power generation. During gasification impurities in the coal that could contribute to air pollution are removed prior to combustion of the gas. Only the clean gas is burned, and air emissions are comparable to those of natural gas. On the other hand, coal combustion is a conventional plant; even using the most modern scrubber technology relies on cleanup after combustion, requiring the much larger volume of stack gases be cleaned. Per unit of coal, the volume of combustion gases from conventional plant is 100 times larger than for a typical coal gasification plant (Ratafia-Brown et al., 2002). This fundamental difference gives coal gasification the environmental and efficiency edge over coal combustion in generating electricity.

In conventional gasifiers, a partial combustion of feedstock entering the gasifier provides energy to drive the heat absorbing chemical reactions, the feedstock reacts in the gasifier with steam and oxygen at high temperature and pressure in a reducing (oxygen starved) atmosphere, that yield a combustible product gas mixture. The produced gas mixture includes the flammable gases (hydrogen, carbon monoxide, methane, and small amounts of hydrocarbons). The primary composition of carbon monoxide and hydrogen can be used as a fuel burned to generate heat and/or electricity or steam. The integrated gasification combined cycle IGCC, and gasification processes in general, is also the only advanced power generation technology capable of co-producing a wide variety of commodity and premium products, in addition to electricity, to meet future market requirements.

It is this ability to produce value-added products that has made gasification economical in selected situations and will be a key driver in a deregulated power market. These higher efficiencies translate to lower operating costs and lower carbon dioxide emissions. In addition, the gasification process can be readily adapted with advanced technologies for the concentration of CO with little impact on cost and thermal efficiency. The ability of a technology to achieve higher efficiencies and concentrate CO with minimal impact on the cost of final products will be major factors in technology selection for future energy plants. Because gasification operates at high-pressure with a reducing atmosphere, the products from the gasifier are more amenable to cleaning to reduce ultimate emissions of sulphurs and nitrogen oxides, as well as other pollutants, than those from combustion processes. In general, the volume of the fuel gas processed in an IGCC plant for contaminant removal is typically one-third that from a conventional power plant.

Processing lower volumes of gas translates to lower capital cost for pollution prevention. The removal of sulphurs, nitrogen, and other contaminants from the reducing gas is also much easier than from combustion products. This results in sulphur and nitrogen oxide emissions being more than an order of magnitude less than those of conventional combustion processes. Gasification plants can also be configured to reach near-zero levels of emissions when required. Unlike that of combustion processes, the by-product ash and slag from the gasification technologies have also been shown to be non-hazardous. The material can be readily used for landfill without added disposal costs or can be used in construction materials or further processed to produce value-added products, leading to a zero-discharge plant.

Although current cost for green field sites are high, gasification processes can be economically integrated into existing refineries and chemical plants. With proper integration and the use of existing infrastructure, the overall cost of a project can be significantly reduced.

2.2 Integrated Gasification Combined Cycle (IGCC) System

IGCC plants are extremely clean and more efficient than traditional coal-fired systems. In IGCC plants, coal is not burned in a traditional boiler but is converted into a hydrocarbon vapour (syngas) in a gasifier. The syngas is then cleaned, stripped of impurities and used as fuel instead of natural gas in a conventional combined cycle plant (see description of the natural gas combined cycle plant, below). The result is an integrated gasification combined-cycle configuration that provides ultra-low pollution levels and high system efficiencies. The IGCC systems that are operating commercially have demonstrated exceptional environmental performance. Emissions of SO_2 and NO_x are less than one-tenth of those allowed under U.S. New Source Performance Standards limits. Moreover, IGCC efficiency levels can be as high as 45%. Most of the existing IGCC plants were built on a demonstration basis with government subsidies; however, these plants are nearing full commercial operation. For example, it is reported that the Wabash River plant in Indiana had an overall reliability of 79% in 1999 and operators are now receiving a lot of interest in their technology. The numerous benefits of coal IGCC are prompting electric utilities and independent power producers to consider the use of coal:

2.2.1 Ultra-Low Emissions

There is increasing pressure to consider the environmental impacts associated with the use of fossil fuels. Depending on the gasification technology that is used, IGCC can be the cleanest means of producing electricity from coal, resulting in lower emissions of both gases and solids. IGCC plants would dramatically reduce emissions of sulphur dioxide, nitrogen oxides, mercury, particulates, and carbon dioxide compared to levels produced by conventional coal-fuelled plants. In fact, sulphur dioxide and nitrogen oxides can be reduced substantially below the Clean Air Act's new source performance standard ("NSPS") requirements for coal-fuelled facilities.

Carbon dioxide emissions can also be controlled more effectively with IGCC technology than with other coal-fuelled or natural gas fuelled technologies. Capture of carbon dioxide emissions reduces the power output of an IGCC power plant by only 14%, whereas the decrease is 21% for natural gas-fuelled plants and 28% for conventional coal-fuelled plants when comparing similar percentage levels of carbon dioxide reduction (O'Brien et al., 2004).

2.2.2 Air and Solid Emissions

IGCC can achieve greater reductions of air emissions at lower cost than less advanced technologies (ChevronChevron, 2002), offers the lowest emissions of sulphur dioxide (SO_2) and NO_x of any coal-fed technology. In addition, the reductions of carbon dioxide (CO_2) and particulates from an IGCC plant are significantly better than those achieved by plants using competing clean-coal technologies. Due to IGCC's high efficiency, CO_2 emissions are low (the higher the conversion efficiency, the lower the emissions of CO_2). This process produces a high pressure and high quality CO_2 product that can be recovered for sale. During gasification, virtually all of the carbon in the feedstock is converted to syngas. The mineral matter in the feedstock separates from the gaseous products, the ash and other inert materials such as metals fall to the bottom of the gasifier as non-leach able, glass-like solids or other marketable material. This material can be safely used for many construction or building applications. In addition, more than 99% (ChevronChevron, 2002) of the sulphur in the coal can be removed and converted into marketable elemental sulphur. Competing technologies for generating clean power from coal cannot match the environmental performance of IGCC (Table 2.2). For instance, utilities using circulating fluidised bed combustion (CFBC) and pulverised coal boilers with FGD must remove sulphur from post-combustion flue gases. This generates large amounts of waste. Utilities using IGCC can readily remove more than 99 percent of the sulphur, pre-combustion, while producing marketable sulphur products instead of waste.

Table 2.2: Emission comparison (ChevronChevron, 2002)

	NGCC	IGCC	CFB
SCR	Yes	No	No
Stack Gas Scrubber	No	No	Yes
NO_x	3 ppm	< 9 ppm	85 ppm
Sulphur Recovery	-	> 98 %	95 %
CO_2 (lb/kWh)	0.81	1.95	2.26

2.2.3 Great Diversity of World Fuel Supply

Around the world, there is a growing appreciation for the need to diversify the energy supply and to avoid the dependence on limited fuel sources. IGCC technology allows for the clean, sustainable use of the UK's coal reserves, which increases energy self-sufficiency, and lessens reliance on foreign energy sources.

2.3 Overview of Other Combined Cycle Technologies

All coal combustion technologies rely on the generation of high pressure steam using heat produced by burning coal. This high pressure steam then drives a turbine, and electricity is produced from an electrical generator attached to the steam turbine. The combustion of coal in the boiler can be accomplished in various ways, described below. In general, the most energy-efficient plants have the lowest emissions, as they produce more electricity per unit of coal burned. However, emissions from less-efficient plants can be reduced with "add-on" pollution control options.

2.3.1 Natural Gas Combined Cycle (NGCC) Process

The best standard for today's power generation technology is set by the NGCC system which provides high efficiency, low environmental emission and low cost. Coupled with the relatively low cost of natural gas, NGCC offers the most cost-efficient way of generating electricity. However due to the fact that natural gas costs are on the rise, environmental requirements are becoming ever more stringent, and there is an urgent need to diversify the world's fuel supply. It is not a coal combustion process, but a description is included here for comparison with the various coal-fired options. Commercial-grade natural gas burns more cleanly than other fossil fuels because it consists mostly of methane and has already been cleaned of sulphur. In NGCC plants, natural gas is used as fuel in a gas turbine. Electricity produced from the generator coupled to the gas turbine, hot exhaust gas from the turbine is used to generate steam in a waste heat recovery unit. The steam is then used to produce more electricity.

2.3.2 Subcritical and Supercritical Pulverised Coal Combustion (PCC)

Coal combustion has traditionally occurred at atmospheric pressure using subcritical steam, but today, greater efficiencies can be obtained by using higher steam pressures in the supercritical range. Both of these processes begin with coal being ground into a fine powder. The powdered coal is blown with air into the boiler through a series of burner nozzles where combustion takes place at temperatures from 1300-1700°C, depending largely on the coal type. Combustion occurs at near-atmospheric pressure, which simplifies the burner and coal handling facilities. Subcritical PCC plants use steam in the range of 16 MPa pressure and 550°C while supercritical PCC plants use steam with pressures as high as 30 MPa and 600°C. The higher steam pressure in supercritical plants results in higher energy efficiency, 38-45%, compared with 33% for subcritical plants. While supercritical plants have higher capital costs and some added risk due to the higher pressure and temperature, they have been in commercial use for many years.

2.3.3 Atmospheric & Pressurised Fluidised Bed Combustion (AFBC & PFBC)

FBC processes are commonly used with high sulphur coal. In a FBC plant, hot air blown up through the floor of the boiler suspends or "fluidises" powdered coal mixed with a sorbent such as powdered limestone. The combustion of the coal in the presence of the sorbent facilitates the capture of SO_2. Conventional boilers, by contrast, simply burn the fuel on a grate in the firebox. FBC plants can remove up to 98% of the SO_2 and the coal burns more efficiently because it stays longer in the combustion chamber. AFBC plants operate at atmospheric pressure, and NO_x generation is minimised due to lower combustion temperatures (815-875°C) than in conventional PCC plants. In contrast to AFBC plants, PFBC plants operate at elevated pressures (Sadownik et al., 2004). PFBC plants are typically more compact than similar capacity AFBC and PCC plants due to the higher pressure. The PFBC design allows for potentially greater efficiency, reduced operating costs and less waste than the AFBC design. PFBC plants use the same process as AFBC plants to fluidise or float the coal/sorbent mixtures. In both AFBC and PFBC plants, the reacted sorbent forms a dry, granular material that is easily disposed of or used as a commercial by-product. The reacted sorbent is removed with the bed ash through the bottom of the boiler and with the fly ash that has been collected in the dust collectors at the top of the boiler stacks.

2.3.4 Environmental Control Comparison of IGCC with PC & FBC Power Plants

IGCC, PC, and FBC power plants use different methods of environmental control due to their different design configurations. Generally, stringent emission requirements favour IGCC over PC and FBC power plants. Coal gasification can meet strict air pollutant emission standards, produce only a small amount of inert solid waste, and recover sulphur as valuable elemental sulphur or sulphuric acid. PC and FBC plants can also achieve relatively low levels of emissions by utilising advanced low-NO_x burners and SCR for high-efficiency NO_x control, high-efficiency FG for SO_2 control (95%+ removal), and state-of-the-art particulate control (e.g., fabric filter). The major environmental benefit of selecting FBC technology is the removal of SO_2 (90-95%) and NO_x (emission is less than 100 ppm) in the combustion process without adding post-combustion cleaning equipment, such as wet or dry FGD systems and selective catalytic reduction (SCR) systems. The available published comparison of environment control methods for IGCC, PC and FBC power generation technologies have been tabulated in Table 1-9, page 1-29 in Ratafia-Brown et al. (2002).

2.3.5 Status of the Current Gasification Process

In the EU, many companies have actively been developing IGCC technology. Globally, gasification – of coal, petroleum, petroleum coke and biomass/waste is used to fuel more than two dozen power plants in 12 countries (Rhodes, 2006) as shown in Table 2.3.

Table 2.3: Worldwide gasification use in power plants source (Rhodes, 2006)

Plant Owner	Country	Year Started	Status*	Total No. Gasifiers	MWth Output	Feed
Steelhead Energy	United States	2010	D	2	0	Coal
Excelsior Energy	United States	2009	D	3	0	Coal
Sistemas de Energia Renovavel	Brazil	2006	D	1	68.4	Biomass
ATI Sulcis	Italy	2006	D	2	956.9	Coal
Sokolovska Uhelna, A.S.	Czech Republic	2005	C	1	787.4	Coal
EPZ	Netherlands	2000	O	1	84	Biomass
IBIL Energy Systems Ltd.	India	2002	O	1	109.1	Coal
Sekundärrohstoff-GmbH	Germany	1999	O	1	155.6	Biomass
Lahden Lämpövoima Oy	Finland	1998	O	1	48	Biomass
Elcogas SA	Spain	1997	O	1	587.8	Coal
Tampa Electric Co.	United States	1996	O	1	451.1	Coal
Sokolovska Uhelna, A.S.	Czech Republic	1996	O	26	636.4	Coal
Nuon Power Buggenum	Netherlands	1994	O	1	465.9	Coal
Sydkraft AB	Sweden	1993	O	1	14.4	Biomass

D = Development, C = Construction, O = Operating

Europe has three large IGCC demonstration projects: at Buggenum in the Netherlands (operated by Nuon), Puertollano in Spain (Elcogas) and Priolo Gargallo, Italy (ISAB Energy). The 253 MW Buggenum plant uses a Shell coal gasifier with a Siemens V94.2 gas turbine and a Siemens KN steam turbine on a single shaft. The plant has been running since 1994, and has supplied the Dutch grid on a commercial basis since 1998. Two Siemens V94.2k gas turbines are used in the 521 MW Priolo plant, which has a Texaco gasifier fed by refinery residues. The 340 MW Puertollano plant uses a Krupp-Uhde Prenflo gasifier burning coal and petroleum coke to supply a Siemens V94.3 turbine (Parkinson, 2004). Europe is also a world leader in Biomass-Fueled IGCC (BIGCC) plants. Notable projects include Arbre Energy (Eggborough, UK) and Sydkraft (Malmo, Sweden), both of which are based around 5 MW Typhoon gas turbines from Demag Delaval Industrial Turbomachinery (Lincoln, UK), formerly Alstom and now part of the Siemens group.

2.4 The Need for Hot Fuel Gas Cleaning

Hot fuel gas cleaning generally refers to the removal of fuel gas impurities at temperatures above 250℃ (Mitchell, 1998) before the gas stream enters the gas turbine. The integration of hot gas clean-up (HGCU) technology to remove pollutants from coal-derived fuel gas offers the prospect of increasing thermal efficiency whilst simultaneously reducing the capital and operating cost of IGCC systems without compromising the environmental performance.

2.4.1 Environmental Requirements

The important goal of gas cleaning is to ensure that emission levels from power plants conform to existing environmental standards especially with regards to the three major pollutants i.e. solid particulates or dust, SO_2 and NO_x. Air pollution legislation is being established worldwide as concern over air pollution and its local, regional and transboundary effects increase (McConville, 1997). Existing emission standards in the industrialised nations of Western Europe, North America and Japan are being tightened whilst countries in Central and Eastern Europe are putting into place new air pollution legislation, mainly adopted from the EC. Existing and new coal-based power plants in Asia have to conform to increasingly stringent national air pollution regulations, which are very much driven by changes in international legislation.

A number of international standards have been established to control transboundary air pollution (McConville, 1997). These include protocols made under the United Nations Economic Commission for Europe (UNECE) Convention on Long-Range Transboundary Air Pollution (or LRTAP Convention) signed by European countries as well as US and Canada, the European Community's (EC) environmental legislation which is binding on its 15 member countries and which also influences Central and Eastern European countries, and the world Bank environmental guidelines which are increasing in developing countries in which projects are funded by the World Bank. Table 2.4 lists the emission standards for particulates, SO_2 and NO_x from various sources having plant size greater than 50MWth in selected countries as well as several international standards. The emission standards range from 20 to 37℃ mg/m^3 for particulates, 30 to 3400 mg/m^3 for SO_2 and 95 to 1690 mg/m^3 for NO_x.

Table 2.4: Environmental legislation, plant size >50MWth (IEA, 2003)

	Particulates		NO_x*		SO_x*	
	New Plant	Existing Plant	New Plant	Existing Plant	New Plant	Existing Plant
USA	37 – 123	123	220 – 1058	185 – 1058	740 – 1480	1480
UK	25 – 50	50 – 100	40 – 1300	650	200 – 2000	400 – 2000
Germany	47 – 54	54 – 150	200 – 500	200 – 1218	375 – 2000	375 – 2143
Japan	30 – 200	30 – 200	205 – 720	205 – 720	Plant-by-plant basis	
Taiwan	25 – 429**	25 - 1430	1289	1545 - 2575	572	1430
mg Nm^{-3} at 6% O_2			** Maximum emission calculated from sliding scale			

2.4.1.1 Energy Policy in Europe

Energy use continues to be dominated by fossil fuels. Despite continued growth in renewables, substantial further growth is required to meet the EU indicative renewables targets of 12 % of total energy consumption and 22.1 % of electricity consumption by 2010 (EEA, 2002). Emissions of nitrogen oxides, sulphur dioxide and carbon dioxide from electricity production fell while electricity output increased, due largely to switching to fuels that produce fewer emissions, introducing emission-specific abatement measures, efficiency improvements and increased use of non-fossil fuel. Electricity production from combined heat and power increased, but increasingly liberalised energy markets may challenge the EU indicative 'combined heat and power in electricity' target of 18 % by 2010.

The UK is committed to reducing annual emissions of sulphur dioxide to 585 thousand tonnes by 2010 under the EC National Emission Ceilings Directive. The aim is to reduce acidification and ground level ozone across Europe. The Directive sets emission ceilings for all Member States to achieve from 2001, as well as a set of indicative ceilings for the whole of the European Union to be reviewed in 2004. Figure 2.3 shows how levels of sulphur dioxide emissions have changed since 1970, together with the targets for the UK and the EU. The main source of emissions in 2006 was coal use in power stations and other industries.

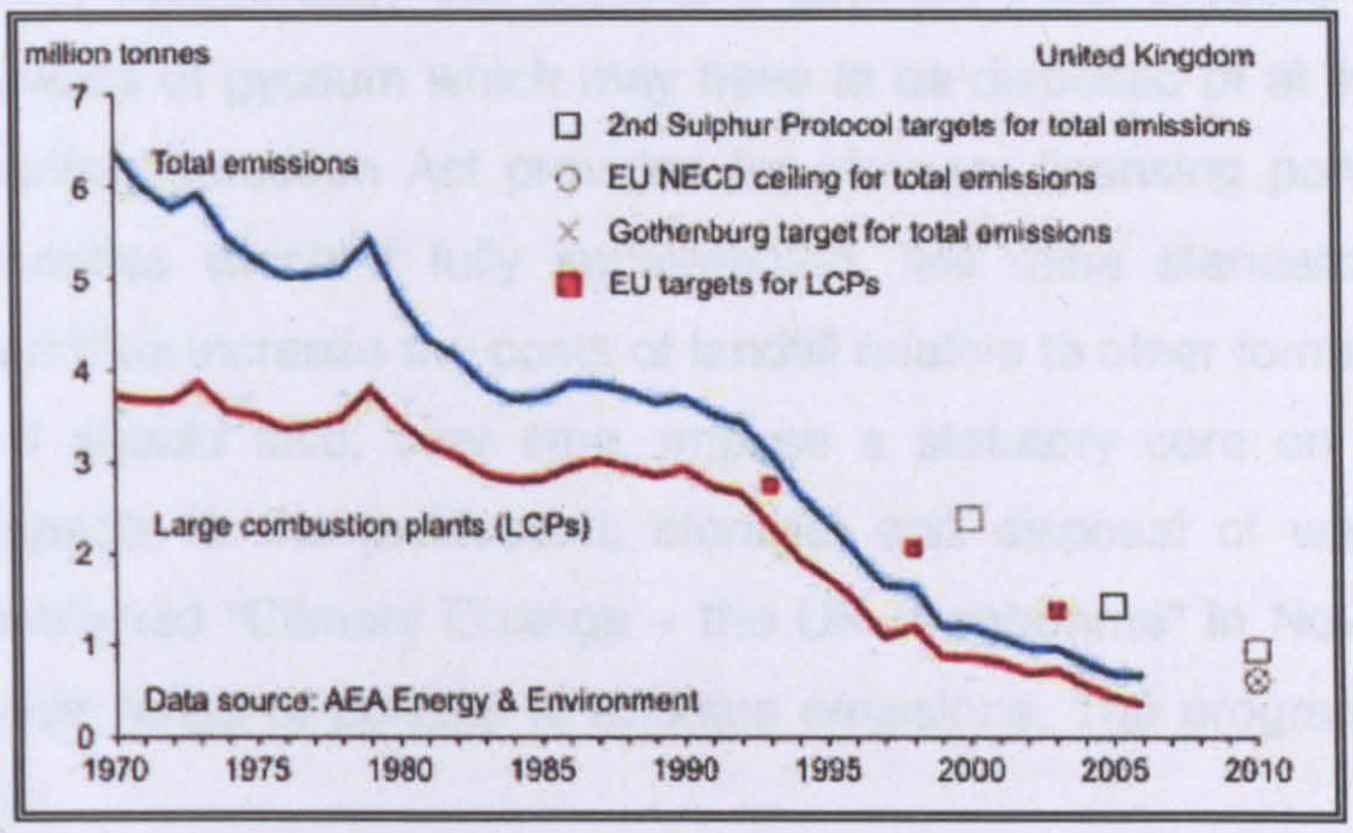

Figure 2.3: Sulphur dioxide emissions and targets: 1970-2010 (DEFRA, 2008)

2.4.1.2 Legislation Regarding Discharge to Water

Electricity generation can have a significant impact on rivers and estuaries which are used as a source of cooling water and also for the disposal of surface water and certain permitted liquid wastes. Most Flue Gas Desulphurisation (FGD) processes may also produce liquid effluent. These discharges are regulated by National Rivers Authority (NRA) and the Scottish River Purification Boards Association, and will be incorporated into the conditions required by HMIP under Integrated Pollution Control. In addition, the Water Resources Act 1991 enables the Secretary of State to set statutory water quality objectives which will incorporate the existing requirements of relevant EC Directives.

2.4.1.3 Legislation Regarding Emission to Air

The EC Large Combustion Plants Directive requires member states of the European Community to reduce total SO_2 emissions from existing combustion installation, with an annual capacity to greater than 50 MW (thermal), of 20 % by end of 1993, 40 % by 1998 and 60 % by 2003 taking 1980 emissions as the baseline.

Those target reduction have been formally set out in the UK National Plan. Emissions from large combustion plants in the UK in 1996 were 57 % below the 1980 baseline, well ahead of the EC target. With the agreement of HMIP, power station quotas can be reallocated to other stations within the company provided the total quota of SO_2 and NO_x emissions is not exceeded.

2.4.1.4 Legislation Regarding Waste Disposal

Over 10 millions tonnes of ash and other solid wastes are produced by UK power stations annually. Additionally, the limestone gypsum FGD process will produce significant quantities of gypsum which may have to be disposed of at licensed sites. The Environmental Protection Act provides for stronger licensing power for waste regulation authorities which if fully implemented, will raise standards for landfill substantially and thus increase the costs of landfill relative to other forms of treatment and disposal. It should also, over time, impose a statutory care on producers of waste with respects to the production, storage, and disposal of waste. The UK Government published "Climate Change – the UK Programme" in November 2000, setting out a wide range of policies to address emissions. The programme included (DEFRA, 2006):

- An obligation on electricity suppliers to source 10 per cent of electricity from renewable sources by 2010, subject to the cost to the consumer being acceptable. This was extended in 2004 to a requirement to source 15 per cent from renewables by 2015;
- Measures to improve domestic energy efficiency, including the new Energy Efficiency Commitment that requires electricity suppliers to promote energy savings by households;
- The Climate Change Levy on business use of energy, including exemptions for renewables and Combined Heat and Power (CHP);
- Climate Change Agreements with energy intensive sectors and the implementation of Integrated Pollution Prevention and Control (IPPC);
- Voluntary reductions through the first stage of the UK Emissions Trading Scheme launched in 2002;
- The Ten Year Plan for Transport.

The Energy White Paper, published in February 2003 (Heath, 2004), committed the UK Government to work towards reducing carbon dioxide emissions, the major greenhouse gas, by 60 per cent from current levels by about 2050, with real progress by 2020. The White Paper, entitled "Our energy future – creating a low carbon economy" also set three further goals for UK energy policy, these being to maintain the reliability of energy supplies; to promote competitive energy markets in the UK and beyond; and to ensure that every home is adequately and affordably heated.

2.4.2 Gas Turbine

The operation of a gas turbine puts high demands on the quality of the gas to the turbine combustor. Properties of concern are the heating value, gas composition and possible contamination comprising solid particulates, sulphur (H_2S, COS) and nitrogen compounds (NH_3, HCN) as well as minor contaminants of alkali metals (Na, K), alkaline earth metals (Ca, Mg), heavy trace metals (Pb, V, Zn, As, Se, Hg, Cd), halogens (Cl, F), and polycyclic aromatic hydrocarbons (PAHs). In long term perspective, contamination of the gas will be important as it will influence the over all lifetime of the gas turbine and degradation of downstream equipment such as deposition, erosion and corrosion (Simms et al., 1995), (Oakey et al., 2004). The National Research Council's (NRC) reported to DOE was that an assessment of hot gas cleanup systems for advanced IGCC and PFBC should be undertaken to determine the ability to meet, within the next three to five years, all requirements for future high temperature (>1260°C) turbine operation and environmental acceptability (Rutkowski et al., 1996). Turbine tolerance estimates and current NSPS requirements are shown in Figure 2.4.

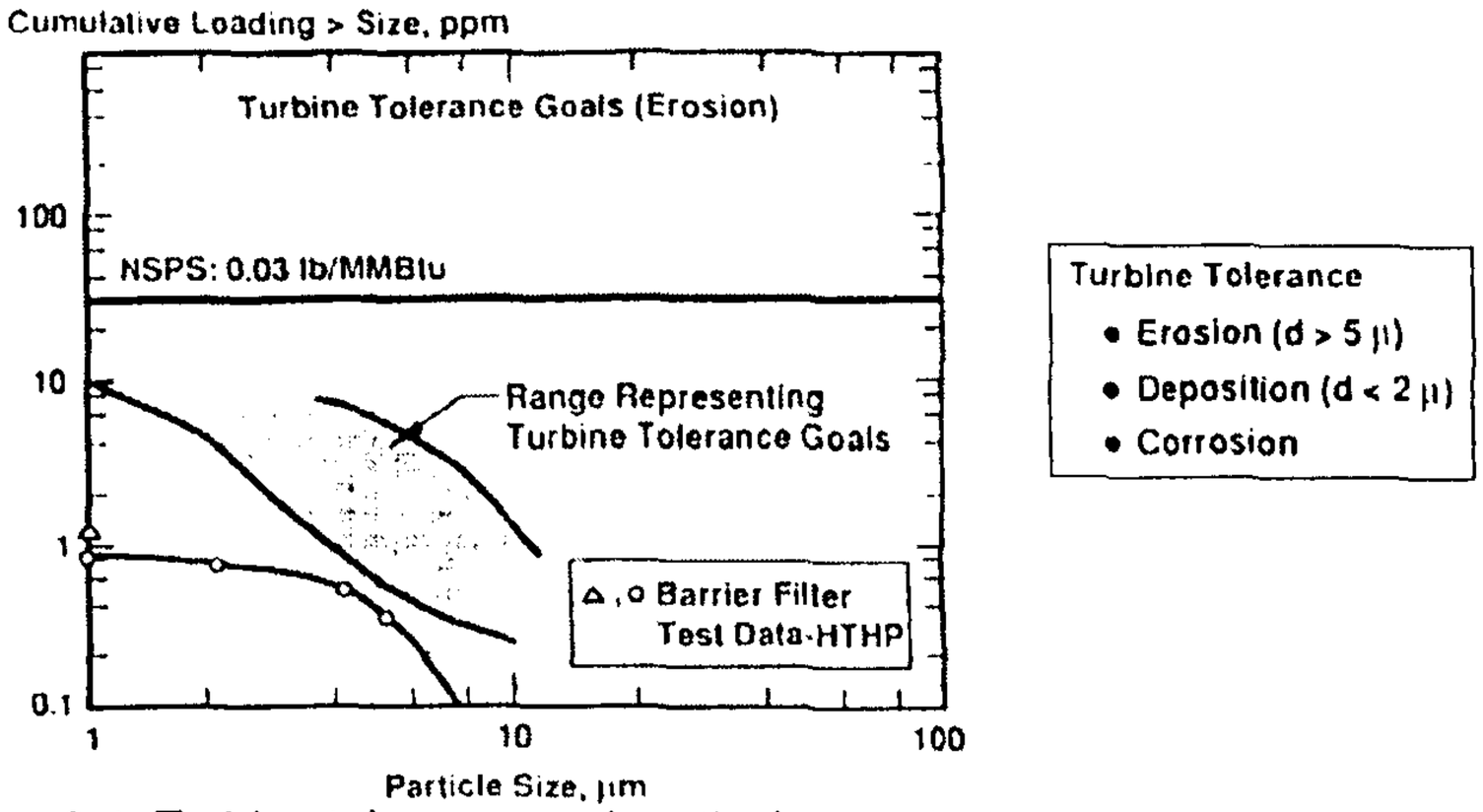

Figure 2.4: Turbine tolerance and particulate emission requirements in coal fueled gas turbine applications (Lippert et al., 1996)

A recent gas turbine specification for maximum concentrations of contaminants is given in Table 2.5 for the Siemens Westinghouse VX4-3A gas turbine. Particles are allowed up to 2 ppmw with further specification of the size distribution: less than 7½ %-wt should be larger than 2 µm. These values, aiming at preventing erosion and fouling of the turbine blades are more stringent that current emission standards, which are typically in the order of 30 - 50 ppmw in countries where these new technologies are being implemented (Scott, 1997).

Table 2.5: Gas quality specifications for a gas turbine (Ron and Pia, 2004)

Contaminant	Chemical Formula	Emission Limit	Comment	
Particulates		2 ppmw	Grain size:	10 µm: 0 2-10 µm: 7.5% 0-2 µm: 92.5%
Hydrogen halides	HCl + HF	1 ppmw		
Sulphur compounds	$H_2S + COS + CS_2$	20 ppmw	Emissions – Only corrosive in combination with alkalis	
Alkalis	Na + K	0.03 ppmw		
Heavy metals	V Pb	0.05 ppmw 1 ppmw		
Calcium	Ca	1 ppmw		

2.4.3 Fuel Gas Cleaning versus Flue Gas Cleaning

End-of-pipe commercial flue gas treatment systems such as conventional fabric filters (bag house), electrostatic precipitators, SCR and FGD technologies can be used to reduce most coal gas pollutants to levels conforming to current emission standards. However, it is commonly considered more energy-and cost-efficient in combined cycle systems to clean the fuel gas stream at high temperature and pressure prior to being combusted in the gas turbine (Mitchell, 1998; Ron and Pia, 2004). Prospective advantages of fuel gas cleaning includes better thermal efficiency, lower capital and operating cost attributed to cleaning of smaller volume of high-pressure coal gas before expansion in the gas turbine compared to the more voluminous flue gas after the turbine, better system control, the utilisation of a more advanced, high efficiency gas turbine and the reduction or possibly the removal of costly gas and water treatment facilities.

2.4.4 Hot Fuel Gas Cleaning versus Cold Fuel Gas Cleaning

There are many different technologies to clean the synthesis gas. They can be divided by the operating temperature. These are generically termed the cold gas clean-up (CGCU) and the hot gas clean-up methods (HGCU) according to the operating fuel gas temperatures. Conventional cold gas cleaning produces a pure fuel gas that satisfies the gas turbine manufacturer's specification and gives low environmental emissions. However, it has a negative impact on efficiency and economics. Advanced hot gas cleaning has yet to be demonstrated and may be wanting with regard to alkali metals, halogens and NH_3 removal efficiency. However, it has the potential to produce a pure fuel gas with low environmental emissions and could provide a competitive advantage over the other systems.

A good overview about high temperature gas cleaning is given in the report by Stevens (2001). Advanced hot gas cleaning is most beneficial to the BCABG and Texaco systems, the advantage to Shell is modest and it is not applicable to BGL due to the high tar content in the off-gas. There is little efficiency and economic advantage to be had by operating the hot gas clean-up system at 600℃ as opposed to 400℃ and there are certainly many more technical problems at the higher temperature. A comparison between conventional cold gas cleaning (below 200℃), partial hot gas cleaning (260-540℃) and hot gas cleaning (above 550℃) is given in Figure 2.5.

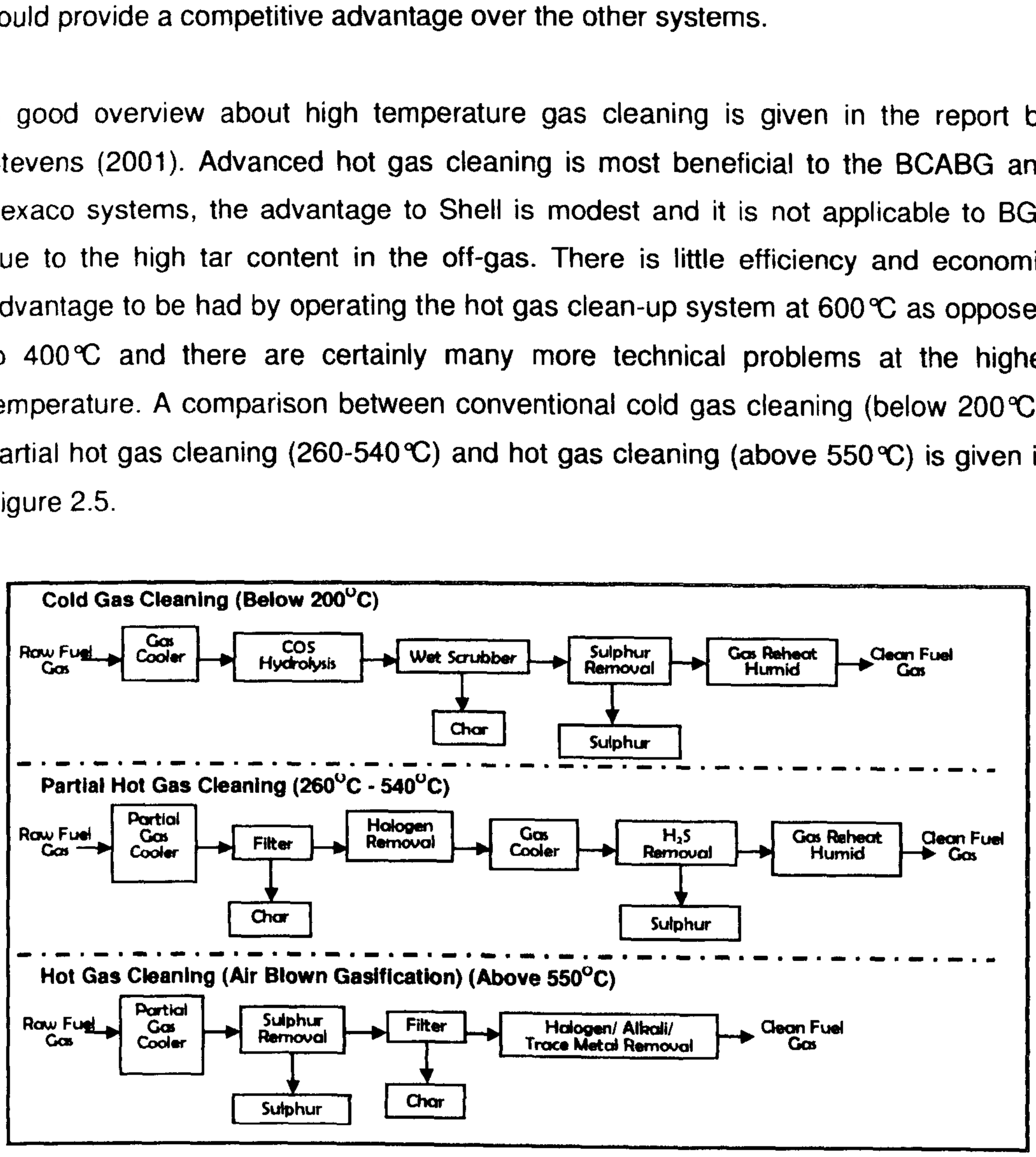

Figure 2.5: Options for HTHP gasification fuel gas cleaning (Lippert et al., 1996)

2.5 Identification and Characterisation of Air Pollutant Criteria

A range of pollutants are generated from coal-fired and coal co-fired power generating plants and some are more specific to a particular technology. Historically, attention has focused mainly on controlling emissions of SO_2, NO_X and particulates. Numerous systems have been developed and applied for their control. Some control specifically one type of pollutant, whereas others may integrate several control systems, thus allowing for the control of two or more pollutants (e.g. combinations of SO_2, NO_X and particulates) (IEA, 2003).

2.5.1 Sulphur Dioxide (SO_2)

During high-temperature gasification of coal (or other solid fuels), most of the sulphur constituent is released and converted to hydrogen sulphide (H_2S), as well as a small amount of carbonyl sulphide (COS), due to the reduced oxygen environment. The concentration levels of these so called acid gases, in the raw syngas exiting the gasifier, are almost entirely dependent on the levels of sulphur in the solid fuel (e.g., coal) (Pahl, 1983). These H_2S and COS are mostly removed from the syngas in the acid gas removal equipment prior to combustion or other forms of fuel conversion. There are inherent advantages in removing syngas contaminants prior to utilisation of the syngas. These advantages are:

- Removal prevents potential damage to the conversion devices, such as gas turbines, that result from contamination, corrosion, or erosion of materials;
- Relatively high concentration of H_2S in syngas, versus much lower concentration that would be found in the combustion flue gas, improves removal;
- High-pressure gasifier operation significantly reduces the gas volume requiring treatment;
- Conversion of H_2S into elemental sulphur (or sulphuric acid) is technically much easier and more economical than capture and conversion of SO_2 into saleable by-products; and
- The acid gas removal equipment extracts from 95% to greater than 99% of the H_2S and COS, once hydrolysed, from the fuel gas and converts it to a saleable sulphur or sulphuric acid (H_2SO_4) by-product. The small amount of residual sulphur that remains in the syngas is converted to SO_2 in the combustion turbine and released to the atmosphere in the HRSG stack gas.

Other secondary sources of SO_2 emissions in an IGCC plant will typically include the sulphur recovery system's tail gas incinerator stack, auxiliary boilers (if applicable), and the syngas flare during gasifier start-up and system upset conditions. These secondary SO_2 sources are typically significantly smaller than the HRSG stack emissions.

2.5.2 Nitrogen Oxide (NO_x)

The term "NO_x" refers to the sum of the nitric oxide (NO) and nitrogen dioxide (NO_2) emissions from a combustion source. While most of the NO_x produced during the combustion of syngas is in the form of NO, it is subsequently oxidised to NO_2 in the atmosphere. NO_x is formed in fossil combustion systems by two primary mechanisms. "Fuel NO" is formed via the oxidation of chemically-bound nitrogen in the fuel, and "thermal NO" is formed via the dissociation of molecular nitrogen and oxygen to their atomic forms (at high temperatures) and subsequent recombination into oxides of nitrogen. Unlike natural gas, coal contains chemically-bound nitrogen that forms most of the NO_x emissions when it is fired in a typical excess-oxygen environment, such as a utility boiler.

Fuel NO typically contributes over 80% of the total NO_x emissions in a coal-fired combustion unit, and its formation is highly insensitive to the flame temperature. Generally, thermal NO_x increases exponentially with increases in flame temperature and linearly with increases in residence time. The gasification process differs significantly from combustion with respect to the impact of chemically bound nitrogen in solid fuels, like coal. Gasification, because it operates with a deficiency of oxygen, converts most of the fuel nitrogen into harmless nitrogen gas (N_2). While a small portion is converted to ammonia (NH_3) and hydrogen cyanide (HCN), these water soluble species are removed during fuel gas cooling and cleaning and are usually converted to nitrogen in the sulphur recovery process. Therefore, the syngas produced is virtually free of fuel bound nitrogen, and NO_x formation is primarily the result of thermal NO produced at the high temperatures in the turbine combustor.

The following relationships exist between turbine combustor operating conditions and thermal NO_x production:

- NO_x increases strongly with fuel-to-air ratio or with firing temperature
- NO_x increases exponentially with combustor inlet air temperature

- NO_x increases with the square root of the combustor inlet pressure NO_x increases with increasing residence time in the flame zone
- NO_x decreases ex-potentially with increasing water or steam injection or increasing specific humidity.

Therefore, by maintaining a low fuel-air ratio and adding a diluent (e.g., nitrogen from the air separation unit or steam from the steam turbine), the flame temperature can be lowered to significantly reduce thermal NO_x formation. The gas turbines installed in commercially operated IGCC plants have made use of this combustion based control method to minimise NO_x emissions.

2.5.3 Particulate Matter (PM)

While ash is released from the solid fuel during the gasification process, most gasifiers release only a small portion as fly ash that becomes entrained with syngas. Not only does the gasification process provide an inherent capability to remove most ash as slag or bottom ash, but the fly ash that is produced is concentrated in a relatively small gas volume relative to solid fuel combustion processes, which further assists its cost-effective collection. Both the Polk and Wabash River plants use a wet scrubber to efficiently capture fine particulates that are entrained in the syngas.

Additional particulate removal occurs in the gas cooling operations and in the acid gas removal systems. As a result, very low particulate emission levels are achieved. Other particulate matter emission sources include:

- The sulphur recovery system tail gas incinerator;
- The flare system used during cold start-up, shutdown, and during upset conditions, when the combustion turbine may be unavailable;
- Mineral matter in the spray from the cooling towers (if applicable); and
- Coal and ash/slag handling and storage operations.

2.6 Summary: Future of Hot Fuel Gas Cleaning

The future of gasification is clearly impacted by changes in government policy. Continuing convergence of oil, gas, and electric power marketing with deregulation improves the potential for gasification. Increasing interest in improved energy efficiency, reduced emissions, and increased recycle of wastes also helps gasification. Electric power generation is the key market for gasification. Demand for electricity is growing at a rate twice that of other end-use energy forms such as natural gas and transportation fuels. Gasification will become more competitive in the long term as the current dominance of NGCC will lessen as natural gas prices increase. Gasification enables all feedstock to meet the same emission levels as NGCC. Current pitch and petcoke gasification is a bridge to long-term coal gasification. Technical trends, which help gasification, include improving gas turbines and polygeneration. Each increase in combined-cycle efficiency directly reduces the size and cost of the gasification facility required to fire the combined cycle. Advanced intercooled, recuperated, reheat gas turbines have the potential of power-to-cogeneration heat ratio that is an order of magnitude higher than possible with steam turbines. Polygeneration is unique to gasification, and with deregulation this concept will develop.

Gasification has strategic emission, efficiency, and economic flexibility for the future. This research intends to investigate and demonstrate the hot gas cleanup option for use in an integrated gasification combined cycle process. The goal is not to simply meet current environmental emission standards with respects to contaminants gases and particulate emissions, but also to adequately protect high-efficiency gas turbines and to control contaminants and particulate emissions at a sufficient low level to meet more stringent regulatory requirements anticipated in the future. Hot gas cleanup is still under development and may not be available for commercial application immediately. Summing up, hot gas cleaning will continue to play a major role in the development of coal-based combined cycle power generation systems in the foreseeable future. This research will contribute to how coal will continue to make a major contribution to global energy supply in the 21st century. Not only will the huge reserve base of coal be needed, but technological advancement can ensure coal is part of a cleaner energy future.

CHAPTER THREE

Review of Existing High Temperature Gas Cleaning Technologies

Gas cleaning systems for gasification-based power generation are needed to remove dust, S-species, N-species (e.g. ammonia, cyanides, etc), halides and trace metals from the gasifier fuel gases prior to their passage through the gas turbine and their subsequent release. Conventional technologies to remove these pollutants are based on wet gas cleaning systems, which have an adverse effect on cycle efficiency. The development and introduction of HGCU technologies offers the potential of a lower cost approach to pollutant control, leading to simpler cycle configurations with associated efficiency advantages. This chapter reviews the available technologies for hot gas desulphurisation and particulate clean-up. Emphasis is therefore given to the status of regenerable metal oxide sorbents for the removal of hydrogen sulphide from fuel gas under reducing conditions. This is followed by review on the various particulate control technologies available and their potential for high temperature gas cleaning. The final part of this chapter examines previous work on hot gas cleaning using liquid metals which culminates with the proposed molten tin based fuel gas cleaning system that is of interest in this research work.

3.1 Techniques and Development of Particulate Control in Hot Gas Clean-Up

3.1.1 Particulate Cleaning Technology

As part of the recent interest in new coal conversion techniques, there is an increased interest in particulate removal at high temperature and high pressure (HTHP), for hot gas cleaning. The main reasons for considering gas cleaning at HTHP conditions are:

Energy recovery from the gas stream (before use or emission), in particular:

- In combined cycle applications involving a turbine where the turbine has to be protected from erosion and corrosion, further:
- The smaller volume of gas cleaning equipment operating at high pressure may be advantageous.

Particulates are defined here as solid-phase materials entrained in the raw product gas stream as it exits the gasifier (Stevens, 2001). There are several major types of control devices for removing particulate matter from exhaust gases before the gases are emitted into the atmosphere. These include cyclones, wet scrubbers, electrostatic precipitators, and baghouses. In recent years, such steps have been taken in many industries. Nevertheless, no process can be made 100% efficient, and so there will always be some air pollution emissions that must be controlled. The technological and commercial status of hot gas particulate cleaning technology have been extensively reviewed and discussed by Chang (2003); Ron and Pia (2004), Seville (1996, 1997) and Mitchell (1997).

3.1.1.1 Ceramic (Rigid) Barrier Filters

Ceramic barrier filters are the most advanced hot gas filtration technology system with several systems going to commercialisation. They boast of high dust collection efficiencies with only low pressure and temperature drops across the system (Chang, 2003), and the filtration efficiency is "usually extremely close to 100%" (Seville, 1997) with the exception of substantially submicron dust or large filter medium granule or fibre size. They provide a potential opportunity to produce a clean fuel gas while retaining the sensible heat of the fuel gas. Stevens (2001) reported that these filters effectively remove small-diameter particulates in range or 0.5 to 100 μm in diameter from the gas stream. It can be designed to remove almost any size of particulates, including those in the sub-micron range, but the pressure differential across the filter will increase as the pore size decreases.

As a result, there are technical and economic constraints which effectively limit particulate removal to about 0.5 μm in systems such as gasifiers that must handle large gas volumes. Factors that limit the life of ceramic filter include reaction of alkali vapour and/or steam with the amorphous binder phase, oxidation of non-oxide based ceramics, as well as degradation due to thermal and mechanical shocks. Typical failures that have occurred during operation include broken filter elements, deformed filters, reduced permeability due to plugging of ceramic matrix pores by ash, and thermal degradation of the ceramic binder (Huque et al., 1996). Other problems are formation of strongly bonded ash deposits and bridging of ash between candles and hot metal structures.

Mitchell (1997) concluded that individual components of ceramic barrier filters need to undergo long-term assessment under conditions typical of coal or biomass based combined cycle systems in order to gain confidence in commercial applications of this technology. Further research and development will be required to provided insight into the influence of operating temperature and gas phase components on dust cake formation and removal behaviour. For IGCC application, there is now evidence that satisfactory operation of ceramic candle filters is possible at temperature ranging from 250℃ to 450℃. However, operating temperatures above 500℃ and up to 900℃ required of advanced combined cycle designs must be the long-term goal such that high system efficiencies can be achieved (Mitchell, 1997), (Seville, 1996).

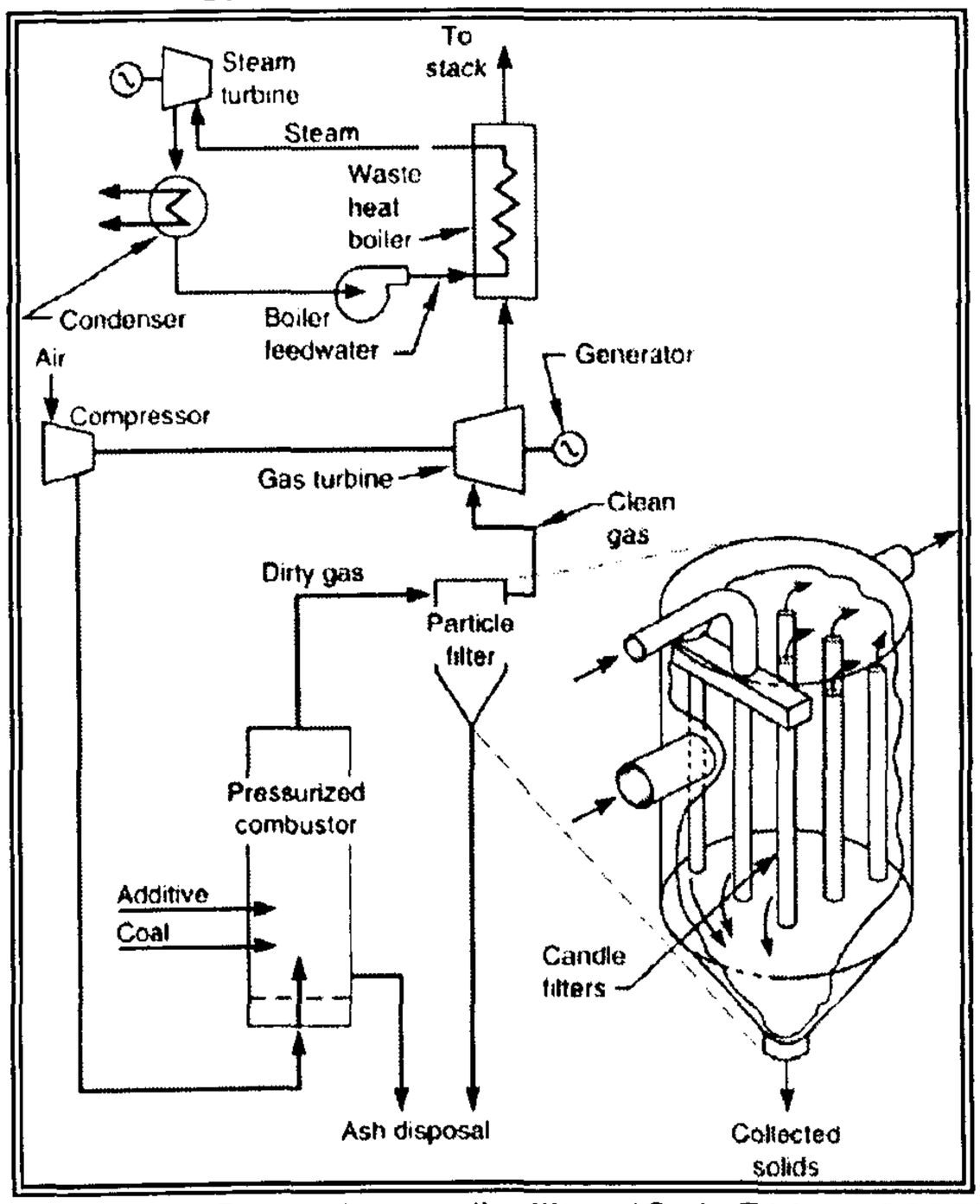

Figure 3.1: Ceramic candle filter (Oak-Ridge, 2005)

3.1.1.2 Cyclones

Cyclonic filters are a primary means of removing bulk particulates from gas streams. They use centrifugal force to separate solids from the gas by directing the gas flow into a circular path. Because of inertia, the particulates are unable to follow the same path and are separated from the gas stream. Cyclones can operate between 0.1 and 10 MPa at temperatures greater than 1000℃. The cyclone is typically a vertically erected conical or cylindrical shaped chamber which receives particle laden flue gas in the upper chamber region, as shown in Figure 3.2. The main limitation of the cyclone is the inability to effectively remove small particles less than 5 μm in diameter. For small particles, the inertial separating force (particle momentum) is low and the particles are more prone to remain suspended in the gas stream.

Cyclone performance is affected by gas flow rate, since this affects the swirling velocity in the cyclone. Cyclone efficiency is relatively insensitive to dust loading, and in fact, the efficiency can increase with higher loading due to particle interactions. Efficiency increases with particle size, typically ranging from 5% for 0.5 µm particles to 50% for 3 µm particles. The cyclone efficiency increases with particles size, density and gas velocity, but decreases with increasing gas velocity and cyclone diameter, hence it is unlikely to improve at high temperatures and pressures (Clift, 1997); (Mitchell, 1997). A number of novel cyclone designs have been developed, however they have not been widely accepted because despite being more costly and complex, their efficiency is not higher than that of a well-designed conventional cyclones (Seville, 1996)

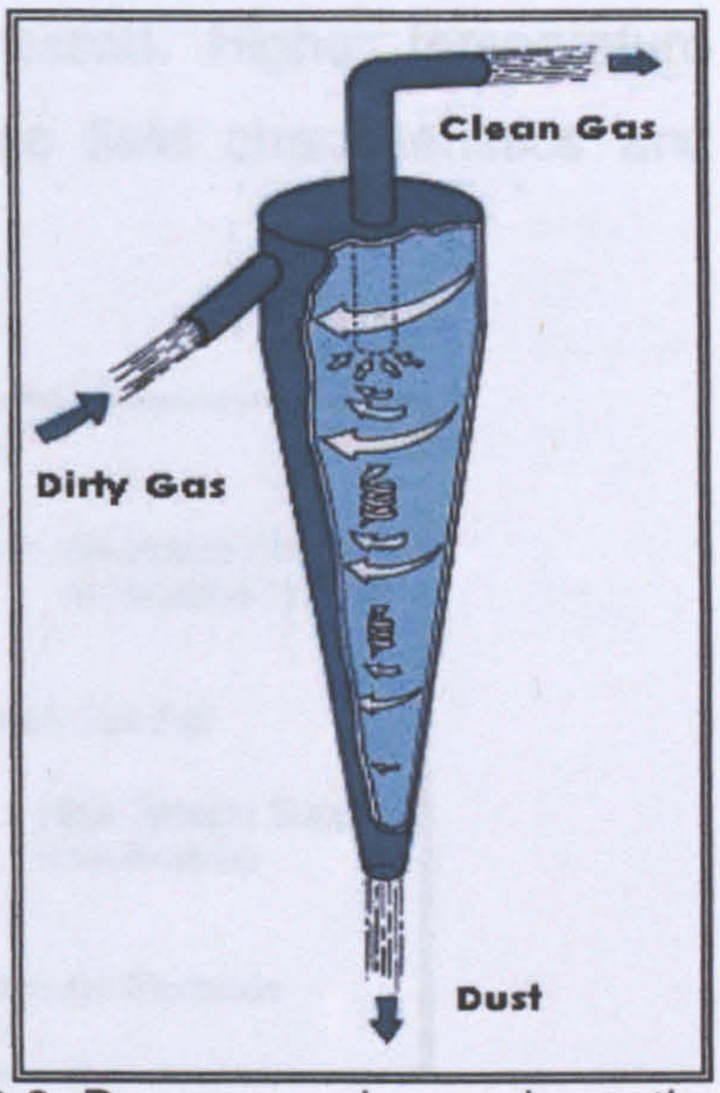

Figure 3.2: Process cyclone schematic

3.1.1.3 Electrostatic Precipitators

Electrostatic precipitator (ESP) filters have also been used extensively in a variety of gas cleaning operations (Noll and Peter-Castle, 1995), typically operated at atmospheric pressure and temperatures ranging from 120 to 450℃, capable for collecting fine particles (less than 2 µm) with high collection efficiencies in excess of 99.5%. ESP are available in a variety of designs and can operate in a dry or wet mode and in hot or cold gas conditions (EPA, 1996). The particulates are charged and attracted to the earthed electrode, separating them from the gas stream as shown in Figure 3.3. ESP efficiency increases with increasing plate area, increasing voltage and decreasing gas flow rate. Capture efficiency is dependent on specific collection area (SCA), operating voltage, and particle characteristics. The main difficulty faced by ESPs in high temperature operations is that the voltage difference between the corona onset and spark over (i.e. when electrical field breaks down) has to be essentially maintained, but this difference decreases with increasing temperatures. However, the voltage difference is increased at higher pressures, indicating the possibility of high-temperature and high-pressure ESP operation.

Also, high electric field strengths can be achieved under these conditions meaning that a smaller collecting area is possible. However at high temperatures, issues concerning corona stability, high energy loss, material durability as well as low-resistivity dust-charging and dust removal difficulties have to be addressed. Higher temperature operation is limited by availability of data on the electric field characteristics and uncertainties concerning the insulator and other materials.

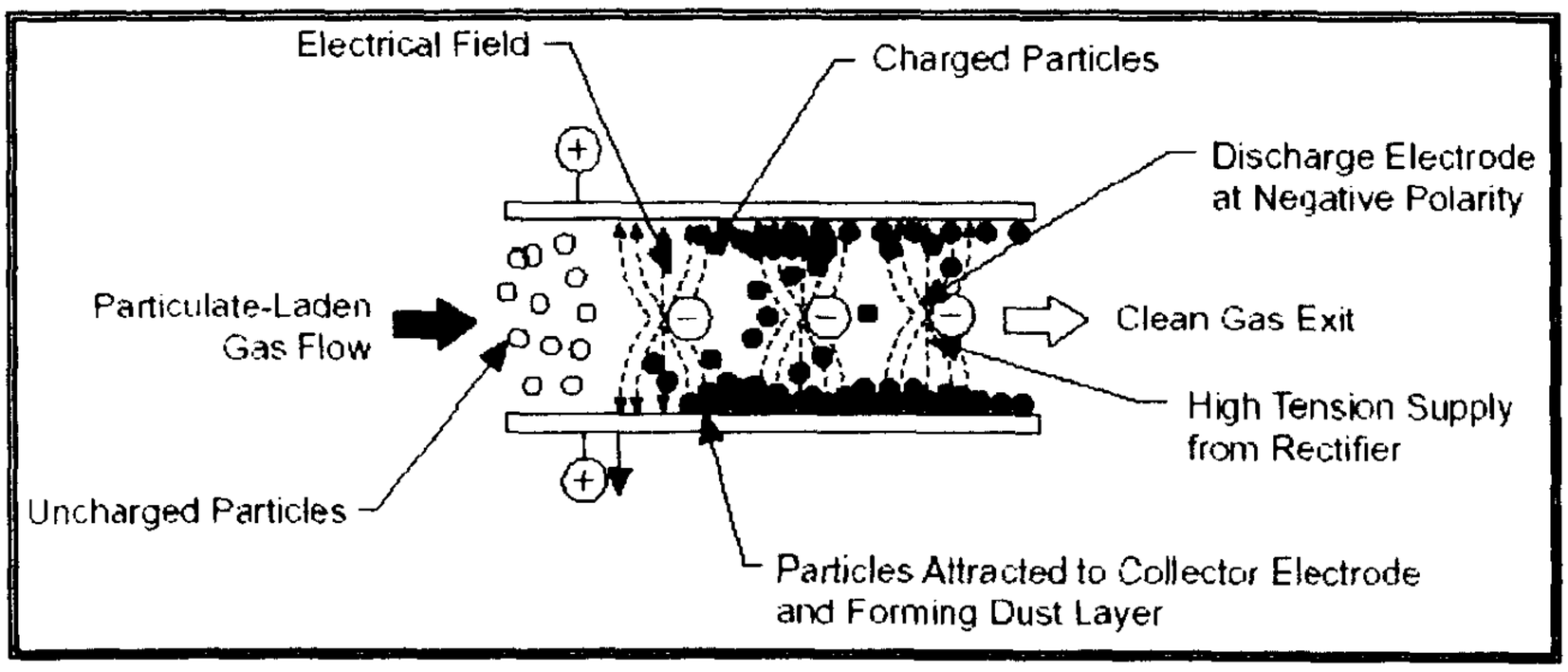

Figure 3.3: ESP particle collection procedure (EPA, 2005)

3.1.1.4 Fabric Filters (Baghouses)

One of the most efficient devices for removing suspended particulates is an assembly of fabric filter bags, commonly called a baghouse. A fabric-filter dust collector can remove very nearly 100 percent of particles as small as 1 μm and a significant fraction of particles as small as 0.01m. Fabric filters, however, offer relatively high resistance to airflow, and they are expensive to operate and maintain. Additionally, to prolong the useful life of the filter fabric, the air to be cleaned must be cooled (usually below 300℃) before it is passed through the unit; cooling coils needed for this purpose add to the expense. Fabric filter efficiencies can range between 99 and 99.99% for particle sizes as low as 0.1μm. Particle capture is relatively insensitive to particle and dust physical characteristics such as particle resistivity and dust loading. Efficiency decreases as the air-to-cloth ratio increases as gas velocity rises. Air-to-cloth ratio is a ratio of the gas volume flow rate to the filter surface area and is a measure of the superficial gas velocity through the filter.

Particle capture efficiency is also dependent on the frequency of bag cleaning, cake build-up, and fabric type and weave, as well as on the physical condition of the bags. A typical baghouse comprises an array of long, narrow bags each about 25 cm in diameter (SugarUdyog, 2005) that is suspended upside down in a large enclosure. Dust-laden air is blown upward through the bottom of the enclosure by fans. Particulates are trapped inside the filter bags, while the clean air passes through the fabric and exits at the top of the baghouses. Several compartments of filter bags are often used at a single baghouse installation.

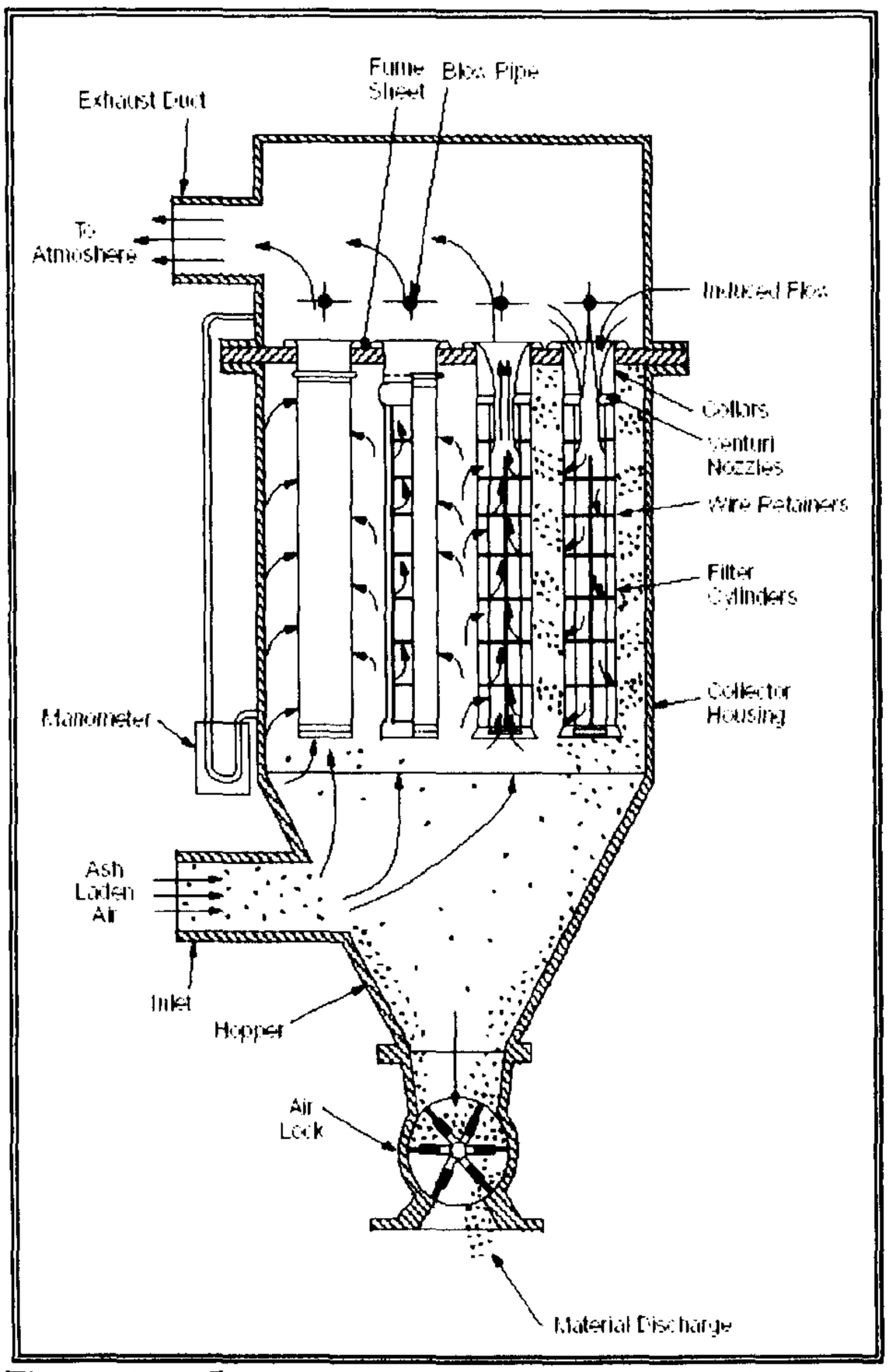

Figure 3.4: Pulse-air-jet - Baghouses (EPA, 2005)

This arrangement allows individual compartments to be cleaned while others remain in service. The bags are cleaned by mechanical shakers or by reversing the flow of air and the loosened particulates are collected and removed for disposal. The bags are usually made of cotton, wool, synthetic, or glass fibers, and there may be hundreds of bags within one structure. Operation is limited to relatively low filtration velocity of less than 5 cm/s to avoid penetration of particulates into the fabric medium and their re-entrainment. Research into their application in combined cycle power systems has been very limited, with the available ones focusing on pulse jet type of ceramic fabric filters. The main issue is to identify suitable materials to withstand long-term-high-temperature operation.

Some composite textile materials that are marketed for high temperature duty, quoted to have an average operating temperature of 300℃ with surges up to 350℃ include 'Tefair' (PTFE/glass fibre) by DuPont and 'Pyrotex' (mineral/ceramic/metal fibers) by BMW (Chang, 2003). 3M's seamless filter bags woven from aluminium borosilicate ceramic filter material 'Nextel' are quoted as temperature-resistant up to 1150℃ for continuous operation and up to 1370℃ for short operation periods. However, the development of SiC composite rigid candle filter by 3M seems to suggest that the bag filter design is not a serious alternative for high temperature applications in combined cycle power systems. At present, fabric filters do not provide the long-term performance necessary for gas turbine protection in combined cycle applications (Mitchell, 1997), (Seville, 1996).

3.1.1.5 Metallic Filters

Metallic filters based on stainless steel have been widely rejected for PFBC operations mainly due to their susceptibility to severe hot corrosion in oxidising environments. However, the possibility remains for their application in gasification at temperatures ranging from 350℃ to 600℃ under reducing conditions. The advantages of metallic filters over ceramic filters include their high resistance to thermal and mechanical shock, lower pressure drop resulting in reduced filtration area and lower capital costs, as well as simpler sealing, fabrication, handling and installation (Anderson et al., 2003); (Grasa et al., 2004). A study to test the long-term corrosion resistance of metal filters in a gasification environment was performed recently by VVT in Finland. Pall's commercial metal filter material comprising 316 and 310 stainless steel, Inconel 600 and Hastelloy X were tested up to 800 hours in simulated gasification conditions with 300 ppmv H_2S at 400℃ and 500℃ (Chang, 2003).

All materials showed good durability at 400℃, the slight corrosion being mainly due to oxidation of chromium to chromium oxide (Cr_2O_3). At 500℃, the stainless steel filters notably the 310 demonstrated good resistances, however the nickel-based filter of Inconel and Hastelloy suffered severe sulphidation forming nickel sulphide (NH_3S_2), blinding the filters. Pall is supplying their sintered stainless steel candle elements for the IGCC project at Polk Power. Pall have developed seamless tube filters using a new corrosion resistance metal alloy of iron aluminide (Fe_3Al) which are claimed to be

exceptionally resistant to corrosion in high temperature, sulphurous environments. The iron aluminide filters will be tested under gasification conditions as well as in an oxidising gas stream. However, there continue to be concern over the ability of metallic filters to endure high and low temperature excursions, as well as short term sulphur level variations (Seville, 1996).

3.1.1.6 Granular Filters

Granular bed filtration was considered a leading hot gas cleaning technology in power generation applications in the early 1980s. The filter consists of a bed of granular solids, typically spherical and 1 to 3 mm in size. The main advantage of this filter is their robustness as various mechanically, chemically and thermal resistant (above 1000℃) granular media can be used as collectors. There generic configurations: fixed or slowly moving beds acting as surface filters, fixed or moving beds operating as depth filters and fluidised beds. The main collection mechanisms involved are inertial impaction and agglomeration. Others include diffusion and interception, as well as gravitational, electrostatic, magnetic and acoustic collection mechanisms. In principle, they can operate at relatively high velocity and all the different designs are capable of relatively high collection efficiencies. However in practice, commercial development has been hindered by cake formation and particle retention difficulties, as well as severe attrition of the collector medium at high temperatures and high velocities.

Commercial granular bed filters are available from the Combustion Power Company, Westinghouse and Kawasaki Heavy Industries (Chang, 2003). In CPC's design, the dust-laden gas travels counter-currently to a downward moving bed consisting of relatively high-value 1 to 3 mm alumina (Al_2O_3) or 6 mm mullite ($Al_2O_2.SiO_2$) spheres. CPC is currently testing an industrial-scale unit in Wilsonville, Alabama. At higher temperatures problems arise due to sintering of the fine particles on the surface of the granules which may lead to filter blinding at short distances from where the dusty gas enters. The efficiency of a granular bed filter depends on the size distribution and shape of the particles to be filtered. Granular beds are unlikely to succeed as a stand-alone particulate filter but may be attractive as a multi-contaminant clean-up device for simultaneous removal of gaseous contaminants and solid particulates (Seville, 1996), (Mitchell, 1997).

3.1.1.7 Hybrid Systems

Hybrid particulate collection systems combine electrostatic precipitation with fabric filtration to achieve high particulate removal efficiencies at low costs. Compact Hybrid Particulate technology (COHPAC) provides a low cost option to upgrade the existing aged or undersized ESPs and, when combined with activated carbon powder injection, a possible means for mercury control. An Advanced Hybrid Particulate Collector (AHPC) system can achieve 99.99% particulate collection efficiency for all particles sized from 0.01 to 50 μm (Ron and Pia, 2004), (Hrdlicka and Swanson, 2003). An AHPC system requires less space and has lower capital cost compared with a conventional ESP or baghouse, and can be designed for new installations as well as retrofits for existing ESPs (Zhu, 2003). Electrostatic precipitators use electrodes to give particles an electric charge that draws them to collection plates. The Advanced Hybrid system puts rows of bag filters directly between the collection plates. The bags stop the particles that get by the collectors and, periodically, inject air in reverse through the filters, dislodging built-up particles and sending them back toward plates to be collected. This not only keeps the bags clean, but also uses less energy drawing air. Reportedly air coming out of the plant is cleaner than that going in, with respect to fine particulate.

3.1.2 Current Limitation

Various technologies have been proposed for hot gas particulate cleaning; however few have undergone sufficient development for commercial application in combined cycle power systems. Further development will be required to enable operating temperatures above 500℃ and up to 900℃ necessary to fully realise the advantages of gas cleaning at high temperatures in advanced combined cycle designs.

3.2 Techniques and Development of Desulphurisation Processes in Hot Gas Clean-Up

Sulphur products in combustion not only pollute the environment, but also are detrimental to combustion systems because of the corrosive action of their combustion products (Kwon, 1998). In the gasification process, coal is reacted with steam and air or oxygen to produce a medium to high calorific value fuel gas. The fuel gas can be subsequently combusted in a gas/steam turbine combined cycle (IGCC). These IGCC-based power generation options offer much higher thermodynamic cycle efficiencies that promise to reduce all forms of pollutants released from a coal conversion process through lower fuel consumption and the use of more energy efficient high pressure and/or temperature unit operations for the removal of environmental pollutants.

3.2.1 Conventional Gas Cleaning Technology for Power Generation Plant

The conventional method of removing H_2S and sulphur recovery involves a number of steps including amine scrubbing at low temperature followed by amine regeneration using steam to produce a concentrated H_2S-containing gas. This concentrated H_2S-containing gas is then combusted to produced a gas with a H_2S to sulphur dioxide (SO_2) ratio 2:1 in a Claus furnace (Kwon and Gangwal, 2004). This is followed by up to three stages of Claus reaction at a temperature of around 250 - 280℃ over an alumina catalyst to recover elemental sulphur:

$$2\,H_2S\,(g) + SO_2\,(g) \leftrightarrow 3S\,(l) + 2\,H_2O \qquad (3.1)$$

The Claus reaction is exothermic and equilibrium limited. To circumvent the equilibrium limitation, the reaction is conducted in up to three reaction stages with interstage cooling/sulphur condensation followed interstage re-heating. However, even with three stages, the reaction is not complete due to thermodynamic limitation at 250℃ (Turk et al., 2001). The Claus tail gas contains sulphur that must be further treated in an expensive tail gas treatment plant (e.g., SCOT) before discharge. Thus, overall H_2S removal and sulphur recovery using this conventional sequence is extremely cumbersome, equipment intensive, and expensive.

3.2.2 High-Temperature Sulphur Removal Using Sorbent Technology

✱ Disposal Sorbents (In-Situ Desulphurisation)

The disposable sorbents are mainly calcium-based materials, for instance dolomite ($CaCO_3.MgCO_3$), lime (CaO) and limestone ($CaCO_3$) which are cheap and abundantly available. They are used in a once-through mode in the fluidised bed gasifier (as well as in fluidised bed combustion systems), removing up to 90% (Mojtahedi et al., 1994) of sulphur in the fuel. The sorbents can be incorporated in-bed., injected into the gas stream, or directly contacted in an external reactor unit. This in-situ high-temperature desulphurisation process is well-proven and involves the following reaction for H_2S removal under reducing conditions:

Sulphidation: $CaO\ (s) + H_2S\ (g) \text{ --- } CaS\ (s) + H_2O\ (g)$ (3.2)

Direct sulphidation: $CaCO_3\ (s) + H_2S\ (g) \text{ --- } CaS\ (s) + CO_2\ (g) + H_2O\ (g)$ (3.3)

Unstable CaS is formed which is then reacted with air forming the environmentally stable $CaSO_4$ (gypsum) to be disposed off with the gasifier bottom ash. There are several disadvantages associated with the use of these disposable sorbents. Sintering and pore plugging at high temperatures reduce calcium availability, inhibiting CaS stabilisation to $CaSO_4$ and necessitating a secondary oxidiser for complete conversion of CaS to $CaSO_4$. In-bed sulphur retention within the gasifier is limited by thermodynamics at low temperatures.

Sulphur removal is 80 to 90% which is lower than the desirable level of 95 to 99% for IGCC (Gangwal, 1995), necessitating post-bed H_2S polishing to further reduce the residual H_2S. The resulting $CaSO_4$ has no market value, requiring land filling which incurs additional removal costs and may pose a problem where land is scarce. Although H_2S is the main sulphur component in the fuel gas and hence is the focus in the literature regarding gas desulphurisation, similar sorbent sulphidation reactions to those represented by equations 3.2 and 3.3 should apply to COS as well.

UNIVERSITY OF SHEFFIELD LIBRARY

❋ Regenerable Sorbents (Post-Bed Desulphurisation/Polishing)

A good sorbent will allow for a deep desulphurisation to ppm levels and have good regeneration properties. This means the combination of a high affinity towards the reaction with H_2S and COS, as well as the formation of a sulphide which can be converted back to the oxide through oxidation with air or dilute air. Next to the residual H_2S and COS level, sorbent durability is the critical issue. The thermodynamics of the reaction should be favourable enough to achieve the desired level of H_2S and COS removal (as much as 99% or more) (Gangwal et al., 1998), (Sanchez et al., 2005). According to Elseviers and Verelst (1999), for economical operation, a good sorbent has to maintain a large fraction of its desulphurisation properties for at least a hundred sulphidation-regeneration cycles, requiring excellent sorbent stability. Over the last two decades a number of studies have been reported on high-temperature H_2S removal, primarily using various transition metal oxides as regenerable sorbents. The sulphidation (absorption) and regeneration (desorption) reactions involving metal oxide sorbents can be represented by the following general equations:

Sulphidation: $M_yO_x\,(s) + xH_2S\,(g) \rightarrow M_yS_x\,(s) + xH_2O\,(g)$ (3.4)

Regeneration: $M_yS_x\,(s) + (3/2)xO_2\,(g) \rightarrow M_yO_x\,(s) + xSO_2\,(g)$ (3.5)

$M_yS_x\,(s) + 2xH_2O \rightarrow M_yO_{2x}\,(s) + xH_2S\,(g) + xH_2\,(g)$ (3.6)

Gangwal et al., (1998) reported that various oxides of materials such as activated carbon (Bandosz, 1999), (Cal et al., 2000), ZnO (Sasaoka et al., 1992; Sasaoka et al., 1994; Slimane and Abbasian, 2000), Fe_2O_3 (Sasaoka et al., 2001), CuO (Abbasian and Slimane, 1998), Mn_2O_3 (Wakker and Gerritsen, 1993; Slimane and Hepworth, 1994a; Slimane and Hepworth, 1994b; Slimane and Hepworth, 1995) and $ZnFe_2O_4$ (Pineda et al., 1997) have been researched.

These oxides are sometimes mixed with secondary oxides such as silica, alumina, titania and chromic which do not take part in the sulphidation reaction but instead give additional mechanical support, stabilise the main metal oxides and minimise sorbent losses, as well as aid regeneration. Table 3.1 lists the main metal oxides used as regenerable sorbents and their characteristics. The sorbent most intensively studied in the 1980's was iron oxide, which yields equilibrium H_2S concentrations in the few

hundred ppm range for a composition representative of low-Btu coal derived gas and temperatures of above 500℃. While the sulphidation kinetics of iron oxide are very good (Tamhankar et al., 1981), this sorbent cannot be used for single-stage coal gas desulphurisation to reduce the H_2S content of the fuel gas down to a few ppm of sulphur. Among the various mixed metals evaluated, zinc-based materials are the most promising for high temperature intensive desulphurisation (Slimane and Williams, 2002).

Table 3.1: Sorbents general characteristics (Williams and McMullan, 1998)

Sorbents	Absorption Temperature (℃)	Regeneration Temperature (℃)	Sorbents Utilisation (%)	H_2S Outlet Concentration (ppmv)
Tin dioxide	350 – 500	400 – 500	85	<100
Copper oxide	350 – 550	650	70	<20
Manganese oxide	350 – 870	900	50	<10
Iron oxide	360 – 500	500 – 650	25 – 45	<100
Zinc oxide	480 – 540	500 – 700	50 – 70	<1
Zinc ferrite	450 – 600	600	20 – 80	<20
Zinc titanate	450 – 750	600 – 750	40 – 60	<10
Copper chromite	650 – 850	N/A	40 – 80	<10
Cerium oxide	750 - 1000	600	90	<100

The bulk of research on regenerable sorbents has been on zinc-based sorbents because sorbents based on zinc oxides appear to have the fewest technical problems among all sorbents (Gangwal et al., 1998). Zinc oxide (ZnO) has highly attractive thermodynamics for H_2S adsorption and can reduce the H_2S to parts-per-million levels over a very wide temperature range. It has been used as a non-regenerable sorbent in "guard beds" protecting catalyst beds from trace sulphur impurities. More recently, zinc oxide has also been investigated as a regenerable sorbent (Lew et al., 1989). The thermodynamic equilibrium for sulphidation of ZnO is quite favourable, yielding desulphurisation down to a few ppm H_2S (Jothimurugesan et al., 1986). The ZnO-based sorbents that have been researched include zinc ferrite, zinc titanate, Z-Sorb, and METC-10 (Gupta et al., 1998). The sulphidation kinetics of ZnO, however, are slower (Westmoreland et al., 1977) compared to those of pure iron oxide, and the regenerability of ZnO is restricted above 700℃ by the loss of surface area and the formation of zinc sulphate at low regeneration temperatures. In the late 1980's, it was shown that certain mixed oxides have superior properties compared to single oxides for hot gas cleanup (Lew et al., 1989).

A compound of zinc and iron oxides, zinc ferrite, $ZnFe_2O4$, developed by DOE/METC was tested at the pilot stage for desulphurisation of low-Btu gases (Ayala and Venkataramani, 1998). Gupta et al., (1996) reported that pure zinc oxide sorbents are not suitable because they are prone to undergo reduction in coal gas resulting in zinc vaporisation. Similarly, zinc ferrite sorbents have limited applicability due to excessive attrition, iron carbide formation, and carbon deposition (Gupta and Gangwal, 1993). Zinc titanate sorbents do not suffer from these problems and therefore have emerged as alternatives to zinc ferrite sorbents. Physical durability of the zinc ferrite sorbent in long-term testing precluded further use at that time, but recent work suggests that improved performance can be obtained with new preparation techniques (Abbasian and Slimane, 1998). Because of the apparent limitations of the zinc ferrite sorbent, many investigators have been conducting research to develop a superior mixed metal oxide sorbent (Patrick et al., 1989).

Earlier experimental studies that pioneered the use of mixed-metal oxides were performed at the Massachusetts Institute of Technology (MIT) (Lew et al., 1989), Research Triangle Institute (RTI), Electrochem, U.S. Dept. of Energy-METC (DOE/METC), (now Federal Energy Technology Centre, FETC) and the Institute of Gas Technology (IGT) (Abbasian and Slimane, 1998). Mixed-metal oxide sorbents have been studied in the past both as straight zinc titanate, (e.g., Zn_2TiO_4 and $Zn_2Ti_3O_8$) or as combinations of oxides of vanadium, copper, manganese, cobalt, and others (Ayala and Venkataramani, 1998).

Work on zinc titanate such as $ZnTiO_3$, Zn_2TiO_4, and $Zn_2Ti_3O_8$ (Lew et al., 1989), (Jun et al., 2001) has shown that titanium oxide is a better alternative to iron oxide additives in terms of the higher stability of the titanate over the ferrite compounds of zinc, and their similar sulphidation equilibrium. With zinc titanate, the sulphidation temperature has been shown to extend to 700℃, and sintering of the ZnO was greatly reduced. Although zinc titanate has also shown better attrition resistance than zinc ferrite in pilot tests, this sorbent also suffers gradual loss of reactivity in long-term cyclic operation, resulting in high fresh sorbent makeup rate to maintain the desired level of desulphurisation (Abbasian and Slimane, 1998). Other mixed metal oxides such as copper-based and cobalt-based sorbents have also been investigated (Ayala and Venkataramani, 1998); however, the research has been limited to laboratory-scale equipment.

Although higher temperature application offers better overall process efficiency, the stringent requirement for sulphur removal efficiency at temperatures above 538 °C limits the choice of the sorbents to a few metal oxides (based on thermodynamic equilibrium), that have been shown to have other limitations as described earlier. The thermodynamic equilibrium of many metal oxides significantly improve as the temperature decreases, making many metal oxide sorbents suitable for hot gas cleanup application in the temperature range of 343-538 °C.

Although the initial chemical reactivities of the sorbents generally decrease with decreasing temperature, the lower thermal stress incurred can lead to better sorbent reactivity after a large number of cycles, reducing the sorbent replacement cost. In general, the benefit to be gained by lower temperature application may outweigh the slight loss of efficiency, resulting in lower overall cost of electricity. However, no extensive study has been done on the development of advanced sorbents for the lower temperature application. In order for a metal oxide to be considered suitable for high-temperature desulphurisation, the material must exhibit desirable properties in the following areas (Abbasian and Slimane, 1998):

- Rate of H_2S absorption and low equilibrium H_2S achievable in the gas phase
- Ease of regeneration of the sulphide species formed during absorption
- Likelihood of sulphate formation and ease of sulphate decomposition
- Metal/sorbent evaporation and temperature of incipient evaporation
- Formation of low-melting eutectic phases
- Reduction to metal during absorption due to highly reducing coal gases
- Interactions between active metal oxide, stabilisers, and support with other components and contaminants in coal gas (e.g., H_2, alkali metals, halogens)
- Sulphur loading of metal oxide and sulphur loading capacity limitations
- Disposal of spent sorbent metals and deleterious effects of volatilised sorbent metals to other IGCC components (e.g., turbine)
- Cost of support and/or cost of active metal oxide

The feasibility of operating a moving-bed high-temperature desulphurisation system in an economically competitive and technically feasible manner currently restricts its use to a temperature between 400-750℃ and pressures above 10 atmospheres during absorption. Operation below 400℃ does not take full advantage of higher system efficiency compared to low-temperature cleanup systems, while operation above 750℃ requires a trade-off between more sophisticated material properties/higher capital costs and reliability of process operation. Although this operation may expand in the future, these current boundaries of operation are considered realistic (Abbasian and Slimane, 1998).

3.2.3 Current Limitation

From their reviews of existing hot gas desulphurisation technologies, Mitchell (1998) and Chang (2003) concluded that no fully commercialised desulphurisation sorbent is available as yet, while Williams and McMullan (1998) documented that "the perfect sorbents is still a long way from commercial reality". There are still issues to be resolved regarding sorbents performance during long-term operation in different reactor systems. In particular, problems related to sorbent mechanical strength, chemical attrition resistance, long-term durability and reactivity have yet to be fully addressed. According to Turk et al., (2001), currently, the limitations of sorbent-based gas desulphurisation processes may be summarised as follows:

- Inability to reduce H_2S concentration of syngas to sub-ppm (parts per million) levels
- Relatively slow kinetics at temperatures below 427℃
- Relatively low sulphur capacity at low temperatures 204 to 427℃
- Poor regenerability at temperatures below 538℃

3.3 Development of Hot Gas Desulphurisation & Particulate Cleaning by Liquid Metal

The concept of using liquid metals for gas desulphurisation dates back to the late 1970s when Meissner (1976) first patented the concept of removing sulphur from hot reducing gases using liquid lead. However since then, only few others have propounded the use of liquid metals for gas cleaning. They were Meissner and Shora (1981); Schüermann (1984); Reitz (1985); Hedden et al., (1986) and most recently, Warner (2000, 2001).

3.3.1 Early Work – Gas Desulphurisation with Molten Lead

Meissner (1976) put forward the concept of using molten lead for sulphur removal from hot reducing gases. Lead was selected as the reagent metal due to its relatively low melting point of 327℃. In the proposed process, incoming hot gases containing sulphurous compounds such as hydrogen sulphide are contacted with a slurry or solution mixture of lead sulphide in molten lead in a refractory-lined clean-up chamber. In the clean-up chamber, a rotating wheel that is partially immersed in the melt disperse the mixture into droplets in the gas phase, providing intimate contact with the sulphur compounds in the incoming gases and breaking up the solid lead sulphide skin (if any) on the surface of the melt. The sulphur content in the hot gases reacts with lead forming lead sulphide. The slurry of unreacted molten lead and the formed lead sulphide is withdrawn to a refractory-lined regeneration chamber. Regeneration is carried out by electrolysis of the lead sulphide producing molten lead at the cathode and elemental sulphur at the anode.

The regenerated lead together with any unconverted lead sulphide (in solution or slurry form) is recycled back to the clean-up chamber in a volume that is in excess of that required to react with the predetermined sulphur content in the incoming hot gases and to at least form a pumpable mixture of molten lead and solid lead sulphide. The elemental sulphur is removed as a volatilised gas from the regeneration chamber. Building on the earlier patent by Meissner (1976), Meissner and Shora (1981) proposed a general process for a high temperature heat exchanger between a gas stream and either a molten metal or a molten salt. This is through generation of liquid droplets in a confined gas passageway giving high interphase contact surface area.

The droplet shower can be generated either by impellers or rotating disks partially immersed in a liquid pool, or using submerged gas jets, or with spray heads and nozzles. If required, simultaneous removal of undesired solid, liquid or gaseous components from the gas stream can also be provided for. Although Meissner (1976), Meissner & Shora (1981) patented a system for liquid metal based gas cleaning, there has been no documented evidence to suggest that their idea was explored and further and put into actual practice.

3.3.2 Early Work – Gas Desulphurisation with Molten Tin

In the mid-1980s, the use of molten tin for sulphur removal was investigated by researchers in Germany, Schüermann (1984); Reitz (1985) and Hedden et al., (1986), and the latest investigation was done in 2003 by researchers in United Kingdom, Chang (2003).

✸ Schüermann (1984)

Schüermann (1984) showed that it is thermodynamically possible to remove H_2S with molten tin and then demonstrated it experimentally. The possibility of combining sulphur and dust removal in a spray scrubber was also suggested. The desulphurisation reaction is as follows:

$$Sn\ (l) + H_2S\ (g) \rightarrow SnS\ (s) + H_2\ (g) \qquad (3.7)$$

The reaction is an exothermic process. The enthalpy of reaction varies from -90.5 to -82.43 kJ/mol at temperatures 327 to 727℃. The equilibrium constant for the heterogeneous reaction 3.7 is independent of pressure as follows:

$$Kp = p_{H2}/p_{H2S} \qquad (3.8)$$

Figure 3.5 depicts the dependency of the Gibbs free energy change of reaction ΔG_R for reaction (3.7) on the temperature T for varying partial pressure ratio p_{H2}/p_{H2S}. ΔG_R tends towards a negative value as either the temperature or partial pressure ratio decreases, favouring reaction i.e. H_2S absorption.

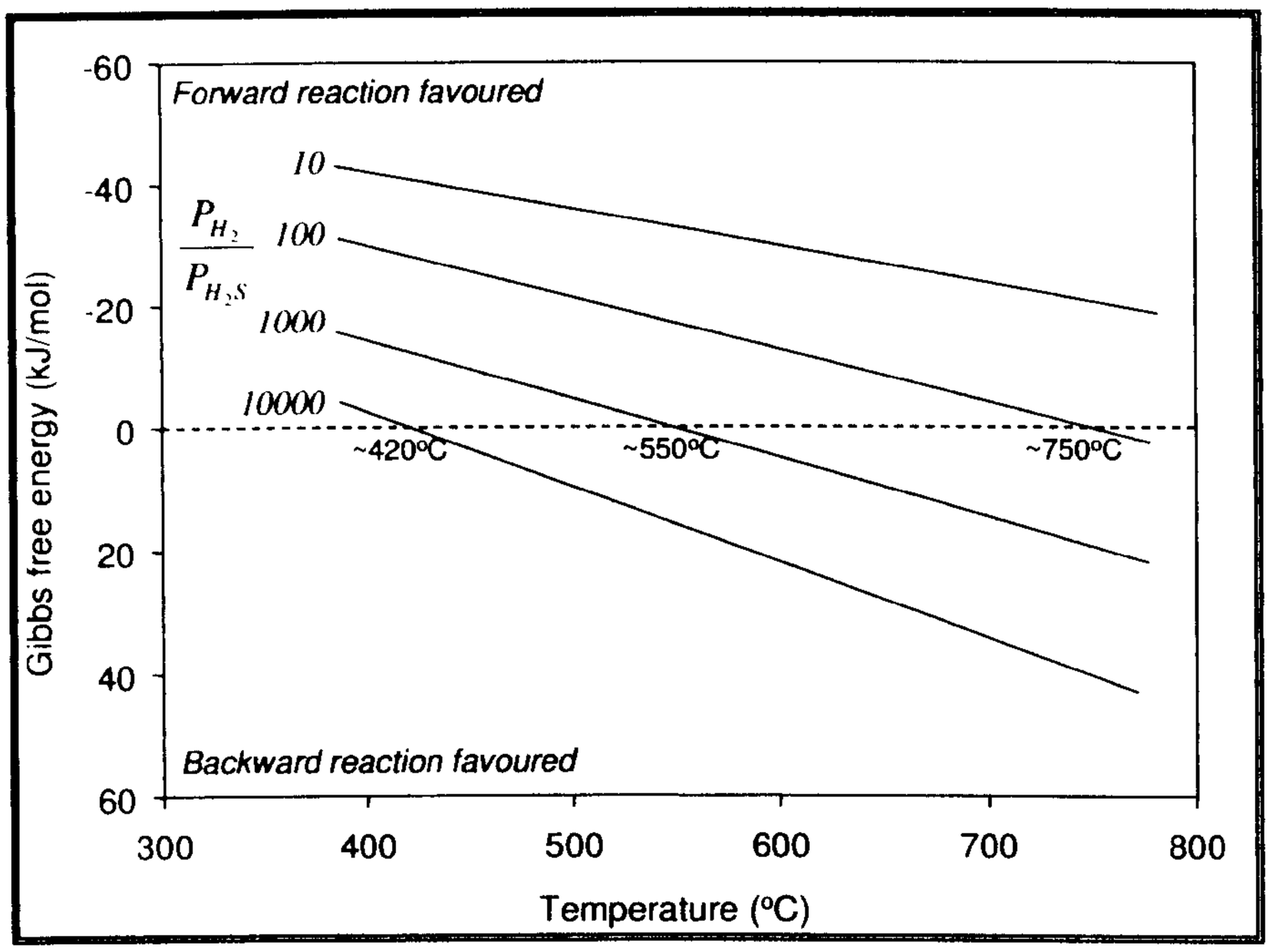

Figure 3.5: Variation of Gibbs free energy for the desulphurisation reaction of tin by H_2/H_2S ratio and temperature (Schürmann, 1984)

Conversely as either the temperature or partial pressure ratio increases, ΔG_R tends towards a positive value, favouring the reverse reaction i.e. SnS decomposition. Therefore either the H_2S absorption or SnS decomposition is favoured depending on the system temperature and gas composition. For a typical fuel gas composition of 30 vol. % H_2 and 0.5 vol. % H_2S, temperatures of less than 527℃ (800 K) have to be kept to achieve H_2S separation of greater than 90%.

A simple test was carried out to investigate the desulphurisation reaction 3.7. 1000 ppmv H_2S in N_2 gas was bubbled through a small amount of molten tin held in a gas washing bottle heated at constant temperature. It was found that as the temperature rose from 400 to 800℃ the degree of H_2S separation increased from approximately 60% to over 90%. According to Schüermann, the temperature dependence of the degree of H_2S separation could only be explained kinetically as complete conversion in all cases could be expected from thermodynamic balance. The kinetic hindrance was probably due to insufficient dispersion of gas bubbles through the molten tin at low temperatures. This problem could be avoided by the dispersion of tin to fine droplets providing a large area for interphase mass transfer.

In addition to sulphur removal, Schüermann also investigated separation of quartz dust and fly ash using liquid tin at pilot scale batch at temperatures about 400℃. Liquid tin was dispersed into droplets by spraying the melt through nozzles by means of compressed nitrogen. The molten tin spray was directed into the path of the dust-laden gas stream. Approximately 60% dust separation efficiency was reported achieved.

❋ **Reitz, (1985) and Hedden et al., (1986)**

Research at the University of Karlsruhe, Germany, Reitz, (1985) and Hedden et al., (1986) proposed the following liquid tin based desulphurisation and tin regeneration process of which reaction 3.9, 3.11 and 3.12 were investigated:

Desulphurisation	:	$2\ Sn\ (l) + 2\ H_2S \rightarrow 2\ SnS + 2\ H_2$	(3.9)
Roasting	:	$SnS + 2\ O_2 \rightarrow SnO_2 + SO_2$	(3.10)
Sulphur Production	:	$SnS + SO_2 \rightarrow SnO_2 + 2S$	(3.11)
Reduction	:	$2\ SnO_2 + 4\ H_2 \rightarrow 2\ Sn\ (l) + 4\ H_2O$	(3.12)
Overall Reaction	:	$2\ H_2S + 2\ H_2 + 2\ O_2 \rightarrow 4\ H_2O + 2\ S$	(3.13)

The bulk of experiment studies (Hedden et al., 1986) focused on the desulphurisation reaction (reaction 3.9) in a bubble column, stirred vessel and double-stirred cell reactors at temperatures ranging from 400 to 700℃ and at pressures higher than atmospheric. It was found that the increase in reaction temperature, surface renewal frequency (i.e. reactor impeller speed) or the residence time improved the degree of H_2S conversion. However, the degree of H_2S conversion dropped slightly with an increase in H_2S partial pressure. The presence of other gas components i.e. H_2, H_2O, CO and CO_2 in the gas mixture did not affect the degree of H_2S conversion with tin.

The authors concluded that the simple N_2/H_2S gas mixture would suffice as a simulation fuel gas to predict the desulphurisation of gases produced by coal gasification, with the exception of fuel gases with $H_2/\ H_2S$ ratios such that the equilibrium conversion of H_2S would be affected. From their investigation, Hedden et al. concluded that the reaction H_2S with liquid tin in the reactors was first-order with respect to the H_2S concentration at the chemically active interfacial area.

The effective interfacial area for reaction was found to be reduced by the formation of solid tin sulphide film on the liquid tin surface, preventing further sulphide formation and hindering desulphurisation. Hence, besides the system temperature and H_2S concentration, the desulphurisation reaction rate was also dependent on the interfacial area sulphur renewal frequency. The sulphur production reaction (3.11) was investigated (Hedden et al., 1986) in a fixed bed reactor at 500 to 800℃. It was found that some of the elemental sulphur produced from the reaction of SnS with SO_2 accumulated on the solid SnS/SnO_2 surface forming polysulphides (SnS_2, SnS_3). Additional heating of the solid to 800℃ in a N_2 stream was necessary for complete recovery of the accumulated sulphur. The reduction of SnO_2 (3.12) was effected by H_2 at 480℃ and CO at 540℃. A gas desulphurisation scheme was proposed by Hedden et al., (1986) based on the results obtained from the individual reaction steps. After pre-cleaning in a cyclone, simultaneous sulphur and fine dust removal from the hot fuel gas take place in a molten tin spray scrubber at 500℃ and 20 bars. The unreacted molten tin containing solid tin sulphide product and dust particles is removed from the scrubber, the solids scraped off and the cleaned tin is transport back to the scrubber. The separated solid tin sulphide, SnS is treated with O_2 and SO_2 in a rotary kiln at 800℃ to form tin oxide, SnO_2 and elementary sulphur. The tin oxide is reduced by purified fuel gas (H_2 or CO) in a second rotary kiln, regenerating molten tin. However, there is no reported evidence to suggest that the proposed process has actually been implemented. No subsequent documents were found on the progress of this process.

- **Chang et al., (2003)**

Small-scale gasification of petroleum coke samples was carried out in an electrically heated horizontal furnace using a steam/nitrogen mixture as the gasifying medium. Gasification was performed with and without the presence of tin. The amounts of H_2S sampled from the product gas steam in both occasions were compared. There was roughly 10 % reduction in the sampled H_2S upon tin addition. The reduction was small as any reaction involving the tin was limited by the small surface area of the tin available for contact with the gas stream. At a temperature of about 1000℃, the molten tin reacted with the product gas depositing a solid residue. However at a temperature in the region of 500℃ (could be lower due to possible lower gas phase temperature), the kinetics were too slow for similar reactions between the fuel gas and the molten tin to take place.

The solid residue was most likely a mixture of mainly SnO_2 from the reaction of molten tin with steam and CO_2 with a small fraction of SnS contributed by the reaction of molten tin with H_2S. These small-scale gasification studies provided actual confirmation and evidence of the possibility of sulphur removal by molten tin under gasification environment. Previous work by Chang (2003) presents the results of cold test studies conducted on a non-wetting flow packed bed scrubber and shows the application of these data to the design of a small scale molten tin irrigated high temperature scrubber. The system in the previous study incorporates a fixed bed rather than a moving-bed; nevertheless the results will be useful to the subsequent development of a moving packed bed scrubber. The objective of her research project was to perform studies on an analogous room temperature packed bed scrubber operating under non-wetting conditions, providing insight and understanding towards the development of a high temperature packed bed gas scrubber irrigated by molten tin. A series of cold tests on a Perspex model of the gas scrubber operating under non-wetting flow conditions analogous to liquid metal flow were conducted at University of Sheffield, United Kingdom. The results regarding the cold test studies have been well documented by Chang (2003).

3.3.3 Gas Desulphurisation with Gaseous Metallic Zinc

At the University of Birmingham, Warner (1997) proposed the removal of sulphur from fuel gases based on interaction between H_2S and COS with gaseous metallic zinc producing saleable, premium grade solid ZnS:

$$Zn\ (g) + H_2S\ (g) \rightarrow ZnS\ (s) + H_2\ (g) \qquad (3.14)$$

99% or greater H_2S and COS removal was claimed to be possible. The ZnS concentrate can either be treated on-site by direct smelting (i.e. The Warner Zinc Process) to recover the metallic zinc or it can be sold to a producer. The concentrate has a very small iron content compared to natural ZnS, hence making it an ideal feedstock for the electrolytic Zn industry which is facing heavy environmental pressures regarding the disposal of iron impurities (known as jarosite residues) from Zn concentrates. The leaching of these metal impurities into groundwater and the ecosystem is a matter of serious concern.

3.4 Current Proposal – Particulate Removal/Gas Desulphurisation with Molten Tin

This Chapter sets out the fundamental study of hot gas cleaning by molten tin undertaken during the course of this research project.

3.4.1 Selection of Liquid Metal System

Three possible liquid metal systems were identified (Warner, 2000; Warner, 2001). They were lead (Pb), bismuth-lead mixture (Bi-Pb) and tin (Sn). Lead is the most thermodynamically efficient among the three. It is relatively cheap and is inert to oxidation by fuel gas. Lead's melting point is 327℃. This can be lowered by adding Bi to form a 55.5% Bi – 44.5% Pb eutectic with a melting point of 27℃ which would make system start-up and prolonged stand-by both easier and less energy-intensive. The Bi-Pb is also not susceptible to oxidation by fuel gas. In this mixture, Bi acts as just an inert diluent and by itself it is least effective among the other options in sulphur removal. However, the use of either Pb or Bi-Pb is discouraged due to health hazards associated with in-plant exposure to lead as well as its emissions to the environment.

Lead is a cumulative poison (ASM, 1984). Excessive lead intake either from air, food or water can build up in the body, which leads to lead poisoning. Considering the health risks associated with lead, tin is the remaining choice of the liquid metal system. Tin and its inorganic compounds do not pose a health threat. Tin has a relatively low melting point of 232℃ and negligible vapour pressure at high temperature. This is a major advantage over lead, bismuth and zinc which have relatively high vapour pressure, hence they are easier to evaporate or sublime at high temperature causing massive metal loss. The vapour pressures of these metals are compared in Table 3.2, tin being the least volatile and zinc the most volatile. In addition, molten tin has relatively low viscosity, hence giving easy flow and easy dispersion into small droplets on the packing surface. Molten tin's viscosity is 1.41×10^{-3} kg/m.s at 400℃ as compared to that of water which is 1.13×10^{-3} kg/m.s at 15℃.

Table 3.2: Vapour pressure comparison *(ASM, 1981)*

Vapour Pressure (mm Hg)	Temperature (°C)			
	Tin	Lead	Bismuth	Zinc
10^{-4}	923	548	537	248
10^{-3}	1011	620	609	290
10^{-2}	1190	718	699	343
0.1	1271	821	721	405
760	2272	1745	1421	908
→	Increasing Volatility			

3.4.2 Gas Desulphurisation

Fuel gas is contacted counter currently with molten tin in a moving packed bed of ceramic spheres (typically 100 to 150 mm in diameter). Gas desulphurisation is effected through direct absorption of H_2S and COS in the fuel gas into molten tin:

$$H_2S + Sn \rightarrow SnS + H_2 \quad (3.15)$$

$$COS + Sn \rightarrow SnS + CO \quad (3.16)$$

The reaction should proceed unimpeded as long as the dissolved sulphur in the molten tin is maintained below the saturation level with respect to SnS. This prevents surface drossing by solid SnS formation which can hinder further reaction between the liquid tin and the sulphurous gases as well as to avoid accretion problems which can block the packed bed. This process differs from those employed by Schürmann (1984) and Hedden *et al.*, (1986) in which sulphur is removed as solid tin sulphide at unity activity. According to Warner (2000), it can be shown that the degree of sulphur removal when sulphur is removed as tin sulphide at unit activity is limited by thermodynamic constraints. Indications of this are the limited degree of sulphur removal at high temperature as noted by Schürmann (1984), and at high partial pressure ratio of H_2 to H_2S as identified by both Schürmann (1984) and Hedden *et al.*, (1986). These constraints are removed by maintaining a very low activity of dissolved sulphur in the molten tin, ensuring effective sulphur removal.

3.4.3 Particulate Removal

In addition to gas desulphurisation, simultaneous solid particulate removal is possible in the packed bed which acts as a depth filter. Molten tin having high surface energy exhibits non-wetting droplet and rivulet flow on the ceramic packing surface. The liquid tin droplets and rivulets act as capture sites for primary inertial deposition of solid particulates from the gas stream. A possible secondary entrapment method could be well provided by the naturally adhesive nature of ash and particles at elevated temperatures, promoting deposition and retention on the packing surface. This latter secondary transfer of particulates to sticky packings may be further enhanced with minor flux additions of suitable fused salts. The ability of the hot gas scrubber to function as a multicomponent clean-up device is advantageous as this reduces the number of required vessels and hence the capital cost of the overall gas cleaning system.

3.4.4 Liquid Metal Circulation and Packing Irrigation via Gas Lift

Concern over solid deposition and extensive accretion formation in a fixed bed dictates a moving bed configuration with external cleaning of solid packings. A gas lift is used for liquid metal circulation with the packing spheres in entrainment round the closed-loop system. Injection of a compressed inert gas provides the means to lift the spheres entrained in the liquid metal to the top of the packed bed. Provided that there is sufficient submergence relative to the required lift, this is a simple but reliable method for liquid metal circulation and packing transport.

3.4.5 Metal Recovery

The dissolved sulphur in the molten tin has to be kept below the saturation level with respect to tin sulphide to enable the desulphurisation reaction to proceed unimpeded. Continuous regeneration of metallic tin is thereby essential to maintain a sufficiently low tin sulphide activity in the melt so as to preserve the effectiveness of the molten tin for desulphurisation. Metallic tin is regenerated externally by continuous treatment of the sulphide tin with liquid metallic zinc to produce a saleable premium grade ZnS solid product that is readily stored and transported (Warner, 2000):

$$Zn + SnS \rightarrow ZnS + Sn \qquad (3.17)$$

Regeneration takes place in a fluidised bed where coarse ZnS product is grown on seeds of fine ZnS in fluidised state. These coarse granules can be readily separated from the liquid metal. For zinc recovery, the currently available option is to send the ZnS product to an electrolytic zinc producer (an already well-established industry) for treatment while in the longer term, direct smelting (The Warner Zinc Process) (Warner, 1997) may be adopted.

3.4.6 Effect of Other Constituents in Gasification Fuel Gas

The possibility of reaction between molten tin and typical fuel gas constituents apart from H_2S are considered as follows:

CO_2: Tin reacts with CO_2 at high temperatures according to the following reaction forming solid tin oxide (Hedges, 1960):

$$Sn + 2CO_2 \rightarrow SnO_2 + 2CO \qquad (3.18)$$

Using equal proportions of CO_2 and CO in the test gas, Nielsen and Sigurdardottir (1993) reported that the above equilibria was experimentally found to lie towards the right at a temperature range of 350 to 500℃. However, markedly higher CO concentration compared to CO_2 typical of actual gasifier fuel gas would suppress the forward reaction and the formation of SnO_2.

Steam: Molten tin reacts with steam according to the following reaction forming solid tin oxide (Hedges, 1960):

$$Sn + 2H_2O \rightarrow SnO_2 + 2H_2 \qquad (3.19)$$

The phase diagram depicting the above equilibria is shown in Figure 3.6. Either the H_2O/H_2 ratio in the fuel gas or the system operating temperature must be controlled in order to avoid the loss of tin as SnO_2.

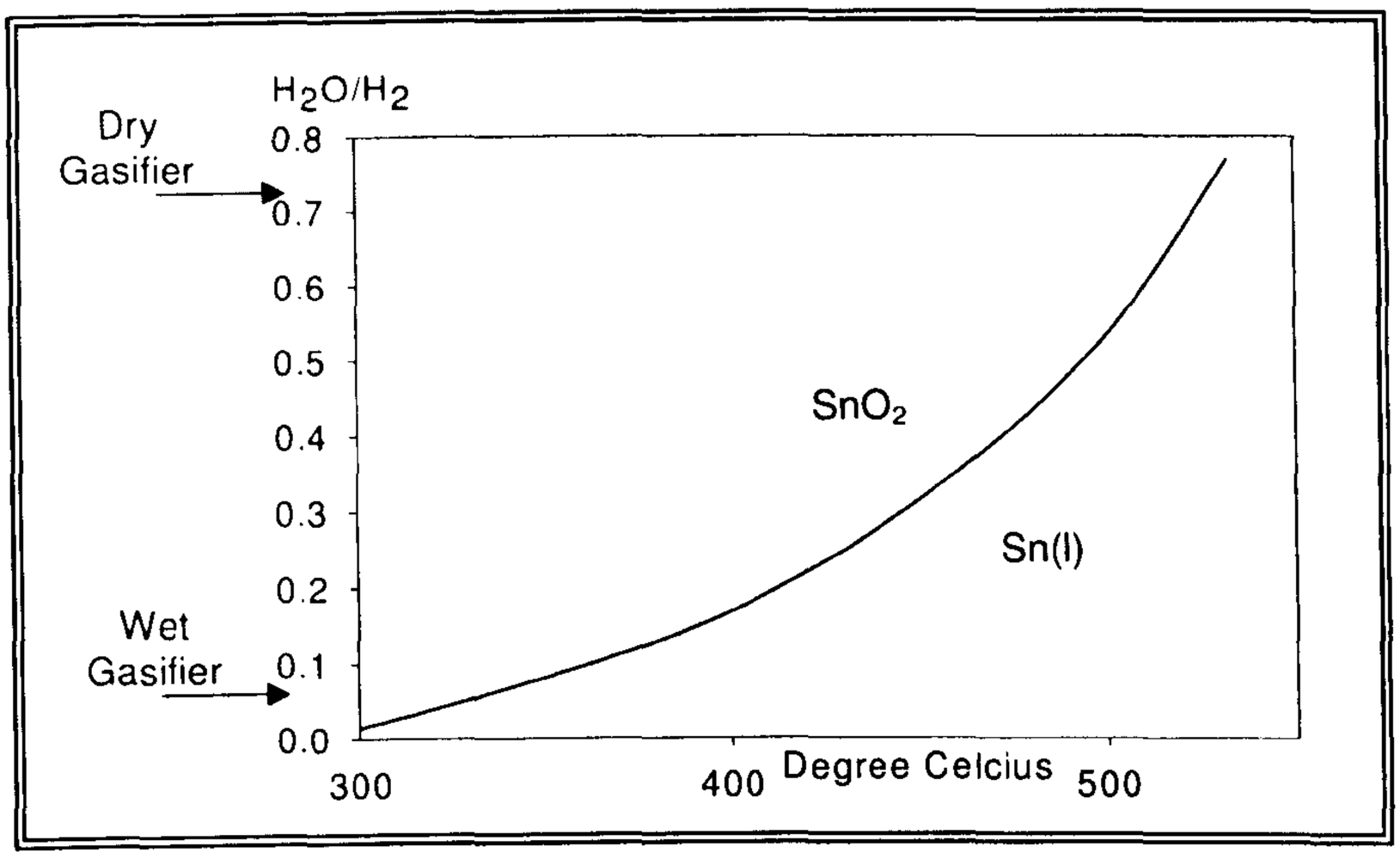

Figure 3.6: Phase diagram H_2O/H_2 molar ratio versus temperature (Nielsen and Sigurdardottir, 1993)

For wet gasifiers such as Texaco, the forward tin oxidation reaction is encouraged by the relatively high proportion of water vapour in the fuel gas relative to H_2. For these systems, the fuel gas temperatures must be kept above 500℃ in the presence of molten tin to avoid SnO_2 dross formation. On the other hand, for dry gasifiers such as Shell, the forward tin oxidation reaction will be suppressed by the low proportion of H_2O to H_2 in the fuel gas. This suggests that higher temperatures and a higher partial pressure ratio of H_2/H_2S shifts the reaction toward H_2S formation. Especially at high H_2/H_2S ratios or higher desulphurisation efficiencies, the dependence on temperature becomes very significant. At a typical H_2 concentration of 30%, for example, temperatures below 550℃ can reduce the H_2S concentration theoretically to 30 ppm (P_{H2}/P_{H2S} = 1000) if the SnS concentration is sufficient in the liquid tin. Therefore, it is essential to suppress the backward reaction by removing SnS in the tin introduced at the top of the counter flow reactor. The dissolved level of SnS can be minimised through the regeneration process using zinc presented in reaction 3.17.

N_2 Tin does not react directly with N_2 (Hedges, 1960)

H_2 Tin does not react directly with H_2 (Hedges, 1960)

NH_3 Tin does not react directly with NH_3 (Hedges, 1960)

HCl: Tin readily reacts with Cl_2 forming volatile $SnCl_4$ (Hedges, 1960)

Although there is no information regarding the reaction between tin with HCl i.e. the main form of chlorine in gasifier fuel gas, it is possible that the reaction, if any, may take the following form:

$$Sn + 4HCl \rightarrow SnCl_4 + 2H_2 \qquad (3.20)$$

However the very high H_2 to HCl ratio in the fuel gas would suppress the forward reaction, and therefore the reaction of HCl with molten tin is highly unlikely.

Trace heavy metals: Molten tin can potentially reduce arsenic, lead and mercury down to very low limits (Warner, 2001). It is worth noting that contrary to Hedges (1960) and Hedden et al., (1986) reported that the presence of H_2, H_2O, CO and CO_2 did not affect the degree of H_2S conversion with tin in tests conducted in a small scale reactor at 400 to 700℃.

3.5 Defining the Research Scope-Investigation of a Packed Bed Scrubber

A fresh and radical approach may provide the key to overcome the inherent limitations of current regenerable metal oxide sorbents employed in hot gas desulphurisation. Warner's (2000, 2001) proposed liquid metal scrubber is one such innovative way forward in hot gas cleaning, processing not only sulphur removal capability but the potential for particulate control as well. The aim of this research project is to perform studies of hot gas cleaning using a pilot unit of the high temperature gas scrubbing by liquid. Liquid tin introduced at the top of the packed bed disintegrates into discrete droplets and rivulets flowing downwards by gravity, countercurrently to an upward nitrogen gas flow. Laboratory hot experiments would concentrate on the particulate removal and gas absorption performance of the packed bed column. The regeneration of tin sulphide by metallic zinc is also of interest in this investigation. It is pointed out herein that the system in the current study incorporated a fixed bed rather than a moving bed as the proposed liquid metal scrubber. Accordingly, the gas lift studies are limited to liquid circulation and are not extended to packing transport. Nevertheless, the findings will undoubtedly be useful in advancing towards an actual moving packed bed scrubber.

CHAPTER FOUR

Packed Bed Wet Scrubber for Hot Fuel Gas Cleaning – Theory

This chapter reviews the fundamentals and theories governing the design and operation of the packed bed wet scrubber used in this project. The theory of packed columns regarding hot gas cleaning has been extensively reviewed by Chang (2003). The major parts of a packed column are first considered followed by the operation of the packed bed scrubber system along with important design criteria. The operating variables affecting wet scrubber operation are then explored, encompassing the pressure drop, liquid-to-gas ratio, gas velocity, as well as the collection efficiency of packed bed scrubbers for particles and gases.

4.1 Gas-Solid Separation (Particulate Cleaning)

The term gas-solid separation used herein refers to the removal of solid particles from a gas stream. Three main processes are involved in the separation of solid particles from a gas:

- Particle transport from the gas onto a collector surface and its retention on the collector
- Removal of the retained particles from the collector surface
- Solids disposal from the gas cleaning equipment

4.1.1 Particle Collection

Wet scrubbers capture relatively small dust particles with large liquid droplets. In most wet scrubbing systems, the droplets produced are generally larger than 50 μm (typically in the 150 to 500 μm). For example, particles produced by mechanical means (crush or grind) tend to be large (above 10 μm); whereas, particles produced from combustion or a chemical reaction will have a substantial portion of small (less than 5 μm) and sub μm -sized particles. The most critical sized particles are those in the 0.1 to 0.5 μm range because they are the most difficult for wet scrubbers to collect. The first phase of gas-solid separation during which solid particles carried by the gas stream are brought into contact with the collector surface is termed the 'collection' or 'capture' process. There are several mechanical collection processes as shown in Table 4.

Table 4: Particle collection mechanisms for wet scrubbing systems (EPA, 2007b)

Mechanism	Explanation
Impaction	Particles too large to follow gas streamlines around a droplet collide with it
Diffusion	Very tiny particles move randomly, colliding with droplets because they are confined in a limited space
Direct interception	An extension of the impaction mechanism. The centre of a particle follows the streamlines around the droplet, but a collision occurs if the distance between the particle and droplet is less than the radius of the particle
Electrostatic attraction	Particles and droplets become oppositely charged and attract each other
Condensation	When hot gas cools rapidly, particles in the gas stream can act as condensation nuclei and, as a result, become larger
Centrifugal force	The shape or curvature of a collector causes the gas stream to rotate in a spiral motion, throwing larger particles toward the wall
Gravity	Large particles moving slowly enough will fall from the gas stream and be collected.

- ***Impaction*** – In a wet scrubbing system, dust particles will tend to follow the streamlines of the exhaust stream. However, when liquid droplets are introduced into the exhaust stream, particles cannot always follow these streamlines as they diverge around the droplet (Figure 4.1). The particle's mass causes it to break away from the streamlines and impact or hit the droplet.

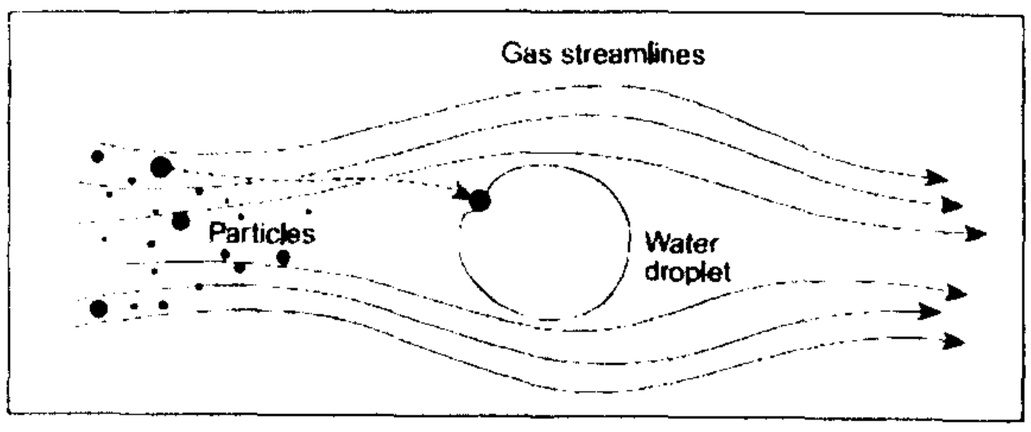

Figure 4.1: Impaction

Impaction increases as the diameter of the particle increases and as the relative velocity between the particle and droplets increases. As particles get larger they are less likely to follow the gas streamlines around droplets. Also, as particles move faster relative to the liquid droplet, there is a greater chance that the particle will hit a droplet. Impaction is the predominant collection mechanism for scrubbers having gas stream velocities greater than 0.3 m/s (Perry and Green, 1997). Most scrubbers do operate with gas stream velocities well above 0.3 m/s.

Therefore, at these velocities, particles having diameters greater than 1.0 µm are collected by this mechanism. Impaction also increases as the size of the liquid droplet decreases because the presence of more droplets within the vessel increases the possibility that particles will impact on the droplets.

- ***Diffusion*** – Very small particles (less than 0.1 µm in diameter) experience random movement in an exhaust stream. These particles are so tiny that they are bumped by gas molecules as they move in the exhaust stream. This bumping, or bombardment, causes them to first move one way and then another in a random manner, or to diffuse, through the gas. This irregular motion can cause the particles to collide with a droplet and be collected (Figure 4.2). Because of this, diffusion is the primary collection mechanism in wet scrubbers for particles smaller than 0.1 µm.

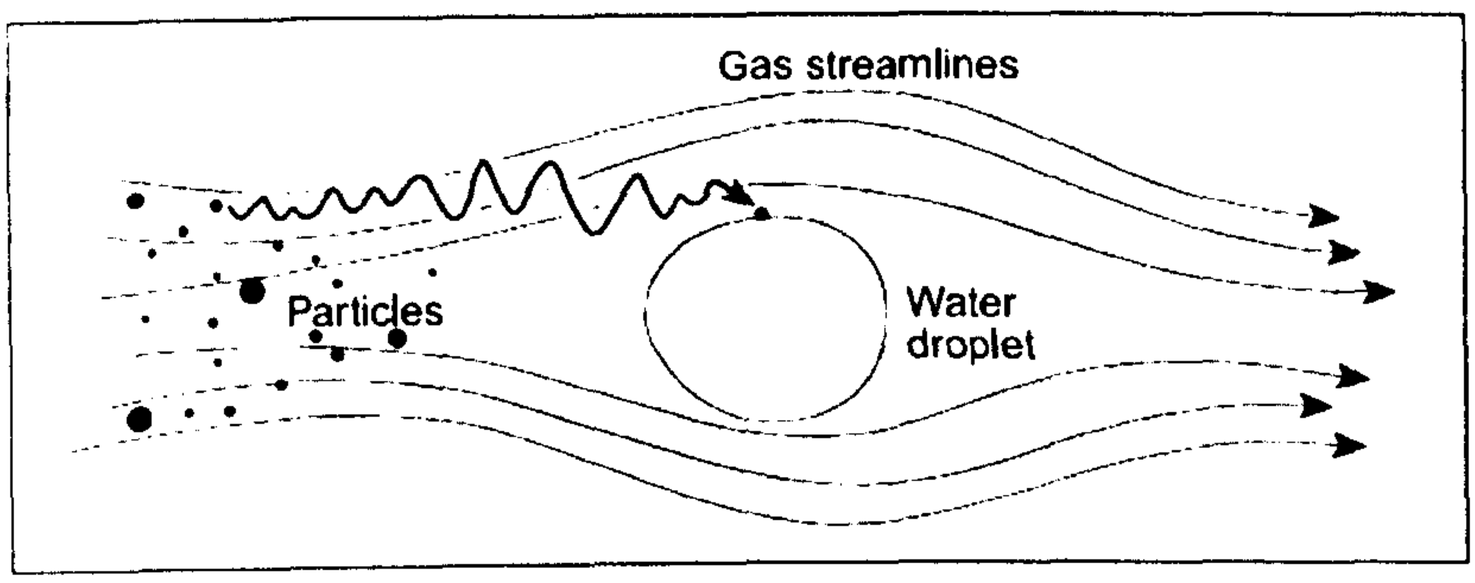

Figure 4.2: Diffusion

The rate of diffusion depends on the following:

- The relative velocity between the particle and droplet
- The particle diameter
- The liquid-droplet diameter.

For both impaction and diffusion, collection efficiency increases with an increase in relative velocity (liquid- or gas-pressure input) and a decrease in liquid-droplet size. However, collection by diffusion increases as particle size decreases. This mechanism enables certain scrubbers to effectively remove the very tiny particles (less than 0.1 µm). In the particle size range of approximately 0.1 to 1.0 µm, neither of these two collection mechanisms (impaction or diffusion) dominates.

* ***Other Collection Mechanisms*** – In recent years, some scrubber manufacturers have utilised other collection mechanisms such as electrostatic attraction and condensation to enhance particle collection without increasing power consumption. In electrostatic attraction, particles are captured by first inducing a charge on them. Then, the charged particles are either attracted to each other, forming larger, easier-to-collect particles, or they are collected on a surface. Condensation of water vapour on particles promotes collection by adding mass to the particles. Other mechanisms such as gravity, centrifugal force, and direct interception slightly affect particle collection.

4.1.2 Particle Rebound or Retention

The 'capture' by the aforementioned mechanisms for a dust particle on the collector surface is not the only deciding factor in ensuring its removal from the gas stream. A dust particle that collides with the collector surface may either rebound and re-entrain back into the gas stream or alternatively it will be retained and thereby removed from the gas. As a result, dust retention is always less than dust collection. Whether particle 'rebound' or 'retention' takes place depends on the relative strengths of the energy of the impacting particle and the detachment energy required to separate the particles from the collector surface (Coury et al., 1987). The total energy of the impacting particles is a summation of its kinetic energy (includes effects due to long-range electrostatic force and fluid drag force) and energy due to short-range Van der Waals forces.

The detachment energy arises from adhesion forces due to Van der Waals interaction, electrostatic and surface tension capillary effects that tend to hold the dust particle against the collector surface, all of which are dependent on the properties of the collector surface and the dust particle itself. Therefore any effects that tend to raise the detachment energy or lower the particle's approaching energy will favour adhesion upon impact. An example of the latter is plastic deformation on collision due to the presence of liquid or adsorbed/condensed films or soft layers on either the dust or collector surface that dissipates that particle's energy. In addition, although capture due to inertial impaction increases as particle inertia increases, the tendency for rebound increases as well and this may eventually dominate.

4.1.3 Separation Efficiency

Consider the following gas-solid separator:

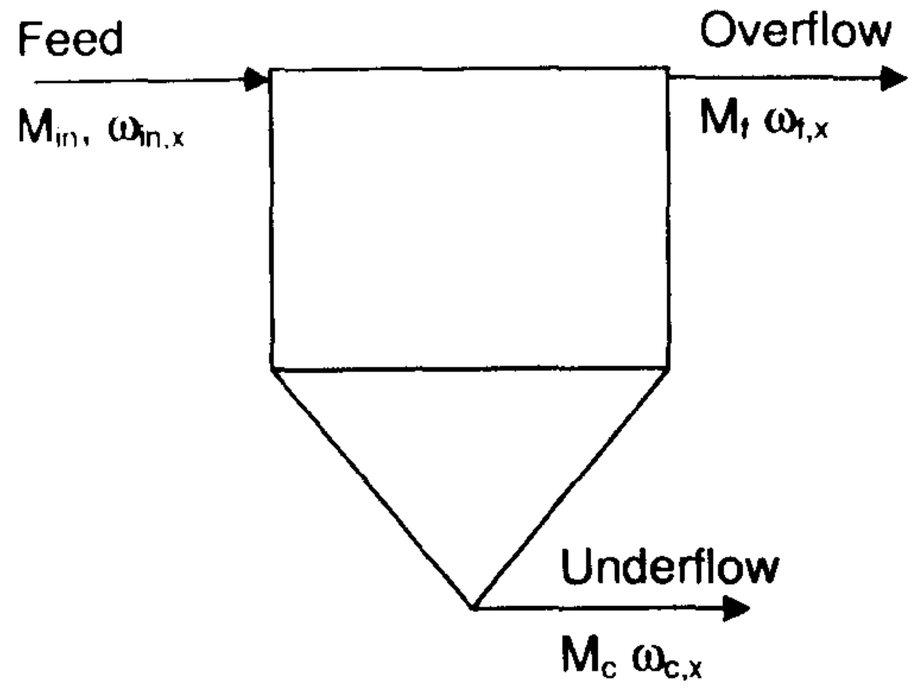

M_{in} = mass flowrate of feed dust (kg/s)
M_c = mass flowrate of coarse (separated) dust in underflow (kg/s)
M_f = mass flowrate of fine (unseparated) dust in overflow (kg/s)
$\omega_{in,x}$ = mass fraction of feed dust at particle size x (kg/kg)
$\omega_{c,x}$ = mass fraction of coarse (separated) dust at particle size x (kg/kg)
$\omega_{f,x}$ = mass fraction of fine (unseparated) dust at particle size x (kg/kg)
x = dust particle size (μm)

Figure 4.3: Schematic diagram of a gas-solid separator

Provided no dust particle accumulation occurs within the separator, the total mass balance is:

$$M_{in} = M_c + M_f \tag{4.1}$$

The mass balance in equally applicable for each particle size x present in the feed, as long as there is no change in solid particle size within the separator i.e. no agglomeration or comminution:

$$M_{in,x} = M_{c,x} + M_{f,x} \tag{4.2}$$

The total mass flowrate of a sample (M) multiplied by the particle size distribution frequency i.e. the mass fraction of particles of size x in the sample (ω_x) gives the total mass flowrate of particles of size x for the samples (M_x). Therefore equation 4.2 becomes:

$$(M_{in})(\omega_{in,x}) = (M_c)(\omega_{c,x}) + (M_f)(\omega_{f,x}) \tag{4.3}$$

4.1.3.1 Total Efficiency, E_T and Number of Transfer Units, N_t

The total or overall efficiency E_T is defined as the ratio of mass of all particles separated to the total mass of solid fed into the separator. Hence

$$E_T = \frac{M_c}{M_{in}} \quad \text{or} \quad E_T = 1 - \frac{M_f}{M_{in}} \tag{4.4}$$

Therefore equation 4.3 can be re-expressed as:

$$\omega_{in,x} = E_T(\omega_{c,x}) + (1 - E_T)(\omega_{f,x}) \tag{4.5}$$

The total efficiency E_T is largely dependent on the size distribution of the feed material and hence is unsuitable as a general criterion of efficiency for gas-solid separation equipment. Efficiency is generally an exponential function of the process variables for most types of collecting devices and therefore is an insensitive function for correlation purpose in the high efficiency range. In this case, the penetration (1-E_T) is generally preferable. Even better is the number of transfer units N_t:

$$N_t = \ln\left(\frac{1}{1 - E_T}\right) \quad \text{(Chang, 2003)} \tag{4.6}$$

$$E_T = 1 - \exp(-N_t) \quad \text{(Chang, 2003)} \tag{4.7}$$

4.1.3.2 Grade Efficiency, G(x)

Generally for most gas-solid separators, the separation efficiency is dependent on particle size, which brings about the application of grade efficiency G(x). The gravimetric grade efficiency G(x) is defined as the mass separation efficiency for specific particle size x:

$$G(x) = \frac{M_{c,x}}{M_{in,x}} \tag{4.8}$$

Using the same argument as that in obtaining equation 4.3

$$G(x) = \frac{(M_c)(\omega_{c,x})}{(M_{in})(\omega_{in,x})} \tag{4.9}$$

From the definition of total efficiency E_T from equation 4.4:

$$G(x) = E_T\left(\frac{\omega_{c,x}}{\omega_{in,x}}\right) \tag{4.10}$$

❋ Grade Efficiency Curve

A typical grade efficiency curve with the grade efficiency function G(x) plotted against particle size x is shown in Figure 4.4. The grade efficiency curve is usually independent of solids size distribution and density and is constant for a specific set of operating conditions. It gives the probability at which particles of any given size in the gas stream will separate from or be retained within the gas stream. The grade efficiency G(x) generally increases from zero for ultra-fine particles to 100 % for coarse particles. The grade efficiency concept is generally applicable to solid-gas separation equipment whose performance does not vary with time if all operational variables are kept constant. Examples of such equipment are cyclones and scrubbers. The grade efficiency when integrated over the particle size distribution gives the total collection efficiency E_T.

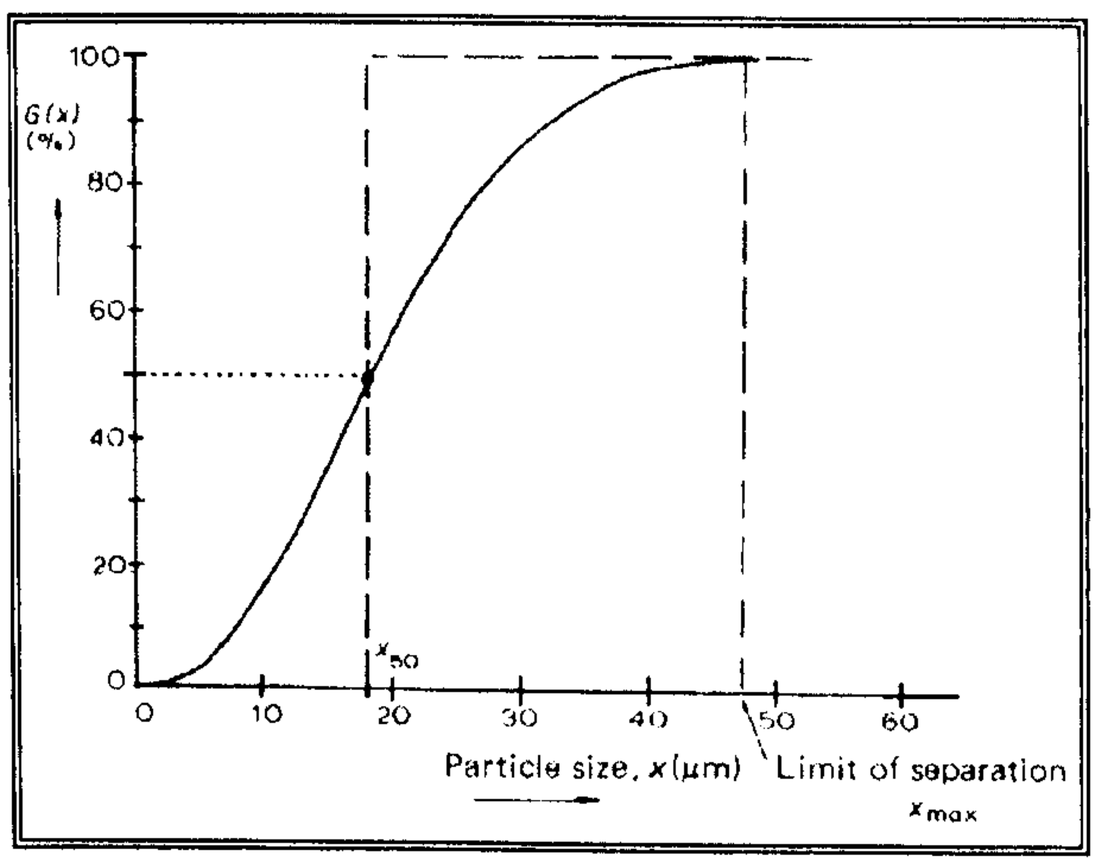

Figure 4.4: A typical grade efficiency curve (Svarovsky, 1981)

❋ Cut Size, x_{50}

The particle size corresponding to 50 % probability of separation on the grade efficiency curve is termed the 'equiprobable size' x_{50} and is usually taken as the 'cut size' of the gas-solid separator. The cut size can be viewed as the equivalent aperture size of an ideal screen that would result in the same separation performance as the gas-solid separator in question. It is taken as the most significant single parameter to describe both the difficulty of dust separation and the performance of the scrubber.

❋ Limit of Separation, X_{max}

The 'limit of separation', X_{max} is defined as the particle size above which the grade efficiency is 100 % for all x. This is the size of the largest particles that can escape with the overflow gas stream. However, the limit of separation is often difficult to ascertain accurately. In this case, an easier defined point termed the 'approximate limit of separation', x_{98} (Chang, 2003); (Svarovsky, 1981), which is the size corresponding to 98 % efficiency, is then measured and used.

4.1.3.3 Factors Affecting Separation Efficiency

The grade efficiency curve is a function of the following factors:

- Gas flowrate
- Gas viscosity
- Solids density
- Solid particle shape
- Gas moisture content (affects dispersion of particles in the gas)
- Solids feed concentration (large influence at higher concentrations)
- Specific water consumption (for wet scrubbers)

4.1.3.4 Packed Bed Scrubber

The scrubber of interest herein is the massive packing scrubber (or simply called the packed bed scrubber in this study) i.e. columns packed with various packing elements usually used for mass transfer. The packing breaks down the liquid flow into a film with high surface area. Packing elements are generally too large to serve as effective collectors except for very large dust particles. In the collection of fine particles, the packings serve mainly to promote fluid turbulence, enhancing particle deposition on liquid films or droplets.

The main collection mechanism is inertial deposition, with some contribution from diffusion for sufficiently small dust particles. Packed bed scrubbers are efficient for separating particles of 10 μm or larger (Strigle, 1994). Smaller packing gives better scrubber efficiencies. Unlike in mass transfer, packing shape is relatively unimportant for gas-solid separation; hence minimal pressure drop is the main selection criterion. Packing elements are subject to plugging, but are removable for cleaning.

At high solid loadings, large packing elements should be used to prevent blockage by the solids; higher liquid rates should also be employed to flush off the deposited solids. In a countercurrent packed bed scrubber, the power supply to the system (as reflected in the bed pressure drop) is limited by flooding of the column, hence restricting the achievable separation efficiency.

4.2 Gas Cleaning (Absorption)

In packed tower or wet-film scrubbers, liquid is sprayed or poured over packing material contained between support trays. A liquid film coats the packing through which the exhaust gas stream is forced. Pollutants are collected as they pass through the packing, contacting the liquid film. Therefore, both gas and liquid phases provide energy for the gas-liquid contact. A wet-film scrubber uses packing to provide a large contact area between the gas and liquid phases, turbulent mixing of the phases, and sufficient residence time for the exhaust gas to contact the liquid. These conditions are ideal for gas absorption. Large contact area and good mixing are also good for particle collection; however, once collected, the particles tend to accumulate and plug the packing bed. The exhaust gas is forced to make many changes in direction as it winds through the openings of the packed material. Large particles unable to follow the streamlines hit the packing and are collected in the liquid. As this liquid drains through the packing bed, the collected particles may accumulate, thus plugging the void spaces in the packed bed. Therefore, wet-film scrubbers are not used when particle removal is the only concern.

For gas absorption, packed scrubbers are the most commonly used devices. The wet film covering the packing enhances gas absorption several ways by providing:

- A large surface area for gas-liquid contact
- Turbulent contact (good mixing) between the two phases
- Long residence time and repetitive contact

Because of these features, packed towers are capable of achieving high removal efficiencies for many different gaseous pollutants. Numerous operating variables affect absorption efficiency. Of primary importance is the solubility of the gaseous pollutants. Pollutants that are readily soluble in the scrubbing liquid can be easily removed under a variety of operating conditions. Some other important operating variables are discussed below.

- ***Gas velocity*** - The rate of exhaust gas flow from the process determines the scrubber size to be used. The scrubber should be designed so that the gas velocity through it will promote good mixing between the gas and liquid phases. However, the velocity should not be fast enough to cause flooding.

- ***Liquid-injection rate*** - Generally, removal efficiency is increased by an increase in the liquid-injection rate to the vessel. The amount of liquid that can be injected is limited by the dimensions of the scrubber. Increasing liquid-injection rates will also increase the operating costs. The optimum amount of liquid injected is based on the exhaust gas flow rate.

- ***Packing size*** - Smaller packing sizes offer a larger surface area, thus enhancing absorption. However, smaller packing fits more tightly, which decreases the open area between packing, thus increasing the pressure drop across the packing bed.

- ***Packing height*** - As packing height increases, total surface area and residence time increase, enhancing absorption. However, more packing necessitates a larger absorption system, which increases capital cost.

4.2.1 Absorption Equipment

Gas absorbers and reactive scrubbers are flexible devices that are very dependable and effective. Figure 4.5 shows examples of the variety of commercial equipment used for gas absorption with or without chemical reaction. The selection of the particular scrubber configuration required for a given control problem is not simple. Almost any type of scrubber will be effective if the pollutants are easily absorbed. In these cases, local costs and availability dictate the type of scrubber.

4.2.2 Packed Tower

Packed bed are used for continuous, counter current or co-current contact of liquid and gases in absorption operations. A counter current packed bed usually consists of a cylindrical column equipped with gas inlet and distributing space at the bottom, while a liquid inlet and distributor at the top, and liquid and gas outlet at the bottom and top, respectively. The column is packed with inert solids called packing which provide relatively large surface area per unit volume. In order to be useful, absorption packing should have large efficiency area, low mass, strong materials of construction, large free cross section when dumped, chemical inertness, small liquid hold-up, and low cost. There are many types of packing; some of them are made of coke, wood, rocks, ceramics, metals, or plastics.

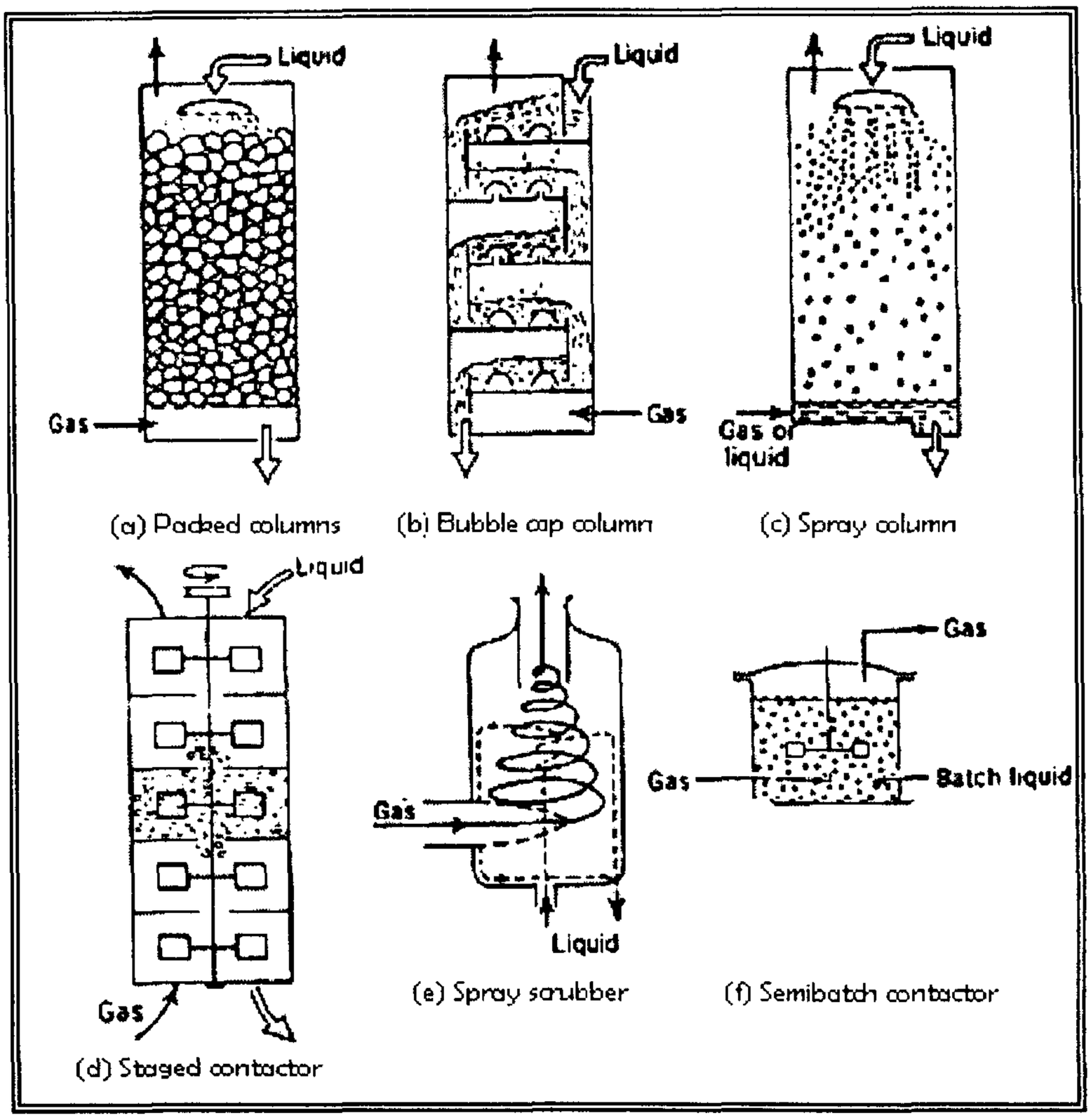

Figure 4.5: Equipment used commercially for gas absorption (McCabe et al., 1993)

4.2.3 Gas-Liquid Equilibrium Considerations

Under a specific condition of temperature and pressure in a gas absorption operation, the solute molecules are transferred from the gas phase to the liquid phase across the gas-liquid interfacial surface. Some solute molecules escape back into the gas phase, the rate being proportional to their concentration in the liquid. As the concentration of the solute in the liquid increases, its rate of return to the gas phase increases as well. In due course, the rate at which the solute enters the liquid equals its rate of return to the gas phase. Simultaneously, each phase achieves uniform concentration through diffusion. A dynamic equilibrium is achieved whereby the net transfer of solute between the phases is zero and the concentration in each phase becomes constant. Hence for a gas-liquid system not in equilibrium, interphase diffusion of the components will take place to eventually bring the system to an equilibrium state. At equilibrium, no net diffusion of components exists between the phases. For ideal solutions, the gas-liquid equilibrium is described by Raoult's Law (McCabe et al., 1993):

$$p_A^* = p_A^o x_A \tag{4.11}$$

Where p_A^* = Equilibrium partial pressure of component A in gas phase (Pa)
p_A^o = Vapour pressure of pure A at the same temperature and pressure (Pa)
x_A = Mole fraction of component A in liquid phase (mol/mol)

Raoult's Law is generally true only for large values of x_A. For slightly soluble gases forming low concentrations of solute in the liquid phase (low x_A) i.e. resulting in only simple solutions with negligible gas-liquid molecules interaction, Henry's Law applies: (McCabe et al., 1993)

$$p_A^* = H\ x_A \tag{4.12}$$

Where H = Henry's Law constant (Pa)

The value of H increases with liquid phase temperature but is relatively independent of pressure. Henry's Law generally describes the equilibrium relationship for dilute concentration of most gases. The partial pressure of component A in the gas phase is proportional to its concentration (McCabe et al., 1993):

$$p_A = y_A P \tag{4.13}$$

Where y_A = Mole fraction of component A in gas phase (mol/mol)
P = Total pressure (Pa)

Combining equations 4.12 and 4.13, the gas phase mole fraction at equilibrium with the liquid phase y^* is:

$$y^* = \frac{p_A^*}{P} = \frac{H\ x_A}{P} \tag{4.14}$$

Absorption will take place as long as the solute partial pressure in the gas phase p_A is higher than the solute vapour pressure above the liquid phase p_A^*. Another way to describe vapour-liquid equilibrium is by the use of the vapour-liquid equilibrium constant, K or alternatively m (McCabe et al., 1993):

$$y_A^* = m\ x_A \tag{4.15}$$

4.2.4 Physical Absorption

4.2.4.1 Mass Transfer Across A Phase Boundary

Several theories have been put forward to describe the conditions at the phase boundary during mass transfer of a solute from the gas phase to the liquid phase. Whitman (1923) put forward the Two-Film Theory treating the mass transfer resistance in each phase as a thin film next to the interface. Steady-state molecular diffusion mass transfer occurs across these films whilst bulk fluid turbulence dies out at the interface. Higbie (1935) propounded the Penetration Theory which assumes that fluid eddies bring fresh materials to the interface and unsteady-state molecular mass transfer into the eddies takes place for a fixed period of time at the freshly exposed surface before the next mixing starts again. Danckwerts (1951) extended the Penetration Theory, resulting in the Surface-Renewal Theory. Whereas the former assumes the same exposure times and averages the varying degrees of penetrations. Toor and Marchello (1958) described the Film-Penetration Theory in which the Film and Penetration Theories were shown to be limiting cases of this more general model.

4.2.4.2 The Two-Film Theory

The Two-Film Theory by Whitman (1923) is extensively used as it gives expressions that are easily applicable to generally available experimental data. In a gas absorption process, the Two-Film Theory assumes that the bulk gas phase is separated from the bulk liquid phase by a thin gas film adjacent to a thin liquid film. Completely mixed turbulent flow exists in both the bulk gas and the bulk liquid phase. Mass transport is by convection currents such that no concentration gradient is present in the bulk phases. The convection currents die out in the vicinity of the thin fluid films. Laminar flow exists in both the gas and liquid films and a solute concentration gradient exists across both films. Resistance to mass transfer is considered to entirely lie in these two films in which mass transport is totally by molecule diffusion. The solute concentration in the gas film at the interface is at equilibrium with the solute concentration in the liquid film at the interface. No resistance to mass transfer exists across the interface. Figure 4.6 illustrates the Two-Film Theory. Solute ***A*** diffuses from the gas phase to the liquid phase. The partial pressure of solute ***A*** in the main body of the gas is p_A and this falls to p_{Ai} at the gas-liquid interface.

Similarly, the solute concentration in the liquid phase falls from C_{Al} at the interface to C_A in the main bulk liquid. The broken lines in the figure represent the hypothetical concentration gradients. The effective film thicknesses are given by z_G (gas film) and z_L (liquid film) respectively. p_{Ai} and C_{Ai} are equilibrium values, given by the system's gas-liquid equilibrium relationship.

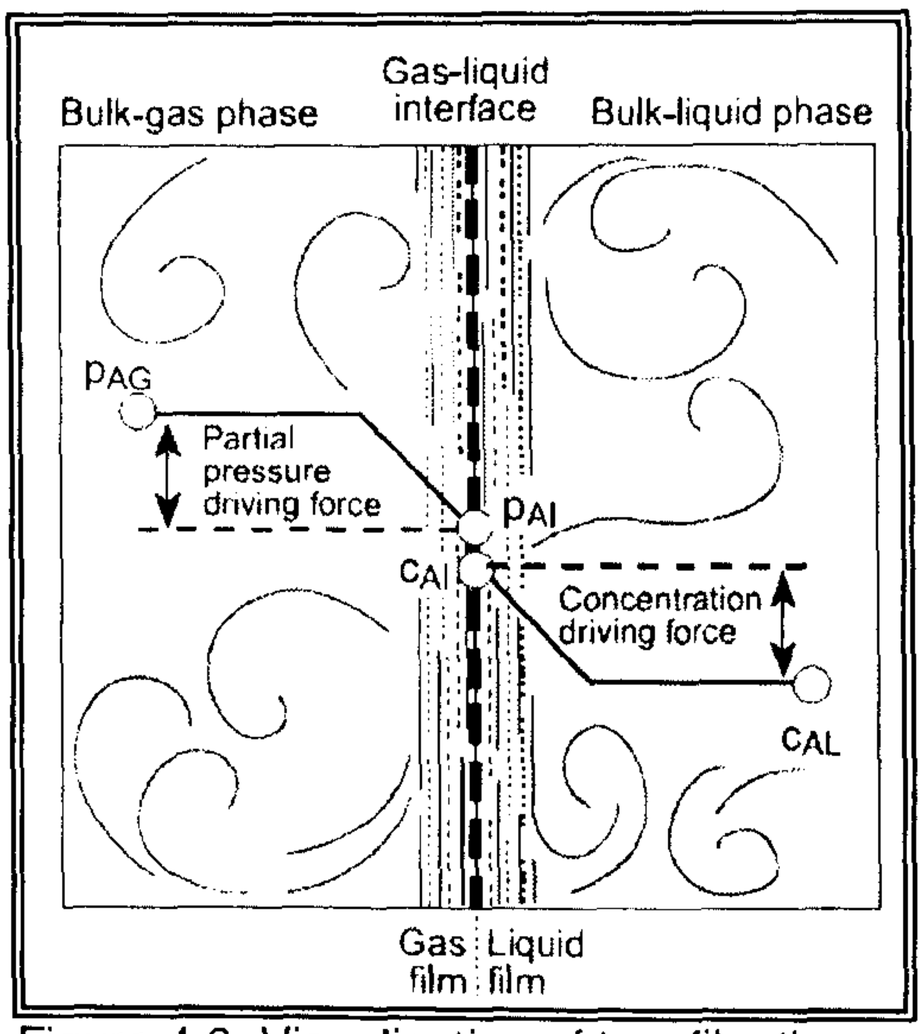

Figure 4.6: Visualisation of two-film theory (EPA, 2007a)

The rate of mass transfer of solute A from the bulk gas phase through the gas film to the interface is expressed as (McCabe et al., 1993):

$$N_A = k_G(p_A - p_{Ai}) \tag{4.16}$$

Where N_A = Total molar flux of substance A (kmol/m^{2}s)
k_G = Gas film mass transfer coefficient (kmol/m^{2}sPa)
p_A = Partial pressure of substance A in bulk gas phase (Pa)
p_{Ai} = Partial pressure of substance A at interface (Pa)

Similar, solute ***A*** is transported from the interface through the liquid film to the bulk liquid phase as follows (McCabe et al., 1993):

$$N_A = k_L(C_{Ai} - C_A) \tag{4.17}$$

Where N_A = Total molar flux of substance A (kmol/m^{2}s)
k_L = Liquid film mass transfer coefficient (m/s)
C_A = Concentration of substance A in bulk liquid phase (kmol/m^3)
C_{Al} = Concentration of substance A at interface (kmol/m^3)

For steady-state mass transfer process, there is neither accumulation nor depletion of ***A*** at the interface. This means that the rate at which solute ***A*** diffuses from the bulk gas phase to the interface equals the rate at which it diffuses from the interface to the main body of the liquid phase. Hence (McCabe et al., 1993),

$$N_A = k_G(p_A - p_{Ai}) = k_L(C_{Ai} - C_A) \tag{4.18}$$

$$\frac{k_L}{k_G} = \frac{(p_A - p_{Ai})}{(C_{Ai} - C_A)} \tag{4.19}$$

For dilute liquid concentration, $k_L = \frac{D_L}{z_L}$ (4.20)

Where D_L = Liquid phase diffusivity (m^2/s)
z_L = Liquid film thickness (m)

4.2.4.3 Overall and Film Mass Transfer Coefficients

In most experimental determinations of mass transfer rate, it is not ordinarily possible to obtain direct measurements of the interface concentrations and hence the film mass transfer coefficients (k_G, k_L). Instead the resulting rates of mass transfer can be expressed in terms of overall mass transfer coefficients which can be derived from solute concentrations in the bulk fluids (McCabe et al., 1993):

$$N_A = K_G(p_A - p_A^*) = K_L(C_A^* - C_A) \tag{4.21}$$

Where K_G = Overall gas phase mass transfer coefficient ($kmol/m^2sPa$)
K_L = Overall liquid phase mass transfer coefficient (m/s)
p_A^* = Partial pressure of A in equilibrium with concentration c_A in liquid phase (P_a)
C_A^* = Concentration of A in liquid phase in equilibrium with partial pressure c_a in gas phase ($kmol/m^3$)

For dilute solutions, Henry's Law applies (H in $Pa.m^3/kmol$) (McCabe et al., 1993):

$$p_A^* = H\ C_A \tag{4.22}$$

It can be shown that when the solution obeys Henry's Law, the relationship between the overall mass transfer coefficients with the film coefficients is in the form of additional resistance as follows (McCabe et al., 1993):

$$\frac{1}{K_G} = \frac{1}{k_G} + \frac{H}{k_L} \tag{4.23}$$

and

$$\frac{1}{K_G} = \frac{H}{K_L} \tag{4.24}$$

For equations 4.23 and 4.24 to be valid, there must be no variation in H over the equilibrium. There has to be negligible interfacial resistance and the two film coefficients must be independent of one another.

The mass transfer equations can be expressed in terms of mol fractions as follows assuming that the total concentrations in the liquid phase remain constant:

$$N_A = k'_G(y_A - y_{Ai}) = K'_G(y_A - y^*_A) \quad (4.25)$$

$$N_A = k'_L(x_{Ai} - x_A) = K'_L(x^*_A - x_A) \quad (4.26)$$

Where x_A, y_A = Mol fraction of soluble component A in liquid and gas phase respectively (mol/mol)

x_A^*, y_A^* = Equilibrium mol fraction (mol/mol)

k'_G, k'_L, K'_G, K'_L = Mass transfer coefficients in terms of mol fractions (kmol/m^{2}s)

If the equilibrium curves relating the solute concentration in the gas phase to the solute concentration in the liquid phase at equilibrium has a slope ***m*** (mol/mol), then:

$$\frac{1}{K'_G} = \frac{1}{k'_G} + \frac{m}{k'_L} \quad (4.27)$$

$$\frac{1}{K'_L} = \frac{1}{k'_L} + \frac{1}{m\,k'_G} \quad (4.28)$$

and

$$\frac{1}{K'_G} = \frac{m}{K'_L} \quad (4.29)$$

The relationship between the mass transfer resistances are as follows:

$$\frac{\text{Resistance in gas film}}{\text{Total resistance, both, film}} = \frac{1/k_G}{1/K_G} = \frac{1/k'_G}{1/K'_G} \quad (4.30)$$

$$\frac{\text{Resistance in liquid film}}{\text{Total resistance, both, film}} = \frac{1/k_L}{1/K_L} = \frac{1/k'_L}{1/K'_L} \quad (4.31)$$

4.2.4.4 Gas Film or Liquid Film Controlled Processes

If ***m*** is small such that at equilibrium only a small solute concentration in the gas will provide a very large solute concentration in the liquid (i.e. very soluble solute in liquid), the liquid film resistance m/k'_L in equation 4.27 becomes minor compared to or with that of the gas film $1/k'_G$. The rate of mass transfer is said to be gas film controlled. In the extreme,

$$1/K'_G = 1/k'_G \quad (4.32)$$

or $$(y_A - y^*_A) \approx (y_A - y_{Ai}) \quad (4.33)$$

In this case, the mass transfer rate is best improved by reducing the gas film resistance as fairly large changes in k'_L will not affect k'_G significantly. Conversely, where values of m are large (i.e. solute relatively insoluble in the liquid), the gas film resistance $1/mk'_G$ in equation 4.28 becomes negligible relative to that of the liquid film $1/k'_L$. The rate of mass transfer is then considered to be liquid film controlled. Ultimately,

$$1/K'_L \approx 1/k'_L \quad (4.34)$$

$$(x^*_A - x_A) \approx (x_{Ai} - x_A) \quad (4.35)$$

Under such conditions, the rate of mass transfer is best improved by reducing the liquid film resistance, i.e. increasing k'_L.

4.2.4.5 The Transfer Unit in Gas Absorption

It is necessary to account for changes in the gas-liquid interfacial area which is not normally directly measured in mass transfer experiments. The interfacial area is allowed for by the use of the volumetric coefficients K'_Ga, K'_La, k'_Ga and k'_La (kmol/m^{3}s) where 'a' is the interfacial area per unit volume of column (m^2/m^3). Figure 4.7 illustrates a gas absorption column through which the gas flows through the column at a flowrate of G' (kmol/m^{2}s) countercurrently to the down flowing liquid at a flowrate of L' (kmol/m^{2}s). It is assumed herein that the amount of solute transferred is small, hence only dilute solutions are formed and concentration changes in the column are small. This is such that K'_Ga, as well as the gas and liquid molar flowrates G' and L' are constant throughout the column. With these assumptions, the height of the packed bed Z (m) required to provide a change in gas concentration from y_B (mol/mol) at the bottom to y_T (mol/mol) at the top is given by:

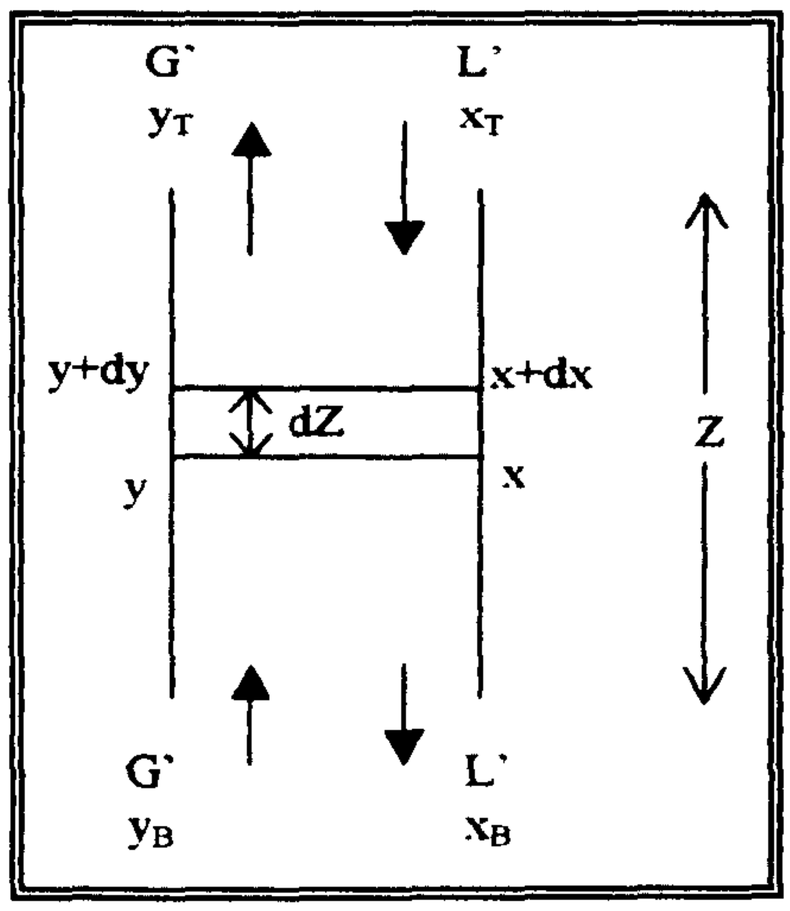

Figure 4.7: Countercurrent gas absorption column

$$\int_0^Z dZ = Z = H_{OG} \times N_{OG} = \left(\frac{G}{K_G a}\right)\left(\int_{y_B}^{y_T} \frac{dy}{y^* - y}\right) \qquad (4.36)$$

The concept of the transfer unit was first put forward by Chilton and Colburn (1934). Similar equations can be written involving the overall liquid transfer coefficient as well as for the individual film coefficients, assuming that dilute solutions are formed and that concentration changes are small (McCabe et al., 1993):

$$Z = H_{OL} \times N_{OL} = \frac{L}{K_L a}\int_{x_B}^{x_T} \frac{dx}{x - x^*} \qquad (4.37)$$

$$Z = H_G \times N_G = \frac{G}{K_G a}\int_{y_B}^{y_T} \frac{dy}{y_i - y} \qquad (4.38)$$

$$Z = H_L \times N_L = \frac{L}{K_L a}\int_{x_B}^{x_T} \frac{dx}{x - x_i} \qquad (4.39)$$

Where H_{OL} = Height of an overall liquid phase transfer unit (m)
H_G, H_L = Height of a gas and liquid film transfer unit respectively (m)
N_{OL} = Number of overall liquid phase transfer units
N_G, N_L = Number of gas film and liquid film transfer unit respectively

For dilute solutions, the operating line and equilibrium line are straight. Conducting a material balance the lower section of the column in Figure 4.7, the operating line:

$$L(x_B - x) = G(y_B - y) \quad \text{or} \quad y_B - y = \frac{L}{G}(x_B - x) \qquad (4.40)$$

The equilibrium line: $y^* = mx + c$ (4.41)

Where ***m*** is the slope of the equilibrium line and ***c*** the y-axis intercept. For dilute solutions the number of overall gas transfer units is (McCabe et al., 1993):

$$N_{OG} = \frac{y_B - y_T}{\dfrac{(y - y^*)_B - (y - y^*)_T}{\ln\left((y - y^*)_B / (y - y^*)_T\right)}} = \frac{y_B - y_T}{(y - y^*)_{lm}} \qquad (4.42)$$

$(y\text{-}y^*)_{lm}$ is the logarithmic mean of the driving forces at the ends of the column, $(y\text{-}y^*)_B$ and $(y\text{-}y^*)_T$. The height of an overall transfer unit is the height of a packed section necessary to achieve a change in concentration equal to the average driving force in that section, this average driving force being $(y\text{-}y^*)_{lm}$. Therefore the rate of mass transfer taking place in the column is as follows:

$$N\ A = G^{'}\left(y_B - y_T\right)A = K^{'}_G aAZ\left(y - y^*\right)_{lm} \qquad \text{(kmol/s)} \qquad (4.43)$$

Where **N** = Molar rate of absorption per unit area (kmol/m^{2}s)
A = Column cross-sectional area (m^2)

Similar to the mass transfer coefficient, the addition of resistance following the Two-Film Theory can also be applied to the heights of the transfer unit, this being first noted by Colburn (1939). The relationship between the film and overall heights of transfer units are as follows, where m is the slope of the equilibrium line and $L^{'}/G^{'}$ is the slope of the operating line. Where mass transfer resistance is essentially all in the gas phase and for dilute solutions:

$$H_{OG} = H_G + \frac{mG^{'}}{L^{'}} H_L \qquad (4.44)$$

Where mass transfer resistance is essentially all in the liquid phase and for dilute solutions:

$$H_{OL} = H_L + \frac{L^{'}}{mG^{'}} H_G \qquad (4.45)$$

4.2.5 Chemical Absorption - Kinetic Regimes for Two-Film Model

When a scrubbing solution contains a compound ***B***, which can react with compound ***A***, the contaminant in gas phase, then removal of ***A*** is referred as chemical absorption. Compound ***B*** will prevent the concentration of ***A*** to build up in the bulk liquid. The overall rate expression for the reaction will have to account for mass transfer resistance, to bring reactants together, and the resistance due to the chemical reaction rate. The relative magnitude of these two resistances can vary greatly and each situation requires its own analysis. The first problem is to identify these time dependent regimes and to select the one which matches the given physical situation. Depending on the relative rates of diffusion and reaction, the absorption systems are classified into five different regions and shown in Figure 4.8 (Levenspiel, 1999). The rate equations for absorption with instantaneous reaction and fast reaction will be developed for their applicable to reactive scrubbing.

4.2.5.1 Rate Equation for Instantaneous Reaction

Consider an infinitive fast reaction of any order:

$$aA_{\text{(from gas)}} + bB_{\text{(liquid)}} \rightarrow \text{Product} \qquad (4.46)$$

If C_B is not too large, the situation is illustrated in Figure 4.9. At steady state, the flow rate of ***B*** towards the reaction zone will be ***b*** times the flow rate of ***A*** towards the reaction zone. Thus, the rate of disappearance of ***A*** and ***B*** are given by (Levenspiel, 1999):

$$-r_A'' = -\frac{-r_B''}{b} = k_{Ag}\left(p_A - p_{Ai}\right) = k_{Al}\left(C_{Ai} - 0\right)\frac{x_o}{x_o - x} \qquad (4.47)$$

Where ***r"*** is the rate of disappearance per unit interface area, k_{Ag} and k_{Al} are the mass transfer coefficients in gas and liquid phases. At the interface, the relationship between P_A and C_A is given by Henry's Law constant for gas liquid systems. Thus

$$P_{Ai} = H_A C_{Ai} \qquad (4.48)$$

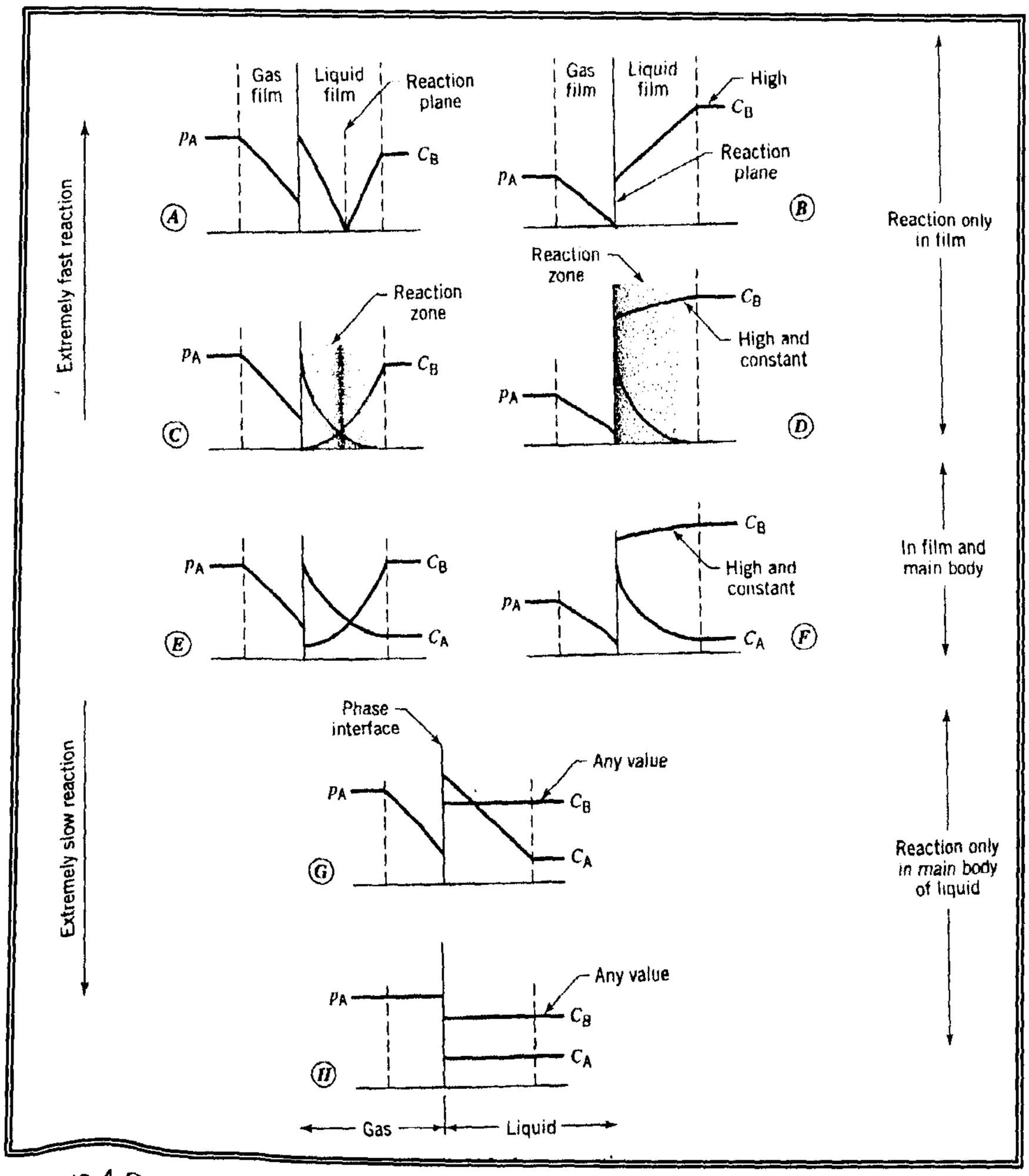

Figure 4.8: Interfacial behaviour for the liquid phase reaction (Levenspiel, 1999)

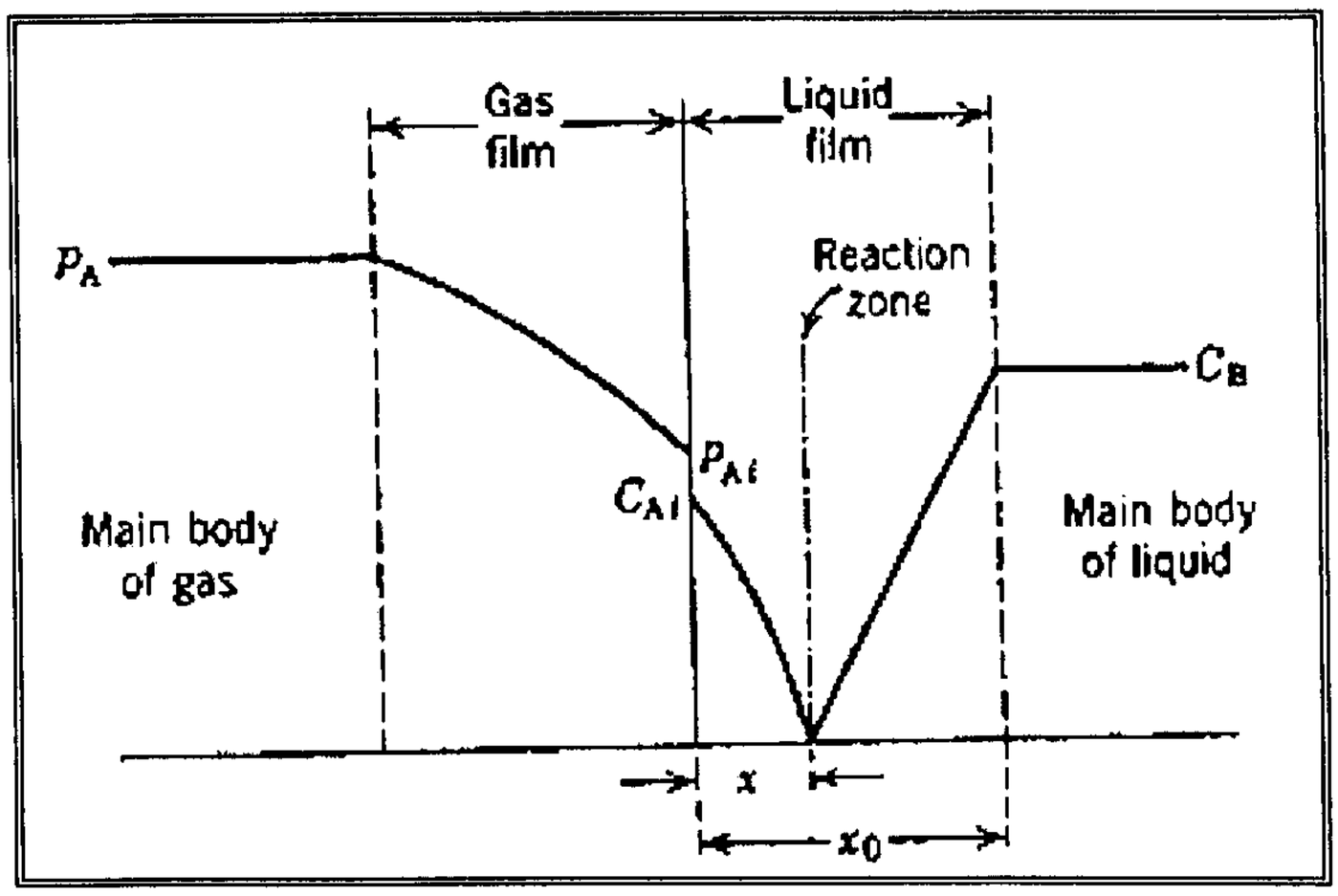

Figure 4.9: Concentration of reactants as visualised by two film theory (Levenspiel, 1999)

Since the movement of material within the film is visualised to occur by diffusion alone, the transfer coefficients for ***A*** and ***B*** are related by (Levenspiel, 1999):

$$\frac{k_{Al}}{k_{Bl}} = \frac{D_{Al}/x_o}{D_{Bl}/x_o} = \frac{D_{Al}}{D_{Bl}} \tag{4.49}$$

Eliminating the unknown in Equations 4.47, 4.48 and 4.49, we obtain:

$$-r_A'' = -\frac{1}{s}\frac{dN_A}{dt} = \frac{k_{Al}}{k_{Bl}} = \frac{\frac{D_{Bl}}{D_{Al}}\frac{C_B}{b} + \frac{p_A}{H_A}}{\frac{1}{H_A k_{Ag}} + \frac{1}{k_{Al}}} \tag{4.50}$$

For the special case of negligible gas phase resistance, K_{Ag} is infinitive, and $P_A = P_{Ai}$. Equations 4.50 reduce to:

$$-r_A'' = k_{Al}C_{Ai}\left(1 + \frac{D_{Bl}C_B}{b\,D_{Al}C_{Ai}}\right) \tag{4.51}$$

Comparing Equation 4.51 with the expression for the maximum rate of mass transfer, or

$$-r_A'' = k_{Al}C_{Ai} \tag{4.52}$$

It is found that the term in brackets represents the increase in rate of absorption of ***A*** resulting from adding reactant B to the liquid. Thus an enhancement factor is defined as (Levenspiel, 1999):

$$E=\left(\frac{\text{Rate reaction}}{\text{Rate for mass transfer}}\right) \tag{4.53}$$

For the case of infinitely fast reaction rate and no gas phase resistance (Levenspiel, 1999)

$$-r_A'' = k_{Al} C_{Ai} E \tag{4.54}$$

where,
$$E = 1+\left(\frac{D_{Bl} C_B}{b\, D_{Al} C_{Ai}}\right) \tag{4.55}$$

for the special case of high C_B (Levenspiel, 1999), or if

$$k_{Al} \le \frac{k_{Bl}}{b} C_{Bl} \tag{4.56}$$

then this condition requires that the reaction zone move to and remain at the interface. When this happens, the resistance of the gas phase controls, and the rate is not affected by any further increase in concentration of ***B***. Equations 4.49 simplifies to:

$$-r_A'' = -\frac{1}{S}\frac{dN_A}{dt} = k_{Ag} p_A \tag{4.57}$$

Note that the reaction rate constant does not enter into Equations 4.49 or 4.56, showing that the rate is completely mass transfer controlled. Also, even though the resistance of liquid film may normally control, when C_B is raised sufficiently, then the resistance always shifts to gas phase control.

4.2.5.2 Rate Equation for Fast Reaction

For a second order reaction between ***A*** and ***B*** (Levenspiel, 1999):

$$-r_{Al} = \frac{1}{V}\frac{dN_A}{dt} = k\, C_A C_B \tag{4.58}$$

In the gas and liquid films (Levenspiel, 1999)

$$-r_A'' = k_{Ag}(p_A - p_{Ai}) = k_{Al} C_{Ai} E \tag{4.59}$$

Eliminating C_{Ai} and P_{Ai} with Equation 4.48 gives

$$-r''_A = \frac{1}{\frac{1}{k_{Ag}} \frac{H_A}{k_{Al} E}} p_A \tag{4.60}$$

For the special case where C_B is sufficiently high to be considered constant the reaction in the liquid becomes pseudo-first order (Levenspiel, 1999), or

$$-r_{Al} = k C_A C_B = (k C_B) C_A = k_1 C_A \tag{4.61}$$

In which case the enhancement factor is a simple expression, as follows (Levenspiel, 1999):

$$E = \frac{\sqrt{D_{Al} k C_B}}{k_{Al}} = \frac{\sqrt{D_{Al} k_1}}{k_{Al}} \tag{4.62}$$

For a special case of high C_B, intermediate concentrations can be eliminated. The rate equation become:

$$-r''_A = \frac{1}{\frac{1}{k_{Ag}} + \frac{H_A}{\sqrt{D_{Al} k C_B}}} \tag{4.63}$$

4.2.6 Chemical Absorption in a Packed Bed

Rate of absorption can be expressed in four different ways by using individual or overall mass transfer coefficients based on the gas or liquid phases. The rate of absorption per unit volume of a packed column is given by any of the following equations, where y and x are the mole fraction of the components which are absorbed in gas and liquid phases respectively (McCabe et al., 1993).

$$r = k_y a (y - y_i) \tag{4.64}$$

$$r = k_x a (x_i - x) \tag{4.65}$$

$$r = K_y (y - y^*) \tag{4.66}$$

$$r = K_x a (x^* - x) \tag{4.67}$$

An absorber can be designed using any of four basic rate equations, but the gas film coefficients are most common. Consider the packed bed shown in Figure 4.5(a). The cross section is ***A***, and the differential volume in height is ***dZ*** is ***AdZ***. If the change in molar flow rate ***F*** is neglected, the amount absorbed in section ***dZ*** is ***–Fdy***, which equals the absorption rate times the differential volume (McCabe et al., 1993):

$$-Fdy = K_y a\left(y - y^*\right)AdZ \tag{4.68}$$

This equation is rearranged for integration, grouping the constant factor ***F***, ***A*** and $K_y a$ with ***dZ*** (McCabe et al., 1993).

$$\frac{K_y aA}{F}\int_0^{Z_T} dZ = \frac{K_y aA Z_T}{F} = \int_b^a \frac{dy}{y - y^*} \tag{4.69}$$

The equation for column height can be written as follows (McCabe et al., 1993):

$$Z_T = \left[\frac{\left(F/A\right)}{K_y a}\right]\int_b^a \frac{dy}{y - y^*} \tag{4.70}$$

The integral in Equation 4.70 represents the change in vapour concentration divided by the average driving force and is called the number of transfer unit (NTU). The other part of Equation 4.70 has the unit of length and is called the height of transfer unit (HTU). Reaction in the liquid phase reduces the equilibrium partial pressure of the solute over the solution, which greatly increases the driving force for mass transfer. If the reaction is essentially irreversible at absorption conditions, the equilibrium partial pressure is zero, and NTU can be calculated just from the change in gas composition from $y^* = 0$ (McCabe et al., 1993).

$$NTU = \int_b^a \frac{dy}{y} = \ln\left(\frac{y_a}{y_b}\right) \tag{4.71}$$

Large parts of the research described in this thesis are designed to evaluate the effects of key parameters, such as temperature, concentration, height of packing, liquid and gas flowrate on H_2S absorption with molten tin. Another part of this research is directed at obtaining the HTU for H_2S absorption in a packed bed hot gas scrubber.

CHAPTER FIVE

Experimental Programme

This chapter presents the experimental set up and the associated design modification work which was undertaken during the course of this research. Details of the experimental setup and operational procedures for various experiments are also discussed in this chapter. The description of the scrubber system originally designed by Chang (2003) is also presented.

5.1 Original Design of Hot Gas Scrubbing System (Chang, 2003)

The selection of the materials of construction is first discussed. The design of the main gas scrubber unit which includes the column and its packing, liquid distributor and the column injector are also presented in this chapter. This is followed by the design of the gas lift for molten tin transport. Other aspects include provisions for loading and removal of tin from the scrubber, tin level indicators, system heating and insulation, temperature measurement and control as well as system operating parameters.

5.1.1 Main Gas Scrubber Unit

5.1.1.1 Materials of Construction

The packed bed scrubber was constructed from austenitic stainless steel Type 316 (16-18% Cr, 10-14% Ni, 2% Mn, 1% Si, 0.08% C, 0.045%P and 0.03% S). This type of stainless steel is one of the materials which has been tested up to 800 hours in Finland (Chang, 2003). It has been used to test the long-term corrosion resistance of commercial metal filters under a simulated gasification environment with 300 ppmv H_2S at 400℃ and 500℃ and a good corrosion resistance was demonstrated (Mitchell, 1997). However there remains the issue of stainless steel corrosion by molten tin, with the dissolution of some of the nickel content into the liquid metal. As each test run involving the irrigation of molten tin through the scrubber is anticipated to be relatively short in duration (typically less than 30 minutes); the degree of molten tin's contamination by dissolved nickel from the steel is expected to be minimal.

5.1.1.2 Design of the Main Scrubber Unit

- **Column and Packing**

In order to compare with results from the water-irrigated cold model scrubber (particulate and gas cleaning), the physical geometry and dimensions of the Perspex column along with its packing have been closely followed herein on the hot scrubber. The close hydrodynamic similarities between both scrubbers include identical packing shape and size, nearly identical column size, similar packing support plate and liquid distributor. 9.53 mm (3/8 inch) high-purity ceramic alumina (Al_2O_3) spheres provided by the precision Ball and Gauge Company were used as packing material (Figure 5.1).

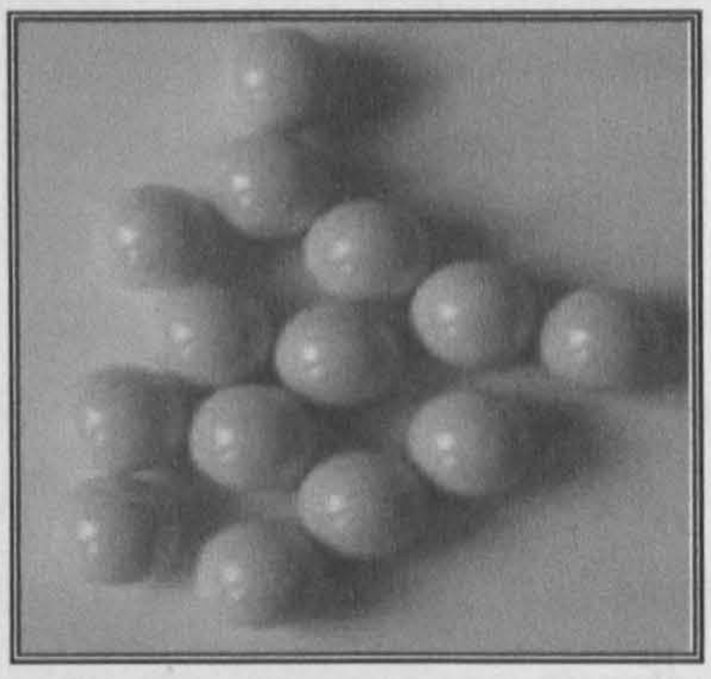

Figure 5.1: High-purity ceramic alumina (Al_2O_3) spheres

Details on the packing are summarised as follows:

Table 5.1: Characteristics of the alumina packing (Chang, 2003)

Diameter d (mm)	9.53
Column to packing diameter ratio (m/m)	8.4
Packing element specific surface area S = 6/d (m^2/m^3)	630
Packed bed porosity ε (m^3/m^3)	0.45*
Packed bed specific surface area $S_B = S(1-\varepsilon)$ (m^2/m^3)	346
Packing specific gravity (dimensionless)	4.0
Alumina critical surface tension σ_C (dyne/cm)	Data unavailable
Molten tin-alumina contact angle θ (degree)	≈ 160-140° at 300-1130°C

To prevent the possible preferential wetting of molten tin on the stainless steel wall, an alumina combustion tube with internal diameter of 8 cm and outer diameter of 9.5 cm was used to line the interior of the stainless steel column (see Figure 5.2). The stainless steel column was sized such as to fit the alumina tube. The alumina tube was 23 cm long allowing an approximately 20 cm packed bed depth.

Figure 5.2: Alumina combustion tube and stainless steel column

- **Packing Support Plate**

The packed bed of alumina spheres was supported on a simple stainless steel sieve-type of packing support plate with evenly-spaced 5 mm perforations, sufficiently small to prevent the spheres from falling through (Figure 5.3). The total fractional free area of the packing support plate was about 0.48. This is slightly smaller than the one used in the Perspex column as the perforations directly above the bottom pressure tapping was omitted. This is to minimise plugging by the splashing liquid droplets.

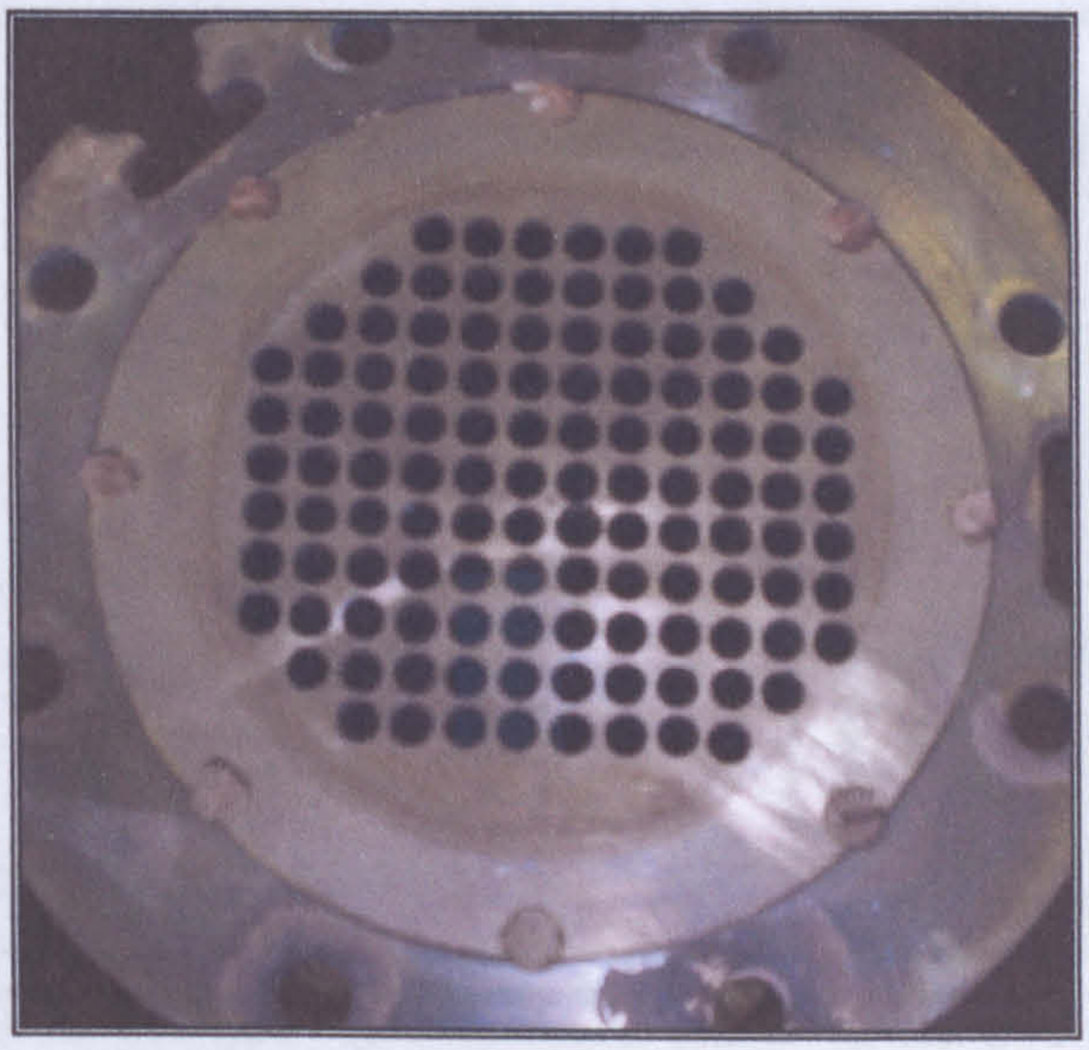

Figure 5.3: Support plate

- **Liquid Distributor**

A stainless steel orifice type of liquid distributor was employed, providing separate paths for gas and liquid flows. The gas flows up through risers whilst the liquid tin flows down through orifices on the distributor floor. The design of the liquid distributor has to fulfil two key criteria (Fadel, 1984). Firstly, the riser height must be higher than the liquid head corresponding to maximum liquid rate to prevent liquid overflow at high liquid rates, thus avoiding liquid misdistribution at the top of the bed. Secondly, the liquid head at minimum liquid rate must be higher than the gas pressure drop through the riser, hence preventing local flooding at the distributor which will eventually lead to flooding of the whole packed bed. Figure 5.4 illustrates the orifice type liquid distributor used in the tests.

- ⇨ Riser: Total = 6; Height = 4.0 cm; Internal diameter = 1.5 cm;
- ⇨ Total flow area = 21% of column cross-sectional area
- ⇨ Orifice:Total = 6; Diameter = 7.6 mm

- **Column Gas Injector**

Gas entered the column via an injector which was made from an 11 mm internal diameter stainless steel pipe with 4 ports distributed at its side at one end. This end was capped, shielding the gas ports from the falling liquid stream.

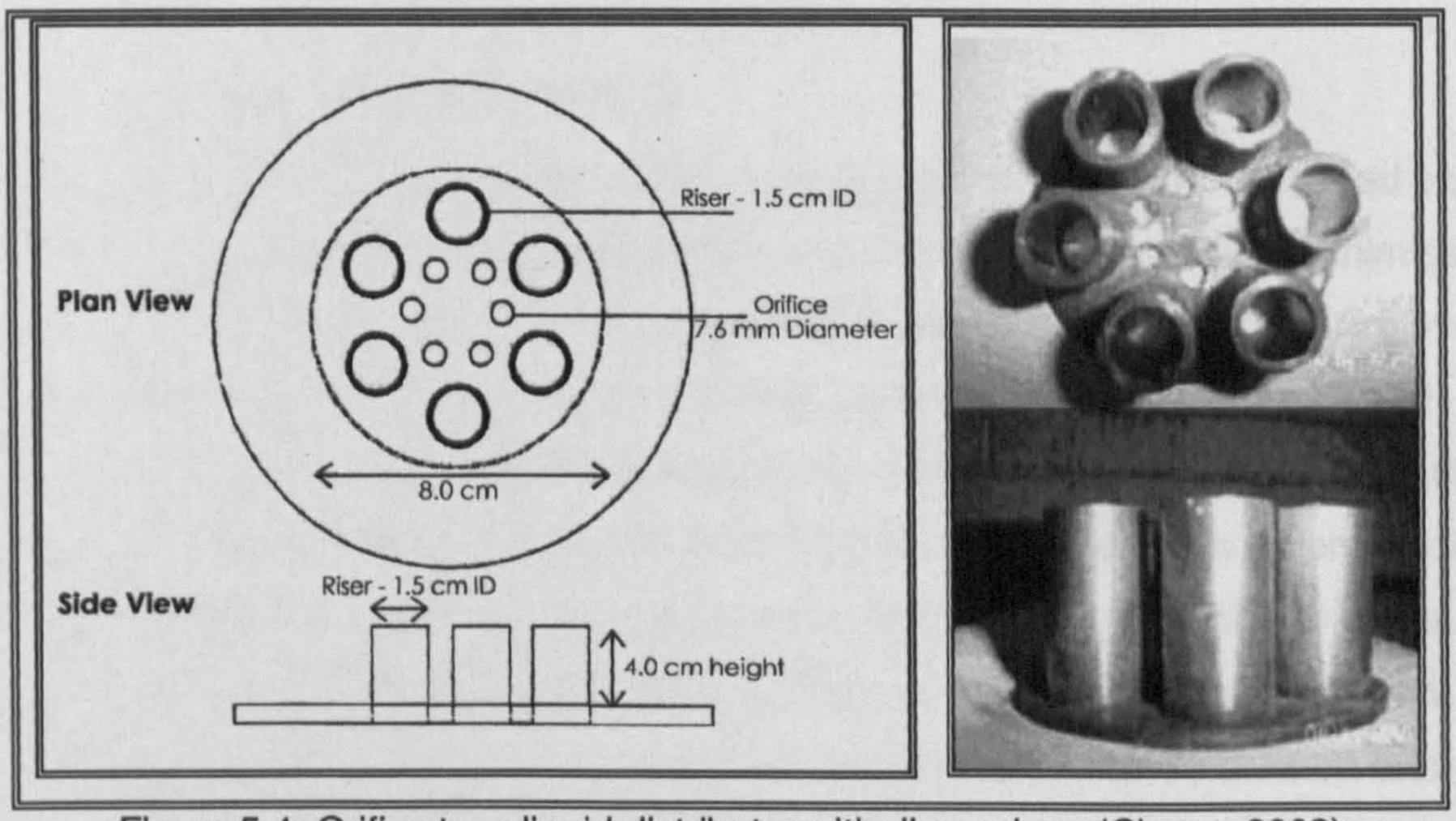

Figure 5.4: Orifice type liquid distributor with dimensions (Chang, 2003)

5.1.1.3 Design of Gas Lift

The irrigation of molten tin through the packed bed scrubber was achieved by a nitrogen U-tube gas lift constructed from a 22 mm inner diameter (D) and 25 mm outer diameter stainless steel pipe. The submergence (S) was 61 cm while the lift (L) was 46 cm, giving a total height of just over 1 m. Nitrogen gas was used for pumping. Figure 5.5 shows the calibration chart of the liquid tin flow rates vs. the N_2 gas flowrates.

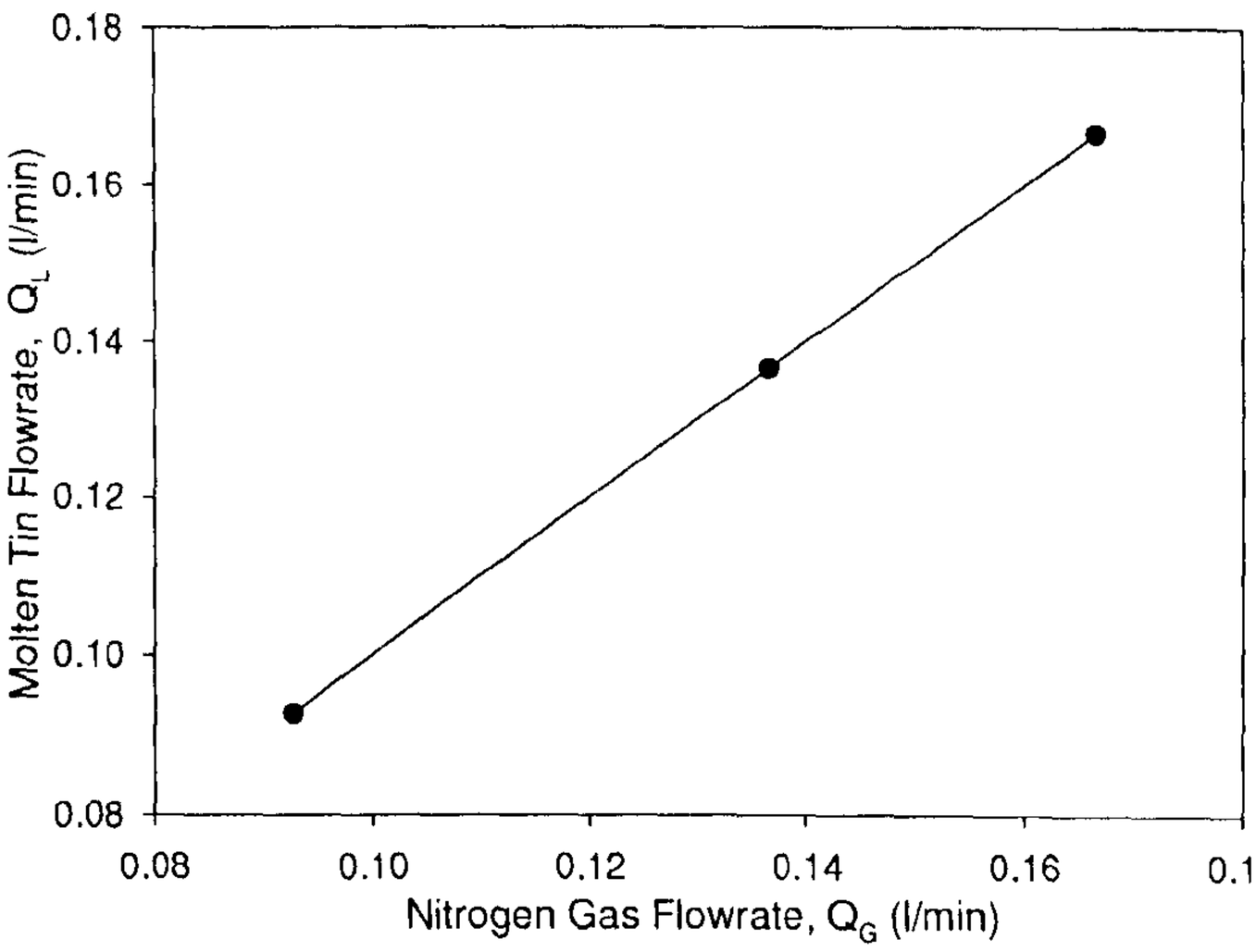

Figure 5.5: Calibration chart of liquid tin flowrates

5.1.1.4 Loading and Removal of Tin

A vessel with a removal lid was provided in which solid tin pellets were loaded before each test (Figure 5.6). It was located at the top of the column in order to minimise the overall cross-sectional area of the space that needed to be heated. An overall compact unit helps to minimise the heating surface area requirement and also reduces heat loss. Once melted, the molten tin flowed from the top vessel down through a downcomer pipe that connected to the side of the bottom reservoir of the column. From the reservoir, the tin flowed down through the downcomer of the gas lift, thus filling the downcomer and the riser legs of the gas lift. The provision of a bottom vessel positioned below the gas lift allowed molten tin to be drained and thus removed from the system at the end of each test. The vessel was provided with a detachable lid so that the solidified tin ingot could be removed. The interior of the vessel was lined with Kaowool paper prior to its use.

Earlier tests using small amounts of tin strips showed that molten tin when solidified fused onto the wall of a bare stainless steel crucible, but the solid tin ingot was easily removed when the crucible was lined with Kaowool paper.

Figure 5.6: Loading vessel

5.1.1.5 Tin Level Indicator

Level sensors were incorporated to indicate the molten tin level in the column reservoir. These were stainless steel probes hanging from the top of the reservoir. The probes were inserted through small ceramic alumina pieces which were attached to the top of the reservoir. The ceramic pieces enable connection of the probes to external wires whilst insulating the probes from contacting the metal body of the column. The wires were connected to an electronic system controller. When the molten tin in the reservoir rises sufficiently high such that it touches the tip of the hanging probe, an electrical contact is made between the system controller, the tin and the metal rig. Since both the control panel and the metal rig were earthed, a complete electrical circuit was achieved; hence an electrical signal was produced and displayed on the control panel showing the tin level in the column reservoir. Three stainless steel probes were used with varying lengths to provide low (L1 = 2 cm), moderate (L2 = 3 cm) and high (L3 = 4 cm) level indicators of the molten tin in the reservoir.

5.1.1.6 Gas Supply

The N_2 gas to both the main column and the gas lift was supplied from separate gas cylinders. For particulate cleaning studies only a N_2 tank was used. For desulphurisation studies, the syngas was modeled as N_2 containing H_2S at various concentrations. As tin is fairly reactive, it can also react with other gas components in actual syngas. The effects of H_2 and other gases are discussed in Chapter 6. The N_2/simulated syngas entered the column via an injector. The gas was preheated by a series of three in-line gas heaters. K-type thermocouples with an inconel sheath and magnesium oxide insulation were used for temperature measurement. H_2S in the outlet stream was analysed using an on-line gas chromatograph (ABB PGC2000) every 5-10 minutes. The GC was calibrated using span gas with H_2S concentration of 4000 ppm ±5%.

5.1.1.7 System Heating and Insulation

Six semi-cylindrical ceramic radiant heaters model CRWS-1215/240-A (3400 watts, 240 volts) supplied by Omega® were used to heat the scrubber. The radiant heater was made from low mass, vacuum formed ceramic fibre with helically wound iron-chrome-aluminium wire elements embedded into the fibre. It provides the convenience of combined heating elements and insulation in a single unit. Each heater was 12 inches in length, 19 inches in external diameter and 15 inches in internal diameter. The six semi-cylindrical radiant heaters were stacked on top of each other, forming a compact semi-cylindrical compartment in which the column, gas lift, top and bottom vessels were fitted. The main gas that entered the base of the column was preheated by a series of three in-line gas heaters model AHP-7562 (750 watts, 240 volts) with a heated length of 14 cm each, supplied by Omega®. The nitrogen gas to the gas lift was preheated by a single in-line gas heater model AHP-5052 (400 watts, 240 volts) with a heated length of 11 cm supplied also by Omega®. Kaowool boards and blankets were used for system insulation. The front of the semi-cylindrical heated compartment was covered by Kaowool boards. The interior of the heated compartment was partitioned by Kaowool blankets in the top and bottom sections to help retain the heat.

5.1.2 Analytical Setup

5.1.2.1 Temperature Measurement and Control

K-type thermocouple probes with inconel sheaths (temperature range 0–1100℃) and magnesium oxide insulation were used for temperature measurement in the high temperature gas scrubbing system. Their individual locations are listed in Table 5.2. Thermocouples T1c, T2c and T3c were connected to the electronic system controller (Figure 5.7). Their set points dictate the extent of heating by the in-line gas heaters and the radiant heaters, controlling the preheated main gas and lift gas temperatures as well as the temperature of the molten tin in the column reservoir respectively. The heaters were cut off once the target temperatures were reached. Thermocouples T1 to T6 were connected to a digital thermometer for temperature display. Low pressure switches P1 and P2 prevent overheating of the in-line gas heaters by cutting off the heaters once the gas pressure falls below 3.8 cm H_2O (g). These were indicated on the control panel.

Table 5.2: Temperature measurements locations

Thermocouple No.	Locations
T1c	Downstream of series of in-line gas heaters, before main gas enters column base. Sets target temperature for series of in-line gas heaters
T2c	Downstream of in-line gas heater, before lift gas enters gas lift base. Sets target temperature for in-line gas heater
T3c	Molten tin in column reservoir. Sets target temperature for radiant heater
T1	Within heated compartment enclosed by radiant heaters
T2	Gas outlet at top of column
T3	Molten tin inlet to column at top of gas lift riser
T4	Main gas inlet to gas injector at column base
T5	Lift gas inlet to gas injector at gas lift base
T6	Gas outlet before entering in-line filter

Figure 5.7: Electronic system controller

5.1.2.2 Gas Analyser

For particulate cleaning studies, an oxygen analyser (Figure 5.8) was used to continuously monitor the level of oxygen concentration in the packed bed scrubber. It is also important to ensure that the system is totally run in inert atmosphere within the scrubber to prevent tin oxidation during the experimental work. For hot gas desulphurisation studies, an online process gas chromatograph analyser (ABB-PGC2000) was used to continuously monitor the concentration of the H_2S at the top of the scrubber.

Figure 5.8: Oxygen gas analyser

5.1.3 Schematic Diagram

The schematic diagram in Figure 5.9 illustrates the original overall layout of the high temperature gas scrubbing system.

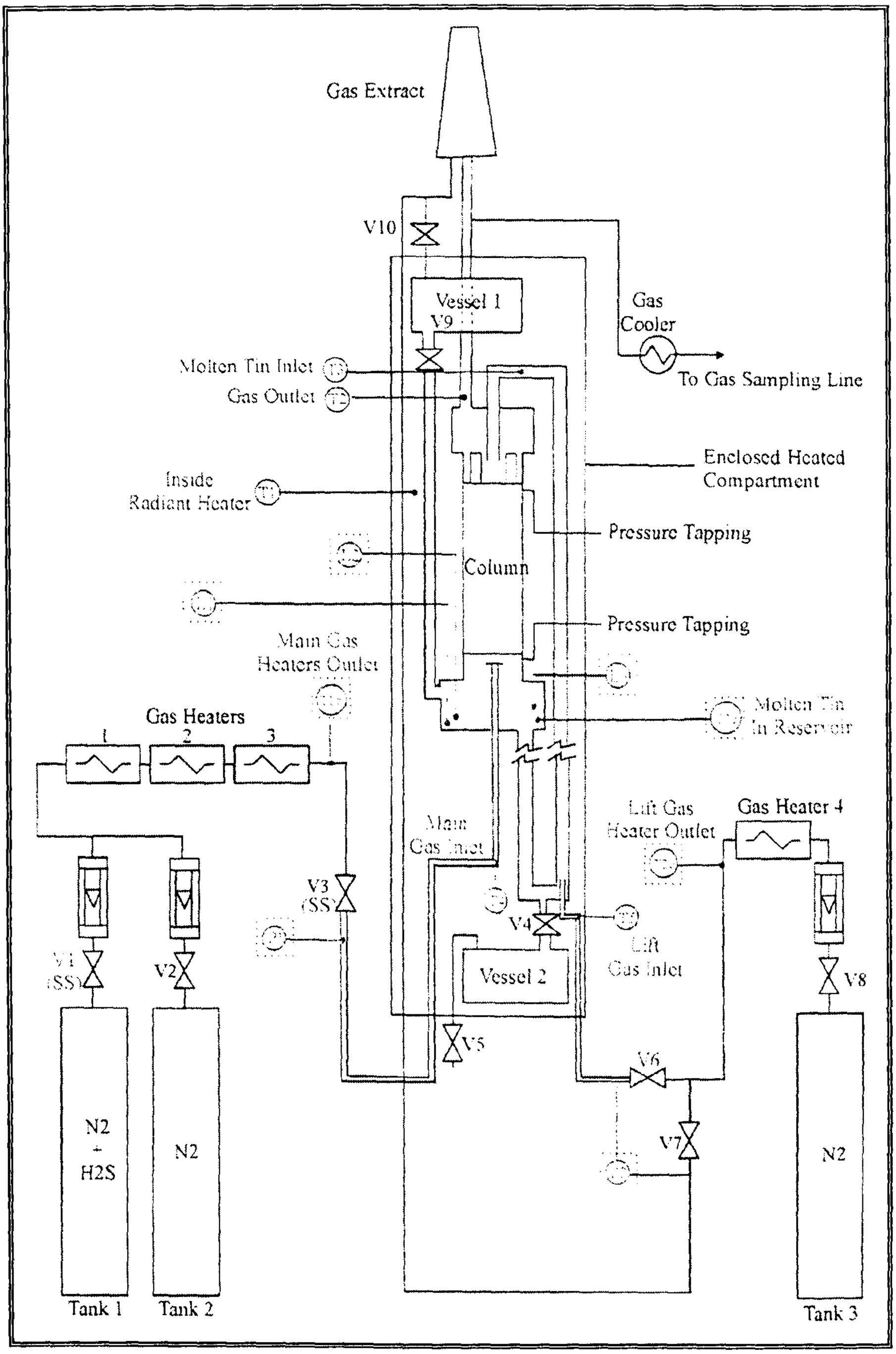

Figure 5.9: Original schematic diagram of scrubbing system (Chang, 2003)

5.2 Modification of the Original Experimental Design

Previously, this equipment was designed to study only the desulphurisation process using liquid tin (Chang, 2003). In this research work, the existing equipment was modified in order to study the desulphurisation process and to investigate the process of particle cleaning. The aim of the design modification was also to ensure that the tin successfully circulates through the gas lift using nitrogen gas. The following sections present the modification and additional work on the rig.

5.2.1 Packing Support Plate

A packing support plate (Figure 5.3) was used in the system in the earlier tests. It was found that this plate was not able to function as expected due to plugging on the surface of the plate (Figure 5.10). In order to rectify the problem, a net support plate was designed and placed at the bottom of the column as shown in Figure 5.11.

Figure 5.10: Packing Support Plate

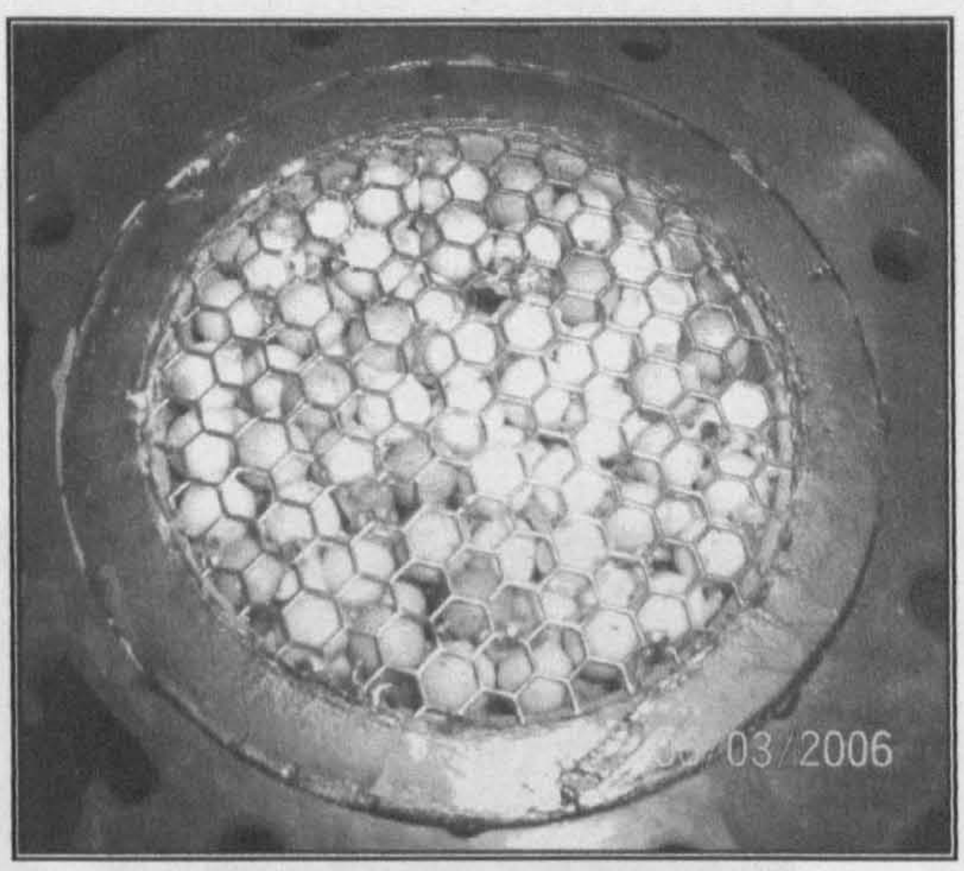

Figure 5.11: Packing Support Net

5.2.2 Gas Heaters

The position of the main heaters (heater 1, 2 and 3) were changed from vertical to horizontal position due to operational problems as recommended by the supplier (RS-Components, 1996).

5.2.3 Air Seal

A glass wool gasket was placed between the two pipe joints (Figure 5.12). It was noted that the glass wool was not able to function efficiently due to leakage. Therefore an o-ring plate made from die cast steel was used as shown in Figure 5.13.

Figure 5.12: O-ring plate (Glass Wool Gasket)

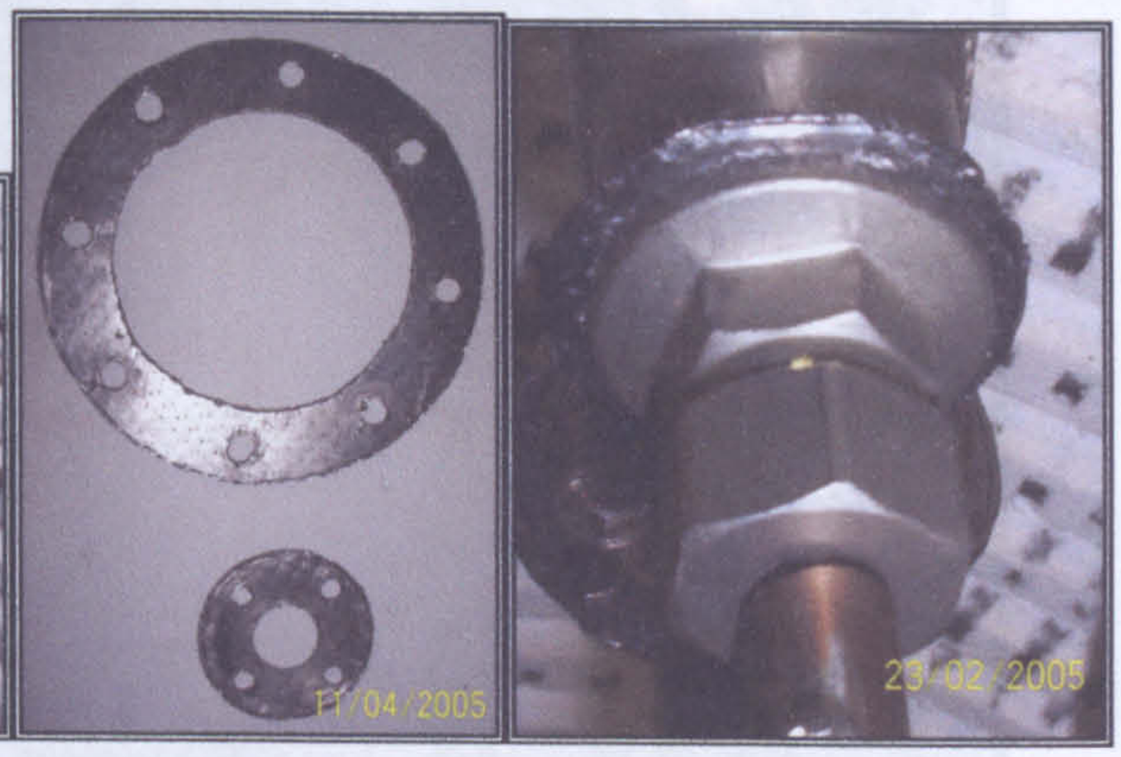

Figure 5.13: O-ring plate (Cast Steel)

5.2.4 Gas Lift

For the gas lift system, an extra route was introduced at the lift gas outlet. It was mainly to avoid the molten tin from the reservoir getting through to the tip of the nitrogen injector as shown in Figure 5.14 and 5.15.

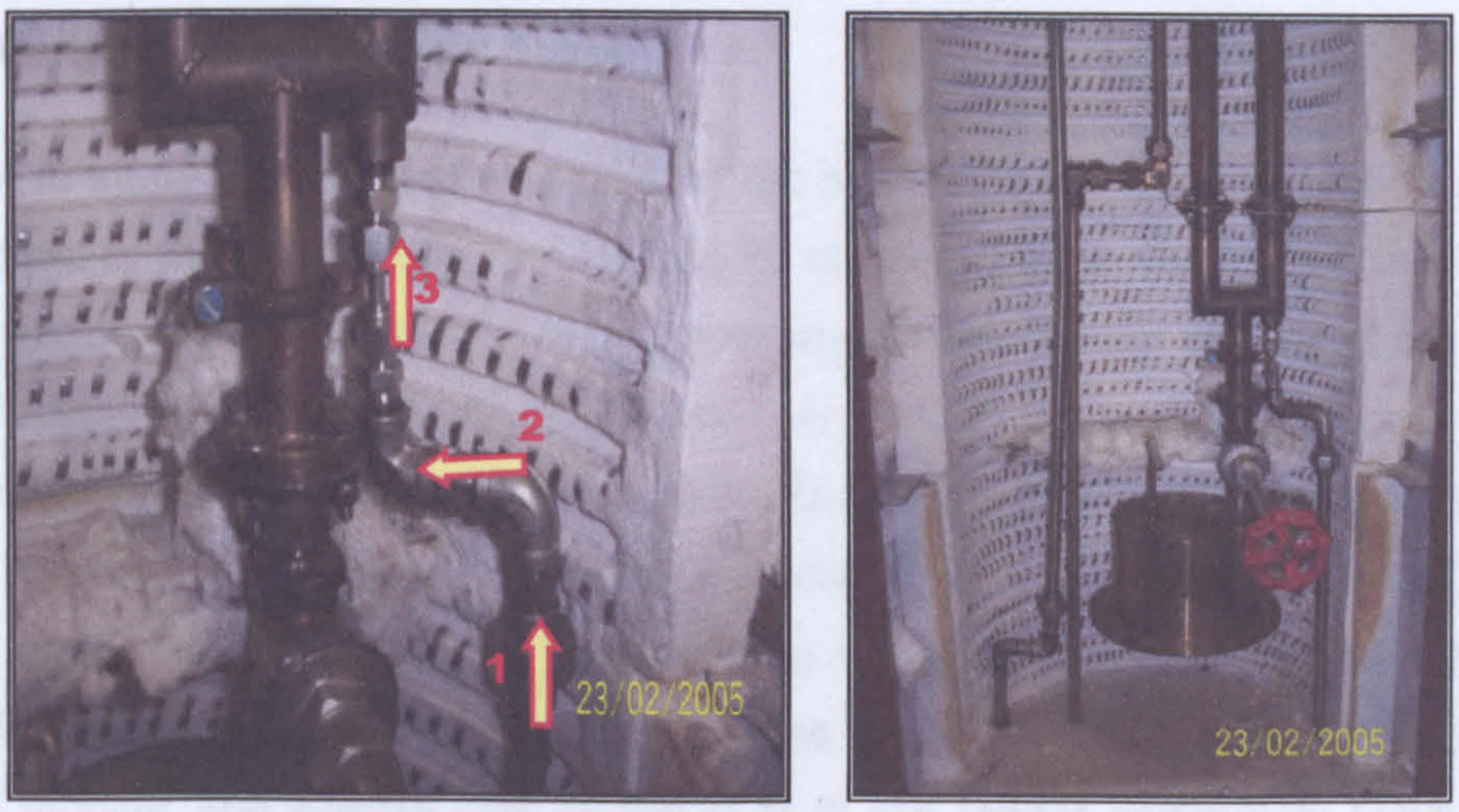

Figure 5.14: Nitrogen injection before modification

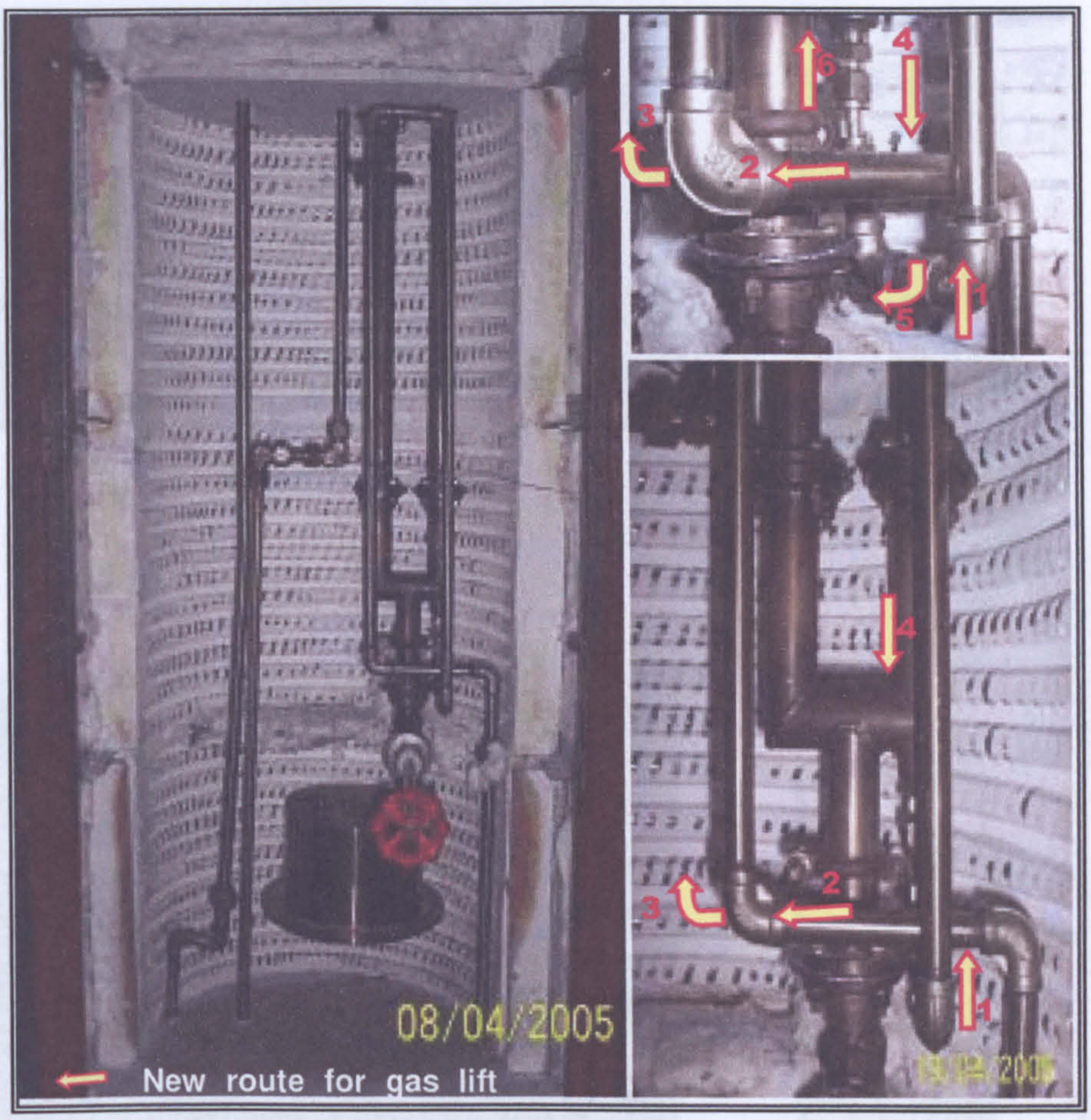

Figure 5.15: Nitrogen injection after modification

5.2.5 Particle Feeder (Screw Feeder)

In order to study the removal efficiency of the system, a particulate injection system was added to the equipment. The possibility of using Malvern's Qspec Dry Powder Feeder for the particles' injection was previously considered but was ruled out due to the difficulties in obtaining uniform particle flow through the hot gas scrubber (HGS) system. Considering all the technical problems associated with Malvern's Qspec Dry Power Feeder, the decision was made to use a screw feeder (Figure 16(a) and 16(b)) for injecting the particles/powder in to the HGS system. The housing was made from stainless steel, and the feeder was closed by transparent perspex. This was to monitor and ensure that all the dust in the feeder completely flows to the scrubber.

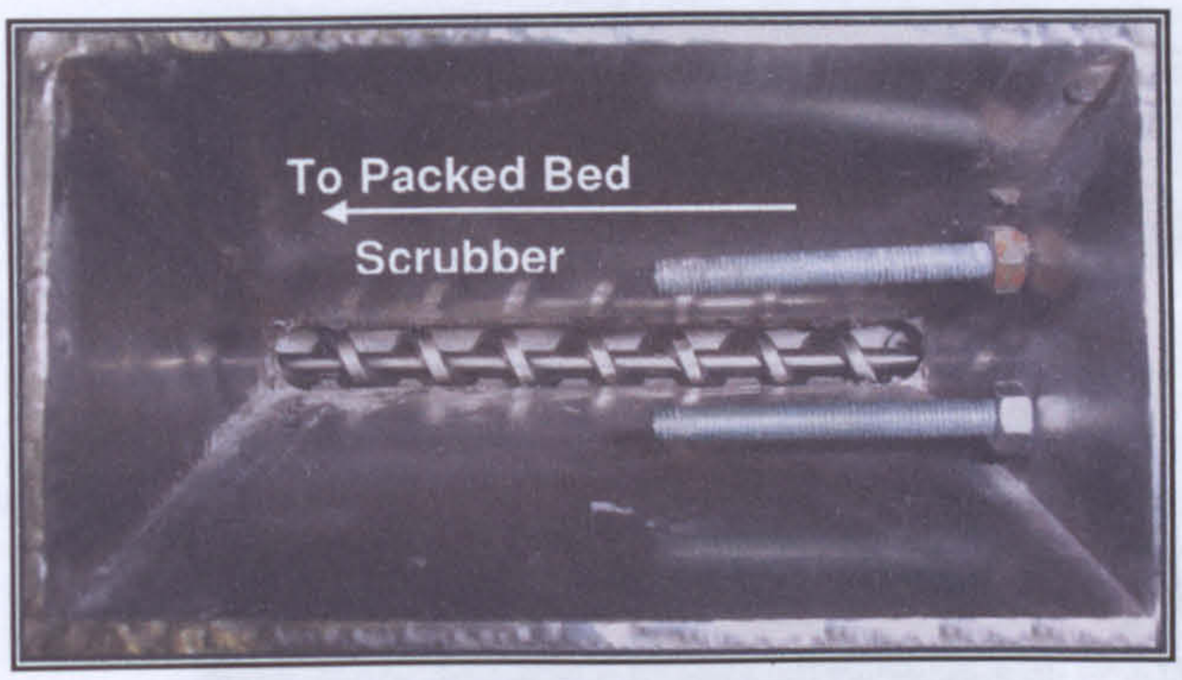

Figure 5.16(a): Screw feeder (top view)

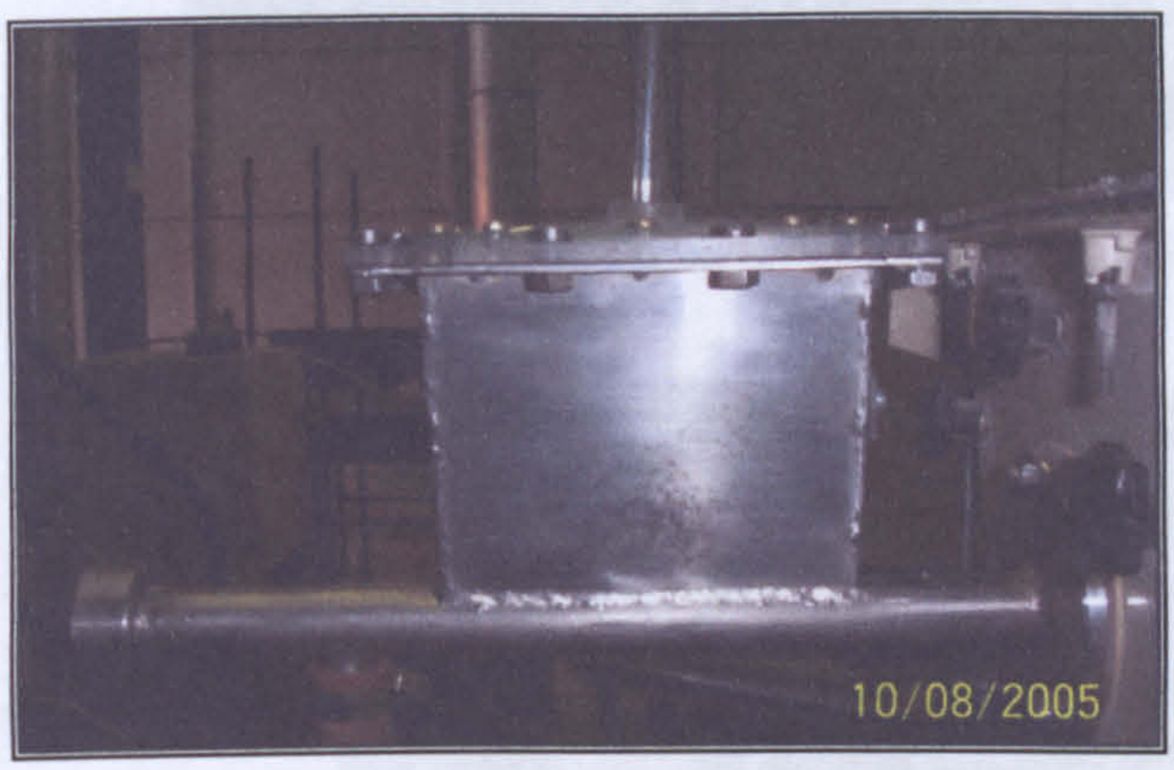

Figure 5.16(b): Screw feeder (side view)

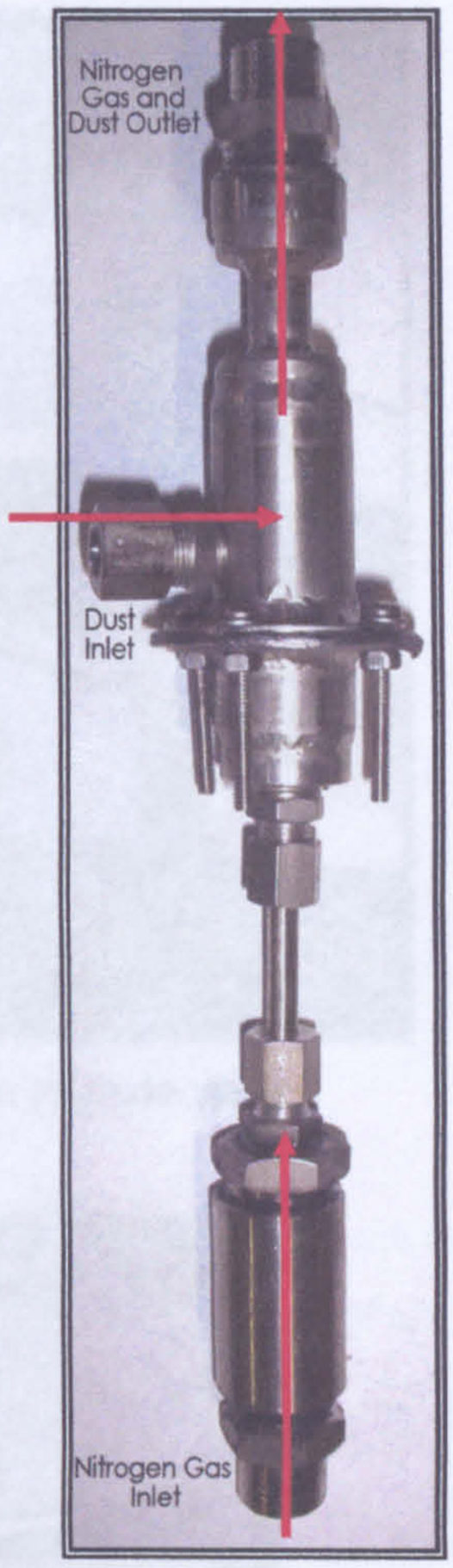

Figure 5.17: Venturi system

Tests were conducted to observe the performance of the screw feeder to generate the minimum flowrate for the particulate injection. In order to make sure that the particles would not block the piping system for the dust injection; a venturi system was introduced as shown in Figure 5.17. The overall particulate injection system for particle cleaning experimental work is shown in Figure 5.18 and 5.19 respectively. Figure 5.20 shows the calibration chart of the screw feeder for different readings.

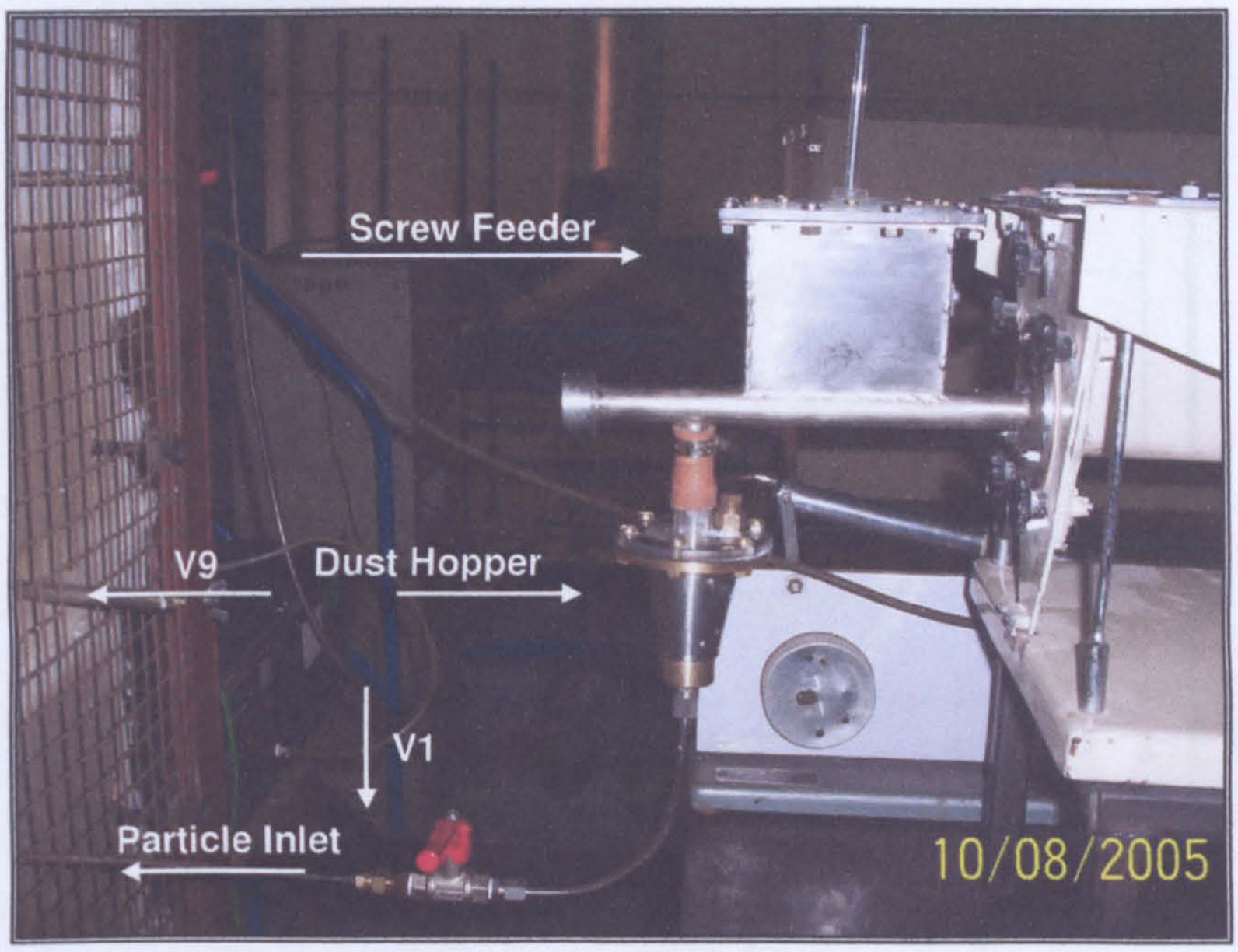

Figure 5.18: Venturi system for dust injection (outside view)

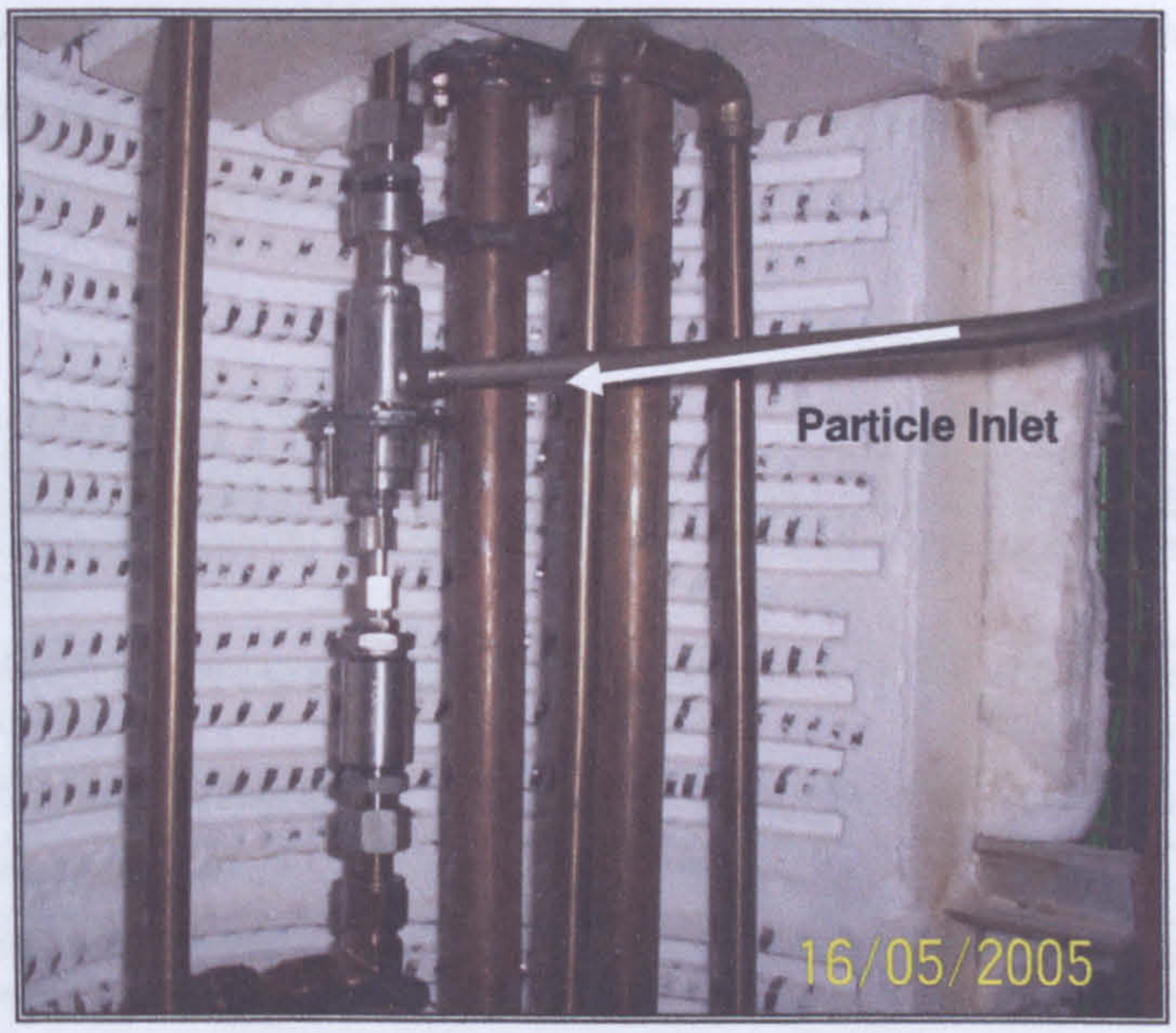

Figure 5.19: Venturi system for dust injection (inside view)

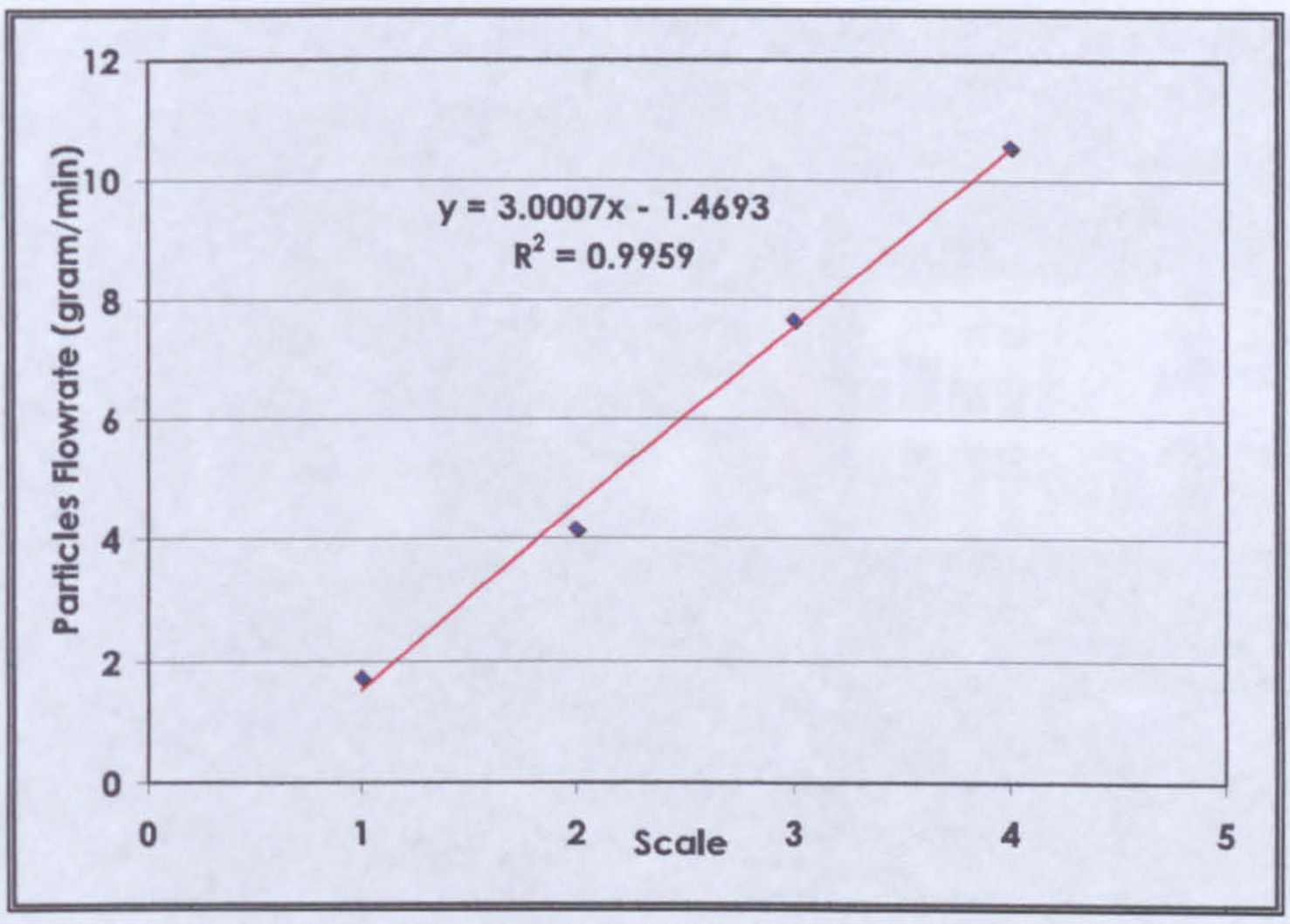

Figure 5.20: Calibration chart of screw feeder

5.2.6 Control Valves

Four extra valves were added to the system to make sure that it was efficient and reliable. The information on location and function of each valve is presented in Table 5.3 and Figure 5.21 respectively.

Table 5.3: New control valves locations

Valve No.	Location	Function
V9	Molten tin outlet to the gas lift limbs	To monitor the liquid level in the reservoir
V10 & V11	Have been renamed and formally known as valve 9 and Valve 10 respectively	
V12	Gas outlet at the top of vessel 1	To purge all air at the top vessel
V13	Gas outlet before entering in-line filter	
V14	Gas outlet to gas extract	To purge all air inside the column

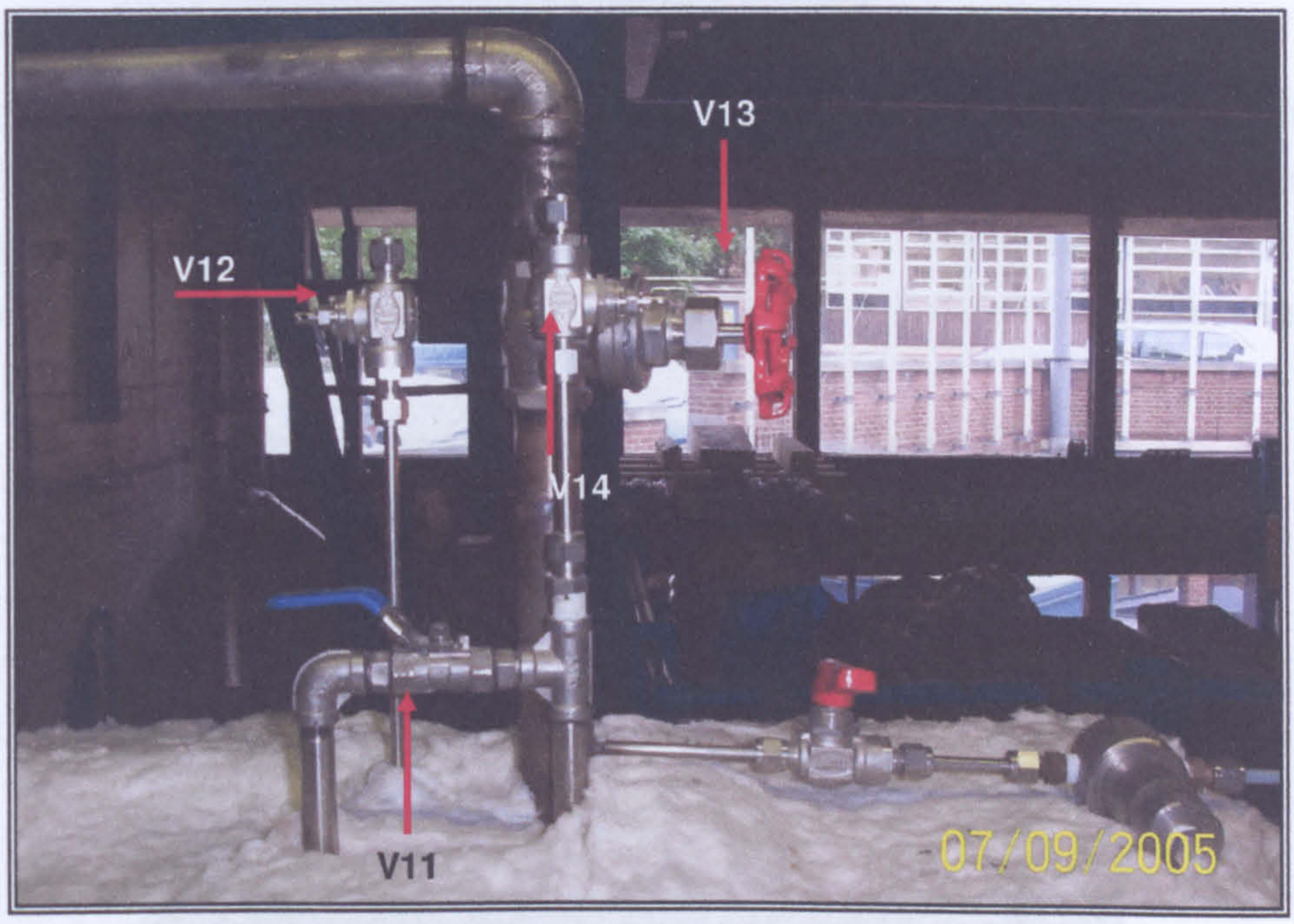

Figure 5.21: New control valves locations

5.2.7 In-Line Filter (Particles Collection)

The original rig was designed for acid gas cleaning (H_2S). For particulate cleaning, in-line filter has to be added to the system in order to measure the amount of particles that cannot be separated through the scrubber. Whatman's Gamma-12 in-line filter was previously considered but the product was no longer available. A fabricated stainless steel in-line filter was used as shown in (Figure 5.22). Another venturi system was added in order to monitor the pressure drop across the in-line filter during the experimental work. The main purpose of this venturi was to make sure that there was no pressure drop (build-up of pressure) across the filter.

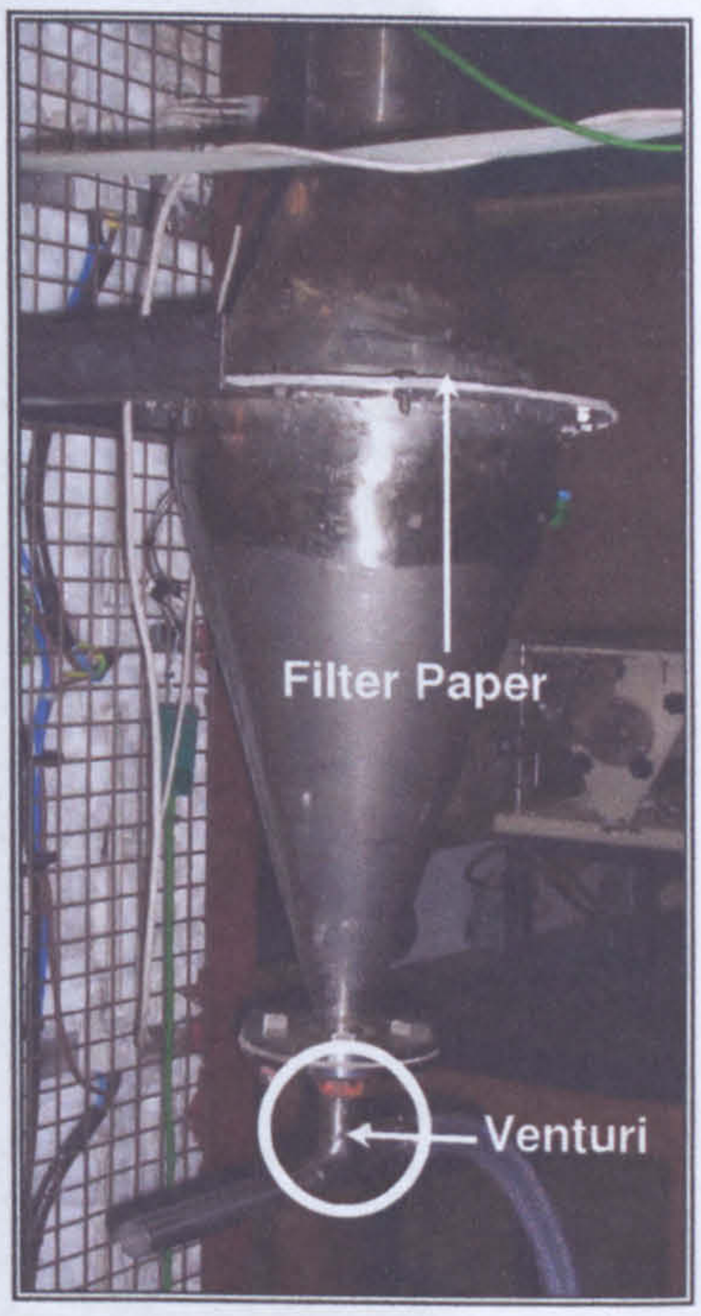

Figure 5.22: In-line filter

5.2.8 Final Modified Design

A photograph of the new scrubbing system is shown in Figures 5.23. Dimensions of the column, gas lift, top and bottom vessels are shown in Figure 5.24. The new schematic diagrams in Figure 5.25 and 5.26 respectively, illustrate the overall high-temperature gas scrubbing system for particulate and acid gases (H_2S) cleaning.

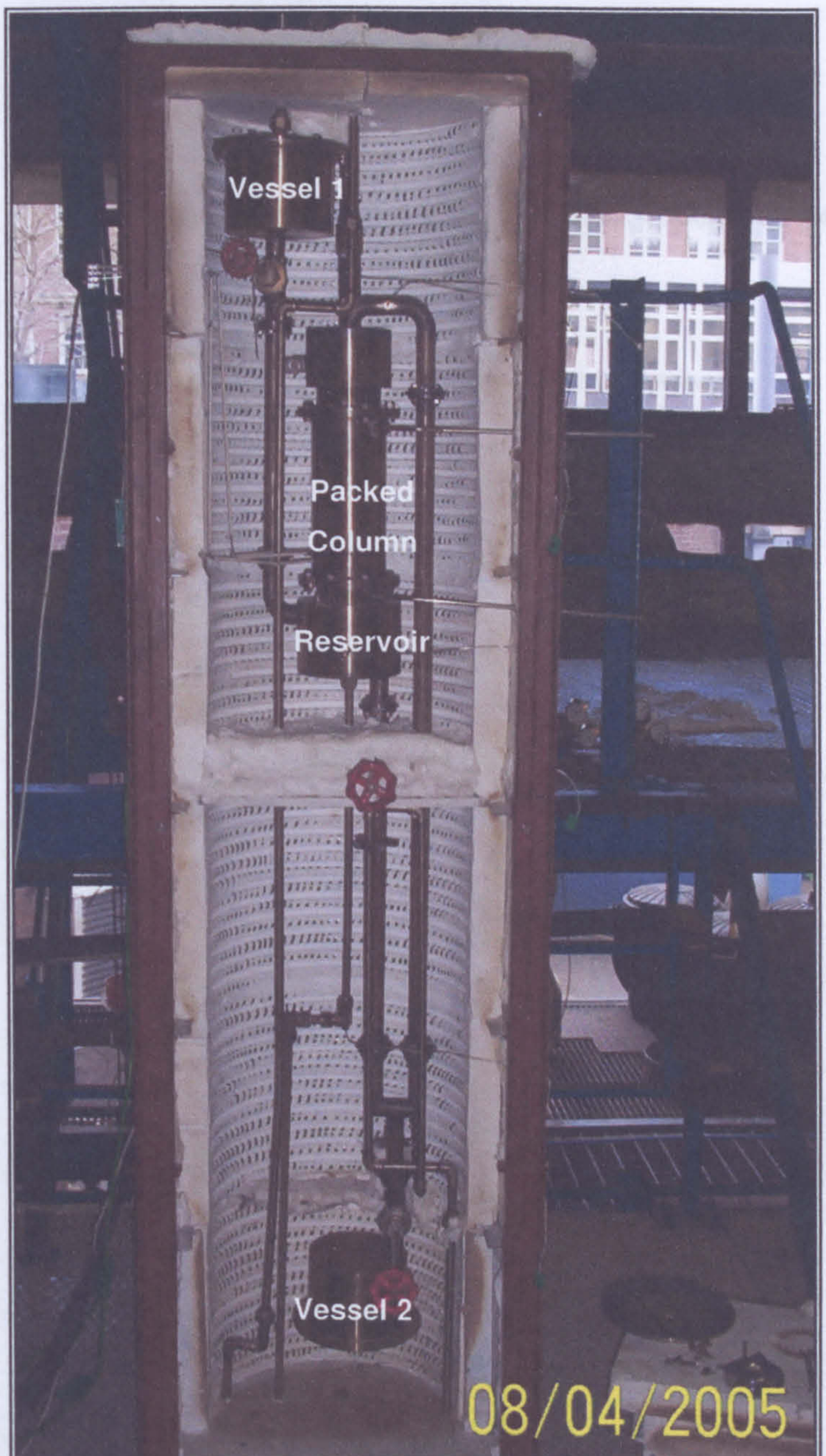

Figure 5.23: Modified hot gas scrubber used for experiments

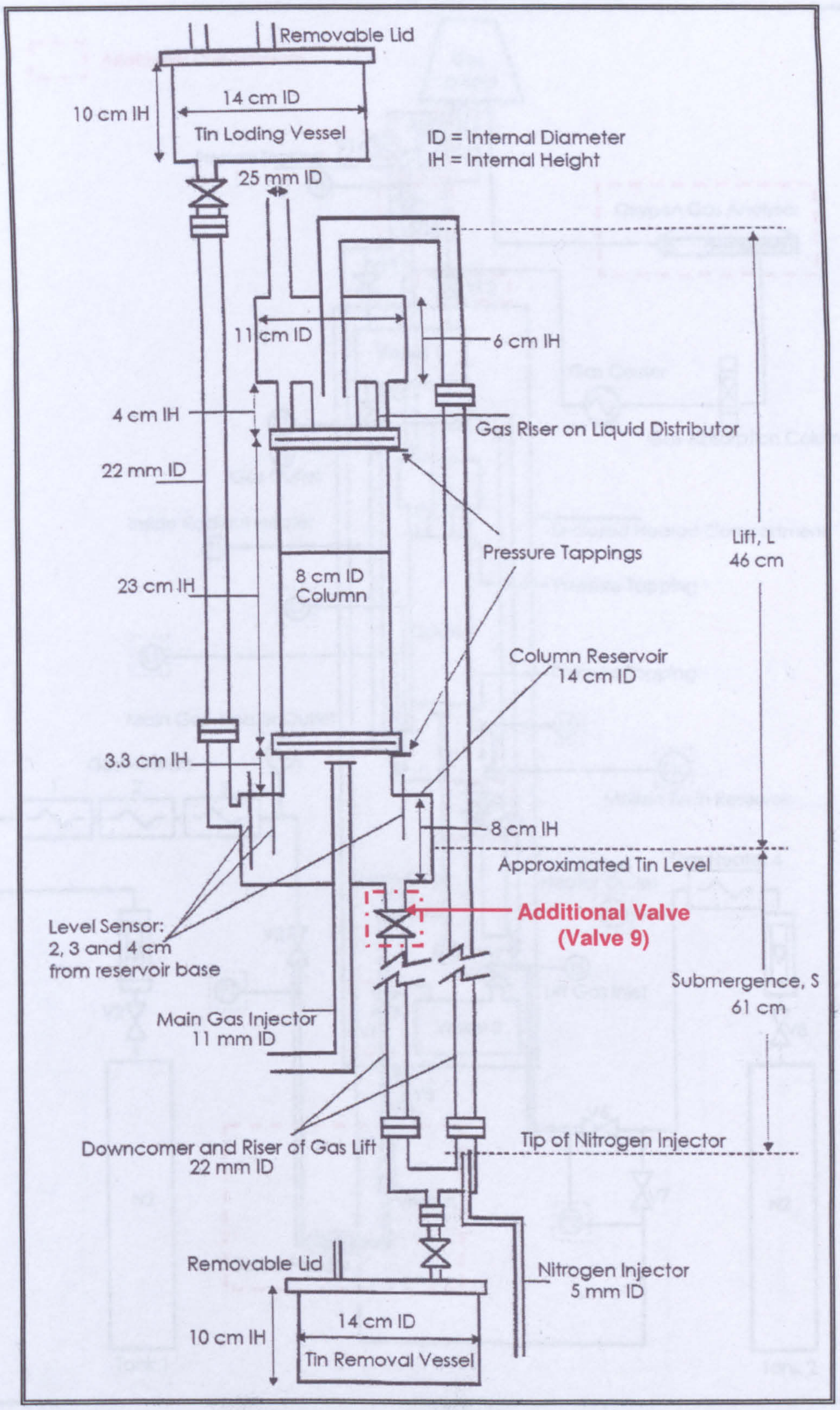

Figure 5.24: Dimensions of the hot gas scrubber with an additional valve

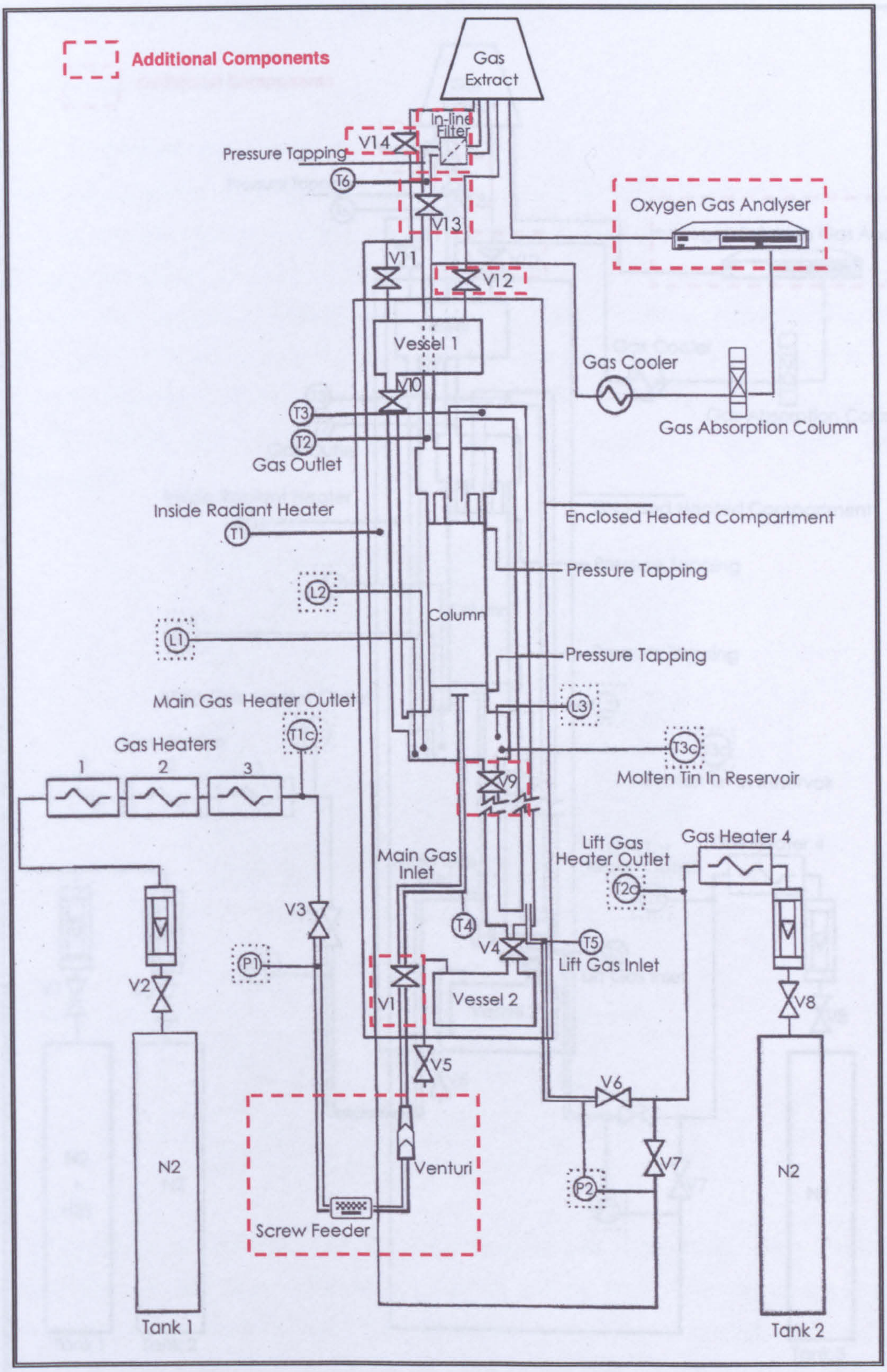

Figure 5.25: New overall particulate cleaning system

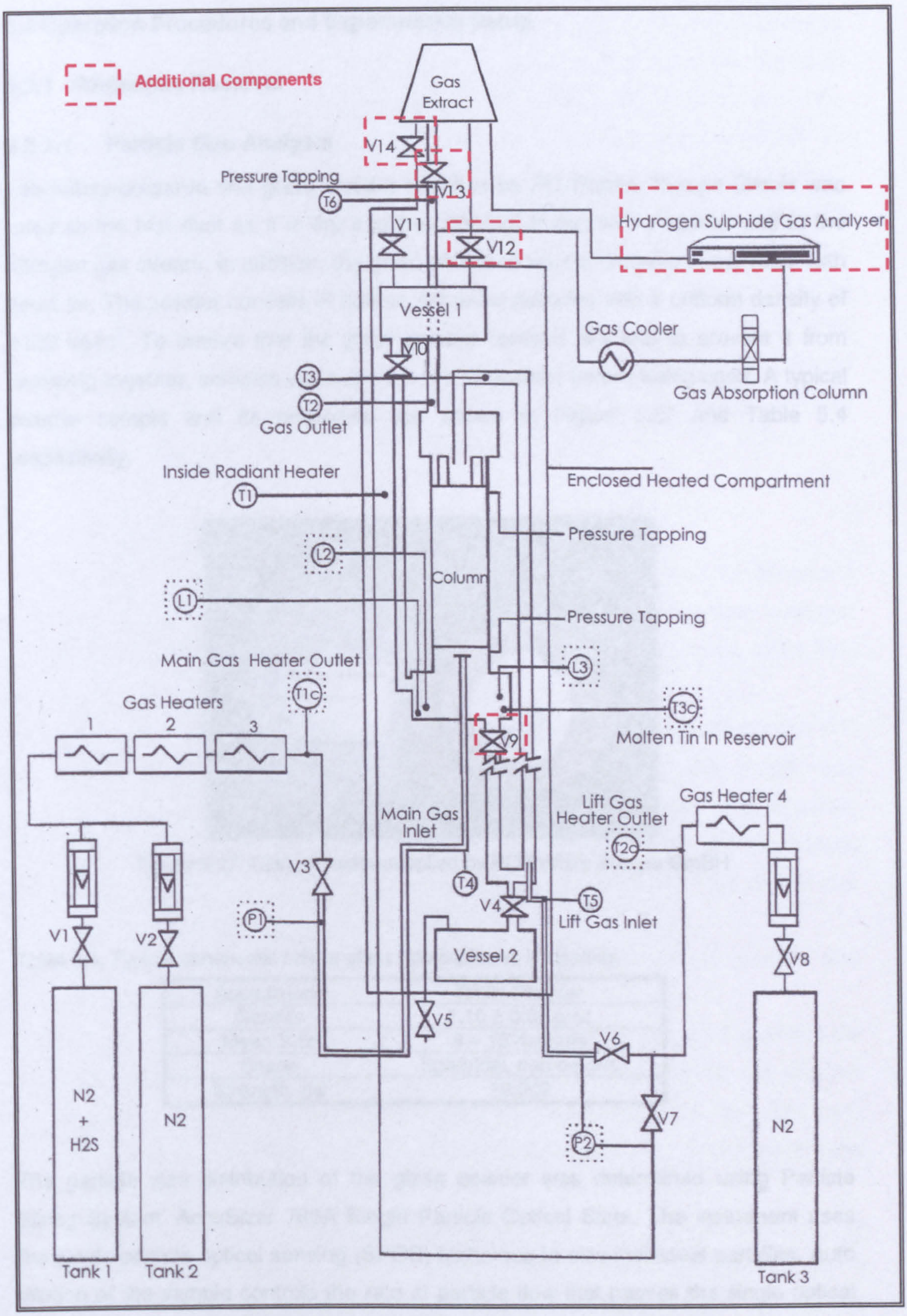

Figure 5.26: New overall H_2S cleaning system

5.3 Operation Procedures and Experimental Setup

5.3.1 Particulate Removal

5.3.1.1 Particle Size Analysis

Laboratory-prepared fine glass powder supplied by PQ Potters Europe GmbH was used as the test dust as it is dry and free flowing. It can also disperse well in the nitrogen gas stream. In addition, the glass powder does not dissolve in nor react with liquid tin. The powder consists of hollow, spherical particles with a uniform density of 1100 kg/m^3. To ensure that the glass powder remains dry and to prevent it from clumping together, samples were dried in the desiccator before being used. A typical powder sample and its properties are shown in Figure 5.27 and Table 5.4 respectively.

Figure 5.27: Glass Powder supplied by PQ Potters Europe GmBH

Table 5.4: Typical spherical® hollow glass microspheres properties

Appearance	White Powder
Density	1.10 ± 0.05 g/cc
Mean Size	9 – 13 microns
Shape	Spherical, non porous
Strength, psi	10,000

The particle size distribution of the glass powder was determined using Particle Sizing System' AccuSizer 780A Single Particle Optical Sizer. The instrument uses the single particle optical sensing (SPOS) technique to size individual particles. Auto dilution of the sample controls the rate of particle flow that passes the single optical particle sensor to a countable rate, preventing any coincidence.

The optical particle sensor uses light scattering principles for sizing particles smaller that several microns and the light obscuration method for larger particles. Individual particles were passed through a laser beam and either the scattering intensity or the amount of light blocked by each particle was measured and transmitted into an electrical pulse. For the former, the scattered intensity pulse height corresponds to the particles' diameter. For the latter, the amount of light blocked and thus the height of the pulse corresponds to the particles' cross section area i.e. the square of the particle diameter. Size distributions were generated from the measurements of thousands of particles. High-resolution particle size analysis was achieved from individual particle sizing. The AccuSizer uses the laser sensor model LE400-0.5SUM having a detectable particle size range from 0.5 to 490 μm. The AccuSizer was controlled via the windows-based CW770 software program.

❋ Experimental Procedures

- ✓ To ensure a representative sampling of the glass powder from its containing bottle, the bottle was gently rolled, changing its orientation continuously such that large and fine particles were mixed thoroughly. A small amount was taken from the bottle.
- ✓ The sample of glass powder was mixed with and dispersed in distilled water in a small container. Using a pipette (10 – 100 μl), 100 μl of this sample was transferred into the AccuSizer dilution chamber containing 60 ml of ultra-filtered, distilled water as the diluent. Sampling was then initiated for 50 ml of the sample suspension at a rate 1 ml/s. Mixing of the sample particles with the diluent was effected by means of a mechanical agitator.
- ✓ A total of 3 sampling runs were carried out and the average particle size distribution obtained.
- ✓ For each sampling, the total number of particles sized was checked such that the maximum limit of 9000 particles/ml (i.e. 450,000 particles for 50 ml) was not exceeded for optimum AccuSizer sampling performance. If the limit was exceeded, the sample in the small container was diluted with distilled water, and the sampling was repeated.
- ✓ Background check: To check whether the distilled water contains particles that can contribute significantly to the overall particle size distribution, the above procedure was repeated but this time without the glass powder i.e. only the distilled water was sampled.

5.3.1.2 Determination of Total Efficiency

❋ **Experimental Setup**

The schematic diagram in Figure 5.25 illustrates the overall hot gas scrubbing system for particulate cleaning. The glass powder was fed into the nitrogen gas supply line using a screw feeder as discussed in section 5.2.5. Isokinetic sampling of the outlet nitrogen stream was carried out using a fabricated in-line filter as illustrated in Figure 5.22 in section 5.2.7. This filter paper was selected for use due to several compelling reasons: it is a resin-bound glass microfibre paper filter that gives exceptionally high particle retention and high loading capacity. Also the disposable filter papers are easily changed in seconds. Filter paper grade GF-A with 1.0 μm particle retention capability was selected for use. The outlet air stream was filtered to determine gravimetrically the mass of test dust unseparated by the packed bed scrubber. The mass of separated dust when divided by the total mass of test dust fed into the column over the period of the experiment gave the total efficiency of particulate removal.

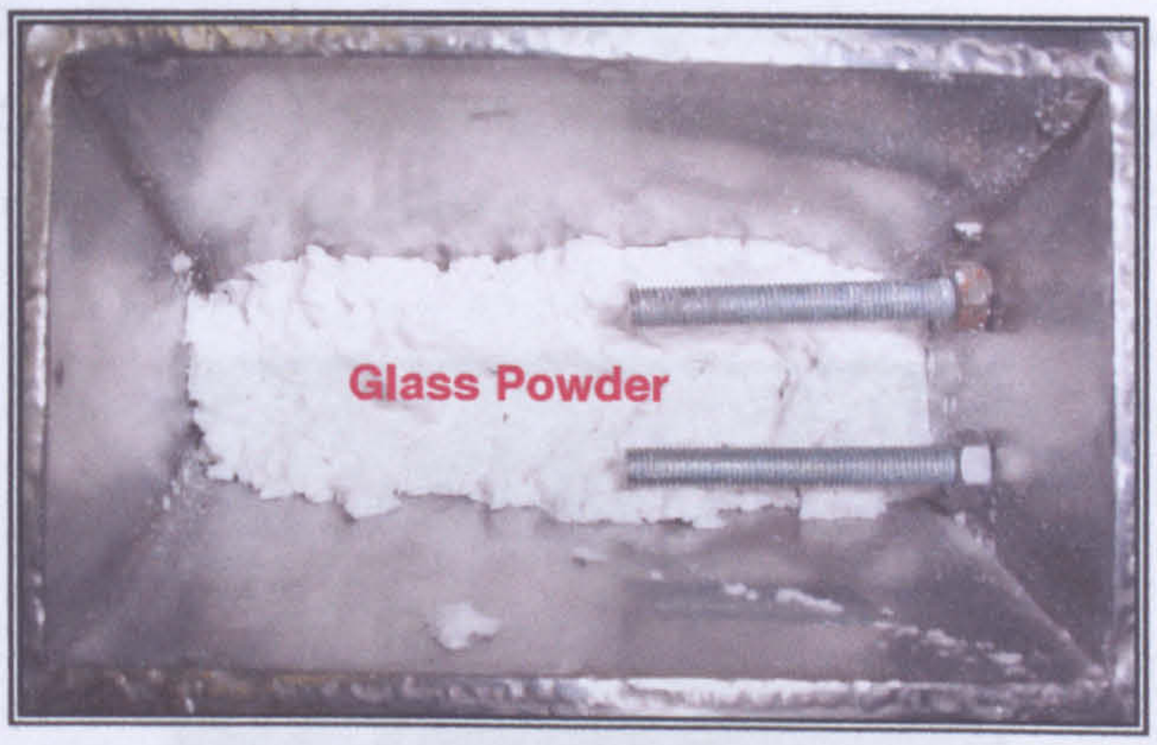

Figure 5.28: Sample in screw feeder

❋ **Operating Parameters**

The key test parameters in this study were gas and tin flowrates. The ranges of test conditions are summarised in Table 5.5. The gas flow rates ranged from 0.245 to 0.581 kg/m^{2}s (gas superficial velocity: 0.490 to 1.161 m/s) with a liquid (tin) flow rate of 2.148, 3.165 or 3.860 kg/m^{2}s (liquid superficial velocity: 3.07×10^{-4}, 4.53×10^{-4} or 5.52×10^{-4} m/s). The operating temperatures were set at 350°C and 400°C.

Table 5.5: Test conditions for hot particulate cleaning in the packed bed scrubber

Test parameters		Unit	Values
N_2 Gas	Flow rate	kg/m^2s	0.245 - 0.581
	Superficial velocity	m/s	0.490 – 1.161
Liquid Tin	Flow rate	kg/m^2s	2.15, 3.17, 3.86
	Superficial velocity	m/s	3.07×10^{-4}, 4.53×10^{-4}, 5.52×10^{-4}
Operating temperature		°C	350, 400

❋ **Experimental Procedures**

- ✓ An unused filter paper was weighed on a microbalance. After about 10 minutes, a constant equilibrium reading was obtained.
- ✓ The filter paper was fitted inside its housing and the whole filter unit was then connected to the nitrogen column gas outlet.
- ✓ Approximately 30 g of glass powder in a plastic container was weighed on the microbalance. The reading was taken after about 2 minutes, i.e. after the reading had stabilised.
- ✓ The glass powder was then placed into the hopper of the powder screw feeder.
- ✓ *Tin Loading*: The Kaowool outer insulating boards were removed from the rig to gain access to Vessel 1. Tin pellets (Figure 5.29) of known weight were loaded into Vessel 1, which was then closed.

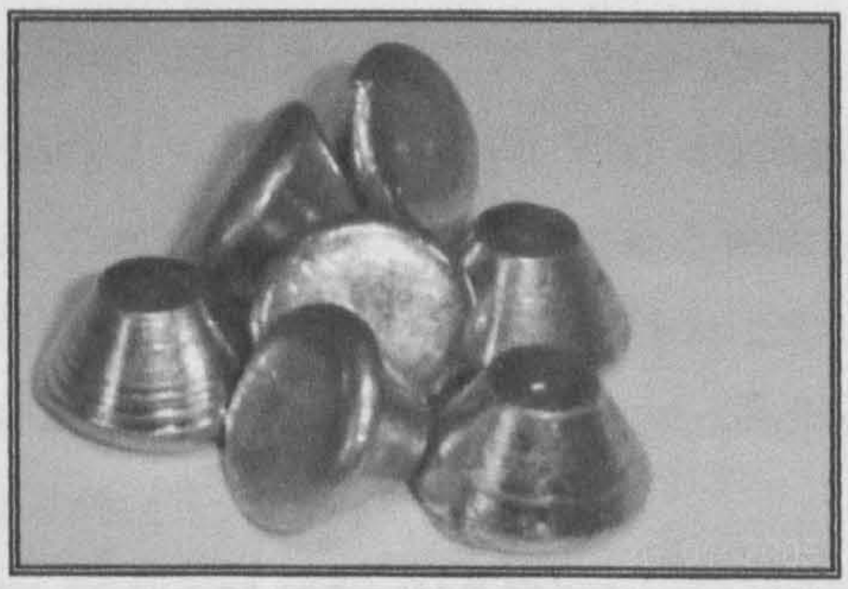

Figure 5.29: Fresh tin

- ✓ *Vessel 2 Lining*: The interior of Vessel 2 was lined with Kaowool paper and then secured back onto the rig. The Kaowool boards were put back onto the rig and the metal cage door screwed.
- ✓ *Ventilation, Gas Sampling Line and Cooling Water*: The room ventilation fans and extract system were turned on. The extract gate was left semi-open to conserve heat. The water supply to the gas cooler (cold finger) was turned on.

- ✓ *System Controller On*: The circuit breaker (i.e. electrical supply to the rig) was switched on. The electronic system controller was tuned on and the desired temperature was set. The oxygen gas analyser was also turned on.
- ✓ *System Purging*: (All valves were initially closed) Valves V4, V5, V9, V10 and valves V3, V7 were fully opened. Valve V2 and V8 were opened and N_2 gas was fed into the system from Tanks 1 and 2 respectively to purge the system of air. Valve V2 was adjusted to minimal flow to conserve the N_2 gas. After a short while, valve V5 followed by V4 were closed.
- ✓ *Radiant Heaters On*: The radiant heaters were turned on using the control panel. The minimal N_2 gas flows from Tanks 1 and 2 were maintained to ensure an inert atmosphere within the scrubber to prevent tin oxidation while the system heats up.
- ✓ *Full Tin Drainage and Full Gas Flow*: Sufficient time was allowed for the tin from vessel 1 to melt and fully drain into the reservoir. This was achieved when level sensors L1, L2 and L3 showed constant readings. At this point, valve V9 was closed. Valves V7 and V8 were closed, shutting off the N_2 supply from Tank 1.
- ✓ The molten tin in the reservoir (T3c) was allowed to reach the desired set point temperature.
- ✓ *Main N_2 Gas at Operating Flow and Heaters On*: The extract gate was fully opened. Valve V2 was adjusted to increase the N_2 flow from Tank 1 to the desired gas flowrate. All gas heaters were turned on from the control panel.
- ✓ *N_2 Lift at Operating Flow and Heater On*: Once the main gas inlet temperature (T4) reached the desired value, valve V6 was opened fully and valve V8 was opened to the gas lift operating flow. Gas heater 4 was turned on from the system control panel. This allows N_2 gas from Tank 2 into the gas lift riser, initiating the molten tin circulation through the packed column. Sufficient time was allowed for the fluid flows to stabilise.
- ✓ Once the oxygen gas analyser indicated there was no air in the system, the dust feeder was switched on at the required feed rate and V1 was fully open to start feed in the glass powder to the system. After approximately 15 to 20 minutes, the screw dust feeder was switched off and the time was recorded. The liquid tin and nitrogen gas supplies were turned off.
- ✓ The glass powder remaining in the screw feeder was removed and weighed. Also filter paper was removed from its housing and weighed. The reading was taken after about 2 minutes, i.e. after the reading has stabilised.

5.3.1.3 Determination of Grade Efficiency

The test dust exiting the packed bed scrubber was collected in an impinger (Figure 5.30) with water as the collecting medium. The particle size distribution of the resulting dust suspension was then determined. This data when used together with the total efficiency determined earlier at the same fluid flowrate and dust loading, and the inlet dust particle size distribution gave the grade efficiency.

- **Experimental Setup**

The experimental setup was essentially the same as that used to determine the total efficiency with the exception of the dust impinger and a valve in place of the in-line filter. The dust-laden nitrogen gas that exited the scrubber entered the impinger via an inlet pipe submerged in about 500 ml of distilled water at a level of about 10 cm. Solid particles entrained in the nitrogen gas stream were removed by direct impingement into water. The clean nitrogen gas then exited the impinger via an outlet pipe. In general as column pressure drop increases, the efficiency of dust separation increases. It was therefore essential that the column pressure drop (whilst using the impinger) was the same as that when the in-line filter was used at the same operating fluid flowrates. This ensured that the dust collected in the impinger would be representative of the dust collected on the filter at the same operating fluid flowrates.

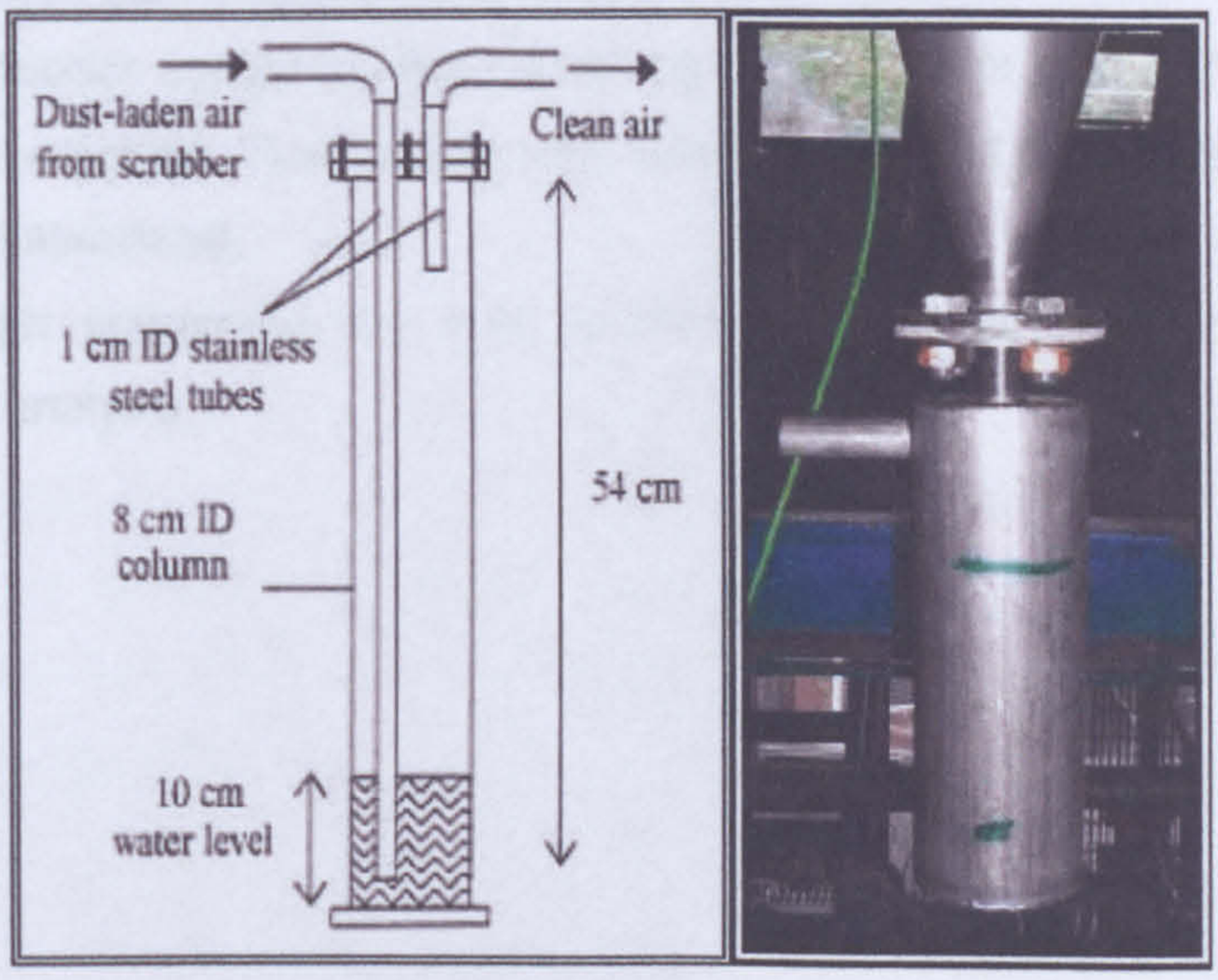

Figure 5.30: Dust impinger

❋ Experimental Procedures

❑ Dust Collection into The Impinger

In this experimental work, the dust exiting the scrubber was collected for only one value of operating fluid and liquid tin flowrates. The pressure drop of the column under steady-state operation at these fluid flowrates was first measured with the in-line filter at the nitrogen gas exit line (Figure 5.31).

- ✓ Approximately 30 g of glass powder in a plastic container was weighed on the microbalance. The reading was taken after about 2 minutes, i.e. after the reading had stabilised. The contents of the plastic container containing the glass powder were then placed into the hopper of the screw feeder.
- ✓ The impinger containing about 500 ml of distilled water was put in place as shown in Figure 5.30. The nitrogen gas supply was turned on at the desired flowrate followed by the liquid tin supply. About 4 to 6 minutes were allowed for steady-state condition to be achieved. The column pressure drop was then measured with a manometer. The valve downstream of the impinger was adjusted until the same column pressure drop was obtained as when the in-line filter was used at the same fluid flowrates. Once this was achieved, the pressure tapping was blocked off.
- ✓ The screw feeder was switched on at the required feed rate. The start time was recorded.
- ✓ After approximately 15 to 20 minutes, the dust feeder was switched off. The liquid tin and nitrogen gas supplies were turned off.
- ✓ The screw feeder containing the remaining glass powder was removed from the hopper and weighed. The reading was taken after about 2 minutes, i.e. after the reading had stabilised.
- ✓ The impinger containing the dust suspension was removed for particle size distribution analysis.

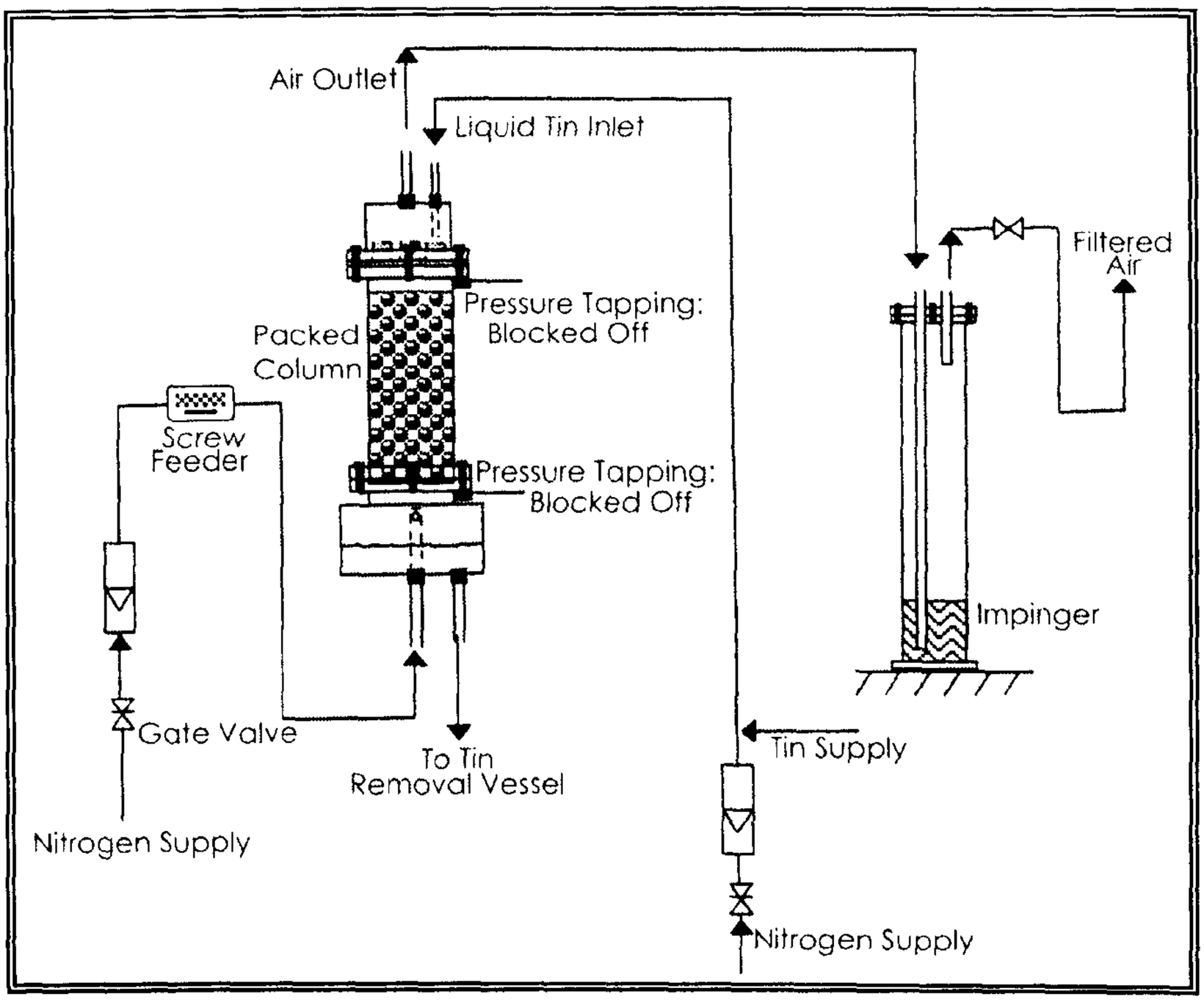

Figure 5.31: Experimental setup to collect unseparated particles for particle size analysis

❑ Particle Size Analysis of Collected Dust Suspensions

- ✓ The dust suspension in the impinger was transferred into a 500 ml beaker. The content of the beaker was magnetically stirred (Magnetic Stirrer SM5 by Stuart Scientific) to ensure uniform mixing of the solid particles in the water. While being stirred, a small amount of sample was drawn off using a pipette into a small container. Then, using a pipette (10 – 100 μl), 100μl of the samples was transferred into the AccuSizer dilution chamber containing 60 ml of ultra-filtered, distilled water as the diluent. Sampling was then initiated for 50 ml of the sample suspension at a rate of 1 m/s.
- ✓ For each test, the total number of particles sized was checked such that the maximum limit of 9000 particles/ml (i.e. 450,000 particles for 50 ml) was not exceeded for optimum AccuSizer sampling performance. If this limit was exceeded, the sample in the small container was diluted with distilled water, and the test was repeated.

5.3.2 Desulphurisation

The following section describes the experimental setup, operating parameters and experimental procedures for gas absorption tests in the scrubber. The schematic diagram in Figure 5.26 illustrates the overall hot gas scrubbing system for the desulphurisation process.

5.3.2.1 Experimental Setup

Hydrogen sulphide (H_2S) from a gas cylinder was mixed with nitrogen gas to provide an inlet gas concentration of 950 ppm H_2S into the column. As the gas mixture rose through the column, H_2S was absorbed into the counter-current flow of molten tin. The gas concentration at the top of the packed bed was measured by an H_2S gas analyser via a stainless steel sampling tube positioned with its open end slightly above the packed bed. The gas that exited from the top of the column was directed into a gas separator.

5.3.2.2 Operating Parameters

The key test parameters in this study were gas flow rate, tin flow rate, inlet H_2S concentration, bed height and temperatures. The ranges of test conditions are summarised in Table 5.6. The gas flow rates ranged from 0.245 to 0.581 kg/m^{2}s (gas superficial velocity: 0.490 to 1.161 m/s) with a liquid (tin) flow rate of 2.148, 3.165 or 3.860 kg/m^{2}s (liquid superficial velocity: 3.07×10^{-4}, 4.53×10^{-4} or 5.52×10^{-4} m/s). The inlet H_2S concentration in N_2 was varied from 300 to 2000 ppm (reference case: 1000 ppm). The height of packing was also varied from 20cm (reference case) to 10 cm and 0 cm (empty column). While the operating temperature was fixed at 400°C as the reference condition for variation of other test parameters, its effect was assessed at 300, 350 and 390°C. Operating temperatures are anticipated to be at least 400°C due to kinetics limitations at lower temperatures as identified from the preliminary gasification test (Chang, 2003), (Schürmann, 1984). As the test gas is a mixture of H_2S in nitrogen, there is no serious concern over SnO_2 formation. However if a simulated fuel gas with a high water vapour content is used, the scrubber will be operated at a temperature above 500°C to avoid SnO_2 dross formation.

Table 5.6: Test conditions for hot gas desulphurisation in the packed bed scrubber

Test parameters		Unit	Values
Gas	Flow rate	kg/m^2s	0.245 - 0.581
	Superficial velocity	m/s	0.490 – 1.161
Liquid Tin	Flow rate	kg/m^2s	2.15, 3.17, 3.86
	Superficial velocity	m/s	3.07×10^{-4}, 4.53×10^{-4}, 5.52×10^{-4}
Inlet H_2S concentration		ppm	300 - 2000
Height of packing		mm	200, 100, 0 (empty column)
Operating temperature		°C	300, 350, 390, 400

5.3.2.3 Experimental Procedures

- ✓ *Tin Loading*: The Kaowool outer insulating boards were removed from the rig to gain access to Vessel 1. Tin pellets of known weights were loaded into Vessel 1, which was then closed.
- ✓ *Vessel 2 Lining*: The interior of Vessel 2 was lined with Kaowool paper and then secured back onto the rig. The Kaowool boards were later placed back onto the rig and the metal cage door screwed.
- ✓ *Ventilation, Gas Sampling Line and Cooling Water*: The room ventilation fans and extract system were turned on; the extract gate was left semi-open to conserve heat. The water supply to the gas cooler (cold finger) was turned on. The necessary sampling equipment was put in place at the end of the gas sampling line.
- ✓ *System Controller On*: The circuit breaker (i.e. electrical supply to the rig) was switched on. The electronic system controller was turned on and the desired temperature was set. The GC on-line analyser (ABB-PGC2000) was also turned on in order to monitor the gas concentration in the system.
- ✓ *System Purging*: (All valves are initially closed) Valves V4, V5, V9, V10 and valves V3, V7 were fully open. Valves V2 and V8 were open and N_2 gas was fed into the system from tanks 2 and 3 respectively to purge the system of air. Valves V2 and V8 were adjusted to minimal flow to conserve the N_2 gas. After a short while, valve V5 followed by V4 were closed.
- ✓ *Radiant Heaters On*: The radiant heaters were turned on from the control panel. The minimal N_2 gas flow from tank 2 and 3 were maintained to ensure an inert atmosphere within the scrubber in order to prevent tin oxidation while the system was heated up.

- ✓ *Full Tin Drainage and Full Gas Flow*: Sufficient time (5 to 10 minutes) was allowed for the tin from vessel 1 to melt and fully drain into the reservoir and gas lift limbs. At this point, valve V9 was closed. Valves V7 and V8 were closed, shutting off N_2 supply from Tank 3. The molten tin in the reservoir (T3c) was allowed to reach the desire set point temperature.
- ✓ *Main N_2 Gas at Operating Flow and Heaters On*: The extract gate was fully opened. Valve V2 was adjusted to increase the N_2 flow from Tank 2 to the desired gas flowrate i.e. the same flowrate as the N_2/H_2S gas mixture, which was to be introduced later. All gas heaters were turned on using the control panel.
- ✓ *N_2 Lift at Operating Flow and Heater On*: Once the main gas inlet temperature (T4) reached the desired value, gas heater 4 was turned on using the system control panel.
- ✓ Valve V6 was opened fully and Valve V8 was opened to the gas lift operating flow. This allows N_2 gas from Tank 3 into the gas lift riser, initiating the molten tin circulation through the packed column.
- ✓ *H_2S Flow Initiation and Gas Sampling*: Once the gas lift inlet temperature (T5) reached the desire value, V2 was closed and V1 opened to allow the N_2/H_2S mixture from Tank 1 into the system at the same flowrate as the initial N_2 gas flow from Tank 2. Gas sampling was then initiated. Typically, 30 to 40 minutes were allowed for the system to acquire constant concentration readings on the GC. For the tests with different H_2S concentrations, N_2 from Tank 2 was added to the N_2/H_2S mixture from Tank 1.

5.3.3 Normal Shut-Down Procedures

- ✓ The gas sampling line was clamped. The gas sampling equipment was switched off and disconnected.
- ✓ Valve V6 was closed followed by V1, stopping the molten tin circulation. Valve V8 was then fully shut.
- ✓ All the gas heaters and the radiant heaters were switched off from the system control panel. The circuit breaker was turned off.
- ✓ Valve V2 was opened to allow N_2 gas into the system.
- ✓ Valve V4 was opened fully to allow the molten tin to drain into Vessel 2. Valve V5 was opened slightly to aid tin drainage.
- ✓ Sufficient time was allowed for the solidified tin as well as all the gas heaters to cool down to room temperature before turning off the N_2 gas supply from Tank 2.

5.3.4 Emergency Shut-Down Procedures

- ✓ All the gas heaters and the radiant heaters were switched off from the system control panel. The circuit breaker was turned off.
- ✓ Valve V6 was closed followed by V1, stopping the molten tin circulation. Valve V8 was then fully shut.
- ✓ Valve V2 was opened to allow N_2 gas into the system, maintaining an inert atmosphere.
- ✓ Valve V4 was opened fully to allow the molten tin to drain into Vessel 2.
- ✓ Sufficient time was allowed for the solidified tin as well as all the gas heaters to cool down to room temperature before turning off the N_2 gas supply from Tank 2.

* ***Normal and Emergency Shut-Down Procedures:***

Tank 2 referring to the main N_2 Gas in H_2S cleaning system while in particulate cleaning system referring to Tank 1.

5.3.5 Tin Sulphide Cleaning

Tin sulphide cleaning tests were carried out in an electrical heated horizontal furnace using zinc powder. Nitrogen gas was used as a cleaning environment. The cleaning process for a known mass of tin sulphide was carried out with and without zinc powder. The effects of zinc and without zinc powder on tin sulphide during the cleaning process were investigated.

5.3.5.1 Experimental Setup

Figure 5.32 illustrates the overall experimental rig used for the tin sulphide cleaning studies. High purity of N_2 gas (99.95%) was used in order to create an inert atmosphere for the cleaning process. The N_2 gas entered the furnace in which a crucible containing the tin sulphide and zinc powder were placed at the central hot zone. Finally, the product gas was removed from the furnace via an extractor. The furnace had double concentric combustion tubes fitted through its centre

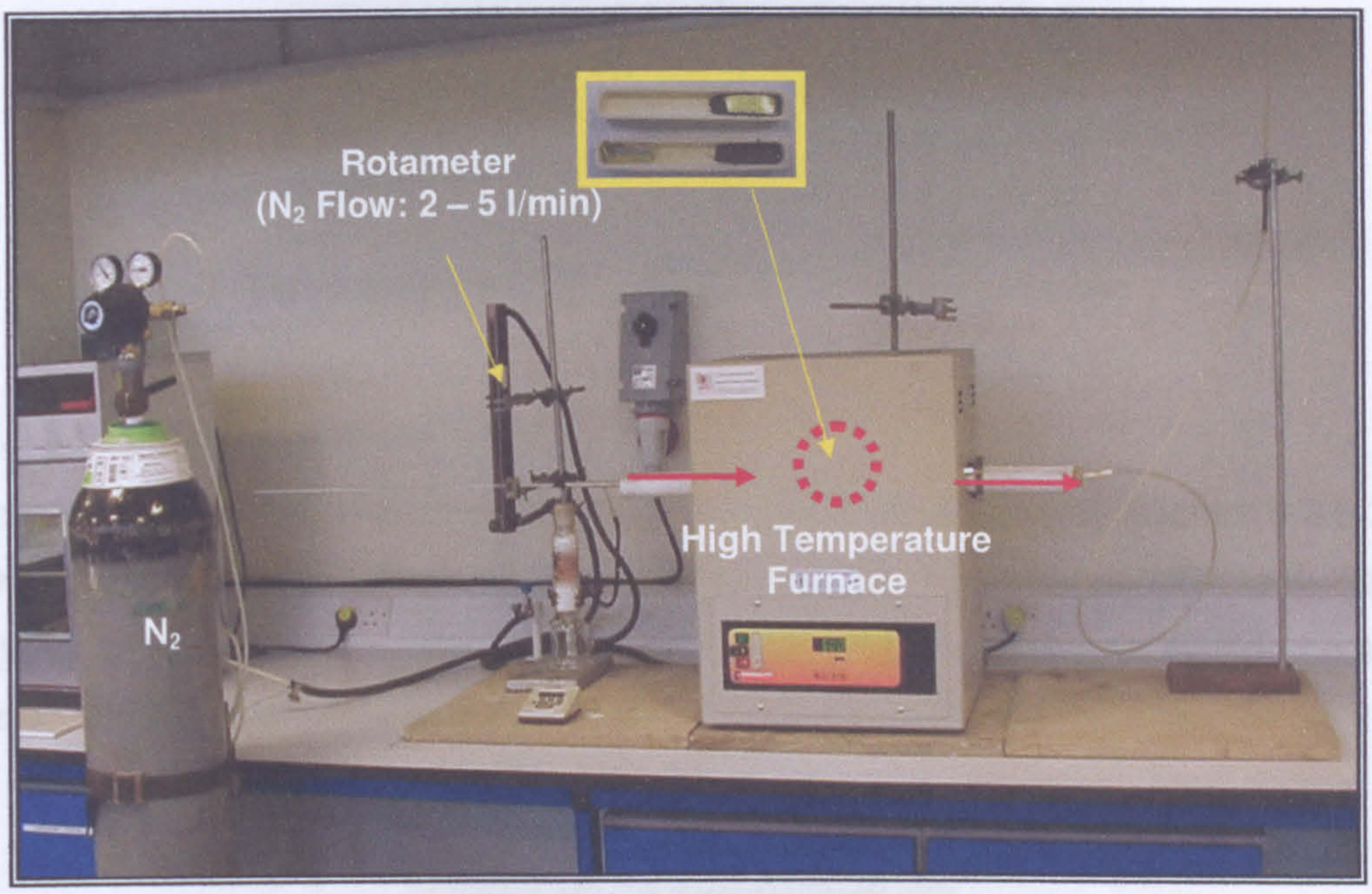

Figure 5.32: Experimental setup for tin sulphide cleaning in the present of zinc powder

5.3.5.2 Operating Parameters

Temperature: Cleaning of tin sulphide was carried out at 400℃ (set point of the furnace) i.e. the temperature of the central hot zone in the combustion tube.

Nitrogen Gas: A continuous flow of nitrogen gas at approximately 2 liter/min was supplied through the hot furnace while the furnace was being heated up to 400℃. This flushed out the air in the cleaning tube and helped to maintain an inert atmosphere, preventing oxidation of the tin sulphide and zinc powder.

Tin Sulphide Samples: Tin sulphide with a known mass was used as a sample.

Zinc Powder: A known mass of zinc powder was used in this investigation.

5.3.5.3 Experimental Procedures

5.3.5.3.1 Cleaning In The Presence of Zinc Powder

Approximately 2 g of tin sulphide samples and 10 g of zinc powder were heated in the central hot zone of the furnace (Figure 5.33) from room temperature to approximately 400℃ in the inert N_2 gas atmosphere. Approximately 4 hours were given for the system to achieve the desired reaction between tin sulphide and zinc powder.

Figure 5.33: Tin sulphide and zinc powder in a crucible

5.3.5.3.2 Cleaning Without Zinc Powder

Essentially the same experimental procedures as that outlined in Section 5.3.5.3.1 were adopted herein. The only difference was that the experimental work took place in glass flask as shown in Figure 5.34. The flask was heated by an electric heater. The tin sulphide sample was weighed before and after each test run.

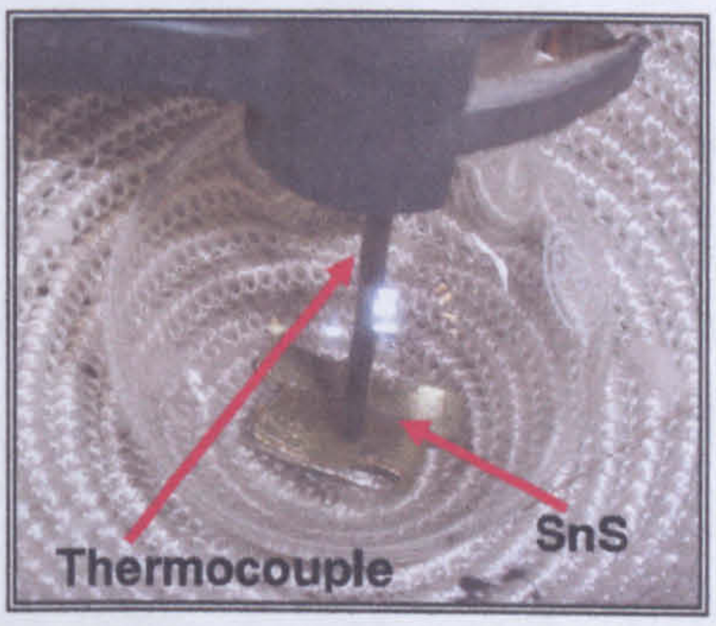

Figure 5.34: Tin sulphide in a flask

The overall setup for the experimental rig used for tin sulphide cleaning without zinc powder is illustrated in Figure 5.35.

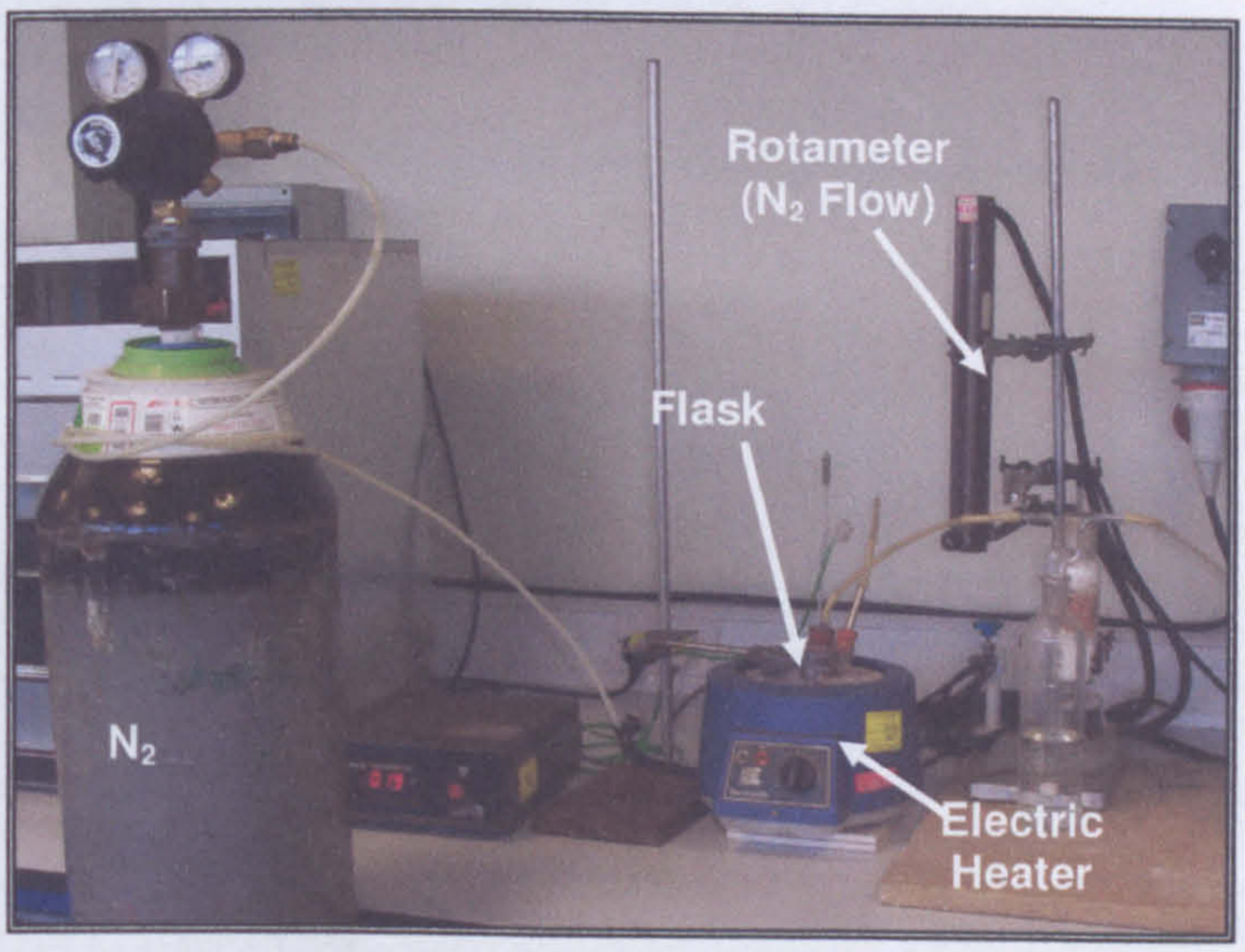

Figure 5.35: Experimental setup for tin sulphide cleaning without zinc powder

5.4 Summary

The main objective of this experimental programme was to study the particulates removal and gas absorption performance of the packed bed hot gas scrubber using molten tin. Previously, this equipment was designed to study only the desulphurisation process. But, in this research work, the existing equipment has been modified in order to investigate the process of particulate cleaning. Various parts of the equipment have been modified such as the packing support plate, gas heaters, air seal and gas lift. For particulate removal tests, an additional system was added to the original design i.e. particle feeder. It consisted of a screw feeder and a venturi system. An on-line filter was also added to the system to determine the total efficiency of particle removal. The key test parameters in particle removal tests were gas and tin flowrates. The operating temperatures were set at 350°C and 400°C respectively. The key test parameters in the desulphurisation tests were gas flow rate, tin flow rate, inlet H_2S concentration, bed height and temperatures. The operating temperature was fixed at 400°C as the reference condition for variation of other test parameters, but its effect was also assessed at 300, 350 and 390°C. Required operating temperatures were anticipated to be at least 400°C due to kinetics limitations at lower temperatures as identified from the preliminary gasification test (Chang, 2003), (Schürmann, 1984). Towards the end of this experimental work, tin sulphide cleaning tests were performed to investigate the effects of zinc and without zinc powder on tin sulphide during the cleaning processes. The results are presented in Chapter 6.

CHAPTER SIX

Experimental Results and Discussion

This chapter presents the results obtained from the experimental studies performed during the course of this research. Comparisons are also made with the published findings from Chang (2003). The results obtained from the particulate cleaning study are considered first, followed by results acquired from the tests on desulphurisation. Finally, the last section of this chapter looks into the tin sulphide cleaning tests which were performed in order to examine the effects of zinc powder addition to the tin sulphide formed during the cleaning processes.

6.1 Particulate Cleaning

6.1.1 Particle Size Distribution of Glass Powder

The suspension of glass powder in distilled water was found to contain particles ranging from 1.5 to 45 μm. In this test the glass powder particles were assumed to be spherical. The average number % distribution was evaluated from results obtained from three dust sampling tests shown in Figure 6.1. This figure also shows almost identical results for all three test runs. It was noted that the size distribution curves were reproducible.

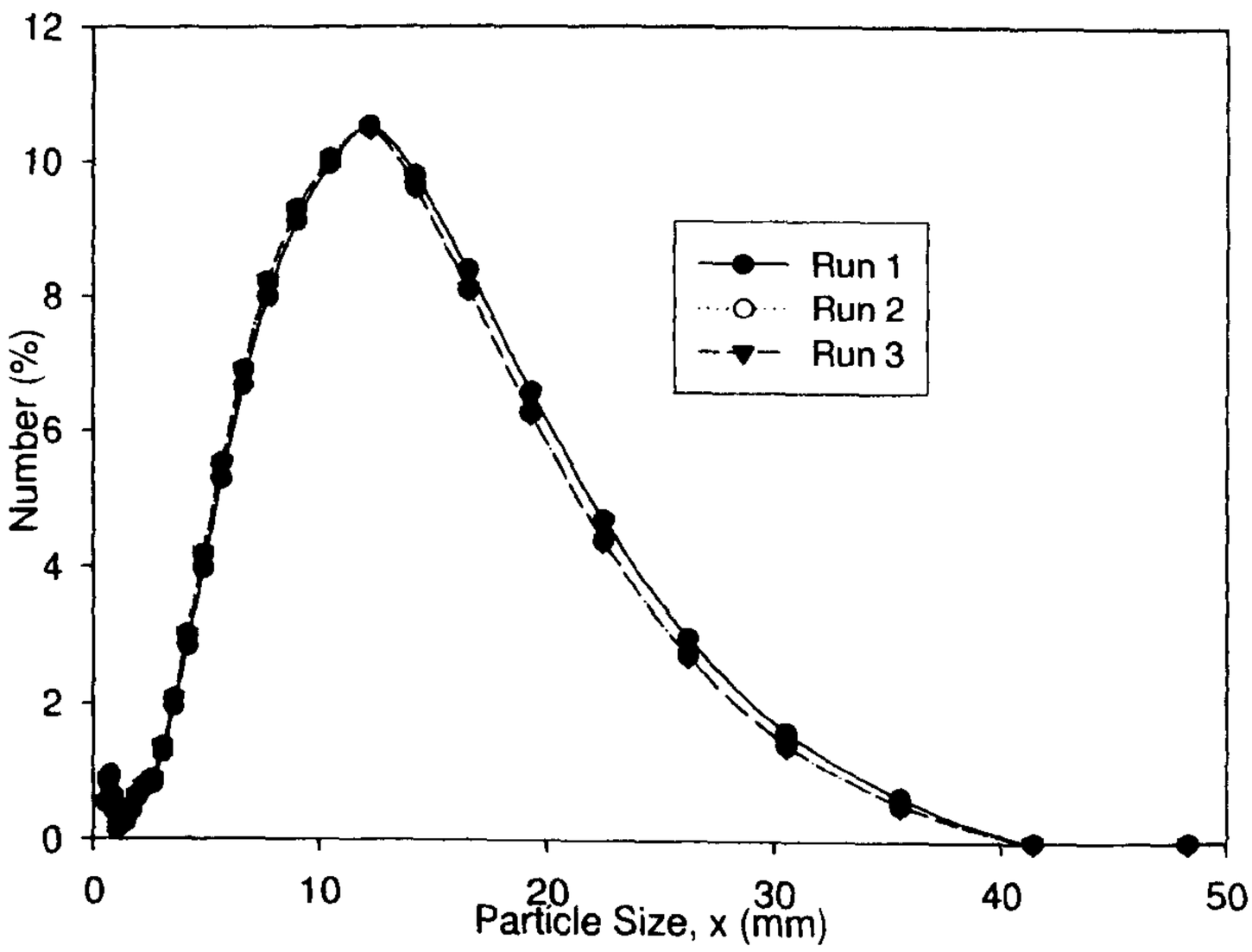

Figure 6.1: Number distribution for glass powder suspension

6.1.2 Experimental Observation

Due to the complex operational characteristics of this hot gas scrubber, several trial runs were carried out before the best start-up procedure was determined. One of the main problems was the solidification of tin especially in valves V4, V9 and V10 after each experiment. Prior to running any experiment, any solid tin had to be cleaned and removed from the valves to prevent blockage. For safety reasons this experimental work could not be performed outside working hours. This therefore introduced a time constraint whereby each experimental run was limited to a maximum of 8 hours. The heat-up of the system was relatively slow and thus it took approximately 6 hours to reach stable conditions. However, after 6 hours the bed temperature was only around 400℃ and this was only just high enough for the most crucial part of the gasification process. Therefore, all the experiments especially for desulphurisation were conducted at 400℃ for about 30mins.

This experimental work was carried out using nitrogen gas for tin circulation at high temperature (350 - 400℃) while the inlet particles were at the ambient temperature of 15ºC. The dust particle feed rate was derived from the N_2 flow rate under different scrubber operating temperatures of 350℃ and 400℃. Solidification of liquid tin from high temperature onto the cool surface of glass particles resulted in solid tin build-up on the surface of glass particles. Inertial deposition was expected to be the main particle collection mechanism whilst Brownian diffusional capture was negligible as the dust particle size was greater than 1.5 μm. Interaction and coalescence of bed materials with the glass particles were considered to be the primary source of agglomeration in the packed bed scrubber. The second source is the accumulation of glass particles and solid tin mixture (Si-Sn). Precipitation of the solid tin mixture deposited inside the column will block the flow and disrupt the circulation. Figure 6.2 is an image of the alumina combustion tube after 3 runs with some accumulation of the Si-Sn mixture. Subsequent test runs showed an increase in agglomerated Si-Sn mixture (Figure 6.3). The reason being that smaller particles tend to coagulate and as the particles grow in size, they will attach to other larger particles. Moreover, the solidification of tin enhances the increase in the agglomerated mixture.

Figure 6.2: A photograph of agglomerates from the solidification of liquid tin and glass powder after 3 runs in the scrubber

Figure 6.3: A photograph of blockage caused by the solidification of liquid tin and glass powder at the end of all runs (8-10 runs)

In this study, particles of 5-7 μm were most abundant at the filter paper exit as shown in the unseparated particles curve of Figure 6.4. Also shown in Figure 6.4, the liquid tin is capable of trapping particles larger than 7 μm inside the scrubber. The volume percent capture decreased for particle size between 10 to 40 μm. This is an indication that the smaller particles are released into the exhaust gas due to heavy attrition.

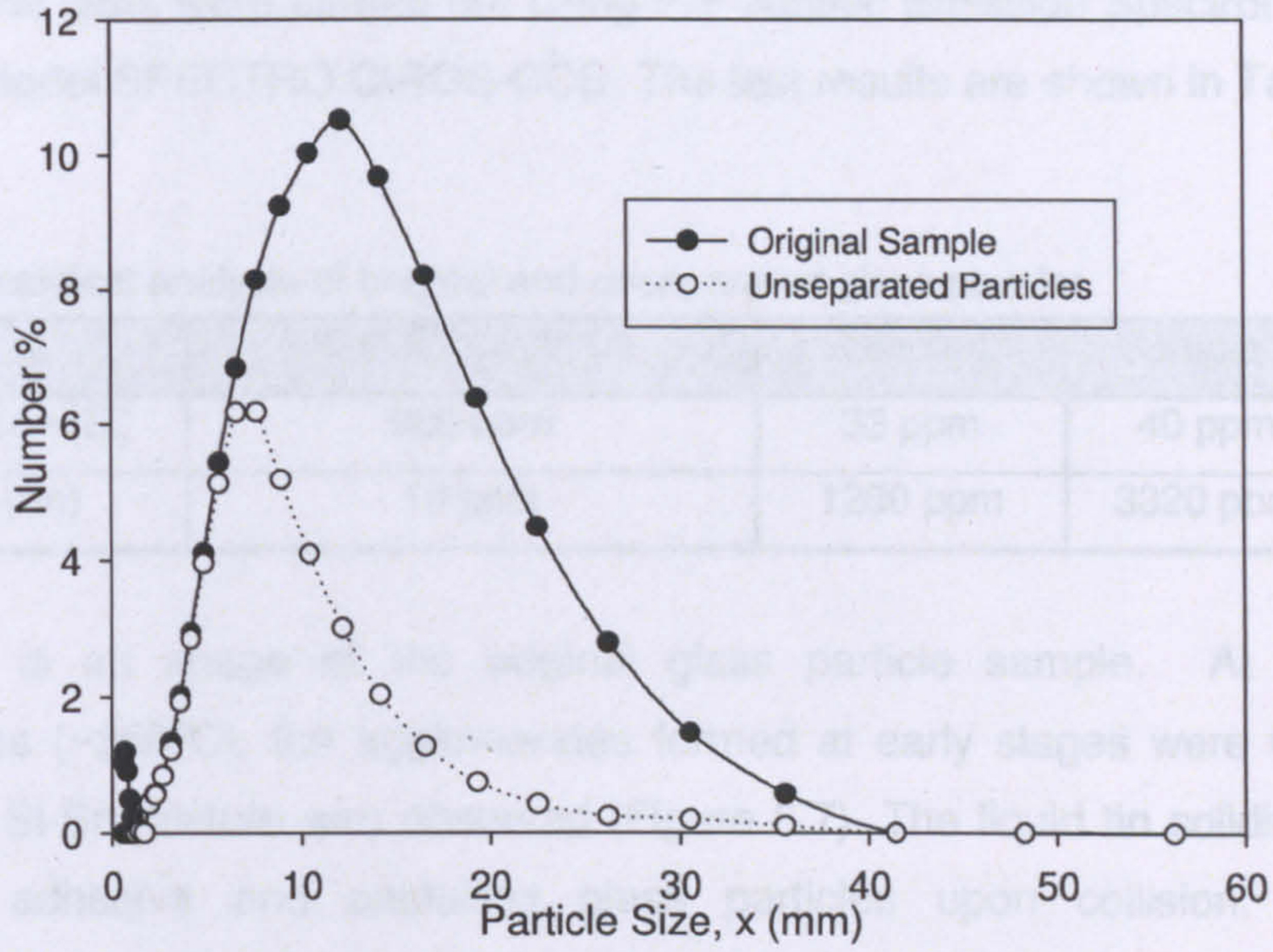

Figure 6.4: Number distribution for unseparated glass particles (Test 1a) and total amount of original particles loading

Throughout the experiments, liquid tin splashes were observed in the exhaust side of the scrubber, which was connected to the filter system. At some point during the particulate removal experiment, some of the liquid tin splashed and accumulated at the exhaust pipe. The deposit on the filter paper consisted mostly of the Si-Sn mixture. The total separation efficiencies obtained from these studies did not represent the actual process. Therefore the total weight of the unseparated sample includes splashed tin, solidification of liquid tin and glass particles (shown in Figure 6.5), which resulted in lower total separation efficiency. The average splashed tin found on the filter paper was around 5.45 g.

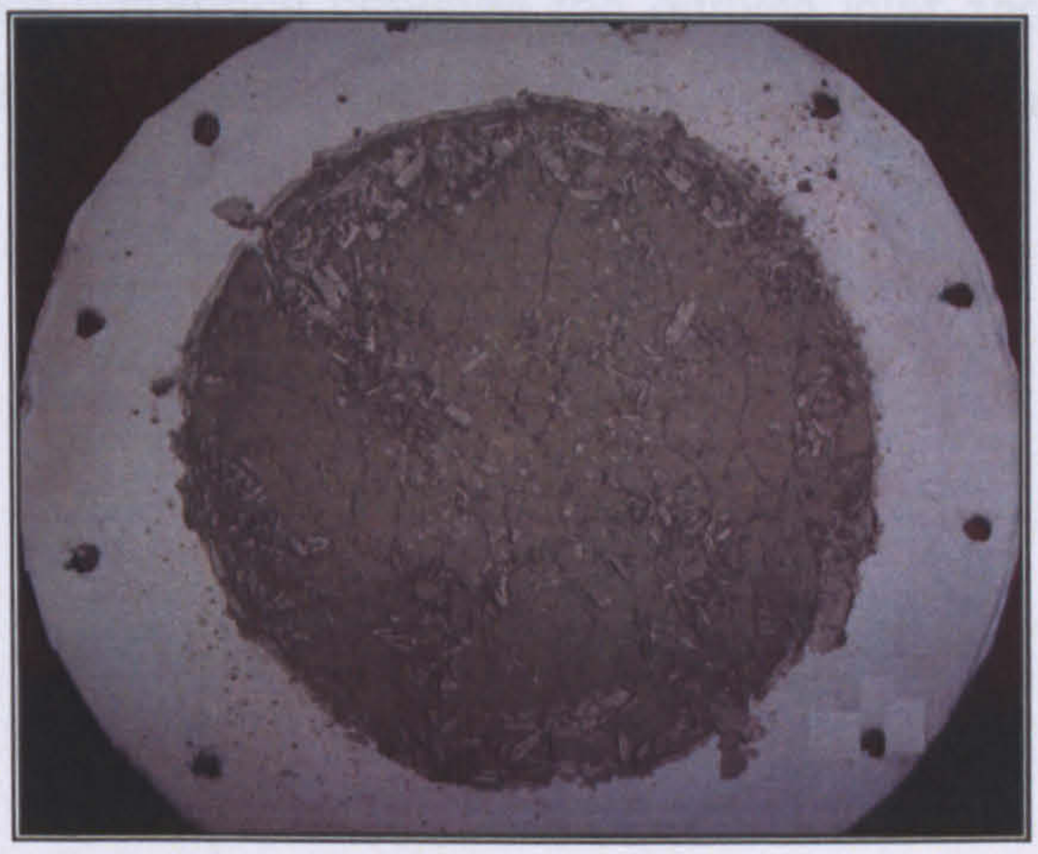

Figure 6.5: Unseparated glass powder on the filter paper

Three samples were sent for analysis to the Chemistry Department, University of Sheffield. The tests were carried out using ICP-Atomic Emission Spectrometry (ICP-AES) with model SPECTRO CIROS-CCD. The test results are shown in Table 6.1.

Table 6.1: Chemical analysis of original and unseparated glass powder

	Sample 1 (Original Sample)	Sample 2	Sample 3
Silicon (Si)	900 ppm	33 ppm	40 ppm
Tin (Sn)	10 ppm	1280 ppm	3320 ppm

Figure 6.6 is an image of the original glass particle sample. At lower bed temperatures (~350℃), the agglomerates formed at early stages were very fragile and a grey Si-Sn mixture was observed (Figure 6.7). The liquid tin solidified slowly, making it adhesive and capturing glass particles upon collision. At higher temperatures (400℃), the formed agglomerates were stronger and had a black colour (Figure 6.8). This is associated with liquid tin, which solidified more rapidly during the filtration process. Images were visually analysed using an optical stereomicroscope and the yellowish tint was caused by the light reflection under the microscope, which resulted in slight colour difference to the actual sample. As can be seen in Figures 6.6, 6.7 and 6.8 respectively, the colour of the glass particles was different when the operating temperature was altered from 350℃ to 400℃. It was mainly due to the rate of solidification of liquid tin during the process and this also proved that the agglomeration processes were sensitive to temperature.

The composition of the glass particles and tin are shown in Table 6.1 and Figure 6.9 respectively. Therefore the higher the operating temperature of the scrubber, the higher the temperature difference between the particle inlet and the scrubber. The higher temperature difference will cause more solid tin to solidify on the glass particle surfaces.

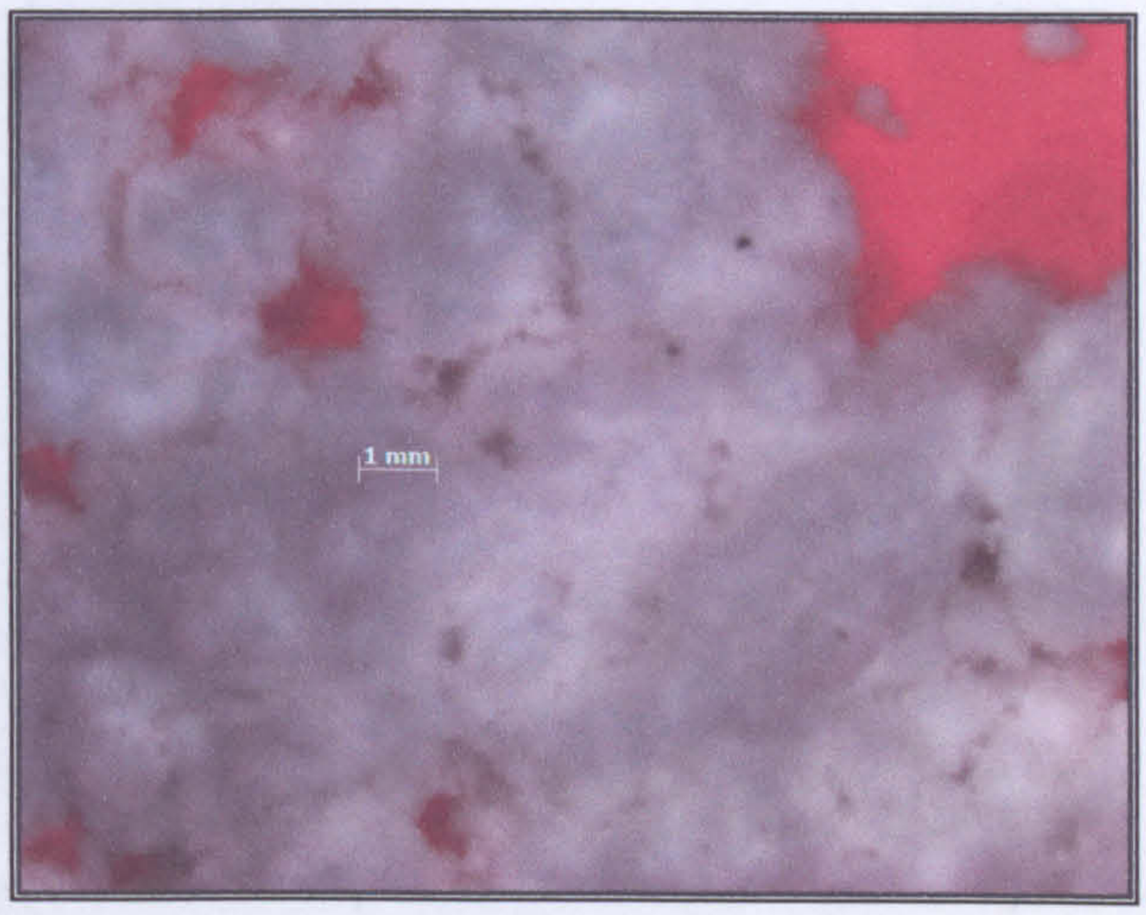

Figure 6.6: Original sample of glass powder (Sample 1)

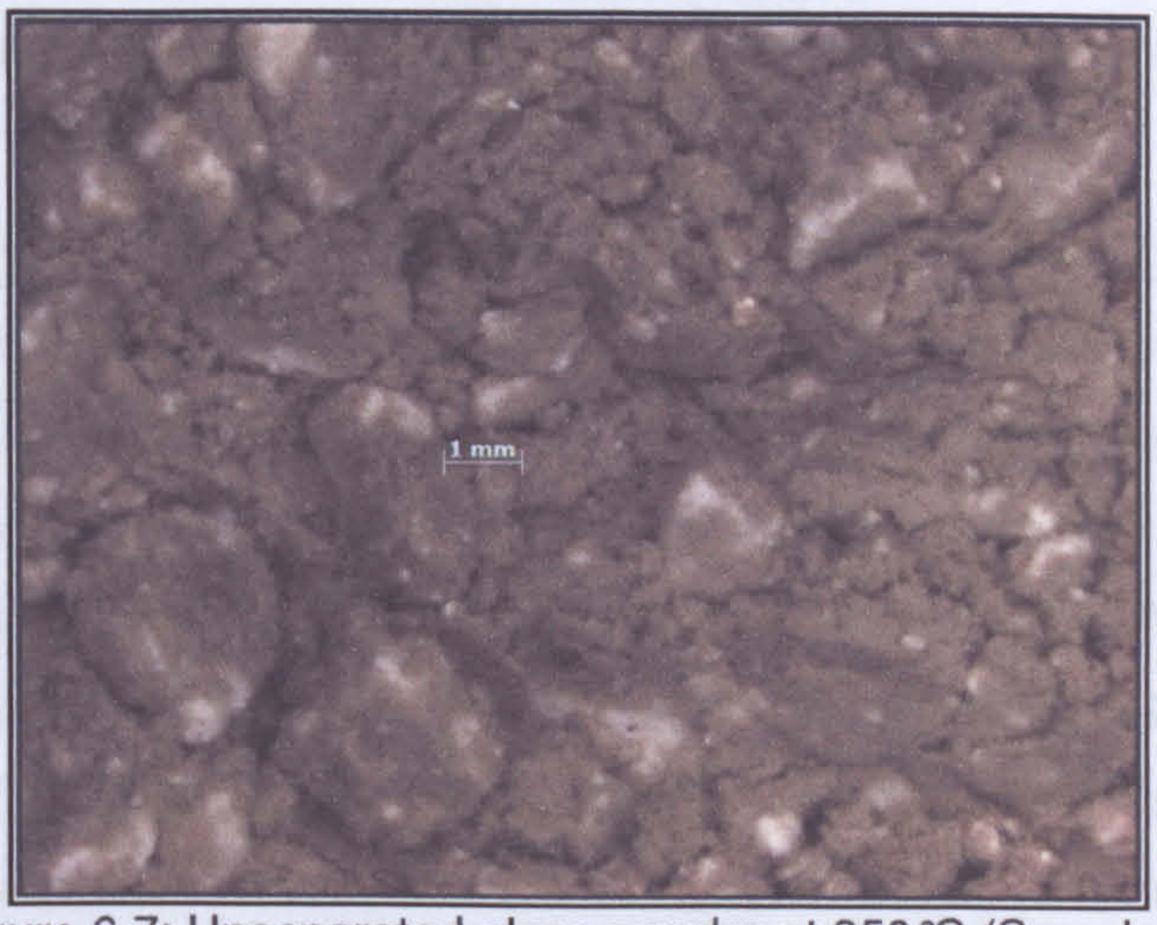

Figure 6.7: Unseparated glass powder at 350 °C (Sample 2)

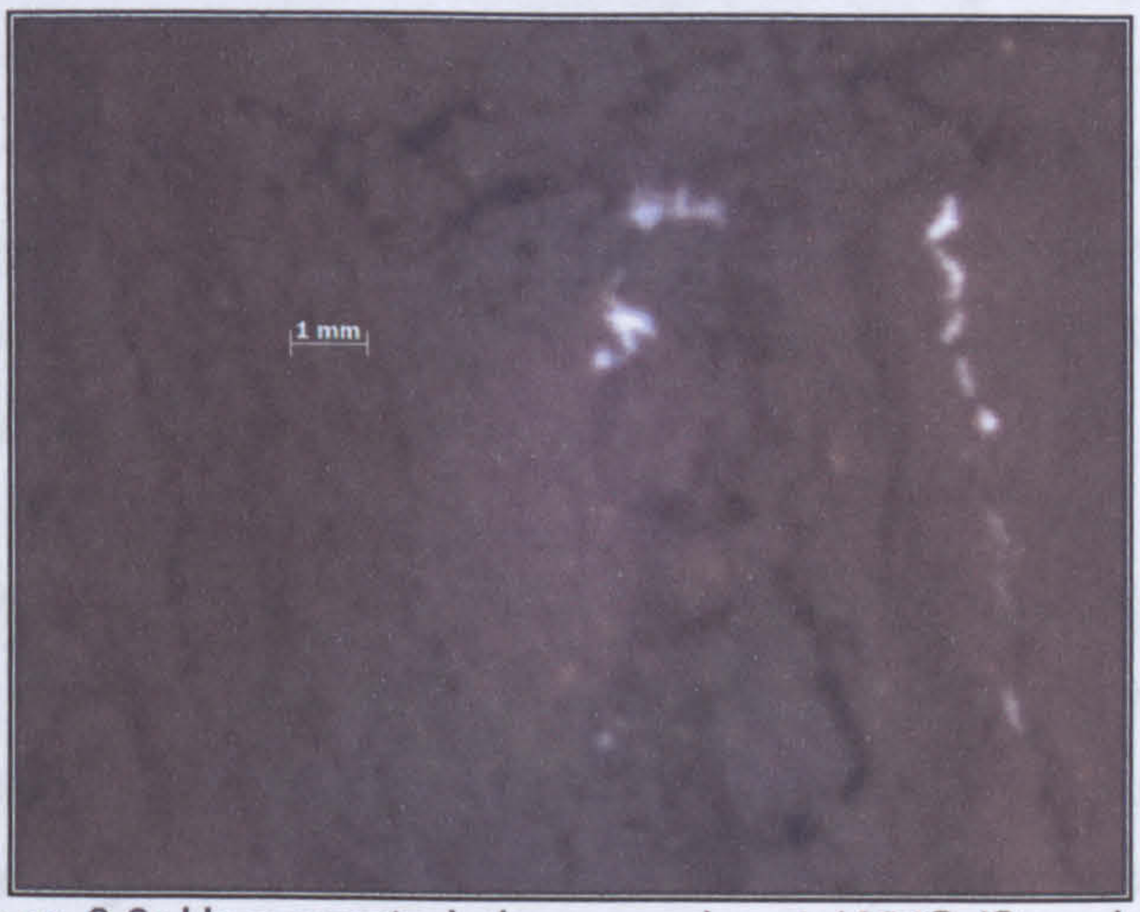

Figure 6.8: Unseparated glass powder at 400 °C (Sample 3)

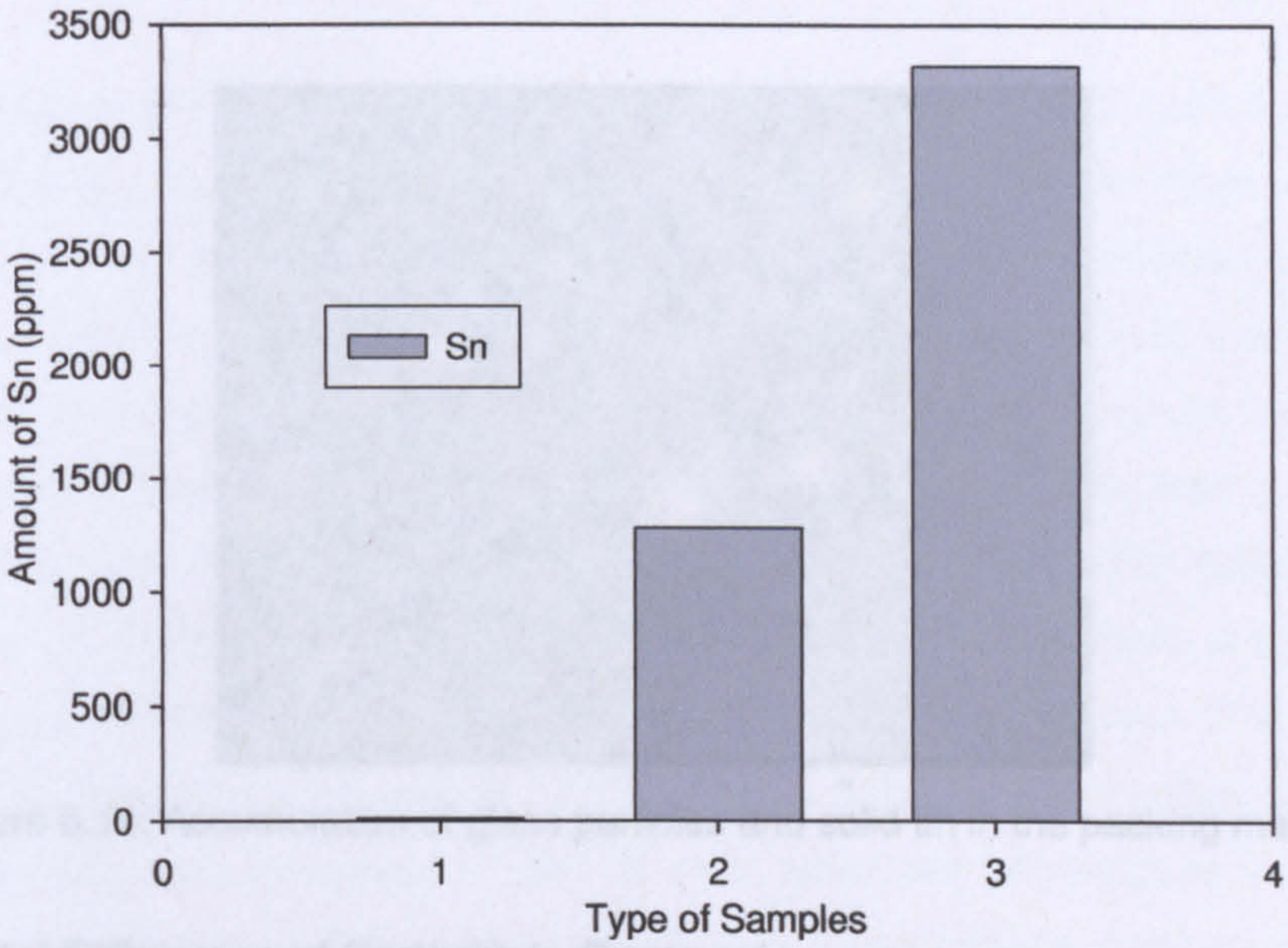

Figure 6.9: Chemical analysis using Atomic Emission Spectrometry – Full element analysis

The solidification of Sn compounds was observed when a coating layer was formed on top of the glass particle surfaces. The formation of the Sn-Si mixture resulted in decrease of the total efficiency. The appearance of the agglomeration between the packing is shown in Figure 6.10. When glass particles collide with liquid tin they may adhere to it, forming agglomerates. When glass particles at lower temperature collide with the hot liquid tin, the liquid tin will solidify and cover the glass particles' surface. The grey and black colours of the mixture provide evidence that solidification of liquid tin had occurred. In these tests, the glass particles either adhered to the liquid tin layer or their surfaces. Results from the analysis during the particulate cleaning revealed that there were agglomerated products, which were a Si-Sn mixture. Figure 6.10 shows the image of glass particles and solid tin products formed during agglomeration. Samples from both operating temperatures gave different surface texture and colour. The presence of Sn was confirmed by ICP-AES and visually by observation of the deposit on the filter paper.

After each run, the high-purity ceramic alumina spheres (packing) together with the column were not cleaned due to time constraint and design limitations. This was identified as another contributing factor, which affected the total efficiency. The limitations of the design were identified and further improvements could be made for future experiments. These are listed in Chapter 9.

Figure 6.10: Accumulation of glass particles and solid tin in the packing material

6.1.3 Total Efficiency of Particulate Removal

There are essentially three material streams containing the dust particles pertaining to the gas scrubber: the feed nitrogen gas stream containing the challenging dust particles, the outlet nitrogen gas stream carrying the unseparated or penetrating dust particles, and the outlet liquid tin stream that washes out the separated dust particles. There is also an accumulation of dust particles within the packed bed that is not washed out by the liquid tin. The material balance around the scrubber is as follows:

$$(M_{in})(\omega_{in,x}) = (M_c)(\omega_{c,x}) + (M_f)(\omega_{f,x}) \qquad (6.1)$$

M_{in} (kg/s) corresponds to the dust in the feed air stream; M_c (kg/s) corresponds to the sum of dust in the outlet liquid tin stream as well as the dust retained within the packed bed. M_f (kg/s) corresponds to the dust in the exiting nitrogen gas stream. ω_x is the mass fraction of particles at size x. The total efficiency E_T is defined by the following equation based on the mass flowrates of the feed dust M_{in} (kg/s) and the unseparated dust in the exit nitrogen gas stream M_f (kg/s).

$$E_T = 1 - \frac{M_f}{M_{in}} \qquad (4.4)$$

Herein, the total efficiency of the scrubber is determined gravimetrically as follows:

$$E_T = 1 - \frac{M_{out}}{M_{in}} \qquad (6.2)$$

Where M_{out} = Mass of unseparated dust in exit air retained on filter (g)
M_{in} = Mass of dust fed into scrubber (g)

m_{out} was obtained from the increase in total weight of the dried and cooled weighing container holding the filter paper and cotton bud used in cleaning. m_{in} was determined from the decrease in the weight of the glass powder contained within the hopper in the dust feeder after a test run. In the scrubbing experiments, studies were conducted to determine the effect of gas flow rates on the percentage removal of glass powder particles. This was achieved using liquid tin as a scrubbing medium. The same experiment was also used to determine the effects of inlet glass powder loading on the percentage removal of glass powder. Experiments were conducted at only one operating liquid tin flowrate of 0.1666 l/min and the particle flow rate (by varying the N_2 flow rate) was kept at 147.73 l/min at constant temperature of 350℃. The nitrogen flow was increased to 221.60 l/min when the temperature was varied from 350 to 400℃. For each gas flow rate the inlet glass particle loading was varied from 20 g/min in four stages, e.g. ~20, ~30, ~40 and ~50 g/min. Table 6.2 is a summary of the operating conditions and experimental results of the particulate cleaning tests. Operating temperature shown in this table were recorded from the electronic system controller. However, as shown in Figure 6.11, the experiment began only when the chamber have reached the set point temperature by making sure that the temperatures of the gas outlet (T2) and the molten tin reservoir (T3c) equilibrates to the set point. This ensures that the column itself was heated to the desired temperature.

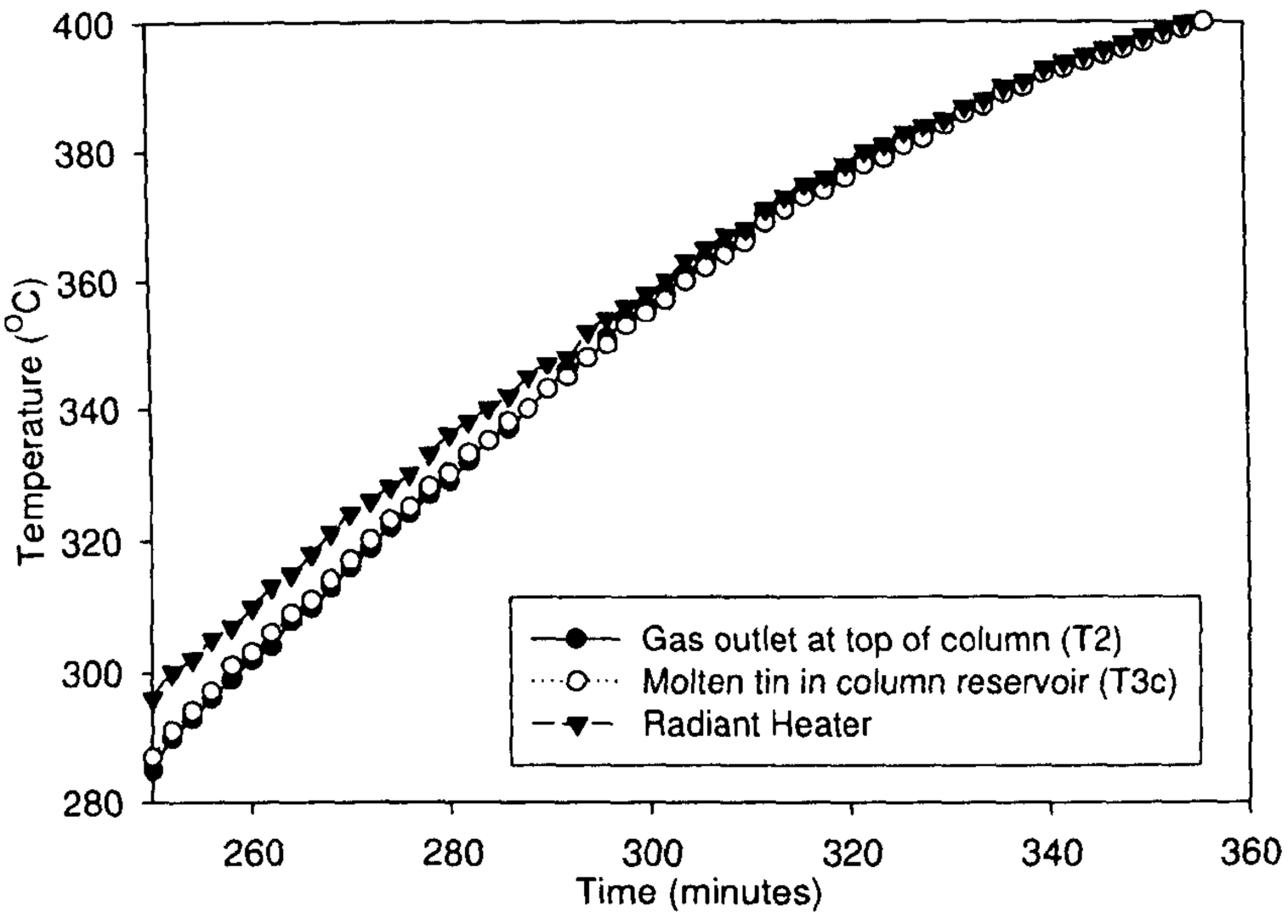

Figure 6.11: Temperature history for three different locations within the hot gas scrubber during heating up of the system

Table 6.2: Experimental data for particulate cleaning

Test No.	Operating Temperature (°C)	Liquid Tin Q_L (liter/min)	N_2 Q_G (l/min)	Dust Inlet (g)	Dust Outlet (g)	Splashed Tin (g) (Average)	Total Efficiency E_T (wt %)
1a	350	0.1666	221.60	20.27	5.41	5.45	98.80
1b	350	0.1666	221.60	31.42	9.93	5.45	82.13
1c	350	0.1666	221.60	40.56	14.58	5.45	73.67
1d	350	0.1666	221.60	50.13	19.57	5.45	68.11
2a	350	0.1666	147.73	20.61	6.31	5.45	93.05
2b	350	0.1666	147.73	31.06	11.34	5.45	76.42
2c	350	0.1666	147.73	41.37	18.41	5.45	63.64
2d	350	0.1666	147.73	51.28	24.34	5.45	58.67
3a	400	0.1666	221.60	20.96	49.62	5.45	67.09
3b	400	0.1666	221.60	32.73	99.49	5.45	-76.81
3c	400	0.1666	221.60	39.26	125.56	5.45	-127.58
3d	400	0.1666	221.60	51.08	190.95	5.45	-203.86

6.1.3.1 Effect of Fluid Flowrates and Solid Loading

The liquid tin-irrigated packed bed scrubber demonstrated particulate removal performance with total separation efficiencies ranging from 60 to 98%. These values were taken only after the effect of splashed liquid tin on the filter paper was considered. Comparisons between results from Chang (2003) on total efficiency E_{Total} with various inlets loading of glass particles, and various operating and flow variables for the scrubber are shown in Figure 6.12. The total efficiency decreases as the inlet dust flow rate increases. This low efficiency is due to the agglomeration of glass particles and solid tin in the scrubber, which were described in the previous section. Several factors were identified which could account for differences observed between results obtained by Chang (2003) and the results from this experiment. When the filtration started, the particles were captured by the bed material of the scrubber, and subsequently the attrition of the particles occurred. As time passes, the accumulation of particles increases, so a strong elutriation of finer particles occurs in the bed. This phenomenon appears at various gas and liquid flow rates. The elutriation of the captured particles affected the removal efficiency and the high collection efficiency was limited when a strong elutriation occurred. Figure 6.12 also shows the effects of solid loading, and as shown in this figure the increase in glass particle loading decreases the percentage removal of the glass particles. Higher inlet loading hinders particle collection in the packed bed column. This is because of the higher particle-particle interaction. It gives agglomeration of Si-Sn mixture and the packing itself.

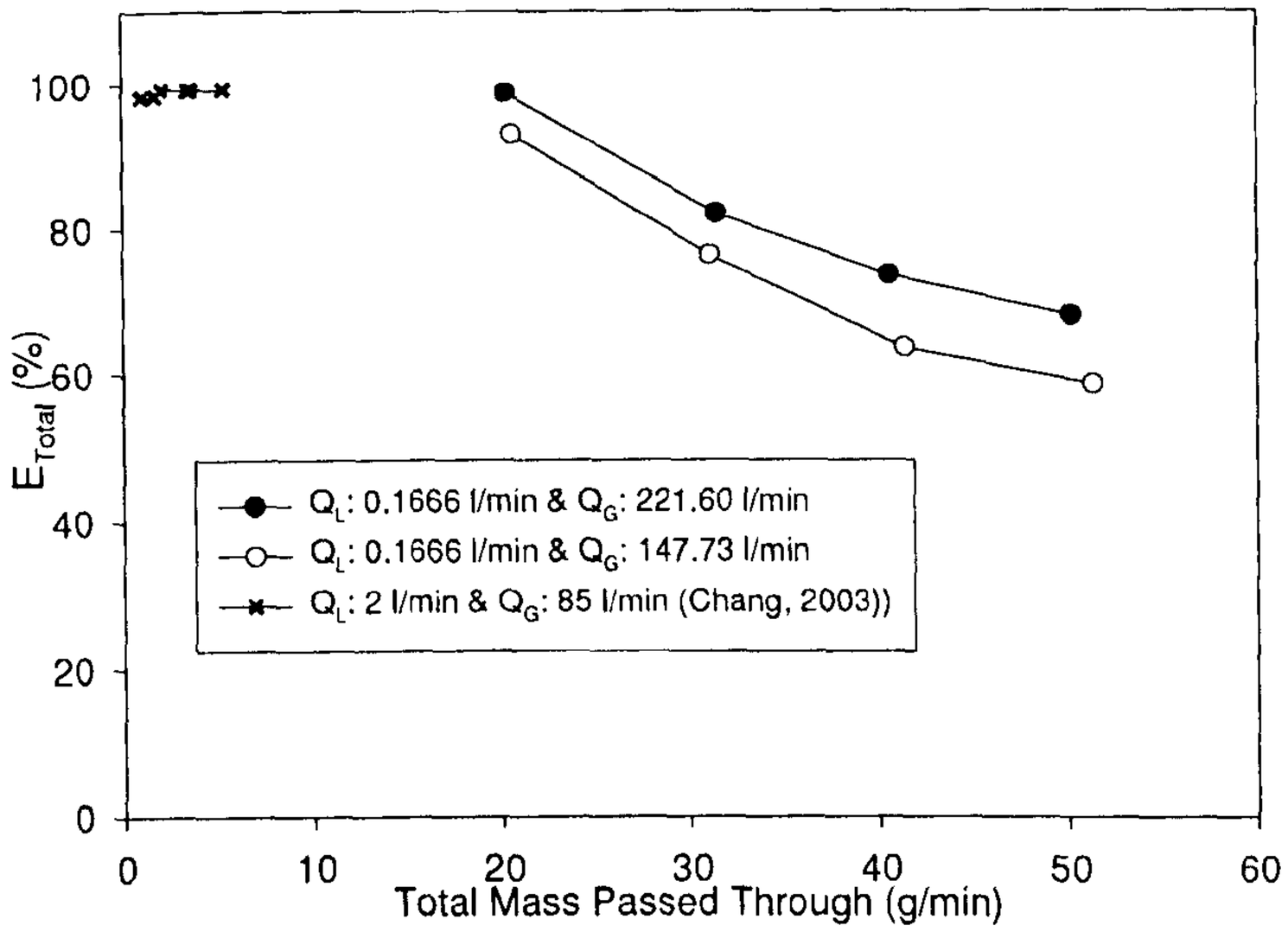

Figure 6.12: Variation of total efficiency with operating temperature 350℃

A higher particle loading increases particle–particle interactions which contribute positively to the removal of particulates. In addition, at high loading rates of glass particles, the importance of particle movement inside the column was increased. This was due to enhanced Brownian motion, which may lead to enhanced collection efficiency at high dust loading. The formation of agglomerated glass particles with solid tin caused by the temperature difference of glass particles at inlet has to be considered because they influence the removal efficiency. The agglomeration formed more rapidly when the solid loading was increased.

6.1.3.2 Effect of Operating Temperature

For the tests of the E_{Total} (total efficiency) with different operating temperatures, the liquid flow rates and solid loading were held constant at 0.116 liter/min and 221.6 liter/min respectively. During these experiments, the variation of the temperature was 50℃. The E_{Total} under various operating temperatures are shown in Figure 6.13. The results show that the influence of temperature on the total efficiency was significant. As temperature increases from 350℃ to 400℃, the E_{Total} decreases. This is mainly caused by the temperature difference between the inlet particles and the scrubber (i.e. 335℃ and 385℃ respectively). A higher operating temperature will form thicker deposits. A large temperature difference between the particle inlet and the scrubber operating temperatures can result in hot spots or zones that will induce sintering.

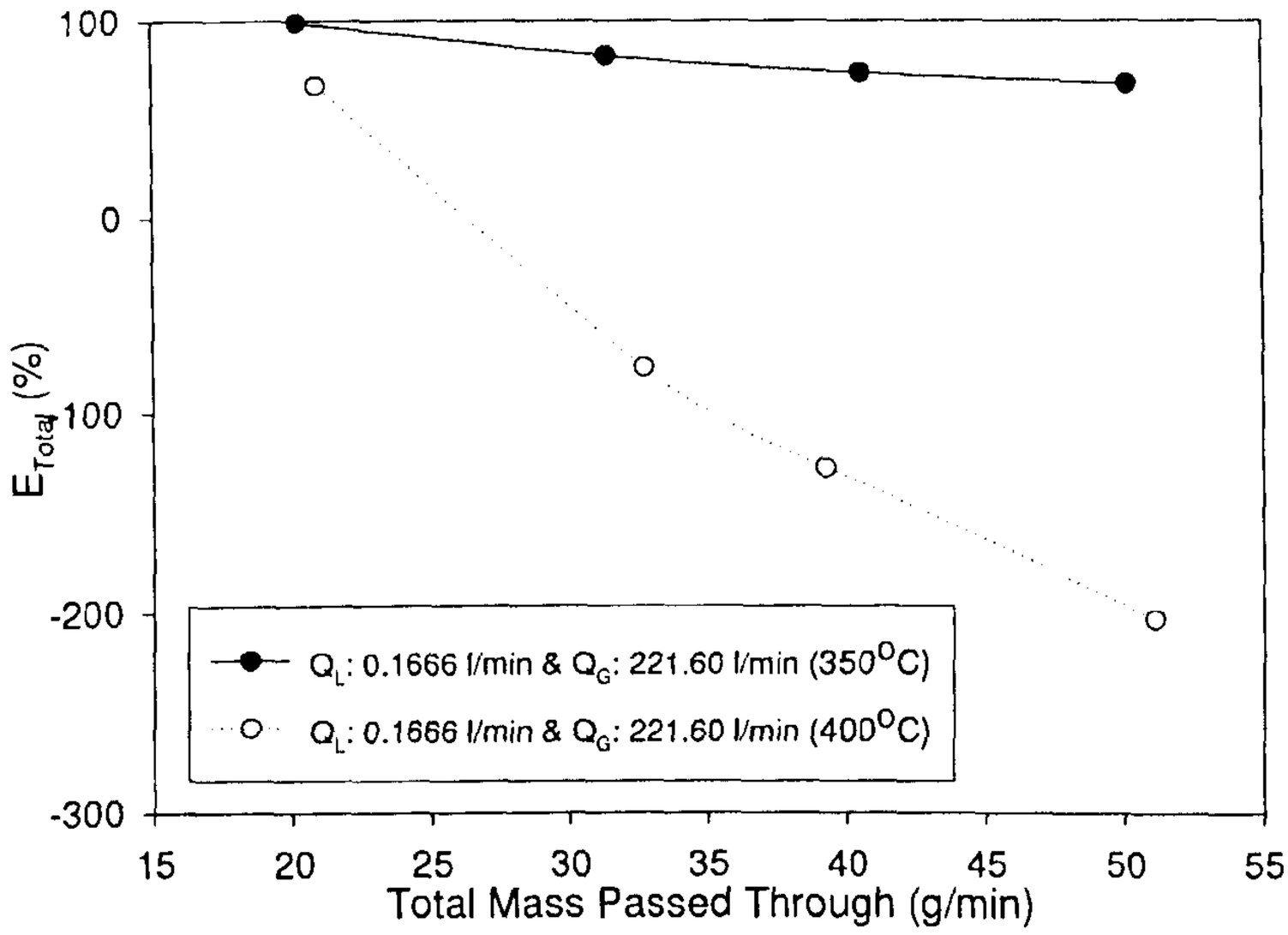

Figure 6.13: Variation of total efficiency with operating temperature

This factor increases the agglomeration of the particles coated by the liquid tin, which decreases the efficiencies of the process. Fine particles, a small amount of the Si-Sn mixture and the splashed tin, which are not collected in the packed bed column, are carried over by the upward moving gas stream. As mentioned earlier, Figure 6.9 also indicates that the Sn content in the filter paper increased with the operating temperature. The E_{Total} decreased gradually as the total mass loading was varied from 20 to 50 g/min. Figure 6.13 shows that the efficiency at 350℃ was reduced from 98% to about 68%. The total efficiency at 400℃, decreased sharply from about 67% to -204% as the total mass loading reached 30 g/min. The efficiency shown in negative values (as low as -204) meant that the mass of Si-Sn mixture in the filter paper exceeded the mass of particle loading. The removal efficiency reduced with the total mass loading since the accumulation of Sn-Si mixture in the filter paper increased with the time. Therefore, minimising the temperature difference between the particle inlet and the operating temperature of the scrubber is important for continuous filtration. An increase in temperature can extend the agglomeration process significantly, probably due to a much faster sintering of the agglomerates at higher temperatures. It is most likely that the agglomerates are initiated by solidification of liquid tin when encountered with glass particles. This may be the dominant cause for the lower efficiency.

6.1.4 Grade Efficiency

6.1.4.1 Dust Collection in the Impinger

Earlier experiments by Chang (2003) showed that the number of particles trapped in the second impinger was insignificant. Therefore the present tests were carried out using one impinger to collect the solids exiting the column. The reproducibility of the grade efficiency curves was less satisfactory as shown in Figure 6.14. As shown in Figure 6.14, glass particles in the range of 1 μm to 5 μm were passing through the packing and liquid tin. The grade efficiency increased in the second test run and it reached the highest value in the third test run. The difference in the particle size distribution contributed to the formation of agglomeration of glass particles and solid tin. Moreover, it was not practical to clean the scrubber after every test run so the results were not reproducible. As discussed previously this is mainly due to the rig design limitations.

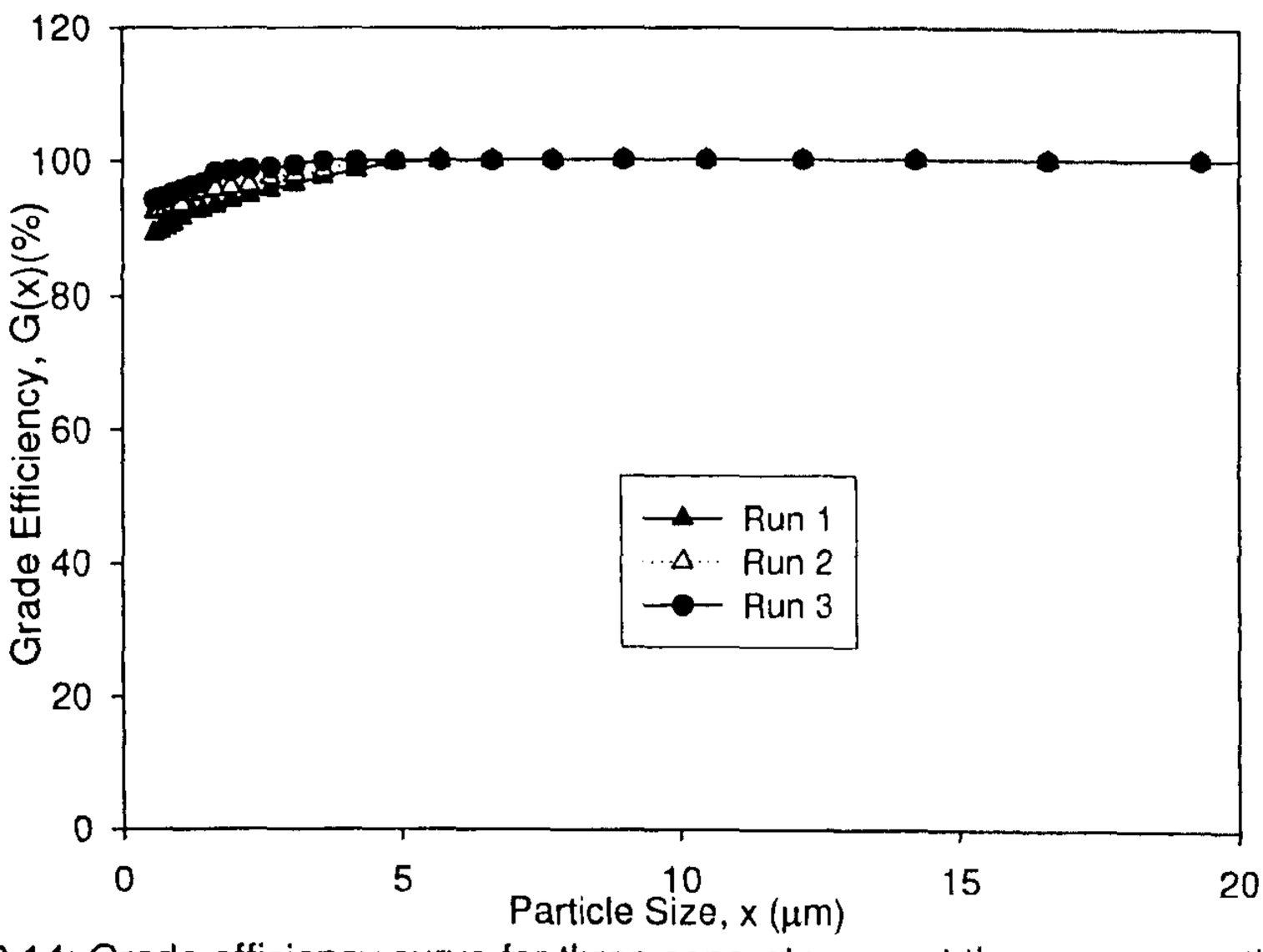

Figure 6.14: Grade efficiency curve for three separate runs at the same operating fluid flowrates and solid loading

6.1.4.2 Determination of Grade Efficiency

The dust exiting the scrubber was collected for only one set of operating liquid tin and nitrogen flowrates (Test 1d), 0.1666 l/min and 221.60 l/min respectively with the same solid particles loading. The grade efficiency was evaluated using the following data:

- ✓ Particle size distribution of dust at inlet (i.e. the original glass powder)
- ✓ Particle size distribution of dust at outlet (i.e. collected in the impinger)

The grade efficiency was calculated using the following equation:

$$G(x) = 1 - (1 - E_T)\frac{\omega_{out,x}}{\omega_{in,x}} \qquad (6.3)$$

Where $\omega_{in,x}$ = Mass fraction of dust fed into scrubber at particle size x
$\omega_{out,x}$ = Mass fraction of unseparated dust in exit nitrogen gas retained in impinger at particle size x

The comparison of grade efficiency was not carried out since it was not possible to reproduce the results at the same operating conditions. This was due to the formation of agglomerates in the column. This is because the particles collected in the impinger cannot represent the same total collection efficiency E_T corresponding to the same liquid flow rates and inlet solid loading. In Figure 6.15, the grade efficiency curves show that glass particles larger than about 5 μm can be separated at efficiencies greater than 98%.

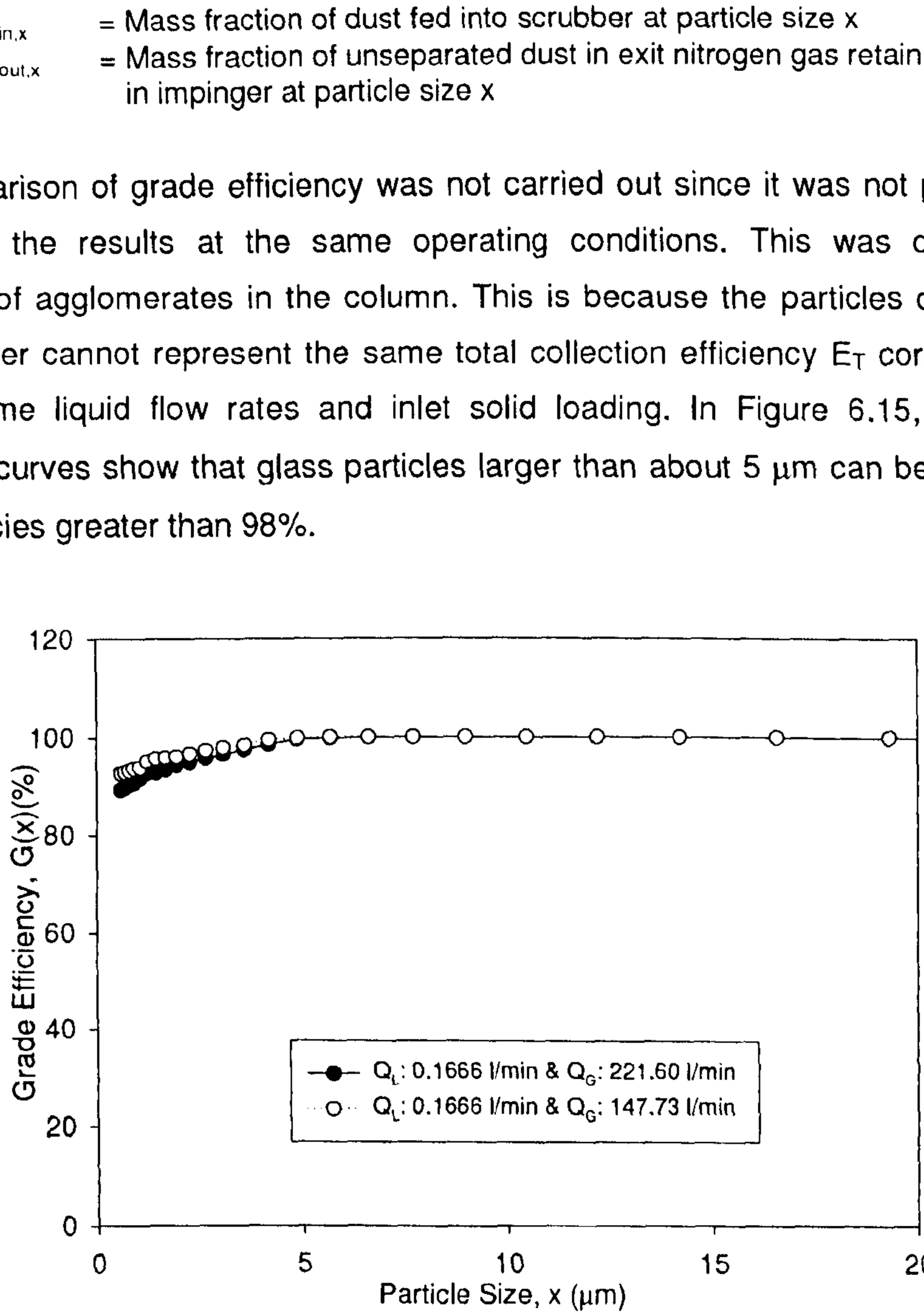

Figure 6.15: Grade efficiency curve for three separate runs at the same operating fluids flowrates and solid loading (Test 1d and 2d)

6.1.5 Experiment Measurement Accuracy

6.1.5.1 Dust Deposition in the Inlet Nitrogen Gas Line

Preliminary tests were carried out to ensure that all or the majority of the glass particles fed by the dust feeder entered the column instead of being deposited in the piping leading to the column. It is apparent that solid deposition in the inlet pipes causes a reduction in the amount of the solids that enter the column i.e. smaller solid loading in the inlet nitrogen gas. In this investigation the nitrogen gas injector was disconnected from the column and switched to a tube. The open end of the tube was closed with a Vacspare^{TM} dust bag. The metal pipes connecting the dust feeder to the nitrogen gas injector as well as the brass nitrogen gas injector itself was earthed. Static charges were drawn and dissipated through a connected wire under the ground. The nitrogen gas supply was turned on and glass particles were fed from the dust feeder into the metal piping, through to the nitrogen gas injector, tubing and dust bag sequentially. The powder captured in the dust bag was weighed and then compared to the amount of glass powder fed by the feeder. It was found that approximately 88% of the dust fed into the system was collected by the dust bag. Hence the amount of powder that left the dust feeder hopper was a reasonably good representation of the amount of solids that actually entered the column, with an error of approximately 12%.

6.1.5.2 Experimental Measurement Accuracy

The accuracy of the equipment used in the particulate removal tests is summarised in the following table:

Table 6.3: Accuracy of equipment used

Apparatus/ Instrument	Measured Quantity	Accuracy
Nitrogen Gas Rotameter	Nitrogen gas volumetric flowrate	± 0.5 l/min
K-type Thermocouples	Bed temperature	±0.0075 ℃ of the actual temperature/±2.5 ℃
Manometer ≥ 10 cm H_2O < 10 cm H_2O	Column pressure drop	± 0.03 cm H_2O ± 0.005 cm H_2O
Microbalance	Mass of glass powder in plastic container; Mass of weighing container + contents	± 0.00005 g
Digital Stop Clock	Duration of test run	± 0.005 sec ± 0.1 sec (human response)

6.2 Desulphurisation

There have been a number of studies of H_2S absorption with metal oxides, which were discussed in Chapter 3 of this thesis. However, there has not been a study on the removal of sulphur from H_2S using molten metal in a packed bed scrubber. The principal goal of this study is to examine the performance of molten tin to remove the H_2S in the hot packed bed scrubber.

6.2.1 Determination of Overall Mass Transfer Efficiency

The mass transfer process of H_2S absorption from H_2S/N_2 mixture into liquid tin in the scrubber was studied. The absorption of H_2S into liquid tin is a known gas film controlled process, with around 80 to 95 % of resistance to the mass transfer lying in the gas phase (Coulson and Richardson, 1990; McCabe et al., 1993). The mass transfer efficiency of the packed bed with high-purity ceramic alumina (Al_2O_3) spheres irrigated by liquid tin was determined from the measured hydrogen sulphide gas concentration in the inlet and outlet gas stream. The gas flow rates ranged from 0.245 to 0.581 kg/m^{2}s (gas superficial velocity: 0.490 to 1.161 m/s) with a liquid (tin) flow rate of 2.148, 3.165 or 3.860 kg/m^{2}s (liquid superficial velocity: 3.07×10^{-4}, 4.53×10^{-4} or 5.52×10^{-4} m/s respectively). The inlet H_2S concentration in N_2 was varied from 300 to 2000 ppm (reference case: 1000 ppm). The height of packing was also varied from 20cm (reference case) to 10 cm and 0 cm (empty column). While the operating temperature was fixed at 400°C (as the reference condition for variation of other test parameters), the effect of temperature was assessed at 300, 350 and 390℃ respectively.

6.2.2 Assessment of Results

From the measured H_2S concentration at the outlet in each test, the desulphurisation efficiency can be derived. It is defined as,

$$\eta\ (\%) = \left(\frac{1 - y_{out}}{y_{in}}\right) x 100 \qquad (6.9)$$

Although this is the simplest way of evaluating the test results, it is case-dependant and does not provide insight on the absorption mechanism. For a packed bed scrubber, the general equation for the scrubber is (Changkook Ryu et al., 2007),

$$-u_G dy = K_o\left(y - y_e\right)a_e dz \tag{6.10}$$

where K_o is the overall mass transfer coefficient (m/s) incorporating the three rate-controlling mechanisms: the gas phase mass transfer (k_G) of H_2S towards the liquid surface, the reaction kinetic effect at the interface (k_r) and the liquid phase mass transfer (k_L) for SnS dissolving into tin. K_o can be expressed simply as,

$$\frac{1}{K_o} = \frac{1}{k_G} + \frac{1}{k_r} + \frac{1}{k_L} \tag{6.11}$$

Rearranging Equation 6.10 gives (Changkook Ryu et al., 2007),

$$-\frac{dy}{\left(y - y_e\right)} = \frac{K_o a_e}{u_G} dz \tag{6.12}$$

Integration of Equation 6.12 yields (Changkook Ryu et al., 2007),

$$N_{OG} = \frac{\overline{K}_o a_e}{u_G} Z \tag{6.13}$$

Where Z is the bed height, $\overline{K}_o$ the overall mass transfer averaged along the bed height. As the H_2S concentration involved was small (less than 0.1 % in the gas), only small amounts of solute were transferred between the gas and liquid phase. This produced a very dilute solution. This meant that both the operating and equilibrium lines for the system are essentially linear. In view of these considerations, the efficiency of mass transfer could be determined as follows:

N_{OG}, the overall number of gas-phase transfer units defined as:

$$N_{OG} = \int_{y_{out}}^{y_{in}} \frac{dy}{y - y_e} \tag{6.14}$$

For a fast absorption process ($y >> y_e$), N_{OG} can be simplified using only the inlet and outlet pollutant concentrations.

$$N_{OG} = \ln\left(\frac{y_{in}}{y_{out}}\right) \tag{6.15}$$

From Equation 6.14, the removal efficiency of a packed bed scrubber can then be expressed in terms of the overall height of the gas-phase transfer unit (H_{OG}) (Calvert, 1972).

$$H_{OG} = \frac{Z}{N_{OG}} = \frac{u_G}{K_O a_e} \tag{6.16}$$

The volumetric overall gas phase mass transfer coefficient:

$$K_G a = \frac{G'}{H_{OG}} = \frac{G'}{Z}\frac{(y_B - y_T)}{(y - y^*)_{lm}} \quad \text{(kmol/m}^3\text{s)} \tag{6.17}$$

Where G' = Molar flowrate of nitrogen per unit cross-section area of column (kmol/m^{3}s)
Z = Packed bed height (m)

H_{OG} represents the height (m) required to achieve a characteristic level of desulphurisation ($y_{in}/y_{out} = e$ or η=63.2%). The smaller the value of H_{OG}, the more efficient is the absorption process. As shown in the Equation 6.16, H_{OG} is affected by the three reaction/mass transfer rates for K_o as well as the interfacial area (a_e) and gas velocity (u_G, or gas residence time in the column).

6.2.3 Correction for End Effects

The H_{OG} and K'_Ga given by equations 6.16 and 6.17 are "apparent values", suggesting higher mass transfer efficiency of the packed bed than the "true values". This apparent higher mass transfer efficiency is due to end effects i.e. additional mass transfer occurring beyond the packed bed region. End effects to mass transfer were expected to be significant due to the use of a short packed bed. The main source of end effect would be the additional mass transfer occurring in the spray of liquid tin below the packing support plate. Another source would be due to gas absorption at the free liquid surface in the bottom reservoir. The other possible end effect contributor was the liquid tin shower above the packed bed, however, this has been minimised by positioning the opening of the gas sampling tube directly above the packed bed. The gas absorption tests were conducted at two different packed bed heights to assess the magnitude of the end effects. The bed heights equivalent to the end effects Z_{end} were determined by plotting the number of overall gas phase transfer units N_{OG} (at the same gas and liquid flowrates) against the packed bed heights, Z and extrapolating the resulting line to zero bed height, shown as Figure 6.16.

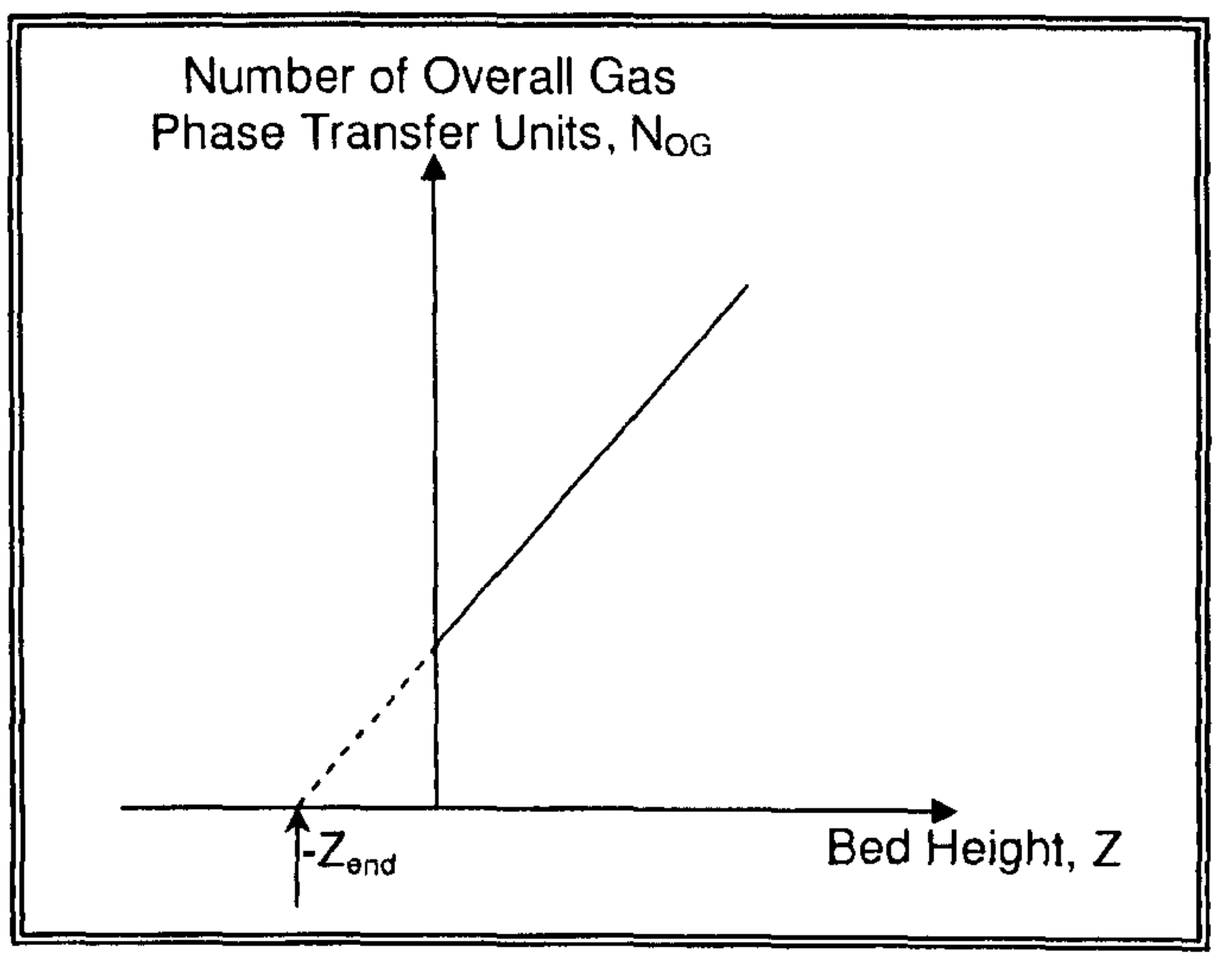

Figure 6.16: Determination of end effects

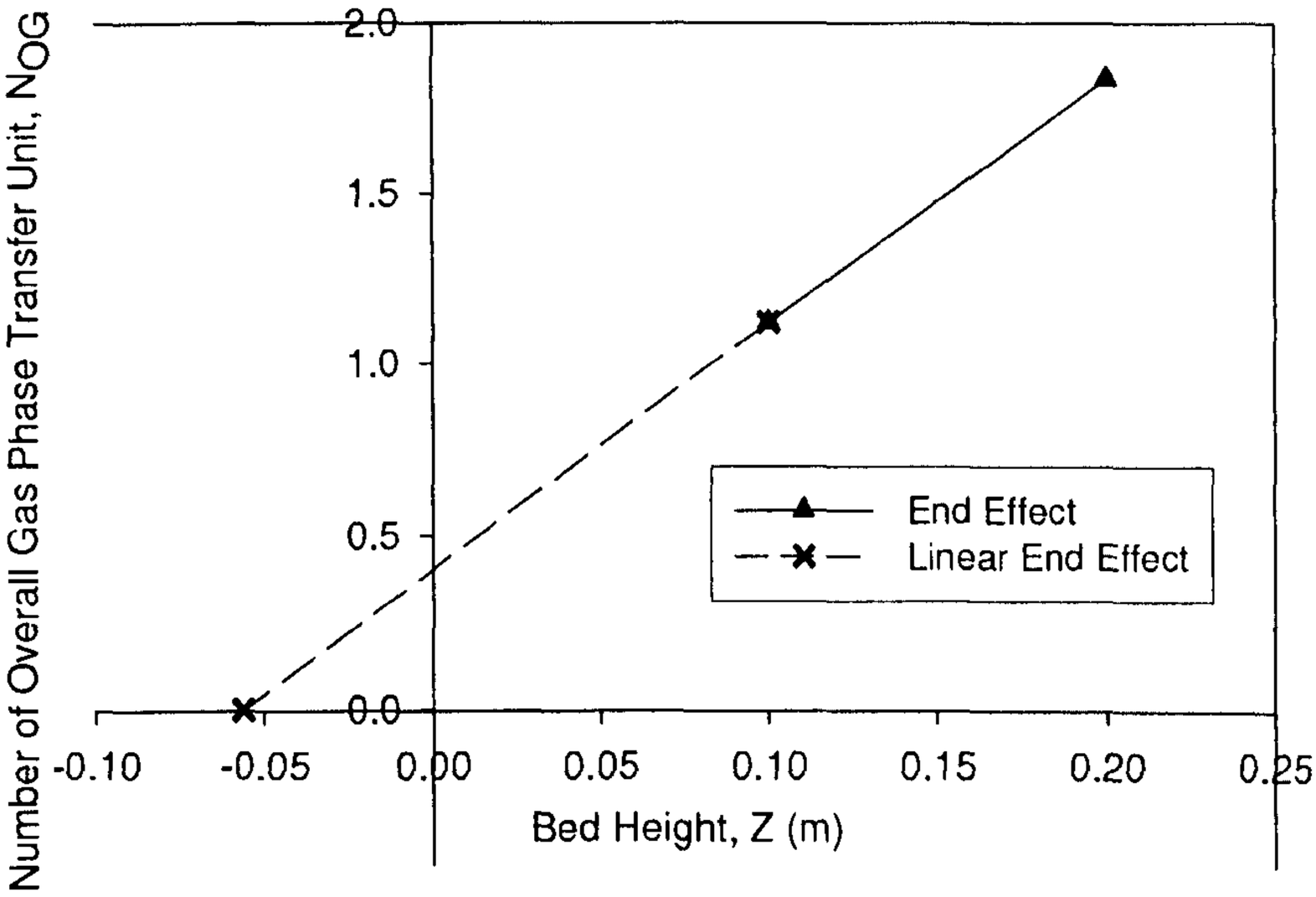

Figure 6.17: N_{OG} versus Ned Height, Z

N_{OG} values obtained from tests using 10.0 cm and 20.0 cm packed bed heights were plotted against Z as depicted in Figure 6.17. As only two data points were available for each combination of fluid flowrates, the use of an average value of Z_{end} for all fluid flowrates seemed more practical than individual Z_{end} at different fluid flowrates. The random errors would be averaged out by the former method. The average Z_{end} was taken to be -5 cm as shown in Figure 6.17. The equivalent height of the end effects (Z_{end} = 20 cm) can be calculated using the following equation (Chang, 2003):

$$H_{OG}(true) = \frac{Z + Z_{end}}{N_{OG}} \qquad (6.18)$$

The correct Z_{end} should result in true values of H_{OG} independent of the packed bed height. Hence the data from both the 10 cm and 20 cm packed bed heights should yield equivalent true values of H_{OG} at the same gas and liquid flowrates.

6.2.4 Blank Test and Test Duration

Figure 6.18 shows the histories of H_2S concentration including a blank test, vs test duration for the desulphurisation process. In the graph, t=0 min is when H_2S was introduced into the column. In the blank test (operation at 400℃ without tin circulation) at 983 ppm inlet H_2S concentration, the outlet concentration (960 ppm) matched the inlet value within the accuracy of the GC (calibrated using standard gas at 4000 ppm (5%). It took 20 min to reach a steady concentration due to the time required for the gas to achieve complete mixing in the reactor and also for the gas retention time in the sampling line to the GC. The two tests for different test durations at 2000 ppm inlet H_2S concentration showed that the tests were repeatable and the outlet H_2S concentration was not affected by the test duration up to 90 min. Although the removal efficiency will be affected by the test duration in the long term, the tin has sufficient sulphur capacity not to be affected by a few hours of tests. The sulphur concentration in the tin after 90 min of test was less than 1% by weight. Therefore, the concentrations at t=30 min were used to evaluate the results.

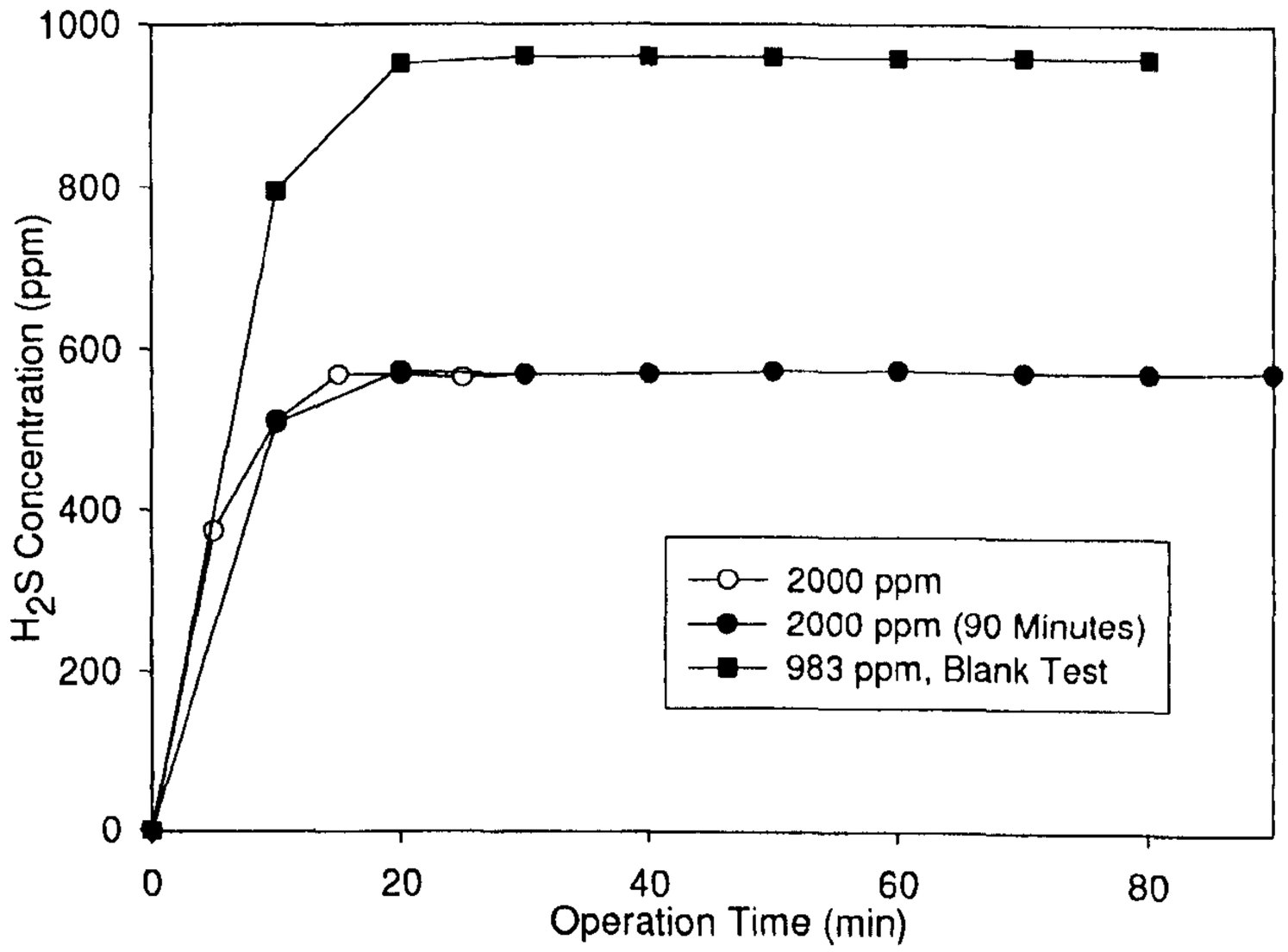

Figure 6.18: History of H_2S concentration for the test duration (m_G = 0.258 kg/(m^{2}s); m_L = 3.860 kg/(m^{2}s) except for the blank test; T = 400℃)

6.2.5 Effect of Gas and Liquid Tin Flow Rates

Figure 6.19 shows the history of H_2S for the test duration with various gas superficial velocities and constant liquid superficial velocities. Figure 6.20 shows the trends of the H_2S removal efficiency (η) and H_{OG} for different gas and liquid superficial velocities for an inlet H_2S concentration of 1000 ppm at 400℃. η ranged from 67% to 91% in the test reactor, which resulted in H_{OG} values of 0.084 to 0.181 m. Increasing the liquid flow rate from 2.148 kg/m^{2}s to 3.860 kg/m^{2}s led to 2-4% higher values of η and, therefore, lower values of H_{OG} by 0.012 – 0.014m. However, larger gas flow rates up to a certain point (0.443 kg/m^{2}s) increased H_{OG} (reduced η) and then started to increase the value. Recalling Equation 6.16 for H_{OG}, these trends can be explained from the way the gas and liquid velocities affect the flow characteristics in the column such as the residence time, interfacial contact area and mass transfer rate. Firstly, the gas velocity determines the residence time of the gas phase in the column, which represents the macro-opportunity for the gas to contact the liquid. For example, the gas residence time in the lab-scale scrubber decreased from 0.183 to 0.078 seconds based on the void volume of the dry column as the mass flow rate increased from 0.245 to 0.581 kg/m^{2}s (see Table 6.4). The actual values are lower than these due to the volume of the liquid retained in the bed, which is known as liquid holdup. The decrease in η from about 90% to about 66% for gas flow rates up to 0.443 kg/m^{2}s is attributable to the reduced gas residence time. Secondly, the gas and liquid velocities affect the liquid holdup in the bed. Higher liquid flow rates directly increase the liquid holdup. As more liquid is retained, it generally creates a larger interfacial contact area (a_e) between the two phases. This results in lower values of H_{OG} at higher liquid velocities. At a constant liquid flow rate, the liquid holdup is not noticeably affected by low gas velocities. When the gas velocity or momentum is sufficiently high to interfere with the liquid droplets, the dynamic liquid holdup begins to increase. Chang (2003) derived the correlation for the liquid holdup of a non-wetting flow below the flooding point from the cold flow tests to be proportional to $u_G^{0.178}u_L^{0.580}$. This suggests that the liquid velocity exerts a stronger influence on the liquid hold-up. Thirdly, increased velocities also resulted in higher mass transfer coefficients of the gas phase (k_G) due to increase in turbulence and interaction between the two phases. Strigle (1994) reported k_G to be proportional to $m_L^{0.22}m_G^{0.79}$. The decrease in H_{OG} at high gas velocities (>0.443 kg/m^{2}s) in Figure 6.20 suggests that the enhancement of desulphurisation by increased liquid hold-up and gas phase mass transfer became more significant at high gas velocities than the adverse effect of reduced gas residence times.

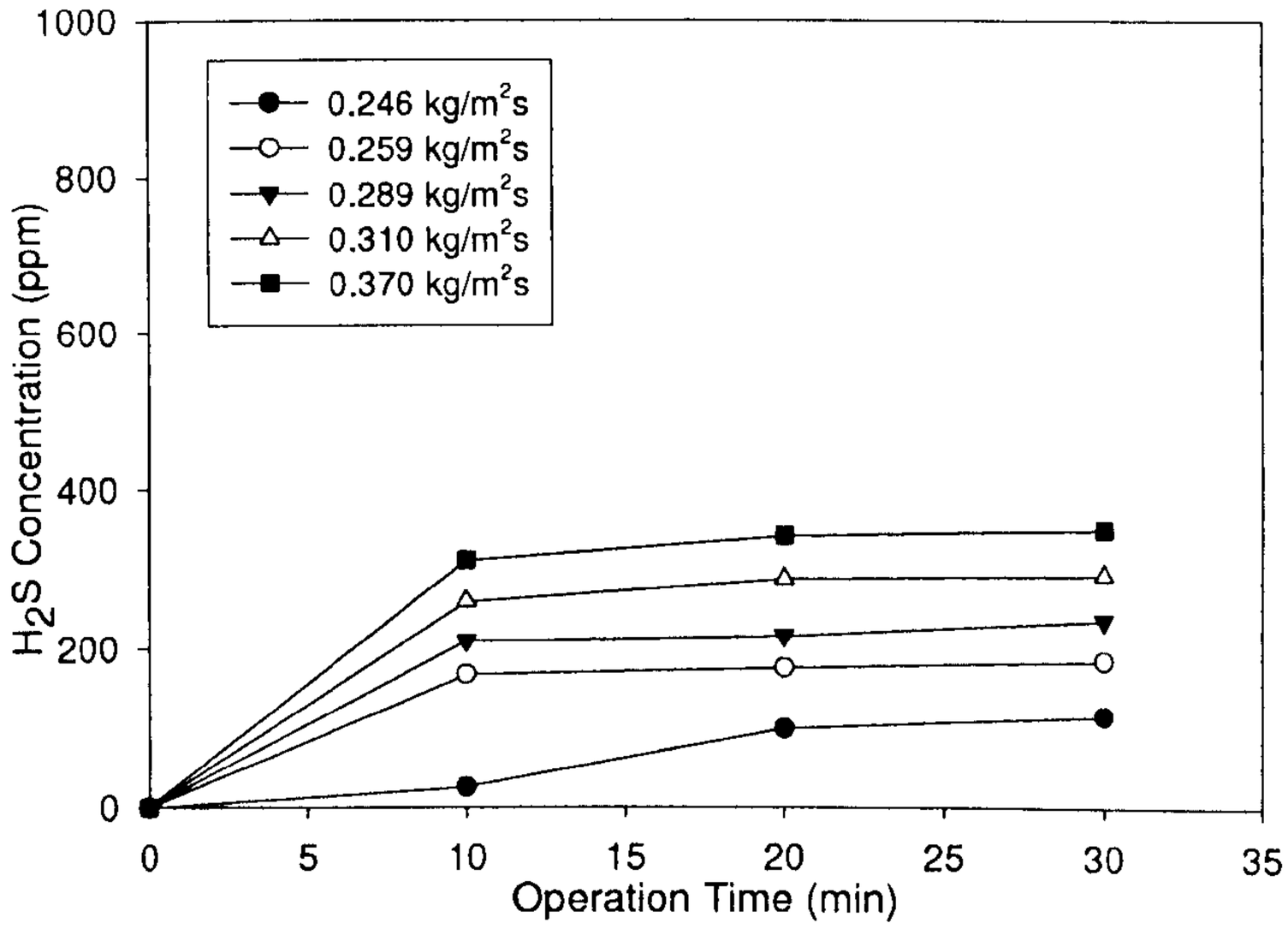

Figure 6.19: History of H_2S for the test duration with various gas superficial velocities and constant liquid superficial velocities = 3.157 kg/m²s (Inlet H_2S concentration: ≈1000ppm)

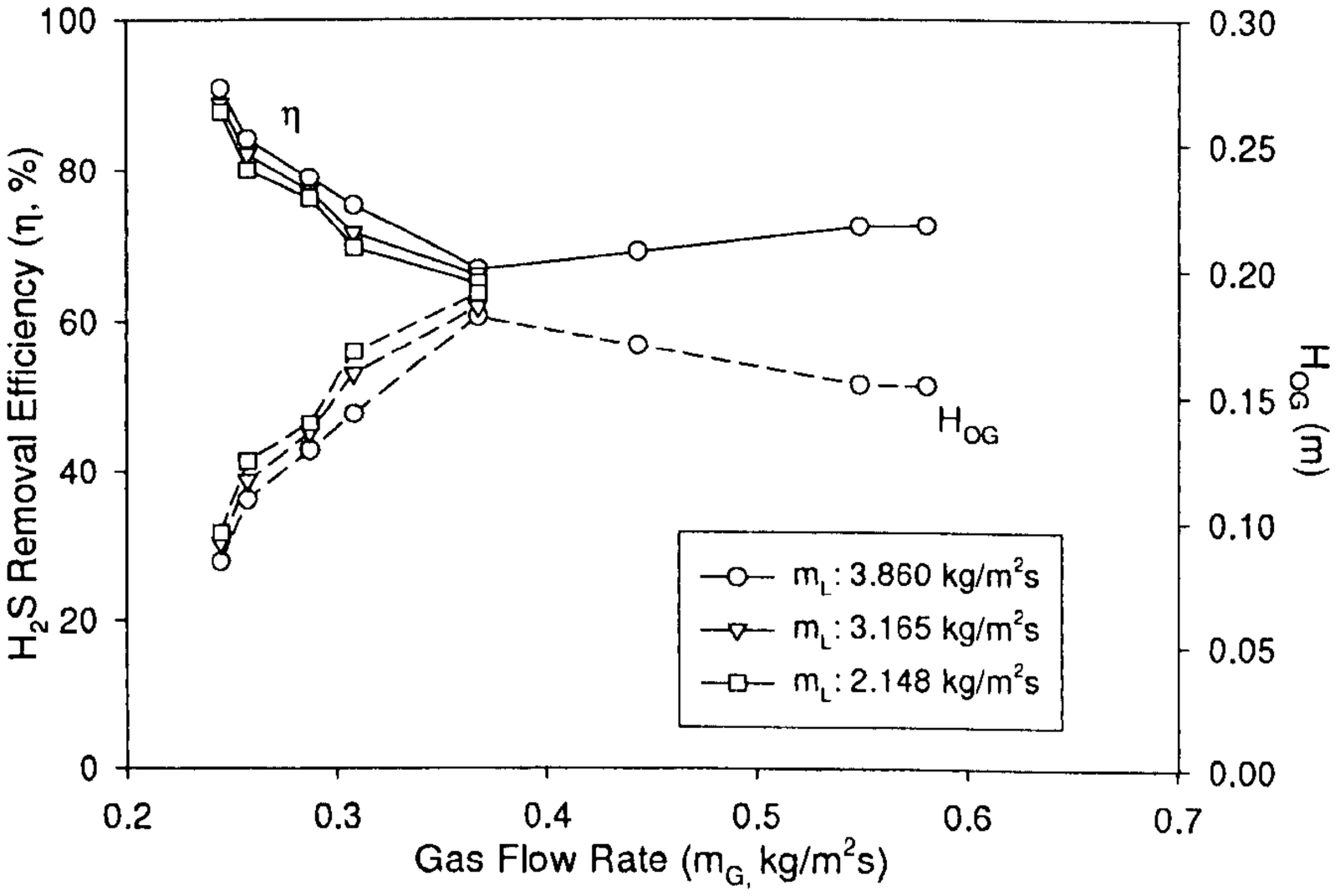

Figure 6.20: H_2S removal efficiency (η) and the gas transfer unit height (H_{OG}) for various gas and liquid superficial velocities (Inlet H_2S concentration: 1000ppm; T=400°C)

Table 6.4: Experimental data for various gas and liquid flow rates

L kg/m²s	G kg/m²s	u_L m/s	u_G m/s	y_B	y_T	x_B mol/mol´10⁶	η %	True N_{OG} (m)	True H_{OG} m
3.861	0.245	5.52E-04	0.490	1000	92	246.36	90.80	1.864	0.0838
3.861	0.258	5.52E-04	0.515	1000	159	239.98	84.10	1.437	0.1088
3.861	0.287	5.52E-04	0.574	1000	211	250.98	78.90	1.216	0.1285
3.861	0.309	5.52E-04	0.617	1000	247	257.14	75.30	1.092	0.1430
3.861	0.368	5.52E-04	0.735	1000	332	271.86	66.80	0.861	0.1814
3.861	0.444	5.52E-04	0.887	1000	309	228.66	69.10	0.918	0.1703
3.861	0.549	5.52E-04	1.098	1000	275	252.32	72.50	1.009	0.1549
3.861	0.581	5.52E-04	1.161	1000	274	281.66	72.60	1.011	0.1545
3.166	0.245	4.53E-04	0.490	1028	115	302.12	88.81	1.711	0.0913
3.166	0.258	4.53E-04	0.515	1028	184	293.73	82.10	1.344	0.1163
3.166	0.287	4.53E-04	0.574	1028	235	307.65	77.14	1.153	0.1355
3.166	0.309	4.53E-04	0.617	1028	292	306.53	71.60	0.983	0.1589
3.166	0.368	4.53E-04	0.735	1028	349	337.03	66.05	0.844	0.1851
2.148	0.245	3.07E-04	0.490	1005	124	429.59	87.66	1.635	0.0956
2.148	0.258	3.07E-04	0.515	1005	201	412.32	80.00	1.257	0.1243
2.148	0.287	3.07E-04	0.574	1005	239	437.91	76.22	1.122	0.1392
2.148	0.309	3.07E-04	0.617	1005	305	429.61	69.65	0.932	0.1677
2.148	0.368	3.07E-04	0.735	1005	352	477.62	64.98	0.820	0.1906

One thing to note is that increased liquid holdup does not always lead to larger interfacial area. High gas and liquid flow rates increase liquid holdup and connect more droplets with each other to change the flow pattern into rivulets. Standish (1968), Mackey and Warner (1973) reported that the interfacial area for the rivulet flow pattern is lower than that of droplet flow. Flooding of the liquid sets the upper operational limits for gas and liquid flow rates. Figure 6.21 compares the test conditions to the flooding line for non-wetting flows proposed by Standish (1973). The liquid and gas flow rates were well below the flooding line. Therefore, the gas and liquid flow rates can be further increased in order to intensify the desulphurisation reactions, thus reducing the volume of the scrubber required to process fuel gases.

Figure 6.22 shows the effects of the gas and tin flow rates on the pressure drop in the bed. The pressure drop increased from 17 to 70 mmH_2O with the increase in the gas and liquid superficial velocities due to higher resistance to the flow and increased liquid hold-up. With very low Reynolds numbers (76-115) for the gas, the trend is almost proportional to the gas velocity. A significant increase in the pressure drop was also noticed for the liquid superficial velocity of 5.52×10^{-4} m/s. This can be due to the liquid accumulating above the support plate at the bed bottom and acting as baffles for the gas flowing through the holes (Mackey and Warner, 1973).

Higher operating temperatures will reduce the pressure drop since lower viscosities of the tin can provide easy flow and dispersion into small droplets on the packing surface.

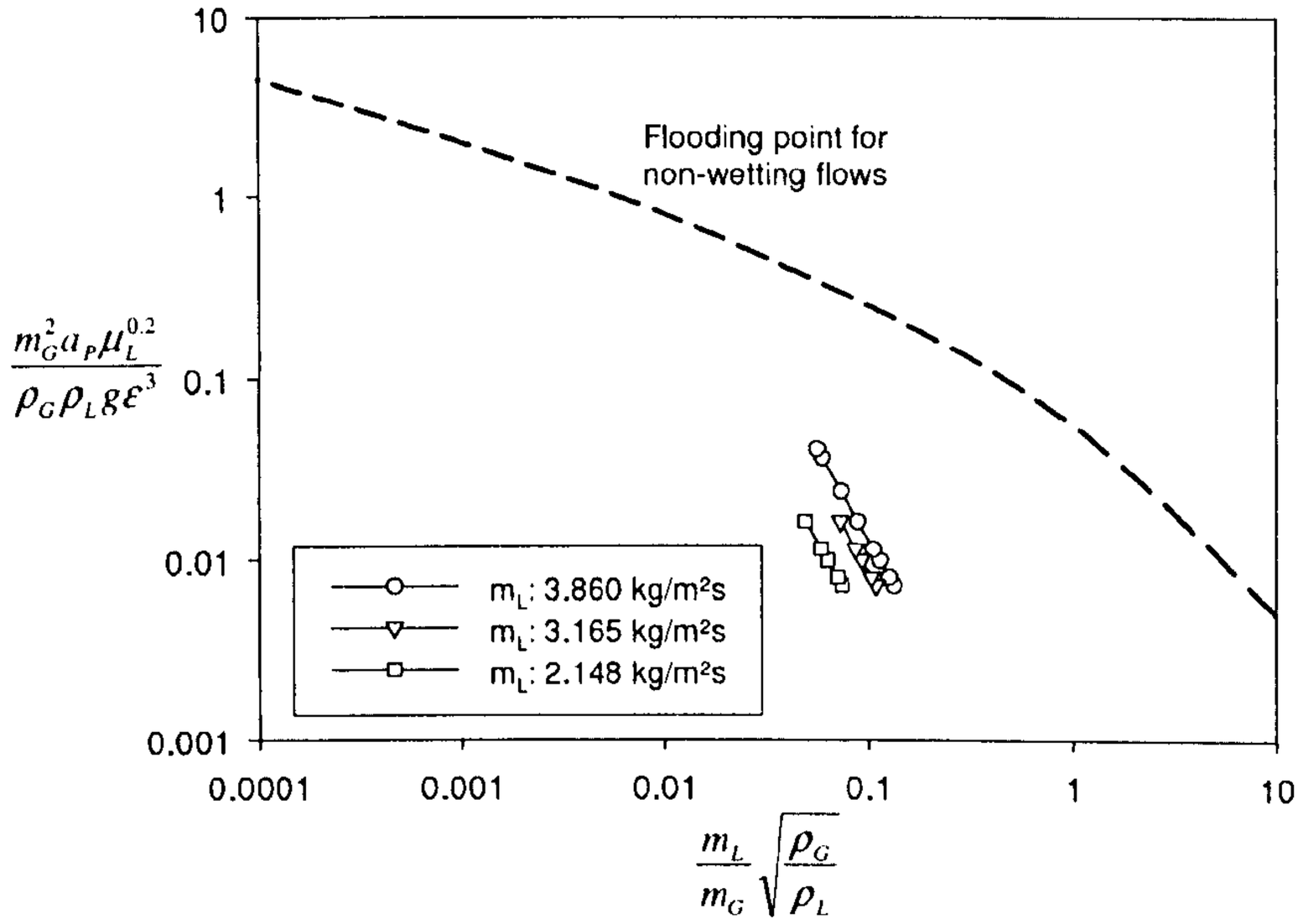

Figure 6.21: Comparison of test conditions to flooding capacity of non-wetting flows

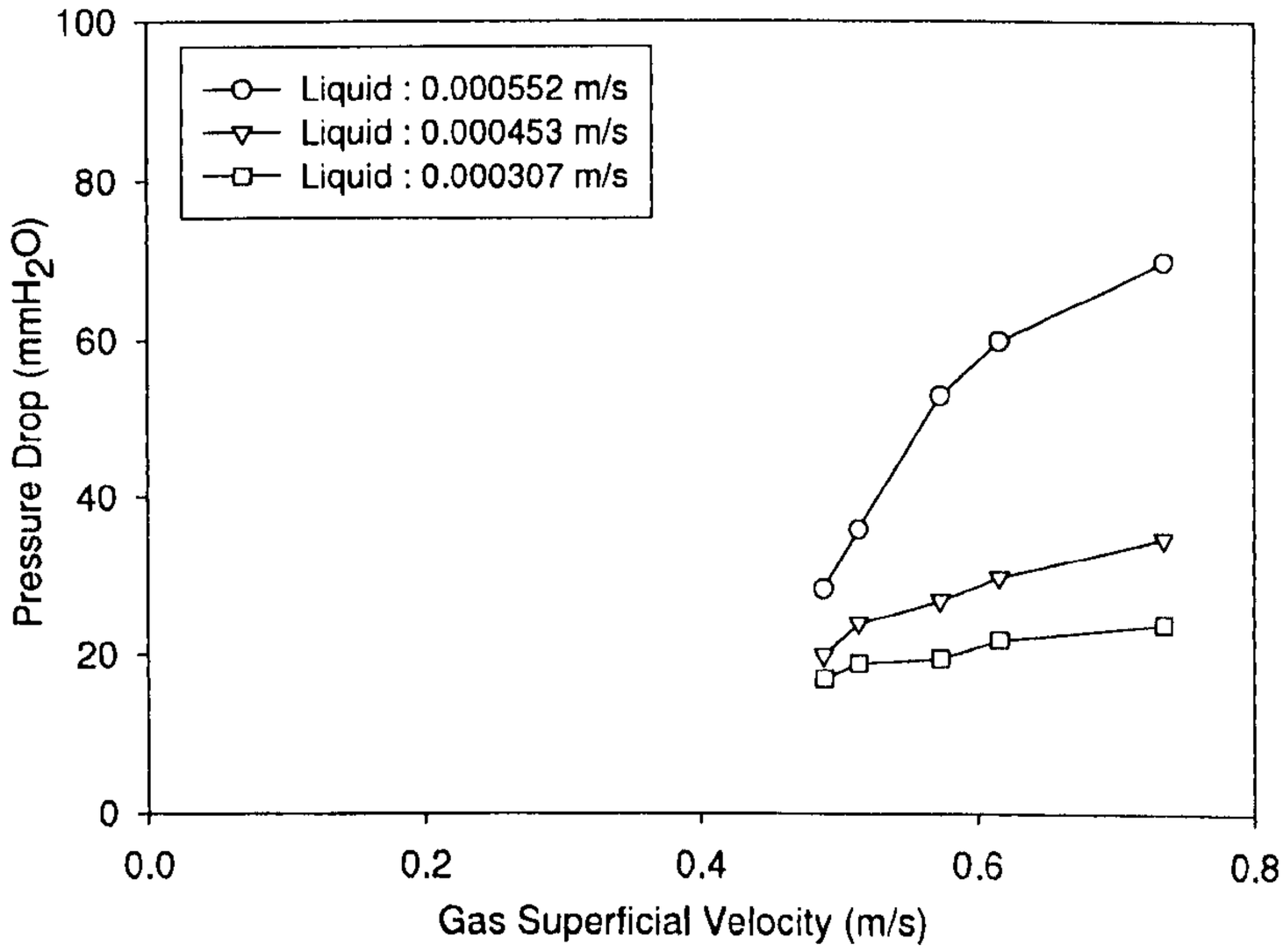

Figure 6.22: Bed pressure drop as a function of gas superficial velocity for three liquid superficial velocities

6.2.6 Effect of H_2S Concentration

Figure 6.23 shows the History of H_2S for the test duration with various gas inlet concentrations. The desulphurisation efficiencies for various H_2S concentration at the inlet are shown in Figure 6.24. The gas and tin flow rates were fixed at 0.258 and 3.860 kg/m^{2}s, respectively, at 400°C. The increase in the inlet concentration of H_2S from 300 to 2000 ppm gradually reduced the removal efficiency from 95.9 to 71.5% (see Table 6.5). Recalling Equation 6.16, this is due to the change in K_o while the gas velocity and interfacial surface area are identical.

K_o is determined by k_G, k_r and k_L. k_G is constant in this set of tests and is expected to be faster than the other rates. Hedden (1986) postulated from the tests in a double-stirred reactor that the reaction of H_2S with Sn is of first order with k_r of 0.012 to 0.020 m/s at 500°C. If the reaction is of first order, then H_{OG} is determined mostly by k_L, i.e., limited mass transfer rate of SnS in tin. In other words, how quickly the liquid surface can be refreshed by dissolving SnS into tin becomes an important rate-controlling factor for increased amount of S (SnS) *due to higher* H_2S *concentrations*.

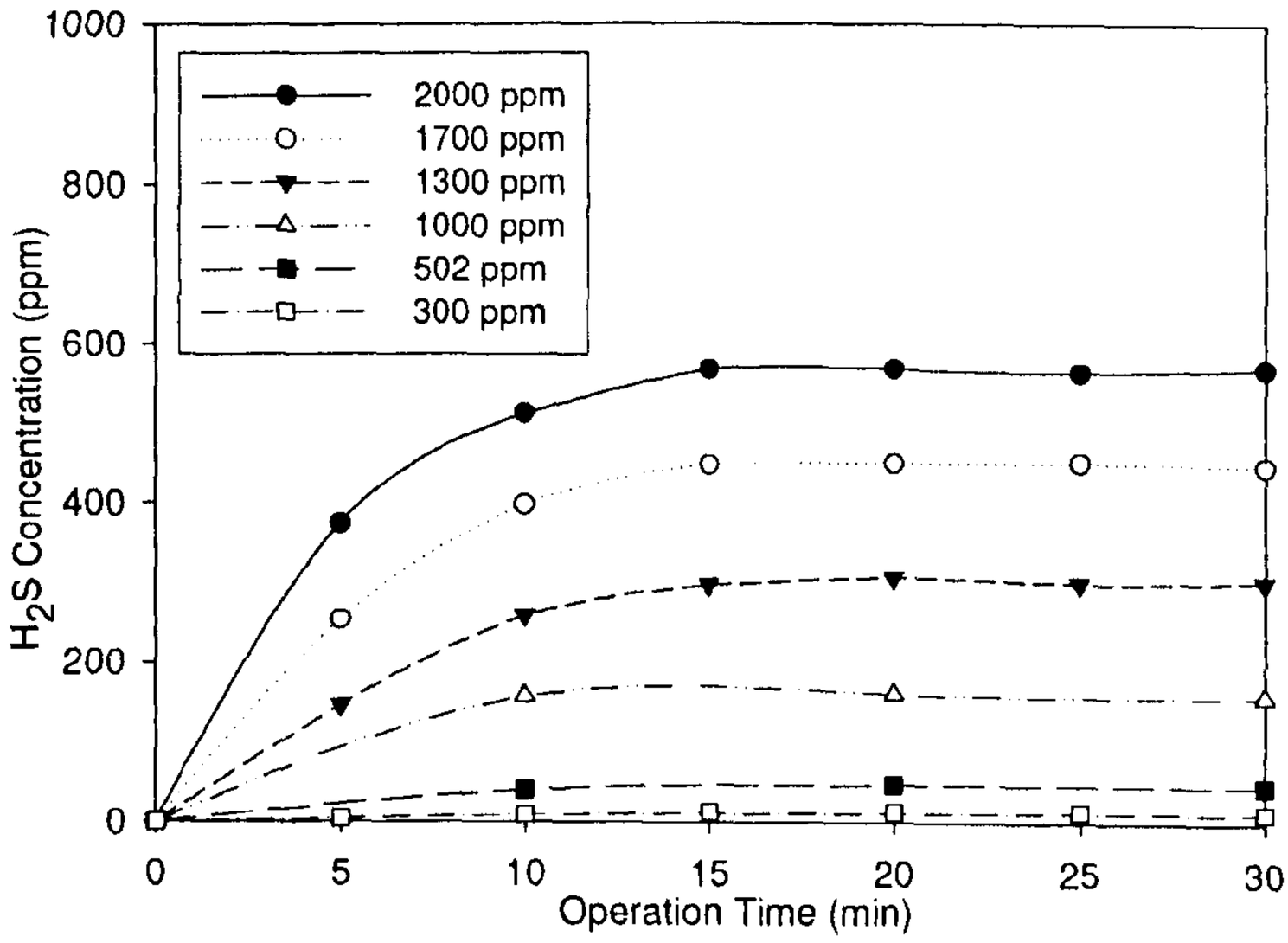

Figure 6.23: History of H_2S for the test duration with various gas inlet concentrations (liquid superficial velocity & gas superficial velocity constant)

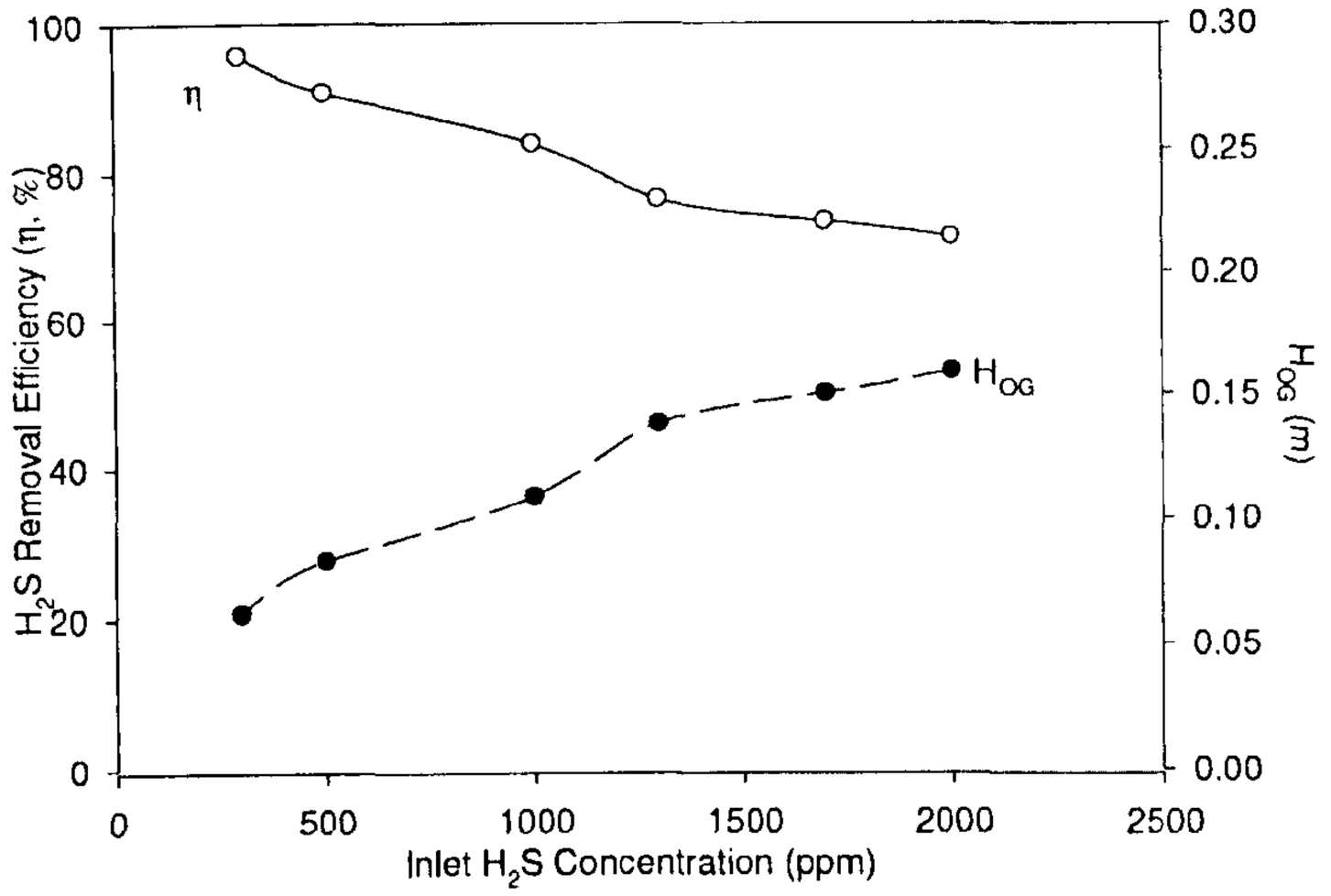

Figure 6.24: H_2S removal efficiency (η) and the gas transfer unit height (H_{OG}) for different inlet H_2S concentrations (m_G= 0.258 kg/m^{2}s; m_L= 3.860 kg/m^{2}s; T=400°C)

Table 6.5: Experimental data for various inlet gas concentration

L kg/m^{2}s	G kg/m^{2}s	u_L m/s	u_G m/s	y_B mol/mol´10^6	y_T mol/mol´10^6	x_B mol/mol´10^6	η %	True N_{OG} (m)	True H_{OG} m
3.861	0.245	5.52E-04	0.490	1995	570	382.69	71.50	0.2740	0.1593
3.861	0.245	5.52E-04	0.490	1695	449	334.62	73.59	0.2906	0.1502
3.861	0.245	5.52E-04	0.490	1304	305	268.29	76.54	0.3178	0.1379
3.861	0.245	5.52E-04	0.490	1000	159	225.86	84.10	0.4022	0.1088
3.861	0.245	5.52E-04	0.490	501.9	46	122.44	90.94	0.5228	0.0833
3.861	0.245	5.52E-04	0.490	304	12	78.36	95.93	0.7034	0.0625

6.2.7 Effect of Operating Temperature

Figure 6.25 shows the History of H_2S for the test duration with various operating temperatures. Figure 6.26 shows the effect of operating temperature ranging from 300 to 400°C. The gas and tin flow rates were fixed at 0.258 and 3.860 kg/m^{2}s, respectively, with inlet H_2S concentration of 1000 ppm. H_{OG} decreased from 0.133 at 300°C to 0.084 at 400°C (see Table 6.6). The desulphurisation became efficient at high temperatures because the increase in the mass transfer and reaction rates is larger than the increase in the gas velocity. However, the effect of thermal equilibrium becomes significant at higher temperatures with high H_2/H_2S ratios (Ryu et al., 2007). Higher temperatures are expected to increase the mass transfer and reaction rate of H_2S while reducing the viscosity of liquid tin. It does not cause a problem with the volatility of liquid tin, but the desulphurisation efficiency at high temperatures would be limited by thermal equilibrium.

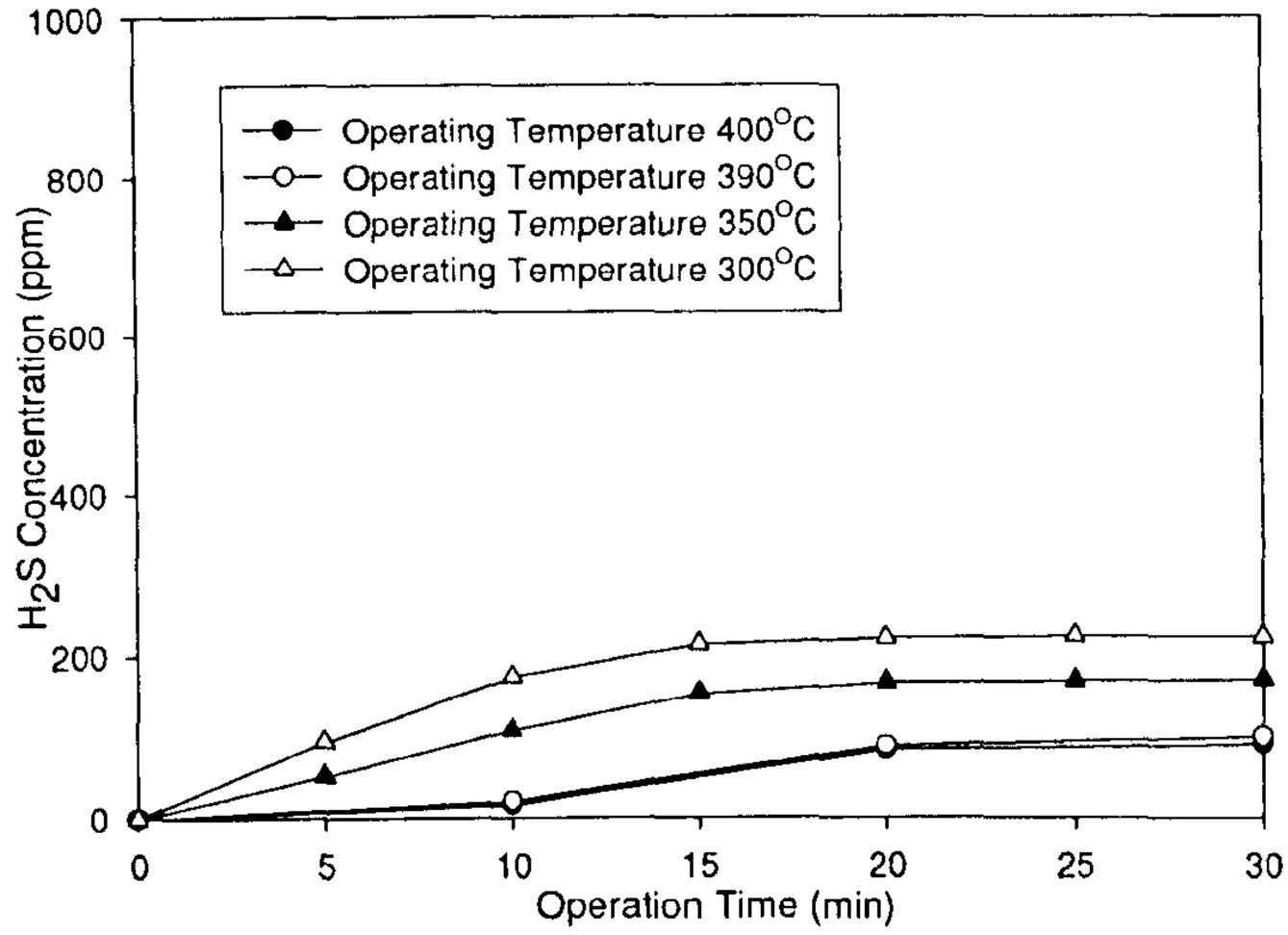

Figure 6.25: History of H_2S for the test duration with various operating temperatures (liquid superficial velocity and gas superficial velocity constant)

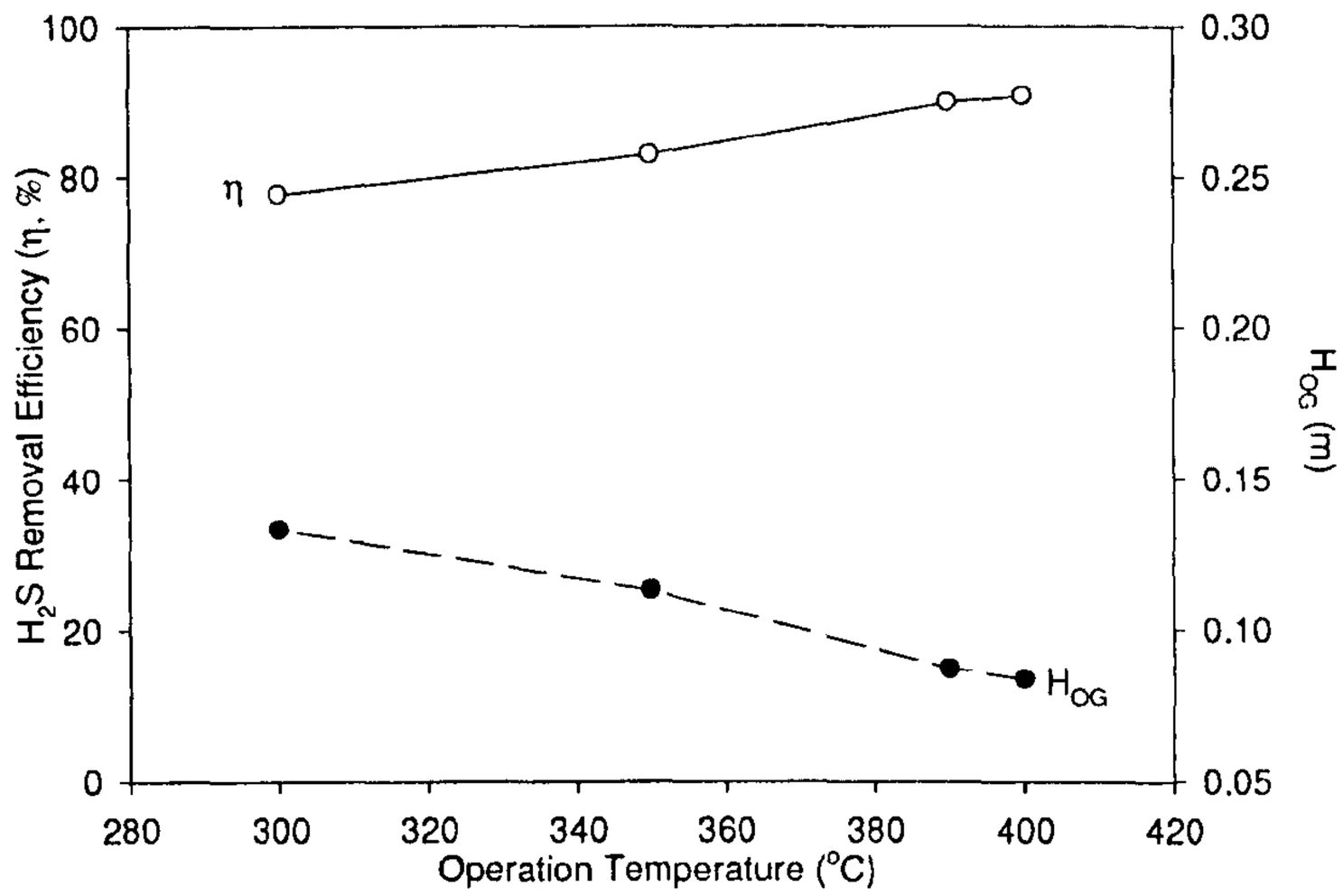

Figure 6.26: H_2S removal efficiency (η) and gas transfer unit height (H_{OG}) for different operation temperatures (m_G= 0.258 kg/m^{2}s; m_L= 3.860 kg/m^{2}s)

In Chapter 3, Figure 3.5 shows the variation of Gibbs free energy for the desulphurisation reaction (Equation 3.7), based on Schürmann's study (1984). Negative Gibbs free energy favours the forward reaction, and vice versa. This suggests that higher temperatures and a higher partial pressure ratio of H_2/H_2S shift the reaction toward H_2S formation. Especially at high H_2/H_2S ratios or higher desulphurisation efficiencies, the dependence on temperature becomes very significant.

At a typical H_2 concentration of 30%, for example, temperatures below 550℃ can reduce the H_2S concentration theoretically to 30 ppm (P_{H2}/P_{H2S} = 1000) if the SnS concentration is sufficient in the liquid tin. Therefore, it is essential to suppress the backward reaction by removing SnS in the tin introduced at the top of the counter flow reactor. The dissolved level of SnS can be minimised through the regeneration process using zinc presented in Equation 3.14. Warner (2000) proposed an external regeneration in a fluidized bed where coarse granular ZnS can be grown on seeds of fine ZnS. The coarse ZnS can be readily separated from the liquid tin. Investigations are required on the theoretical limits and the tin regeneration process.

Table 6.6: Experimental data for various operating temperature

Temp °C	L kg/m²s	G kg/m²s	u_L m/s	u_G m/s	y_B	y_T	x_B mol/mol´10⁶	η %	True N_{OG} (m)	True H_{OG} (m)
400	3.861	0.245	5.52E-04	0.490	1000	92	243.85	90.80	1.864	0.0838
390	3.861	0.245	5.52E-04	0.490	1000	101	241.43	89.90	1.791	0.0872
350	3.861	0.245	5.52E-04	0.490	1000	171	222.63	82.90	1.380	0.1132
300	3.861	0.245	5.52E-04	0.490	1000	223	208.67	77.70	1.172	0.1333

❋ *Kinetic Interpretation*

It is well known that reaction temperature has an effect on the chemical reaction rate during chemical reactions. Arrhenius put forward this semi-empirical regularity from the experimental data and proved that the reaction rate (k_r) variation with temperature (T) was as follow:

$$k_r = A\, e^{\left(\frac{-Ea}{RT}\right)} \tag{6.19}$$

Where k_r = Rate constant (m/s)
A = Frequency factor or pre-exponential factor (m^3/kmol.s)
E_a = Activation energy(kJ/mol)
R = Gas constant (kJ/mol.K)
T = Temperature (K)

Rearranging Equation 6.19 gives,

$$\ln(k_r) = -\frac{E_a}{RT} + \ln(A) \tag{6.20}$$

Comparing the latter form of the Arrhenius equation to the equation for a straight line, $y = mx + c$, it is obvious that a plot of $\ln(k_r)$ versus 1/T will produce a slope of $-E_a/R$ and the intercept of ln(A). The experimentally determined k_r values at various temperatures are graphically provided in the form of an Arrhenius plot (Figure 6.27). The rate constants were obtained from a model developed to study the rate of chemical reaction between tin and sulphur. The range of reaction rate constants from this work is 0.011 to 0.019 m/s for various operating temperature as shown in Table 6.7. These results are within the broad range of values as reported by Hedden (1986) as mentioned in sub-section 6.2.6. The development and results of the model will be discussed further in Chapter 7.

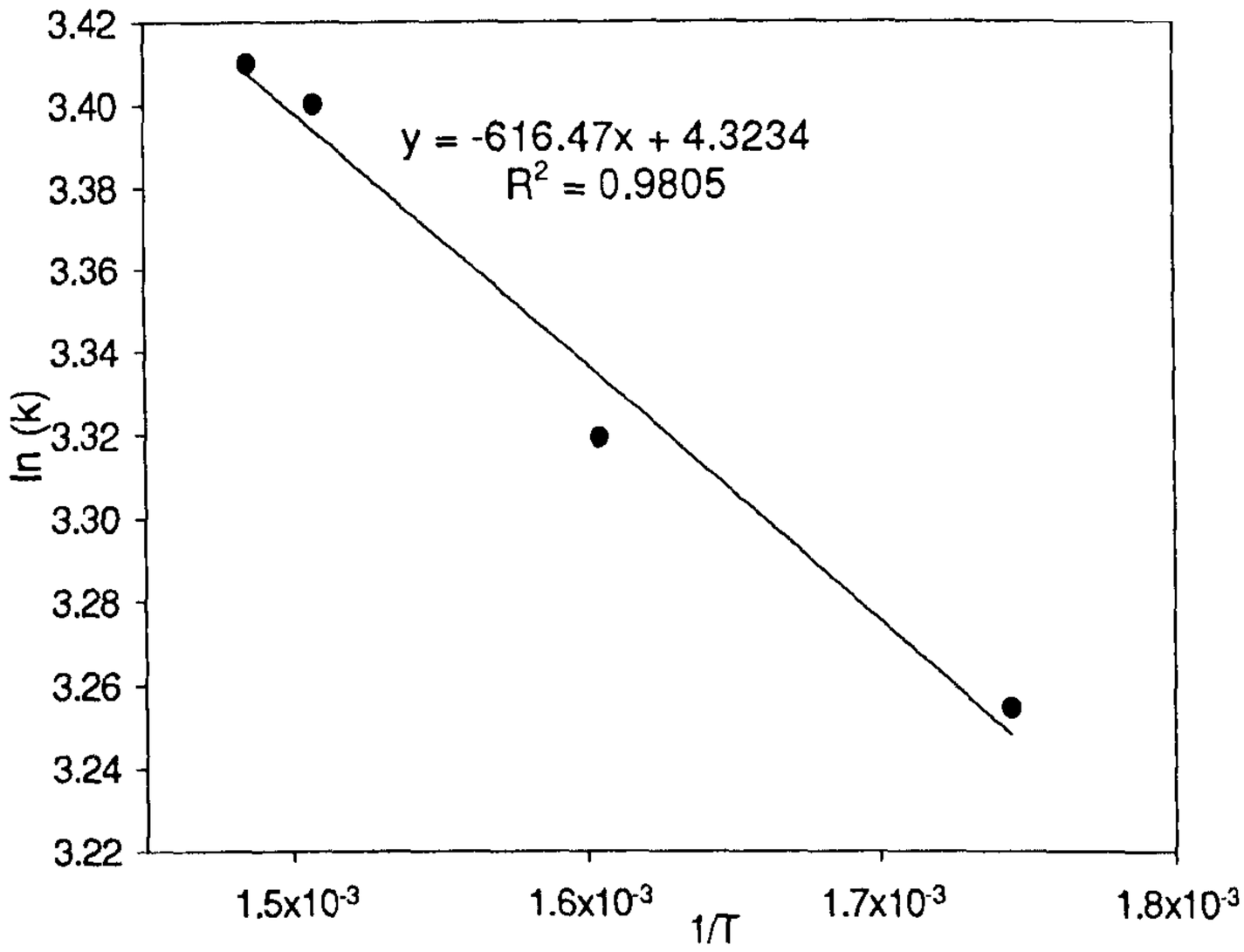

Figure 6.27: Arrhenius plot for the reaction of Sn and H_2S at various operating temperature

Table 6.7: Rate constant value from experimental data for various operating temperature

Temperature (°C)	Efficiency, η (%)	Rate constant (m/s)
400	90.80	0.0188
390	89.90	0.0180
350	82.90	0.0136
300	77.70	0.0114

In this study, when determining the reaction rate constant, the value of a_e was assumed to be 346 m^2/m^3. The activation energy (E_a) and the pre-exponential factor of the desulphurisation reaction were calculated to be 5.13 kJ/mole and 75.45 m^3/kmol.s respectively. However, the E_a value reported by Hedden (1986) (60.0 kJ/mole at 500°C) is significantly higher. The value of E_a obtained from this work is approximately 10 times smaller compared to Hedden. These differences are likely to be related to the differences in experimental techniques (double-stirred reactor) compared to the packed bed scrubber used in this study. This also indicated that the reaction between liquid tin and H_2S in the packed bed was fast compared to the double stirred reactor. It is probably because of the larger interfacial area between liquid tin and H_2S provided by the packed bed scrubber. Moreover, the usage of liquid tin having a non-wetting property will provide a larger interfacial area compared to other scrubbing liquids which have a wetting property.

6.2.8 Effect of Scrubber Packing Height

Figure 6.28 shows η and H_{OG} acquired for three different bed heights (0, 100 and 200mm) with two H_2S concentrations at the inlet (541 and 1000 ppm). The gas and tin flow rates were fixed at 0.258 and 3.860 kg/m^2s, respectively, with an operating temperature of 400°C. The tests with an empty column had η of about 40% due to lack of interfacial contact area, which corresponded to H_{OG} values of 0.40 m. These H_{OG} values were then used to correct the results for the 100mm high packing by removing the effect of the empty half of the column above. Figure 6.28 shows that the increase in the bed height from 100 to 200 mm resulted in an increase in the removal efficiency from 66% to 84% (see Table 6.8). However, the H_{OG} was almost constant for both packing heights at both concentrations, which conforms to its definition.

Table 6.8: Experimental data for different height of packing

Height M	L kg/m²s	G kg/m²s	u_L m/s	u_G m/s	y_B	y_T	x_B	η %	True N_{OG} (m)	True H_{OG} m
					mol/mol´10⁶					
20	3.861	0.245	5.52E-04	0.490	1000	159	225.86	84.10	1.437	0.1088
10	3.861	0.245	5.52E-04	0.490	1000	326	181.03	65.80	0.876	0.2602
0	3.861	0.245	5.52E-04	0.490	1000	613	103.93	35.68	0.382	0.4532
20	3.861	0.245	5.52E-04	0.490	541	67	127.30	87.63	1.632	0.0957
10	3.861	0.245	5.52E-04	0.490	541	176	98.02	67.47	0.877	0.2506
0	3.861	0.245	5.52E-04	0.490	541	327	57.47	39.56	0.393	0.3972

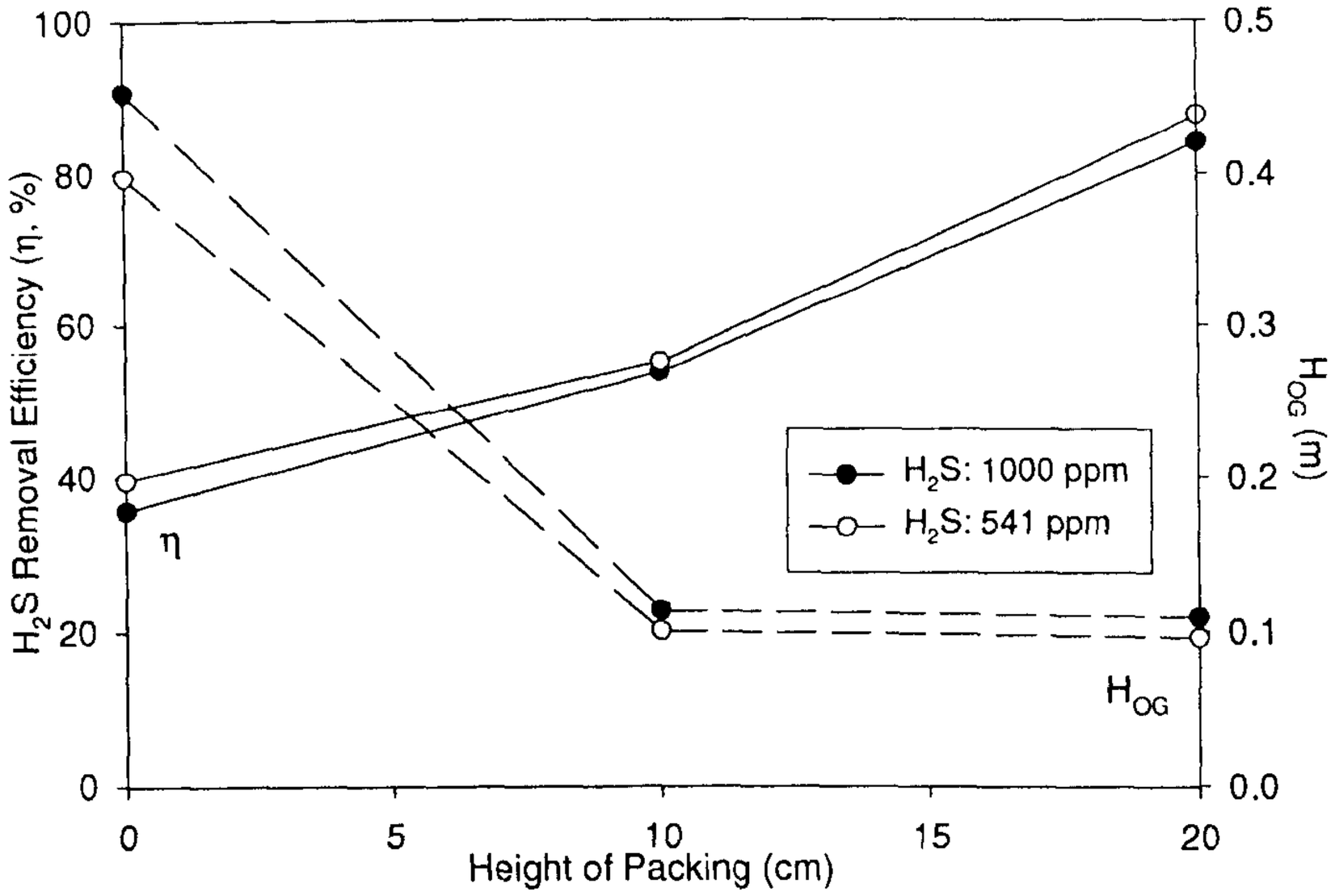

Figure 6.28: H_2S removal efficiency (η) and the gas transfer unit height (H_{OG}) for different packing heights (m_G= 0.258 kg/m^{2}s; m_L= 3.860 kg/m^{2}s; T=400°C)

6.2.9 Experiment Measurement Accuracy

The accuracies of the equipment used in this experiment are summarised in Table 6.9. As some of the equipment employed in the desulphurisation work are similar to the ones used for the particulate cleaning in previous section, only equipment that has no previous examples are described in this section to avoid repetition.

Table 6.9: Accuracy of equipment used

Apparatus/ Instrument	Measured Quantity	Accuracy
H_2S Rotameter	H_2S volumetric flowrate	±0.5 cm^3/min
ABB Gas Chromatograph	H_2Sconcentration in outlet gas	Span gas accuracy±5% (due to reading fluctuations)
K-type Thermocouples	Bed temperature	±0.0075℃ of the actual temperature/±2.5℃
Measuring Tape	Packed bed height	±0.05 cm

6.3 Tin Sulphide Cleaning

6.3.1 Cleaning In The Presence of Zinc Powder

6.3.1.1 Amount of Sulphur Collected

Three separate test runs were carried out to determine the total sulphur removed from the tin sulphide cleaning in the presence of zinc powder. The mass of the sulphur strips from tin sulphide before the test and the mass of the residues after the test are summarised in Table 6.10.

Table 6.10: Results of sulphur determination for SnS cleaning in the presence of Zn

	Run 1 (600℃) (3 hours)	Run 2 (400℃) (4 hours)
Mass of SnS before test (g)	2.7863	2.6997
Mass of residues after test (g)	1.9902	1.9853
Mass loss(-)/gain(+) of contents (g)	-0.7961	-0.7144
Residues as weight % of original tin wires	71.43	73.53

6.3.1.2 Reaction with Zn Powder (1st Method)

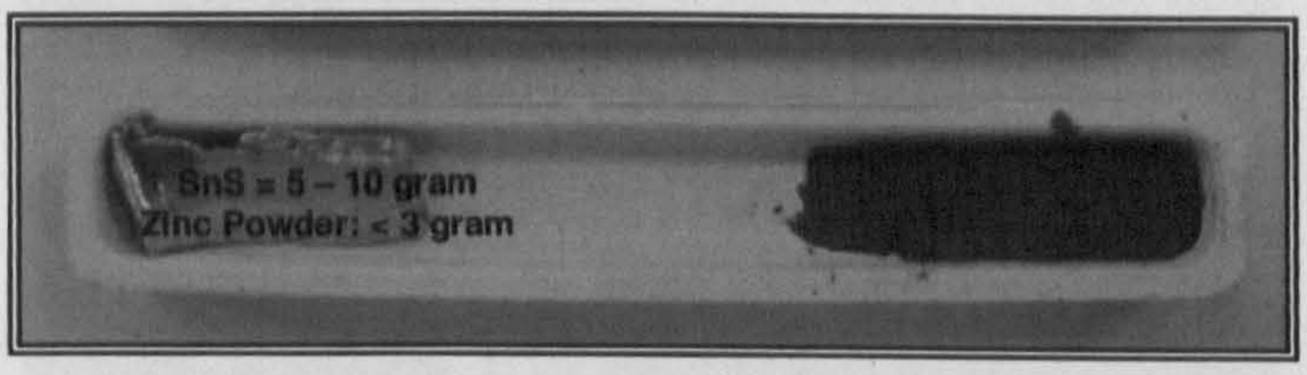

Figure 6.29: Original SnS and zinc powder in the crucible before test

In the first experiment, the sample of SnS and zinc powder were located at different ends of the crucible. Figure 6.29 shows the original SnS and zinc powder prior to the experiment. Figures 6.30 and 6.32 are images of the cooled SnS crucibles containing the residues after the test for different operating temperatures, 400 and 600℃ respectively. The heated SnS reacted with zinc powder forming a significant amount of soft white to yellow colour powder or crystals (Run 1) deposited between the SnS and zinc powder area. The location of this white to yellow solid residues suggests that it was a product of reaction(s) between the SnS and the zinc powder.

Figure 6.31 is a magnification of the zinc sulphide formed in between the SnS and zinc powder area shown in Figure 6.30. Also as can be seen from Figure 6.30, the SnS was coated with a black/white layer. This probably resulted in the formation of SnO or SnO_2 during the cooling process. Upon scraping the solid with a spatula a shiny silver surface was exposed. The weight loss of the SnS was approximately 30% and this confirms the reaction between SnS and zinc powder. The reaction, which resulted in the loss of sulphur from SnS, was described earlier and shown in Equation 3.17 of Chapter 3. The equation indicates that under such conditions (as explained above), ZnS formation from the reaction is extremely favourable. The colour of the solid deposit can also be used to show of the reaction that took place.

Figure 6.30: SnS crucible after test (Run 1)

Figure 6.31: Formation of zinc sulphide during the cleaning process

Figure 6.32: SnS crucible after test (Run 2)

Figure 6.32 showed the colour of the sample was silver-white, which indicated that the sulphur also has reacted with the zinc powder. Although the operating temperature was only 400℃, it was only possible to clean the SnS by prolonging the heating/reaction time between SnS and zinc (same temperature as the desulphurisation operating temperature). The difference between these two operating temperatures was because at 600℃ the rate of reaction between SnS and zinc powder was assumed to be higher when compared to the rate of reaction at 400℃. Table 6.11 shows the physical properties of several compounds of interest.

Table 6.11: Physical properties of tin compounds of interest

Compound	Colour of Solid	Melting Point (C)	Boiling Point (C)	Ref.
Sn	Silver-White	232	2623	(i)
SnO	Black	1050	1425	(i)
SnO_2	White	200	2500	(i)
SnS	Brown	881	1210	(i)
ZnS	White to Yellow	1830	1185	(ii)
Zn	Black	420	908	(ii)

(i)Nielsen and Sigurdardottir, 1993; Vogel, 1989; Samsanov, 1982
(ii)Oxford Chemist, 2007

6.3.1.3 Reaction with Zn Powder (2nd Method)

In the second experimental method, the sample of SnS was placed on top of the zinc powder. The main purpose of this second method is to study the possibilities of SnS cleaning by putting the SnS and zinc powder together. Figure 6.33 shows the original SnS and zinc powder (lumped together) prior to the experiment. Figure 6.34 shows the cooled crucibles containing the residues after the test. The heated SnS reacted with zinc powder, fused together and formed a mixture of Sn, SnS, Zn and ZnS. Considering the Sn will be reused for the desulphurisation process, in this case an additional process needs to be added in order to separate the fresh Sn from the other residues. Therefore this proves that the second method is not practical since it will increase the operational cost of the plant.

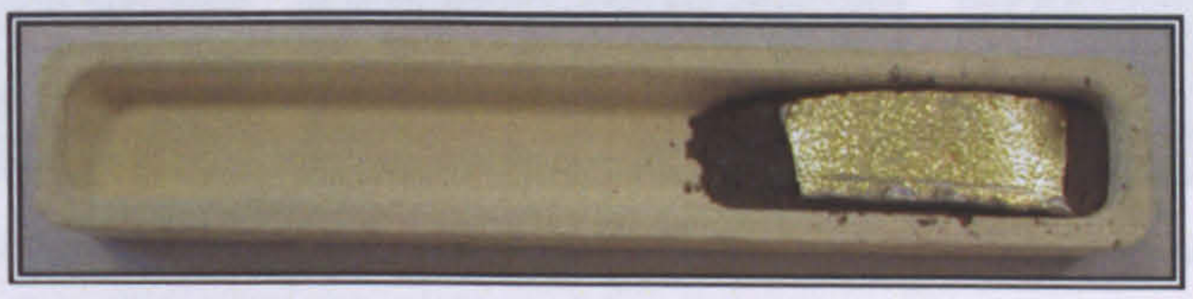

Figure 6.33: Original SnS and zinc powder in the crucible before test

Figure 6.34: SnS crucible after test

6.3.2 Cleaning Without Zinc Powder

6.3.2.1 Experimental Observations

One test run was carried out without the addition of zinc powder. In this experiment, it was observed that the SnS sample changed colour after 2 hours of heating. The molten state of the sample was only observed after 6 hours heating (see Figure 6.35(f)). The change of colour during the cleaning process can be seen in Figures 6.35(a) to 6.35(f). It was noted that the slight change of colour occurred at the temperature of 300℃ (Figure 6.35(d)). This initial change could be attributed some of the sulphur being released during the heating of the SnS sample. Once the SnS started to melt, the colour of the samples changed to gold-silver. The amount of sulphur released during this process is shown in Table 6.12.

Figure 6.35(a)

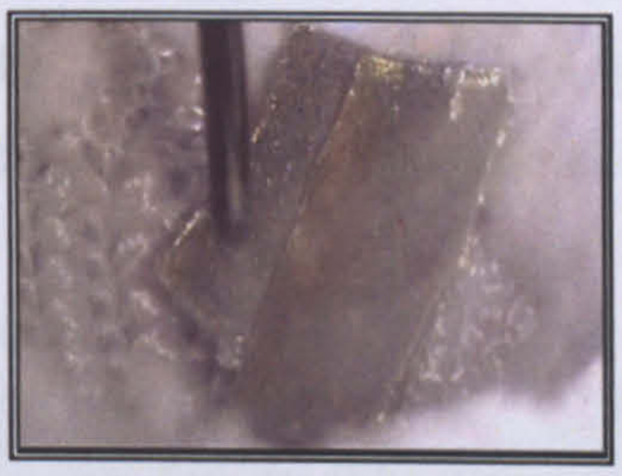

Figure 6.35(b)

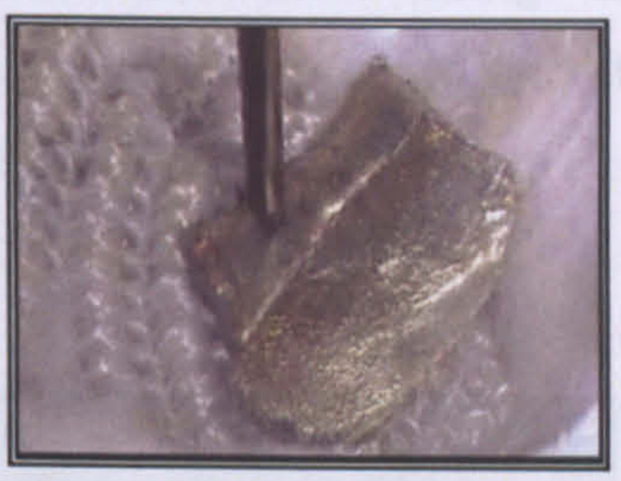

Figure 6.35(c)

Figure 6.35(d)

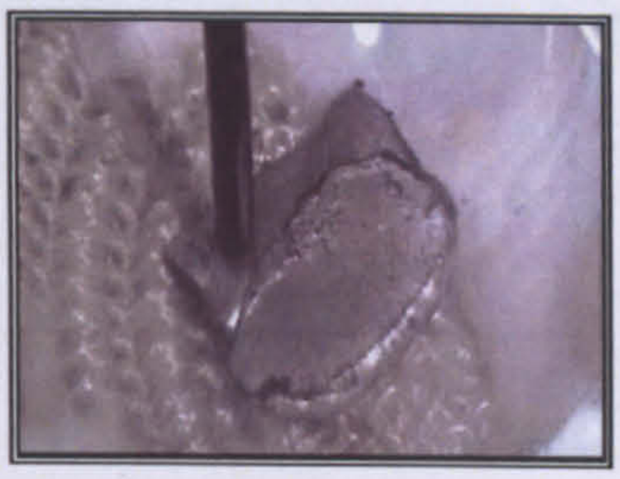

Figure 6.35(e)

Figure 6.35(f)

Figure 6.35: SnS in glass flask during the test

6.3.2.2 Amount of Sulphur Collected

Table 6.12: Results of sulphur determination for SnS cleaning without the presence of Zinc

Mass of SnS before test (g)	2.6321
Mass of SnS after test (g)	1.9289
Mass loss(-)/gain(+) of contents (g)	-0.7032
Residues as weight % of original tin wires	86.92

The weight loss of SnS after the heating process without addition of zinc powder was approximately 13 %. There was roughly 17 % difference between cleaning (heating) process with and without zinc. The reduction was small and any reaction involving the SnS was limited by the small surface area exposed to the gas stream. Since nitrogen gas was considered inert and thus did not react with either with SnS, Sn and S, the decreased in sample weight was definitely caused by the sulphur that was released during the heating process. The presence of zinc gave a significant difference in percent weight loss of SnS.

6.3.3 Experiment Measurement Accuracy

Throughout this experiment there could have been errors that were not accounted for. However, one main source of error associated with this experiment was the determination of the amount of sulphur left in the crucible while using the microbalance. Calibrating the equipment prior to use rectified the error and its accuracy was accounted for during calculations (shown in Table 6.13).

Table 6.13: Accuracy of equipment used

Apparatus/ Instrument	Measured Quantity	Accuracy
Microbalance	Mass of crucible plus contents	± 0.00005 g

6.4 Summary

6.4.1 Particulate Removal

This experimental work was carried out using nitrogen gas for tin circulation at high temperatures (350 - 400℃) and the glass particles inlet was kept at ambient temperature at 15℃. The large temperature difference meant that the liquid (flowing downwards) solidified upon collision with the cool glass particles. This resulted in solid tin build-up on the surface of the glass particles, thus reducing the E_T. In the exhaust side of the scrubber, liquid tin splashes were observed which were then identified in the filter paper. The average splashed tin was found to be around 5.45 g. So the true E_T will have to take account of the amount of splashed tin, the mixture of Si-Sn and the unseparated glass particles on the filter paper. At the lower bed temperature (350℃), the agglomerates formed at early stages were very fragile and contained a grey Si-Sn mixture. The liquid tin solidified slowly, making it more adhesive and it was attached onto the surface of glass particles upon collision. At 400℃, the formed agglomerates were stronger and had a black colour. This is associated with liquid tin, which solidified even more rapidly during the filtration process. The liquid tin-irrigated packed bed scrubber demonstrated particulate removal performance with E_T ranging from 60 to 98%. The E_T decreased as the inlet dust loading increased. The results also showed that the temperature had a significant influence on the E_T. As the temperature increased from 350℃ and 400℃, the E_{Total} decreased. The major reason for this is the temperature difference between the inlet particles and the scrubber, which result in the formation of a thicker bed of agglomerates. The resulting grade efficiency curves were not able to demonstrate realistic results. This is because at the same corresponding liquid flow rates and inlet solid loading, the particles collected in the impinger were not a representation of the same total particle collection as in the total efficiency experiment. As mention earlier the main reason was the formation of agglomerates. Moreover, it was not practicable to clean the scrubber after each test run. The design limitations will be discussed in Chapter 9.

6.4.2 Desulphurisation

The absorption behavior of H_2S in the novel liquid tin irrigated hot gas scrubber was investigated for various operating parameters in a lab-scale packed bed. H_{OG} values ranged from 0.84 to 0.181 m for the test conditions at 1000 ppm H_2S concentration, which showed the good potential of this system for efficient desulphurisation. High liquid velocities increased the removal efficiency due to larger liquid holdup. This created larger interfacial areas. Increased gas velocities influenced the removal efficiency by altering the gas residence times, liquid holdup, and gas-phase mass transfer. The H_{OG} of an empty column was about 5 times higher at the tested conditions due to the lack of contact between the two phases. The H_{OG} gradually reduced at increased H_2S concentrations or at lower operating temperatures. Further fundamental studies are required on various aspects of this scrubber, especially for higher gas and liquid velocities and operating temperatures. It is also anticipated that electromagnetic or mechanical pumps would be used to circulate the tin in an industrial environment.

6.4.3 Tin Sulphide Cleaning

The cleaning of SnS was performed with and without the presence of zinc powder. The amounts of sulphur captured on both occasions were compared. Addition of zinc powder saw around 20% reduction of sulphur in the sample compared to without zinc. Tin recovery at different temperatures (400℃ and 600℃) gave similar results but the formation of ZnS was more evident at a temperature of 600℃. This is because of the higher rate of reaction between SnS and zinc powder. At 400℃, the formation of ZnS was not so apparent in the crucible. This could be due to ZnS formed during the reaction being fused together with the zinc powder. Observation of SnS cleaning without the addition of zinc powder gave a positive result. However, the sulphur reduction of ~13 % could not justify heating the sample to 400℃ for 6 hours. The small scale cleaning process has provided confirmation and evidence of a possibility to clean SnS using zinc in a gasification environment.

CHAPTER SEVEN

Mathematical Modelling

The first section of this chapter presents the results obtained from computational fluid dynamics (CFD) modelling of particulate removal in a hot gas packed-bed scrubber. Grid generation pre-processing was carried out on GAMBIT whilst mathematical calculations were performed using a CFD solver on FLUENT 6.3. Calculations were also carried out in order to simulate the rate of reaction in the packed-bed scrubber using Microsoft Excel. The results are presented in the second part of this chapter. The main reason for developing two different models (particulate cleaning and desulphurisation) was to study the behaviour of the cleaning process using liquid tin in the packed-bed hot gas scrubber. As mentioned earlier in the first chapter, the liquid tin is capable of cleaning both particles and H_2S simultaneously.

7.1 Computational Fluid Dynamics – Particulate Removal

7.1.1 Problem Definition and Geometry Assumptions

The removal of particulates from a gas stream flowing through a packed-bed of spheres under hot liquid tin flow conditions was simulated using FLUENT 6.3. Results from the modelling were then compared to a previous study done by Chang (2003). In the actual packed-bed hot gas scrubber, liquid tin flows downwards counter-currently to the upward flowing gas stream laden with dust particles. Under hot conditions, the liquid flows as discrete droplets and rivulets on the packing surface (Chang, 2003). In this preliminary CFD simulation study, it was assumed that no droplets were present on the packing surface since the aim of this modelling work was to study the effect of different parameters to the total efficiency of particle cleaning. In the actual system, the solid spheres are randomly packed within the column. Graton and Fraster (1935) discussed several instances of systematic packing of spheres. These systematic assemblages are made up of either square or simple rhombic layers (Figure 7.1), or a combination of both types of layers. The square and simple rhombic layers form four major types of systematic packing which are listed in Table 7.1.

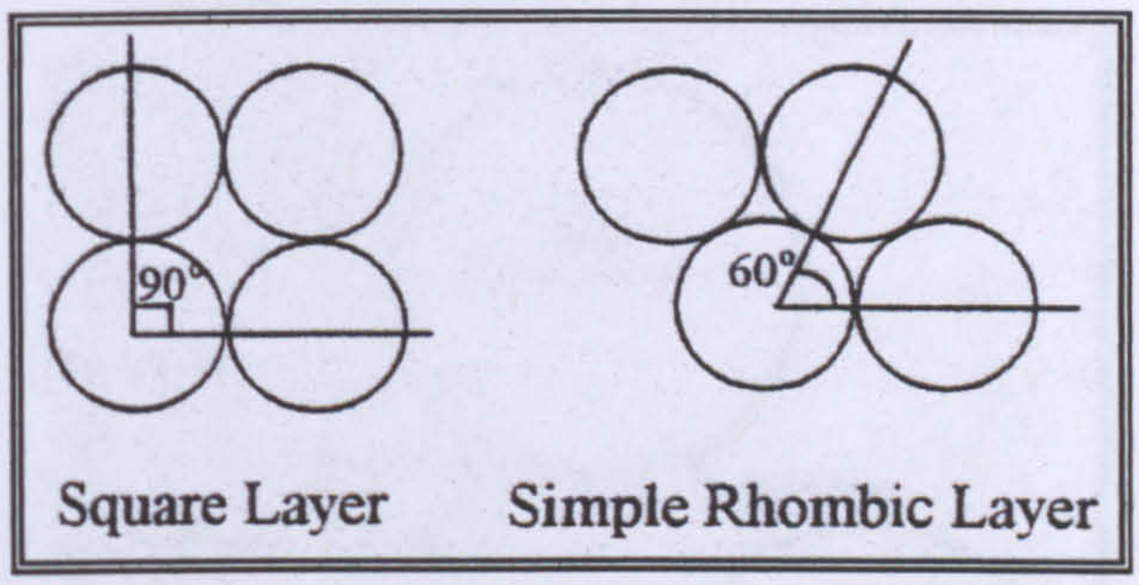

Figure 7.1: Square and simple rhombic layers

In each type of systematic packing, every sphere is arranged identically with respect to every other sphere, and each sphere is identified by the same co-ordination number i.e. the number of adjacent spheres which are in contact with a selected sphere (Gray, 1968). There is a characteristic porosity associated with each systematic packing type.

Table 7.1: Systematic assemblages of spheres (Graton and Fraser, 1935)

Systematic Packing Type	Porosity (%)	Co-ordination Number
Cubic	47.6	6
Ortho-rhombic	39.5	8
Tetragonal	30.2	10
Rhombohedral	26.0	12

The porosity of the packed-bed with 9.53 mm high-purity ceramic alumina (Al_2O_3) spheres is 45%. Based on the porosity, the packed-bed closely resembles a cubic type of systematic packing as shown in Table 7.1. In reality, the packed-bed was randomly filled with the solid spheres which resemble a rhombic systematic packing type.

7.1.2 Geometry Setup and Grid Generation

In this modelling work, the system was assumed to be without any droplets of liquid tin. The total volume of the packed-bed (bed height 19 cm, column diameter 7.8 cm) was 907.89 cm^3 and the packing in the model was made up of spheres having a diameter of 9.53 mm. With the assumption that the solid spheres occupied the column in a randomly packed manner, free space exists between the packing elements. The gap between any given solid sphere was found to be 0.3143 mm. Figure 7.2 shows the basic unit geometry representing the space between spherical solids.

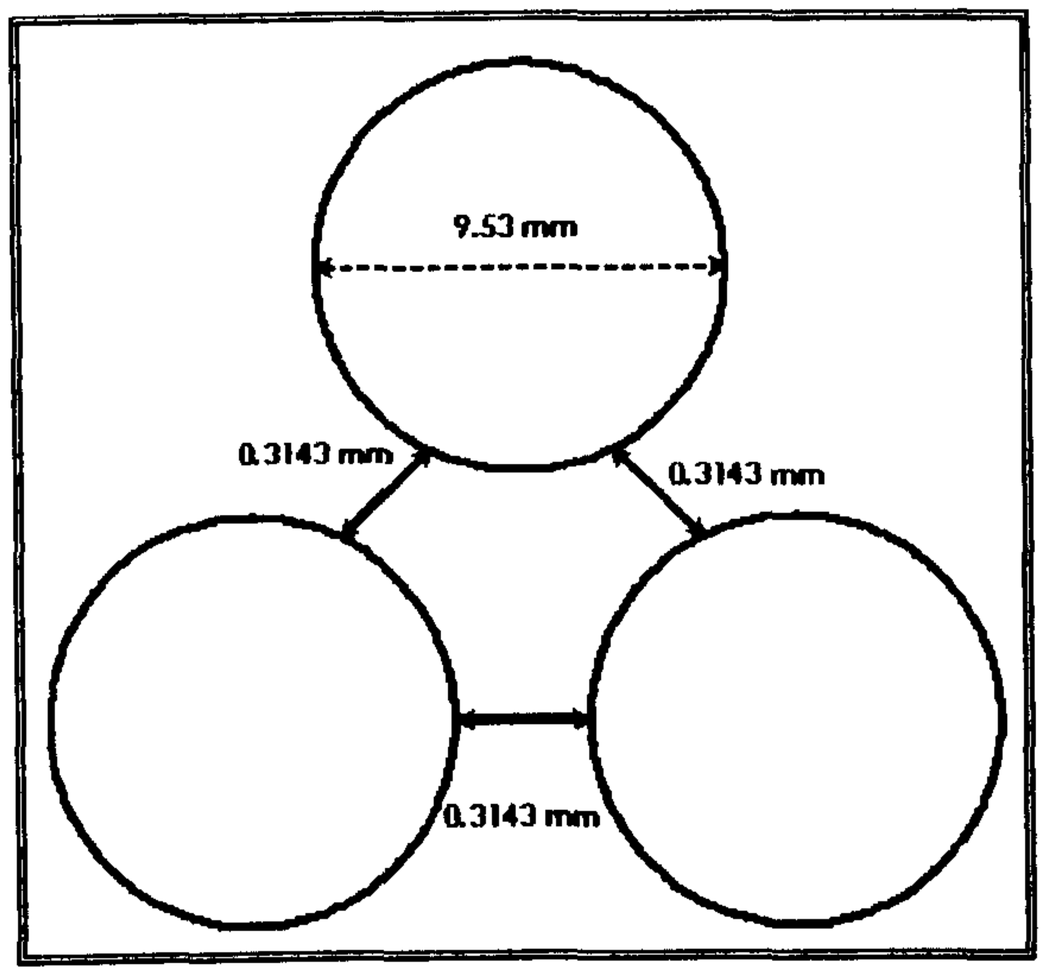

Figure 7.2: Basic unit geometry: Space between solid spheres in column

3-Dimensional geometry setup and grid generation were performed using the GAMBIT CFD Pre-processor (Fluent Inc.). The final 3-dimensional packed-bed geometry was constructed using 2 x 2 x 10 basic units contained within a cuboid. This was the absolute maximum number of basic units which could be achieved by the computer memory during meshing. The total volume of the 2 x 2 x 10 basic units was subtracted from the cuboid volume giving the volume occupied by the gas phase. The cuboid represents an actual model of the packed-bed with the dimensions of 2 cm (width) by 2 cm (length) and the height of 10 cm. The grid of the gas phase volume was generated using the Tet/Hybrid meshing elements in conjunction with the T-grid meshing scheme.

With the above considerations in mind, all the faces were meshed with irregular triangular mesh elements following the Tri-Pave face meshing scheme. The grid volume was meshed with tetrahedral mesh elements. The tetrahedral mesh elements were chosen since they are able to fit into the rounded surface of the spheres with the sharp corners of the intersecting spheres. It was not possible to generate finer meshes with interval size smaller than 0.5 mm because the time taken to complete the mesh was not practical. Also, errors were encountered in FLUENT 6.3 when the mesh size was smaller than 0.5 mm. Figure 7.3 shows the packed-bed model (2 cm x 2 cm x 10 cm cuboid) which houses 11 layers of 2 x (½+1+½) solid spheres. The gas phase volume in between the solid spheres and droplets was completely meshed with the final grid consisting of 148526 cells.

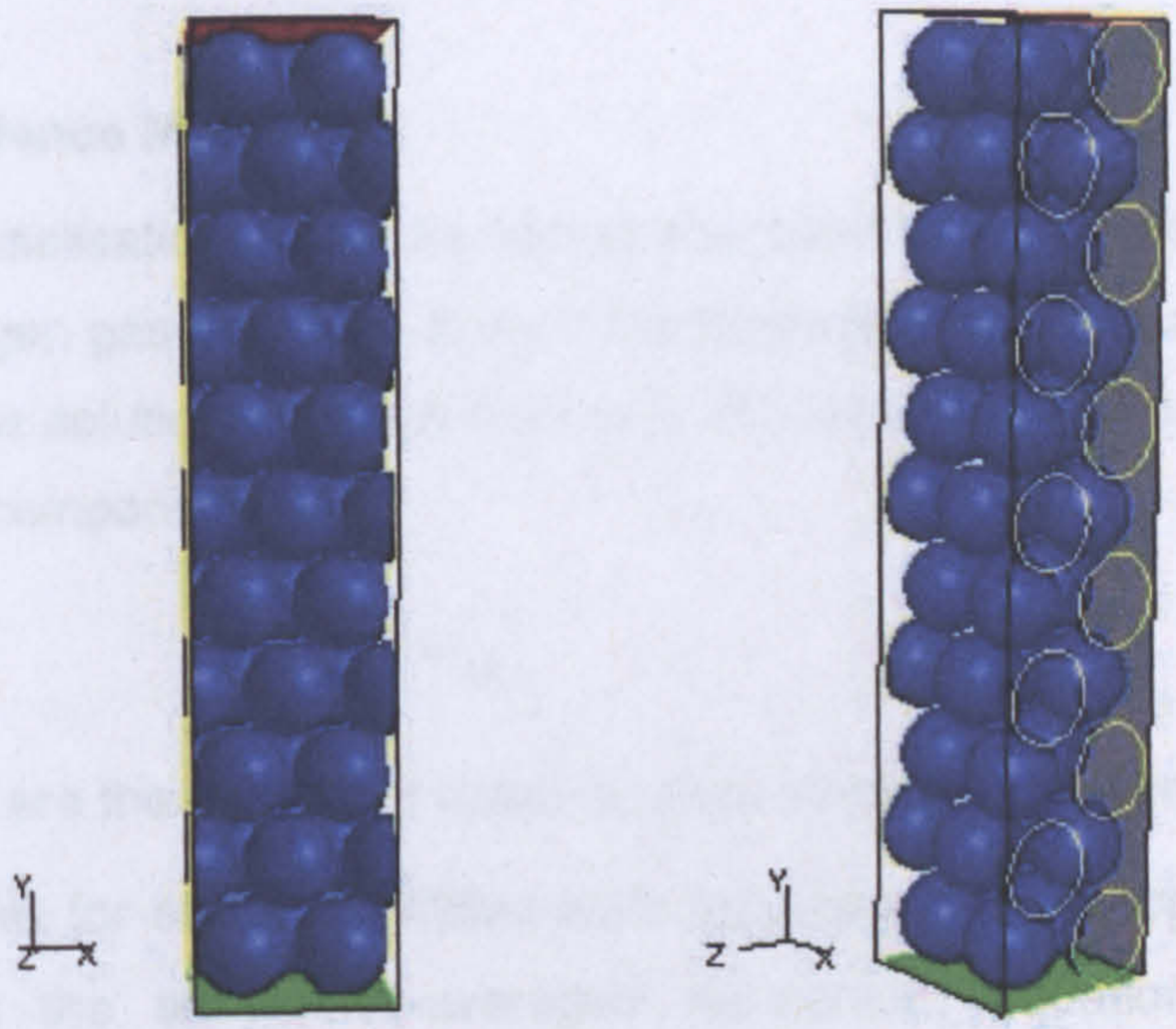

Figure 7.3: Front and side views of meshed packed-bed model

7.1.3 Mathematical Models

The steady-state continuous nitrogen gas phase flow field was modelled using the RNG k-ε turbulence model. Discrete phase particle trajectories were then computed for particles injected from the Mass Flow Inlet face boundary into the flow domain.

7.1.3.1 Continuity and Momentum Equations

The conservation equations of mass and momentum were solved by FLUENT 6.3 for all flows. The conservation of mass or continuity in the i-direction for the continuous phase is represented by equation 7.1. The source term S_m is zero in this case as there is no mass transfer into and out of the continuous gas phase.

$$\frac{\partial}{\partial x_i}(\rho u_i) = S_m \qquad (7.1)$$

The conservation of momentum in the i-direction can be described by the general equation:

$$\frac{\partial}{\partial x_j}(\rho u_i u_j) = -\frac{\partial_P}{\partial x_i} + \frac{\partial \tau_{ij}}{\partial x_j} + \rho g_i + F_i \qquad (7.2)$$

Where P is the static pressure, τ_{ij} is the stress tensor, ρ_{gi} is the gravitational body force, while F_i represents any external body forces impacting the continuous phase. F_i is zero in this case.

7.1.3.2 Turbulence Model

The RNG (renormalisation group) k-ε model was used to model the turbulence in the continuous nitrogen gas flow field. It uses the Reynolds-averaged approach whereby the instantaneous solution variables consist of the mean and fluctuating components. For the velocity components:

$$u_i = \overline{u}_i + u_i \qquad (7.3)$$

Where $\bar{u}_i$ and u'_i are the mean and instantaneous velocity components (i = 1, 2, 3).

The same applies for scalar quantities such as pressure or energy. The turbulence model includes the ensembles-averaged momentum equations containing the Reynolds stress which represent the effects of turbulence, modelled using the Boussinesq hypothesis. In addition to the continuity and momentum equations, the transport equations describing the turbulent kinetic energy k (equals ½ $\bar{u}_i'^2$ for unit mass) and the turbulent dissipation rate ε were solved. The turbulent viscosity μ_t is computed as a function of k and ε. The main reasons for selecting the RNG k-ε model was that it provides an option to use a differential formula for effective viscosity to account for low Reynolds number effect, a feature which is absent from the standard k-ε model. The flow through the packed-bed is affected significantly by the wall boundaries of the solid spheres and the liquid droplets.

7.1.3.3 Discrete Phase Model

A discrete phase of spherical particles dispersed in the continuous gas phase was introduced to represent the solid dust particles in the gas stream. The particle trajectories were computed via uncoupled calculations between the discrete and continuous phases. While the continuous phase impacted the discrete phase constantly, in the uncoupled approach the discrete phase does not affect the continuous phase flow field. The highest solid concentrations used in the simulations were 4800 ppm_w or 0.48 wt. % and the particle was injected with the same velocity as the gas phase at the inlet to the flow domain.

For such low mass and momentum loading of particles, the use of uncoupled calculations is deemed reasonable. The discrete phase trajectory was computed via stepwise integration of the force balance on the particle over discrete time steps. The particle inertia was equated to the thermodynamic drag, the gravitational force and other additional forces acting on the particle.

For steady flow in the x-direction in Cartesian coordinates:

$$F_D(u - u_p) + \frac{g_x(\rho_p - \rho)}{\rho_p} + F_x = 0 \qquad (7.4)$$

Where $F_D(u - u_p)$ is the drag force per unit particle mass; F_D equals $18\mu C_D Re/24\rho_p d^2$; u and u_p are the velocities of the gas phase and particle respectively.

While μ is the gas phase molecular viscosity; ρ and ρ_p are the gas phase and particle densities respectively; d is the particle diameter; Re is the relative Reynolds number which is defined as $\rho_G d|u_p - u|/\mu$ and C_D is the drag coefficient. F_x represents additional forces acting on the particle such as the force required to accelerate the fluid surrounding the particle and the force arising from the pressure gradient in the fluid. Integration in time of equation 7.4 gives the particle velocity u_p at each point along the trajectory and the trajectory itself is computed from:

$$\frac{dx}{dt} = u_p \qquad (7.5)$$

The time integration of the particle trajectory equations is controlled using two parameters:

1. The Maximum Number of Time Steps allowed for integration of equations 7.4 and 7.5 before aborting trajectory computations when the particle does not exit the flow domain was set at 50,000. The trajectory fate was "incomplete" when the trajectory calculation was abandoned. The Length Scale used to set the time step size for integration was 0.05 mm. For turbulent flow, the impact of turbulent eddies present in the continuous phase of particle dispersion is incorporated via the stochastic tracking or the discrete random walk model. The model considers the effect of instantaneous turbulent velocity fluctuations on the particle trajectories. The gas phase velocity u is the sum of the mean gas phase velocity $\bar{u}$. The instantaneous value of the gas flow velocity fluctuation u' is calculated from the following stochastic model:

$$u = \bar{u} + u' \qquad (7.6)$$

2. The random effects of turbulence on the particle dispersion is accounted for by turning on the Stochastic Model and setting a total of five computational (i.e. "number of tries") for each particle trajectory. The Random Eddy Lifetime option was included to set the characteristic lifetime of the turbulent eddy to be random. Particle interaction with the fluid phase eddy occurs over this eddy lifetime. The particles were released from the Mass Flow Inlet boundary surface. The individual mass flowrate of the injected particle stream was scaled according to the area of the face from which they were released. The initial conditions set for the particle stream are listed as follows.

The particle density was varied from 400 to 1800 kg/m^3 in the Material panel.

- Particle type = Inert i.e. particle undergoes no physical or chemical changes
- Particle velocity = 3 m/s and no velocity in the y-direction. Initial particle velocity was assumed to equal the gas velocity i.e. zero slip. Zero velocities in x-direction and z-direction.
- Particle diameter = Varies from 1 μm to 70 μm
- Particle temperature = 673 K
- Total mass flowrate of particles = 9 x 10^{-5} kg/s

The fate of a particle at a boundary zone was set as follows:

- Escapes through Mass Flow Inlet and Outflow boundaries
- Traps/reflects via a fully elastic collision at Wall boundaries of packing spheres and vertical sides of cuboid (z-axis).
- Traps/reflects at Wall boundaries of liquid droplets and passes through interior boundary zone (default)

The fate of a particle trajectory was reported as either "escaped" at flow boundaries, "trapped" at flow boundaries, "incomplete" when the Maximum Number of Time Steps was exceeded, or "aborted" for incomplete trajectories due to round-off reasons.

7.1.4 Material Properties, Operating and Boundary Conditions

The fully meshed packed-bed model was exported to Fluent Inc.'s FLUENT 6.3 for subsequent calculations. The specified material set in this model, referred to as continuous fluid, is nitrogen gas, while the discrete phase refers to the inlet particle.

The density and viscosity of nitrogen gas were set at their constant values at 400℃ while the inert particle density was varied from 400 to 1800 kg/m^3 in the simulation. The reference pressure location (1 atmosphere) was set at the central point of the bottom plane surface of the 'cuboid' and a gravitational acceleration of -9.81 m/s^2 was specified in the y-direction. The boundary conditions of the packed-bed model housed within the 'cuboid' are summarised in Table 7.2 and Table 7.3 which show the inputs for continuous nitrogen gas phase used in this model.

Table 7.2: Boundary conditions of packed-bed column

Regions	**Boundary Conditions and Inputs**	
Solid spheres	Wall face boundary:	Discrete phase trap
Bottom plane surface of cuboid	Mass Flow Inlet face boundary: Mass flow rate of continuous gas phase, M_G = (fixed) Total temperature, T = 673 K Initial gauge pressure, P_g = Static pressure relative to operating pressure, P_{op} = 0 Turbulence intensity (%), = 10 (constant) Turbulent length scale (m), = 1; Discrete phase = Escape	
Top plane surface of cuboid	Outlet face boundary:	Discrete phase = Escape
Vertical sides of cuboid (x-axis)	Symmetry face boundary:	No input required
Vertical sides of cuboid (z-axis)	Wall face boundary	Discrete phase trap/reflect
Interior of cuboid unoccupied by solid spheres and droplets	Interior face boundary: Fluid cell zones	No input required Material = Nitrogen gas

Table 7.3: The inputs used to solve the continuous gas phase

Inputs	**3 m/s nitrogen gas flowrate at 1 atm at base of the column**
Operating pressure, P_{op} (Pa)	101325
Gas Density (kg/m^3)	0.4812
Gas viscosity (kg/ms)	3.21 x 10^{-5}
Gas mass flowrate at Mass Flow Inlet, M_G (kg/s)	9 x 10^{-5}
Turbulent Intensity at Mass Flow Inlet, I (%)	10

7.1.5 Results and Discussion

7.1.5.1 Continuous Gas Phase Results

Figure 7.4 to 7.6 show the CFD derived contours describing the continuous gas phase flow field for gas mass flowrate M_G of 9 x 10^{-5} kg/s. The grid of the packing spheres was superimposed to indicate their locations, although they are partially blocked by the contours. The contours of velocity magnitude (Figure 7.5) show that the gas flow is at its highest velocity in the voids between the spherical packing surfaces. The highest value of turbulent kinetic energy k (Figure 7.6) was observed at the voids between the spherical packing surfaces. Within the bed, k can be as high as 21.6 m^2/s^2.

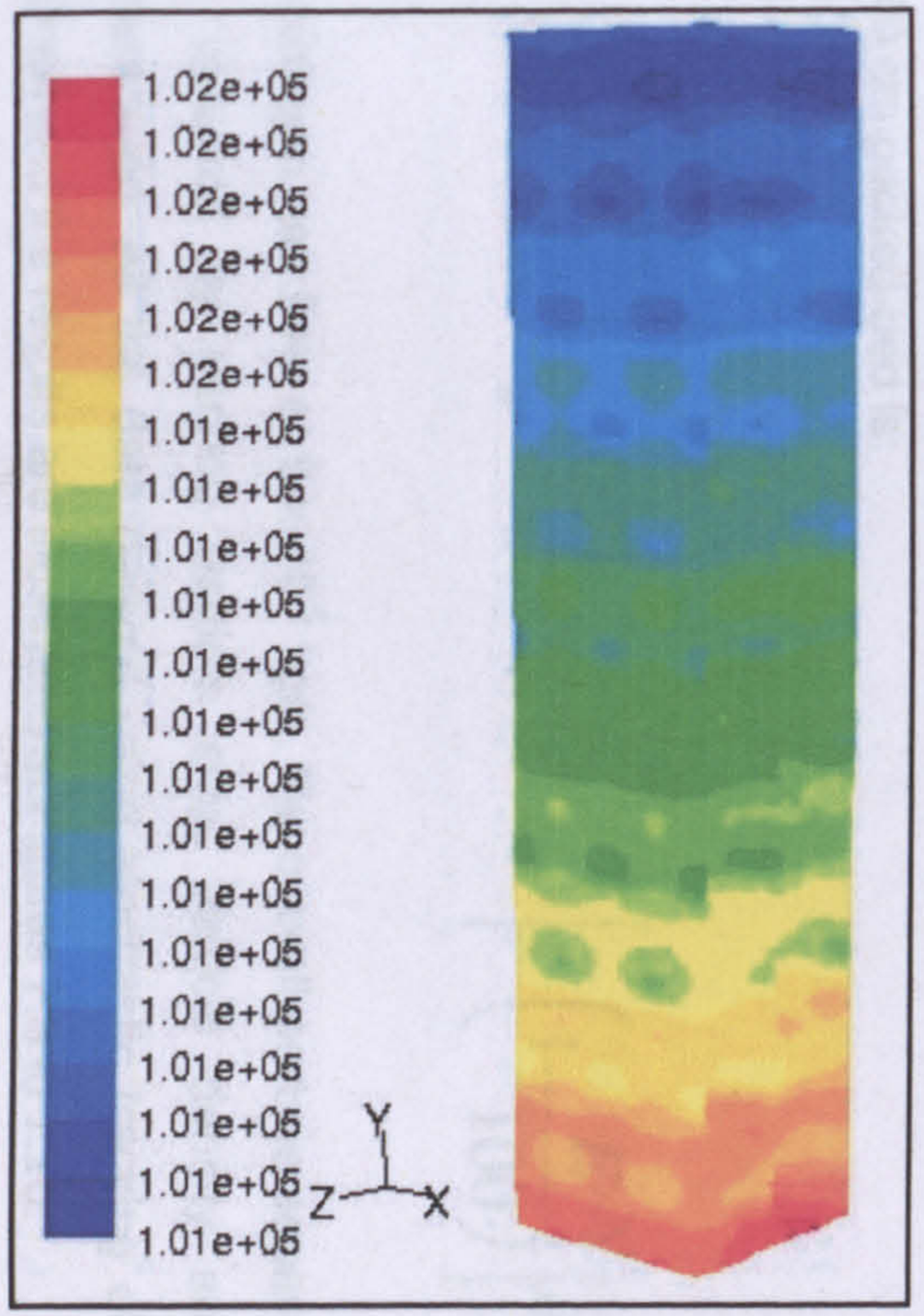

Figure 7.4: Contours of absolute pressure (Pa), [M_G = 9 x 10^{-5} kg/s]

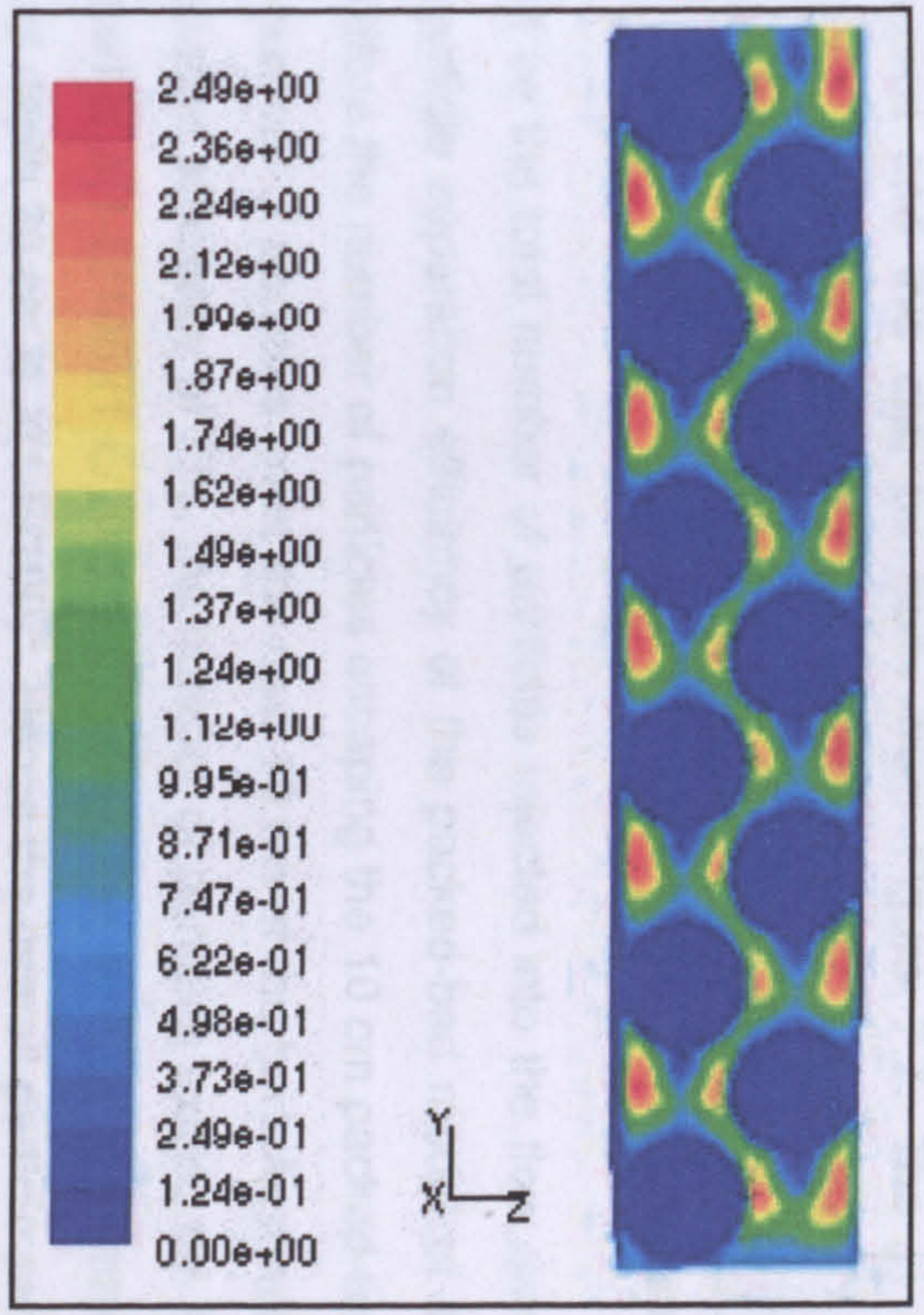

Figure 7.5: Contours of velocity magnitude (m/s) [M_G = 9 x 10^{-5} kg/s]

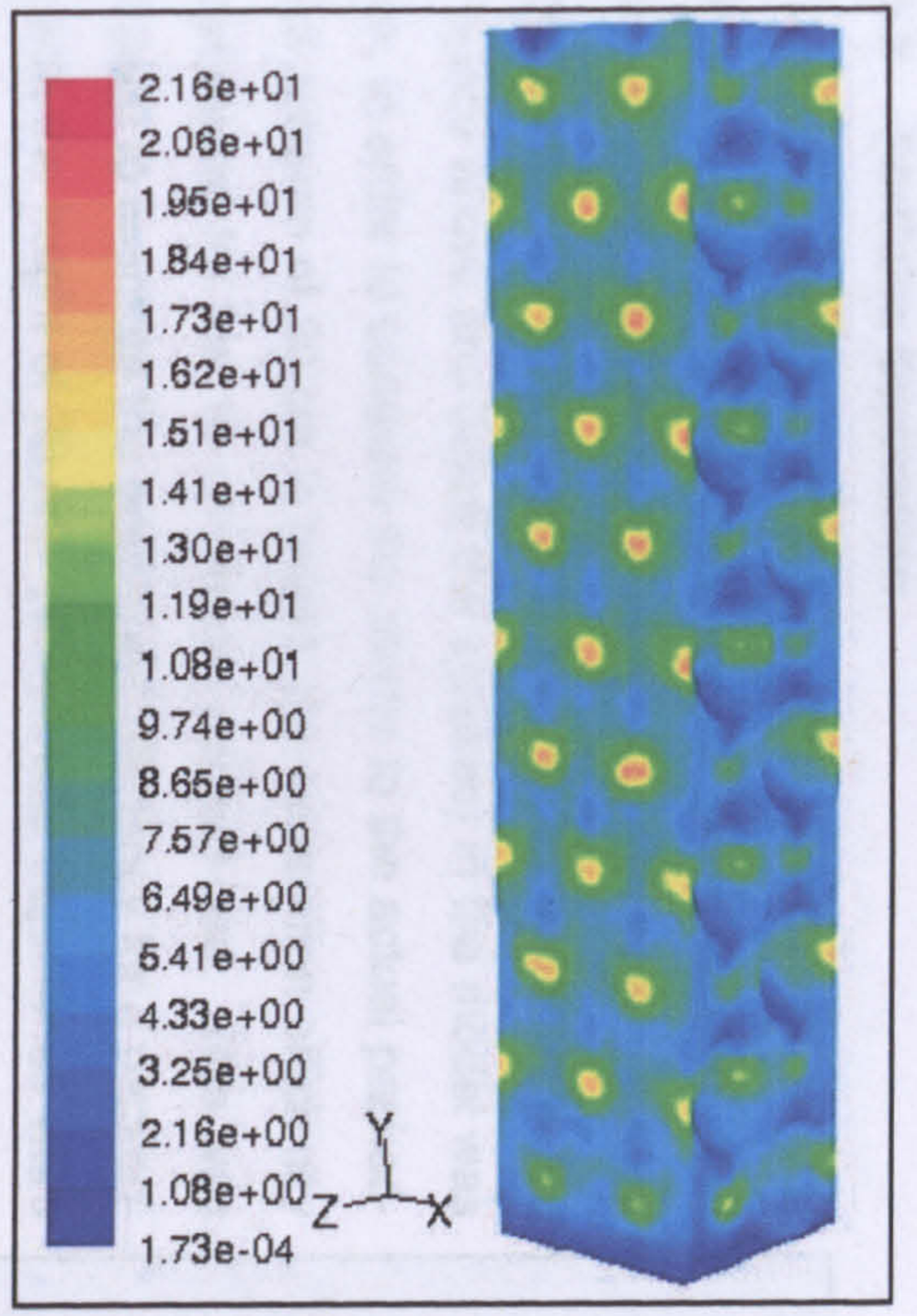

Figure 7.6: Contours of turbulent kinetic energy, k (m^2/s^2) [M_G = 9 x 10^{-5} kg/s]

7.1.5.2 Particles Separation

The particle separation efficiency was determined as the ratio of the "trapped" particles to the total "trapped" and "escaped" particles. The "incomplete" and "aborted" particles were ignored. The total height of the packed-bed (minus the free space above and below the spheres) in the model was 10 cm. In order to compare the model to the actual packed-bed of spheres of 20 cm in height, the separation efficiency was obtained for the 10 cm model packed-bed. This was then used to estimate the equivalent efficiency for a packed-bed with the height of 20 cm. The particle trajectories were simulated and this can be seen from Figure 7.7. The following is a description of the steps used to reach the estimation:

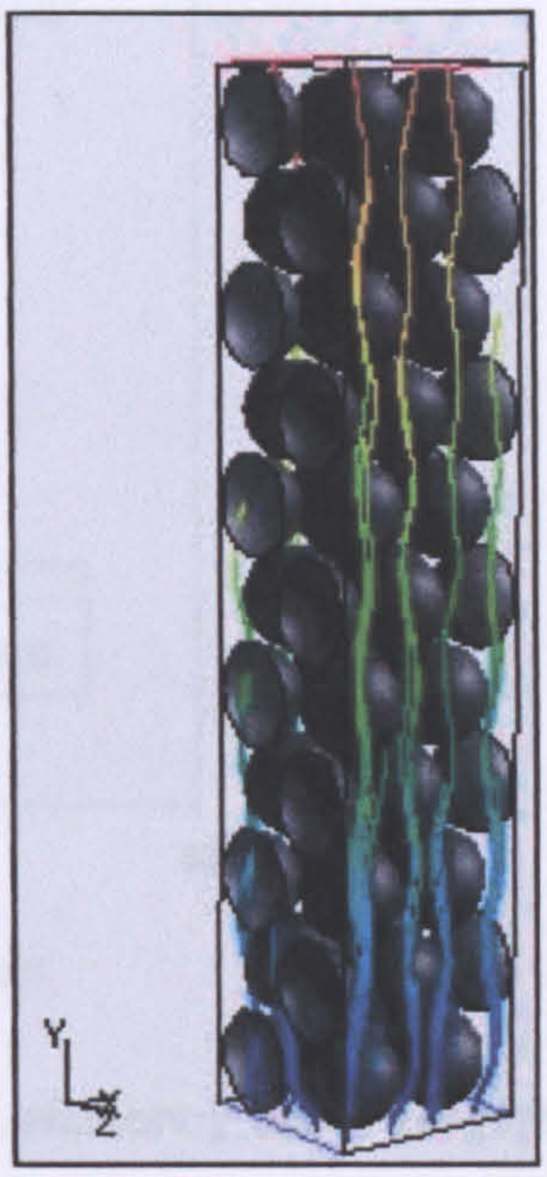

Figure 7.7: Simulated particle trajectories

Let X be the total number of particles injected into the flow domain. Assuming that the particle separation efficiency of the packed-bed model of 10 cm depth is E%. Therefore the number of particles escaping the 10 cm packed-bed is $X(1\text{-}E/100)$. Let this number of particles enter the next 10 cm of the bed. Assuming the same particle separation efficiency of E%, the number of particles exiting the total 10 cm depth of the bed is $X(1\text{-}E/100)(1\text{-}E/100)$. Ultimately, the number of particles exiting a packed-bed of depth 20 cm is $X(1\text{-}E/100)^2$. Hence the overall particle separation efficiency of the 20 cm packed-bed is:

$$E_{total} = \frac{x - x\left(1 - \frac{E}{100}\right)^2}{x} x100\% = E_{total} = \left[1 - \left(1 - \frac{E}{100}\right)^2\right] x100\% \qquad (7.7)$$

For nitrogen gas flow at 9×10^{-5} kg/s, the overall particle separation efficiency E_{total} was obtained by varying particle size, particle density and injected particle concentration. All the data derived using stochastic tracking of the particles were obtained and the results are illustrated in Figures 7.8 to 7.10.

✸ Variation of E_{Total} with Particles Sizes

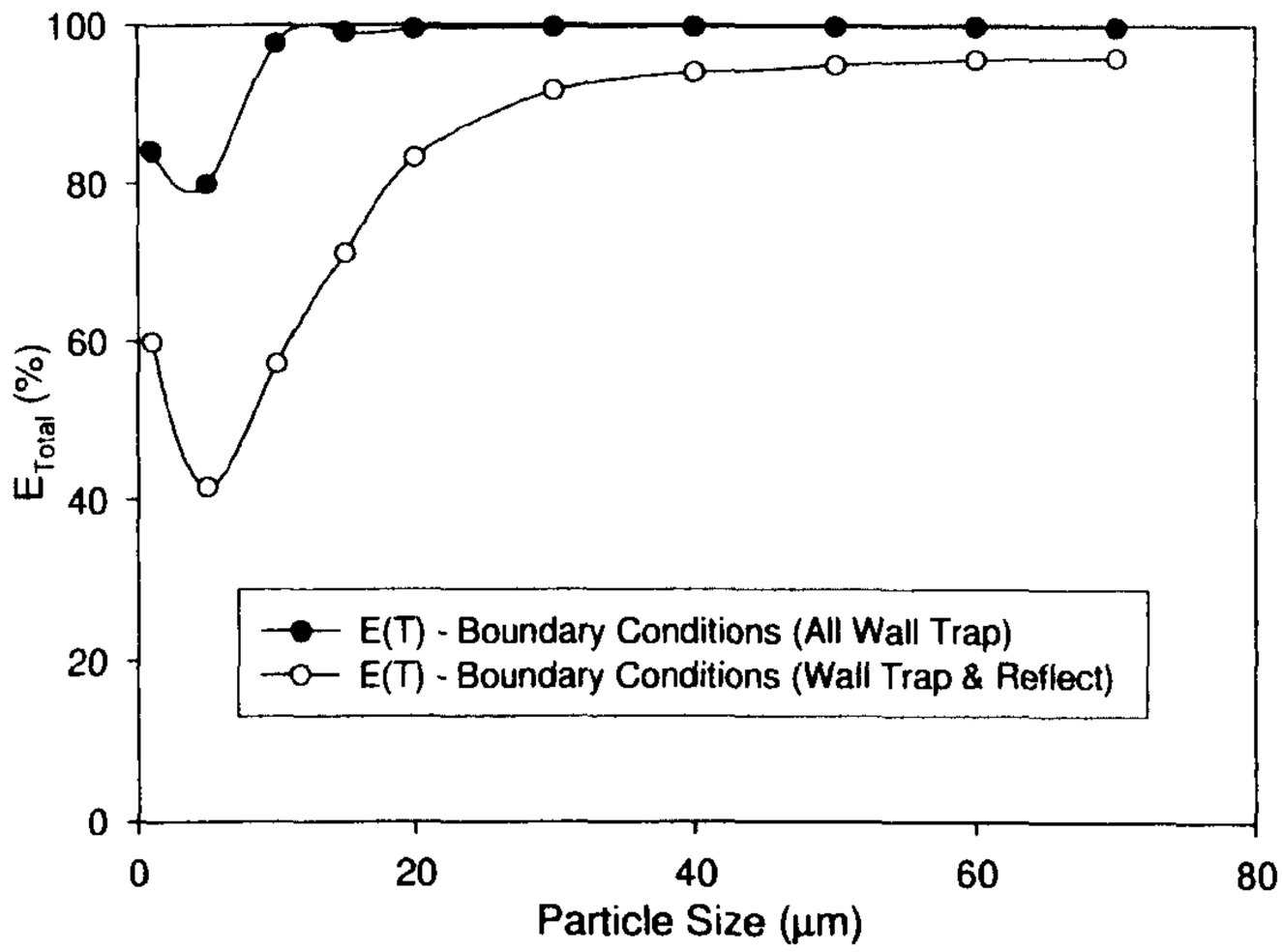

Figure 7.8: Variation of E_{total} with particle size

The variation of E_{total} with particle size is essentially the total efficiency curve (Figure 7.8). E_{total} increases with particle size. Direct interception of particles onto the "trapping" droplets is enhanced with larger particles. Also, as particle size increases, its mass and hence its inertia increases as well. This improves inertial deposition of the particle i.e. there is a greater tendency for it to deviate from the gas streamlines. Larger particles also have higher probability of colliding with the packing spheres. The elastic collisions increase the randomness of the particle trajectories hence improving the chances of particle entrapment by the walls and packing. For "*all wall trap*" conditions, the overall efficiency is 95% (i.e. particles of 10 μm or over). The overall efficiency for the "*wall trap and reflect*" condition was found to be 94% (i.e. 35 μm or above).

✸ Variation of E_{Total} with Particles Density

E_{total} increases with particle density (Figure 7.9). This is due to the effect of greater particle inertia as described in the preceding paragraph. It is also due to the higher mass inducing less velocity for the same momentum.

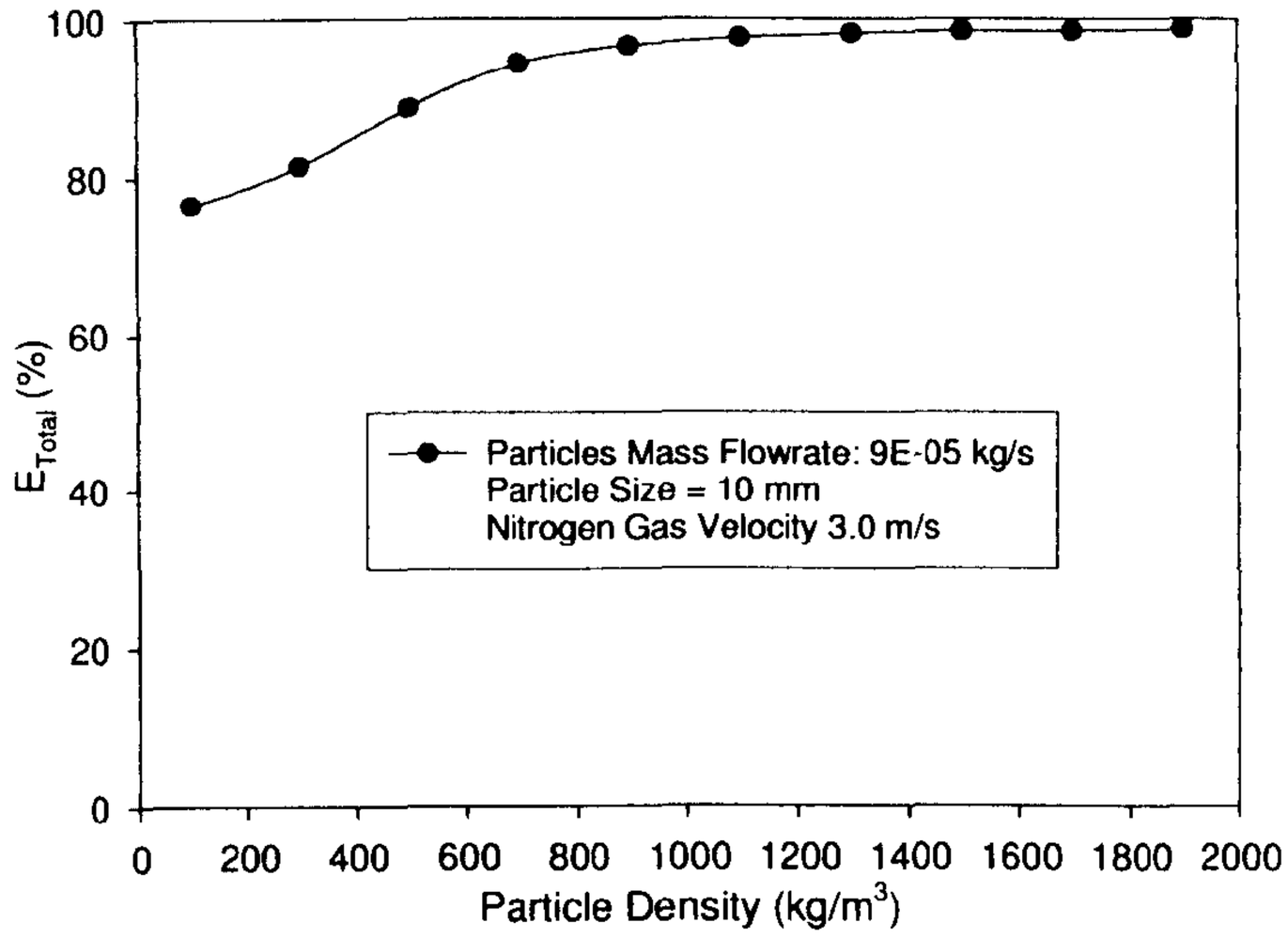

Figure 7.9: Variation of E_{total} with particle density

✸ Variation of E_{Total} with Different Inlet Velocity

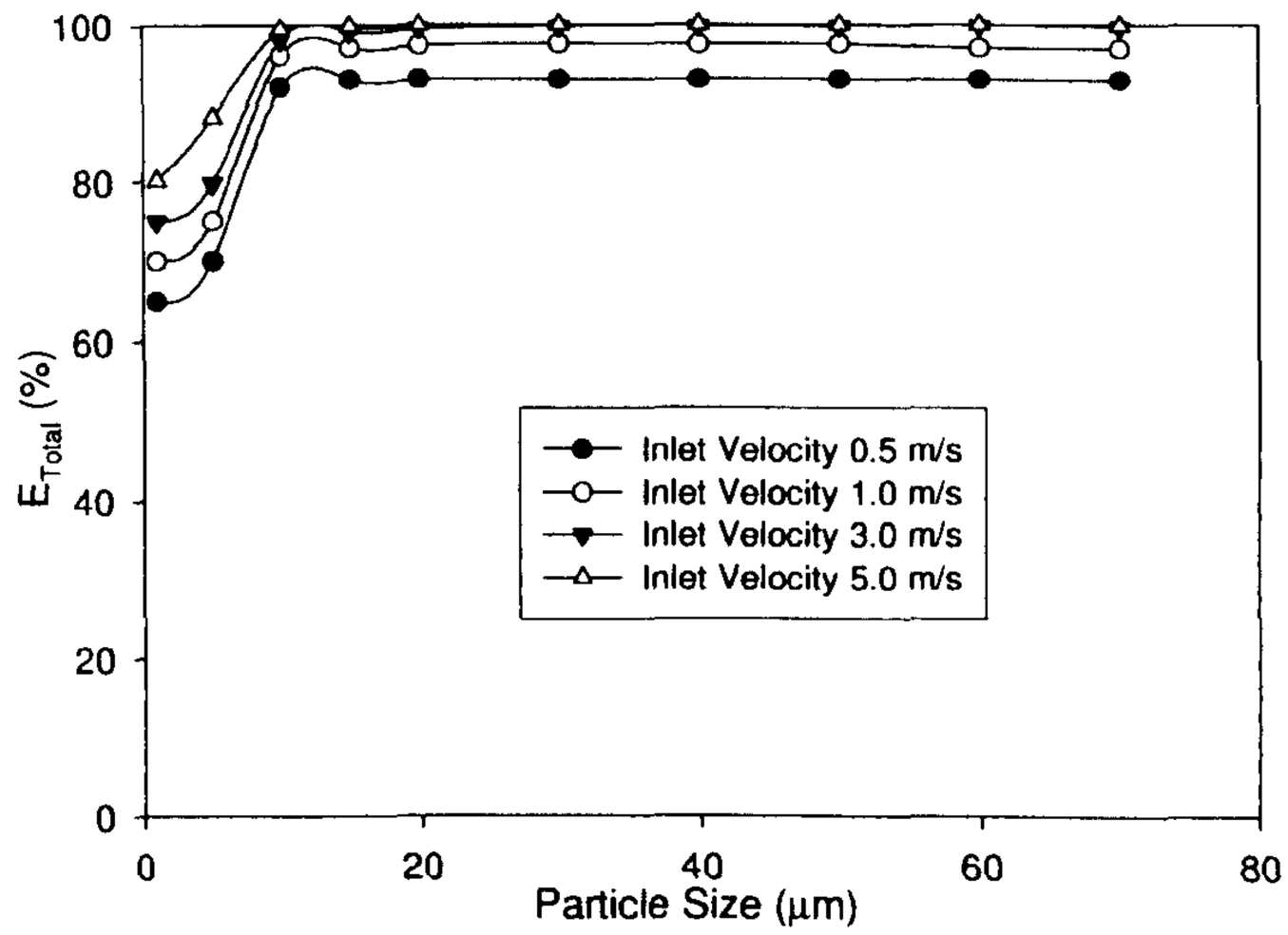

Figure 7.10: Variation of E_{total} with particle size

For nitrogen gas velocities of 0.5 m/s and higher, the total efficiency E_T increased as shown in Figure 7.10. The total efficiency curves at 3 m/s and 5 m/s nitrogen gas velocities were consistently higher for particles larger than 15μm. Therefore, in order to obtain higher efficiency, a high inlet velocity was required. The comparison of total efficiency was not carried out with the experimental results as described in Chapter 6. This was due to the formation of agglomerates in the column. Nevertheless, this simulation work provided basic information on how the mechanisms of particulate cleaning occurred in the packed-bed hot gas scrubber.

7.2 Microsoft Excel - Desulphurisation

The scope of this work is to model the process for better understanding of gas cleaning behavior in the scrubber. This model was programmed as a Microsoft® Excel spreadsheet and used to simulate the rate of reaction in the packed-bed scrubber.

7.2.1 Introduction

The effectiveness of using liquid tin for H_2S absorption was documented in early 1984 (Schürmann, 1984). Due to the limited source of information little effort was made to develop a liquid tin scrubber for pollution control. Nevertheless research on the reaction rate and mechanisms of H_2S with tin was pursued by Hedden (1986) to gain better understanding of the desulphurisation system. Absorption of H_2S occurs with simultaneous mass transfer and fast chemical reaction.

7.2.2 Mathematical Model

Consider a packed-bed column with the following characteristics. The amount of gas absorbed in section *dZ* is *–dy* (Changkook Ryu et al., 2007):

$$-dy = \frac{K_o\left(y_{in} - y_{out}\right)a_e\, dZ}{u_G} \tag{7.8}$$

where K_o = Overall mass transfer coefficient (m/s)
a_e = Effective specific interfacial area (m^2/m^3)
y_{in} = Inlet gas concentration (ppm)
y_{out} = Outlet gas concentration (ppm)
u_G = Gas superficial velocity (m/s)
Z = Column height (m)

This equation is rearranged for integration by grouping together the constant factors *u; a_edZ,* and *K_O,* which have a constant value with *dZ.*

$$\frac{K_O a_e}{u_G}\int_0^{Z_T} dZ = \frac{K_O a_e Z_T}{u_G} = \int_b^a \frac{dy}{\left(y_{in} - y_{out}\right)} \tag{7.9}$$

The equation for the column height, Z_T can be written by integrating *dZ* from 0 to Z_T; as follows:

$$Z_T = \left[\frac{\left(u_G / a_e\right)}{K_O}\right]\int_b^a \frac{dy}{\left(y_{in} - y_{out}\right)} \tag{7.10}$$

As described in Chapter 6, the Ko is the overall mass transfer coefficient (m/s) incorporating the three rate controlling mechanisms: the gas phase mass transfer (k_G) of H_2S towards the liquid surface, the reaction kinetic effect at the interface (k_r) and the liquid phase mass transfer (k_L) for SnS dissolving into tin. K_o can be expressed simply as,

$$\frac{1}{K_o} = \frac{1}{k_G} + \frac{1}{k_r} + \frac{1}{k_L} \qquad (6.11)$$

For the packed-bed hot gas scrubber, the gas-side mass transfer coefficient ($\boldsymbol{k_G}$) may be estimated by the equation proposed by Shulman et al., (1955):

$$k_G = 1.195 u_G \left[\frac{d_p \rho_G u_G}{\mu_G (1-\varepsilon)} \right]^{-0.36} Sc_G^{-2/3} \qquad (7.11)$$

where u_G = Gas superficial velocity (m/s)
d_p = Diameter of a packing element (m)
ρ_G = Density of gas (kg/m^3)
μ_G = Viscosity of gas (kg/m.s)
ε = Void fraction of packing (m^2/m^3)
Sc_G = Schmidt number of gas (Dimensionless)

The liquid-side mass transfer coefficient ($\boldsymbol{k_L}$) may be calculated by an equation suggested by Shi & Mersmann (1985) and Mersmann & Deixler (1986):

$$k_L = 0.86 \sqrt{\frac{6 D_L}{\pi d_{pe}}} \sqrt{\left\{ \frac{u_L^{1.2} g^{1.3} \sigma_L^{0.3} \varepsilon^{1.2} (1-0.93\cos\theta)^2}{\upsilon_L^{1.4} \rho_L^{0.3} a_p^{2.4}} \right\}} \qquad (7.12)$$

where u_L = Liquid superficial velocity (m/s)
d_{pe} = Diameter of a packing element (m)
ρ_L = Density of liquid (kg/m^3)
μ_L = Viscosity of liquid (kg/m.s)
υ_L = Kinematic viscosity of liquid (m^2/s)
σ_L = Surface tension of liquid (mN/m)
θ = Liquid contact angle
g = Gravitational constant (m/s^2)
a_p = Packing specific surface area (1/m)
D_L = Liquid phase diffusion coefficient or diffusivity (m^2/s)

The major assumptions for this computer model are as follows:

(1) Steady-state conditions

(2) The reaction is fast and takes place in the gas film only

(3) Negligible pressure drop in the packing

(4) The effective specific interfacial area (a_e) was assumed to be 90% from the original data of the packing specific surface.

Since the reaction was assumed to be fast and takes place in the gas film only, and also k_L is not rate controlling, Equation 6.11 becomes:

$$\frac{1}{K_o} = \frac{1}{k_G} + \frac{1}{k_r} \qquad (7.13)$$

7.2.3 Source of Data Input

Experimental data from packed-bed hot gas scrubber studies were used to examine the model predictions. In this work, experimental data for verifying mass-transfer prediction from the developed model were generated by performing H_2S absorption into liquid tin. The data were given as the gas-phase H_2S concentration, which can be used to determine the rate of reaction between H_2S and liquid tin in the packed-bed scrubber. The ranges of test conditions are summarized in Table 7.4.

Table 7.4: Test conditions for hot gas desulphurisation in the packed-bed scrubber

Test parameters		Unit	Values
Gas	Superficial velocity	m/s	0.490, 0.515, 0.574, 0.617, 0.735
Inlet H_2S concentration		ppm	2000, 1700, 1300, 1000, 300
Liquid Tin	Superficial velocity	m/s	3.07×10^{-4}, 4.53×10^{-4}, 5.52×10^{-4}
Operating temperature		°C	400, 390, 350, 300

Table 7.5 lists the main references utilised in determining the main parameters. The parameters in Table 7.5 include density, viscosity, surface tension, diffusivity, reaction rate constant, enhancement factor, effective interfacial area, and mass transfer coefficient. The second column in Table 7.5 contains the references to the correlations, method, and procedures for calculating these parameters for the H_2S-Sn absorption system.

Table 7.5: References used to estimate the main parameters

Parameter	References/Method
ρ_L, μ_L, σ_L	CRC Handbook of Chemistry & Physics (2006)
u_L	Experimental Work
ρ_G, μ_G	CRC Handbook of Chemistry & Physics (2006)
u_G	Experimental Work
Packed-bed porosity	Chang (2003)
Packing specific surface area	Chang (2003)
Effective interfacial area	Linek (1984)
Gas-side mass transfer coefficients	Shulman & de Grouff (1952)
Liquid-side mass transfer coefficients	Shi & Mersmann (1985)
Molten tin-alumina contact angle θ	Chang (2003)
Overall mass transfer coefficients	Luke Chen (2002)

The simplified flowchart of Figure 7.11 represents these procedures, and a Microsoft Excel computer program was developed to solve the model equations.

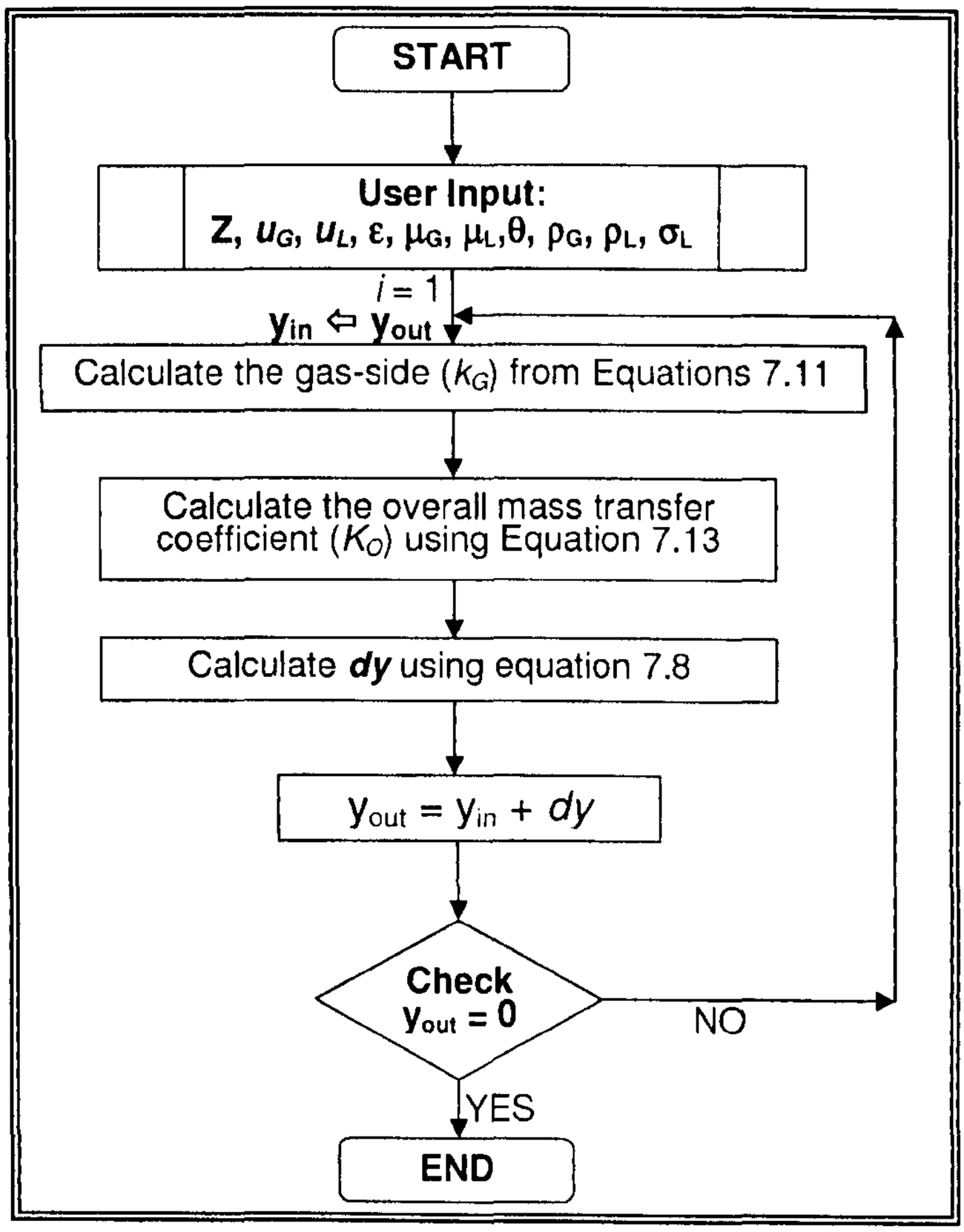

Figure 7.11: Flowchart for the H_2S-Sn simulation model

7.2.4 Simulation Results and Discussion

The validity of the developed mathematical model was confirmed by comparing with the experimental data in this research work. The initial operating conditions of the pilot plant were as follows: simulated flue gas superficial velocity 0.490 m/s, operating temperature at 400℃, liquid superficial velocity $5.5x10^{-4}$ m/s and H_2S inlet concentrations 1000 ppm. Effects of various parameters, such as operating temperature, effective specific interfacial area, gas superficial velocity, liquid superficial velocity, are investigated.

7.2.4.1 Concentration Profiles In the Packed-bed

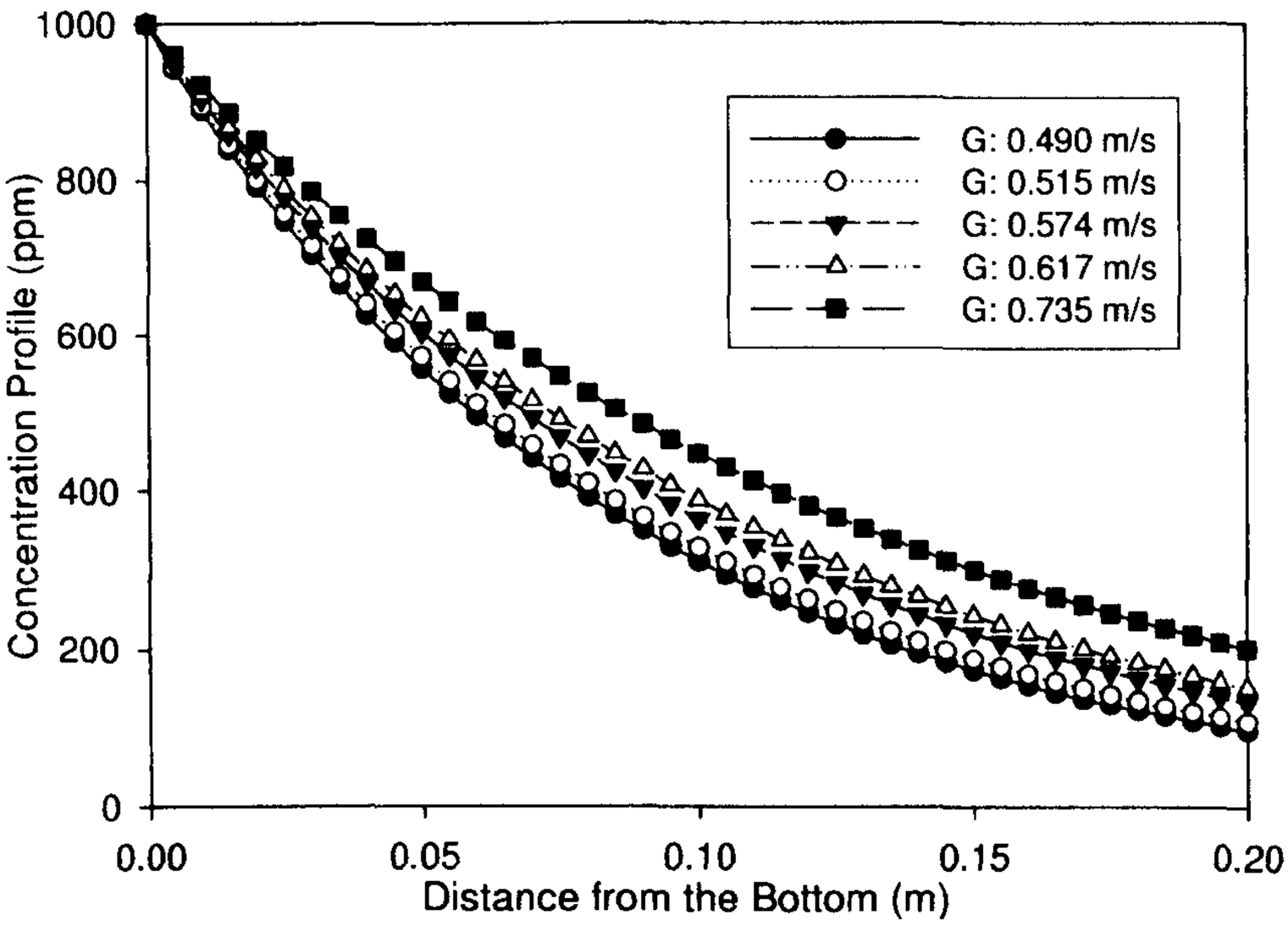

Figure 7.12: Concentration profiles for different gas superficial velocities

The effect of height (height refers to the distance from the inlet of the scrubber to the outlet, along the flow) on outlet concentrations has been shown in Figure 7.12. This figure shows typical plots of simulated gas-phase H_2S concentrations along the absorption column for the H_2S-Sn system. The simulation generally gave results that agreed with the experimental data. As the height of the scrubber increases, the outlet concentration of H_2S in the gas phase decreases but the outlet concentration of H_2S in the liquid phase increases. As the lower height increases, the interfacial contact area increases and so does the time of contact. This causes the gas phase concentration to decrease and the liquid phase concentration to increase, enhancing the H_2S removal efficiency.

7.2.4.2 Comparison of Activation Energy

For the hot gas packed-bed scrubber, which is packed with high-purity ceramic alumina spheres, close agreement is achieved by using the interfacial area as an adjustable parameter. This is a common practice when the existing equations for predicting the interfacial area are found to be inadequate for certain cases of gas absorption processes. Figure 7.13 illustrates the effect of temperature on the apparent reaction rate constant, as correlated by the Arrhenius type relationship over the temperature range 300 – 400°C. The activation energy values are approximately 16.32 kJ/mol and 16.79 kJ/mol from the experimental and modelling work respectively, which are lower than 60±20 kJ/mol reported by Hedden et al., (1986) who conducted his experiments at temperatures ranging from 400 – 700°C in three different types of reactors (bubble column, stirred vessel and double-stirred cell). However, the value for reaction rate constant, k, compares favorably with 0.012–0.020 m/s reported by Hedden et al., (1986) with $a_e = 311.65\ m^2/m^3$.

Table 7.6: Arrhenius constant for high-temperature desulphurisation reaction

	E_a (kJ/mol)	k_r (m/s)
Experimental	16.32	0.01140 – 0.01880
Modelling	16.79	0.01089 – 0.01838
Hedden, Rao et al. (1986)	60±20	0.01200 – 0.02000

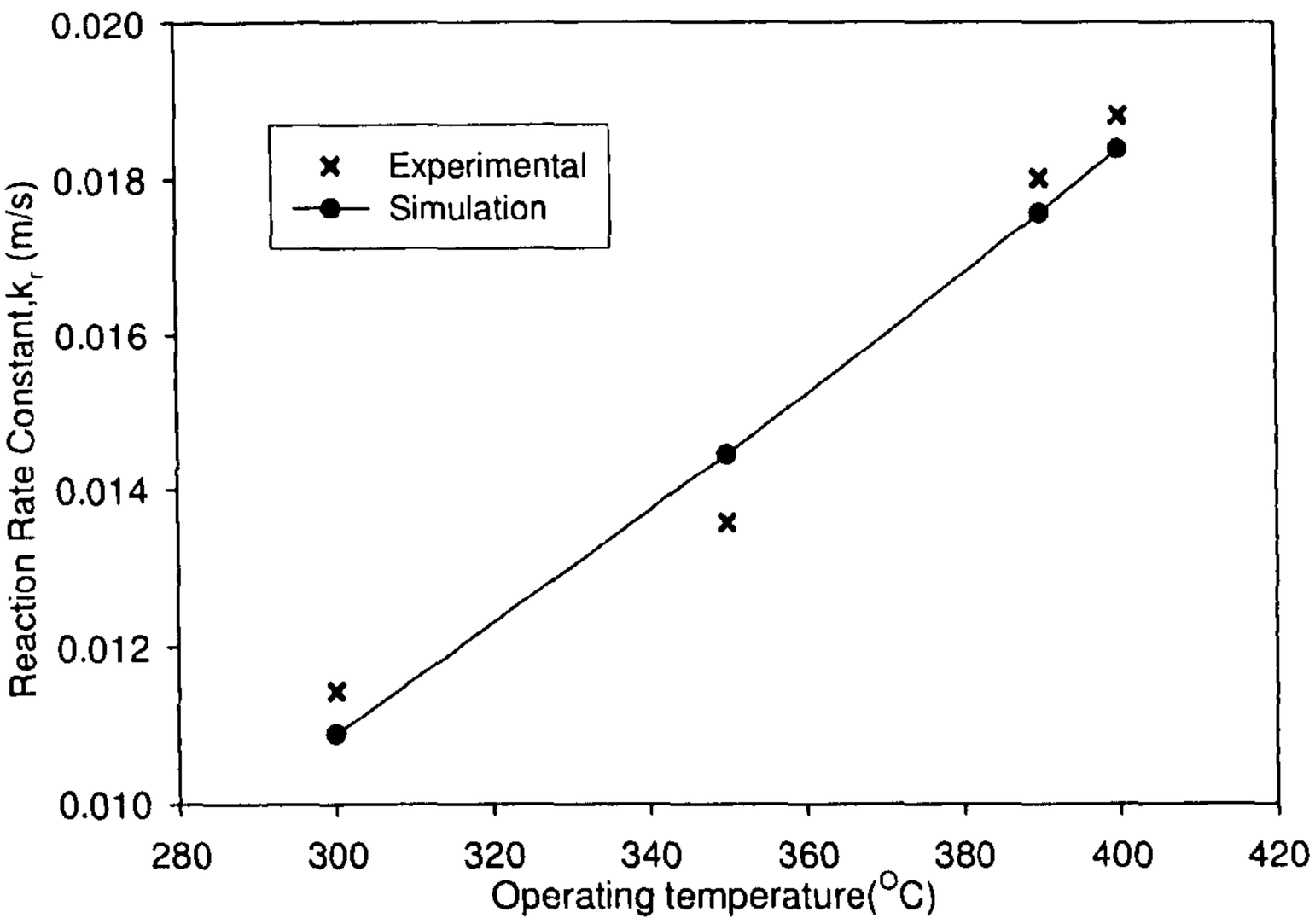

Figure 7.13: Reaction rate constants with different operating temperatures

7.2.4.3 Effect of Operating Temperature

Based on the simulation, the operating temperature also has an effect on absorption performance. Raising the temperature of the bed which also increases the temperature of liquid tin, yields a greater reaction rate constant. As described in the previous chapter, the desulphurisation became efficient at high temperatures because the increase in the mass transfer and reaction rates is larger than the increase in the gas velocity. Higher temperatures are expected to increase the mass transfer and reaction rate of H_2S while reducing the viscosity of liquid tin. Also to be seen in this figure, the efficiency was almost to 100 percent if the operating temperature of the scrubber was set at 700 ℃. It also gives a good indication that the desulphurisation process can be implemented at the same temperature as the gasification process in the real plant.

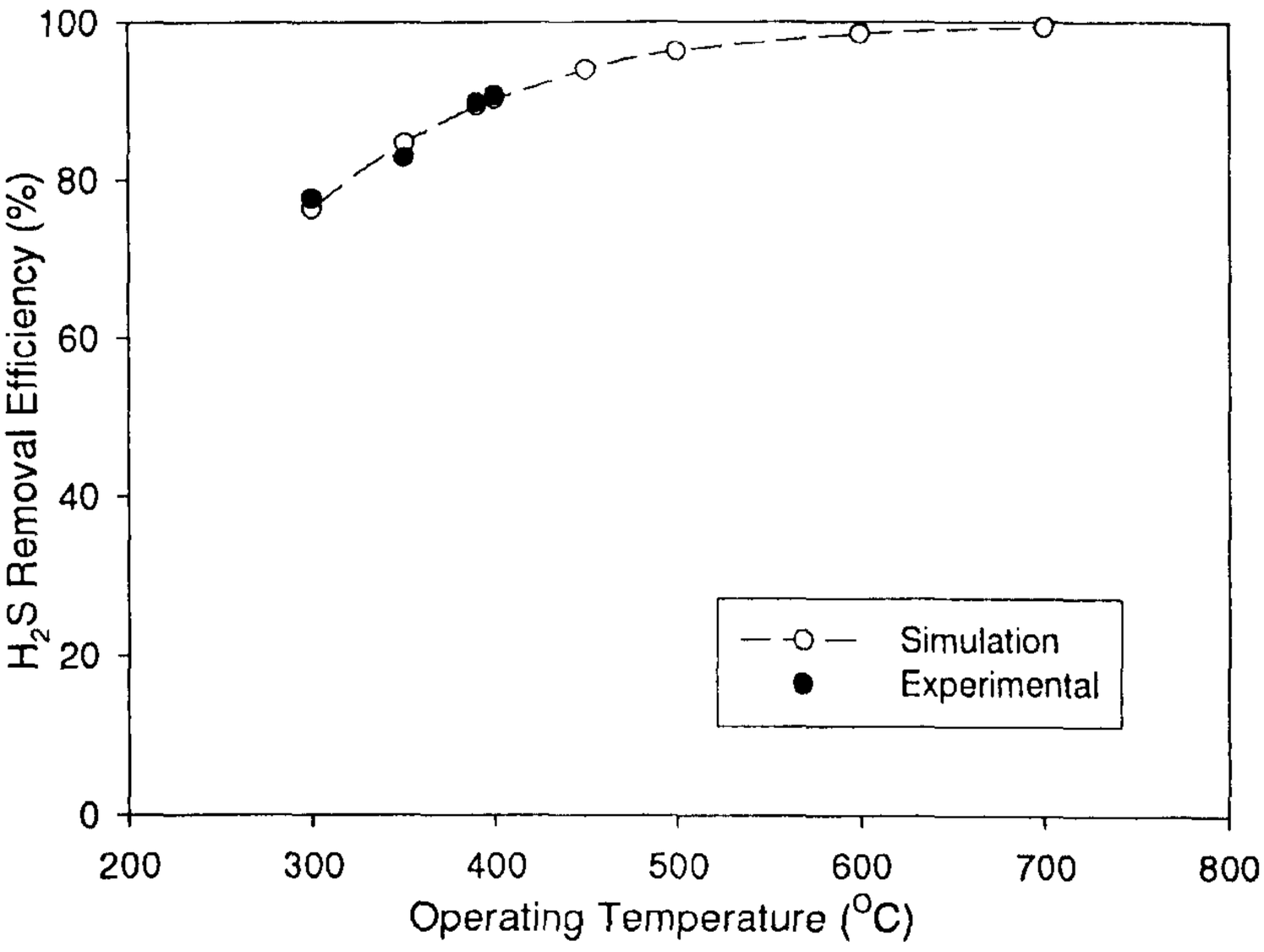

Figure 7.14: Comparison of predicted and measured η for different operating temperature

7.2.4.4 Effect of Gas Superficial Velocities

Figure 7.15 presents experimental data and model predictions for absorption in H_2S. The prediction is accurate except for a lower superficial velocity. But at higher superficial velocities the model predicts higher values than experimental data. It may be explained by the effect of the liquid-side mass transfer coefficient (k_L) which was not taken into account since there are no available correlations for not-wetting liquid. The main reason why the k_L was not considered was in order to simplify the model. In addition to this, the published correlations of k_L were mostly based on wetting conditions and are not compatible with the behaviour of liquid tin (non-wetting).

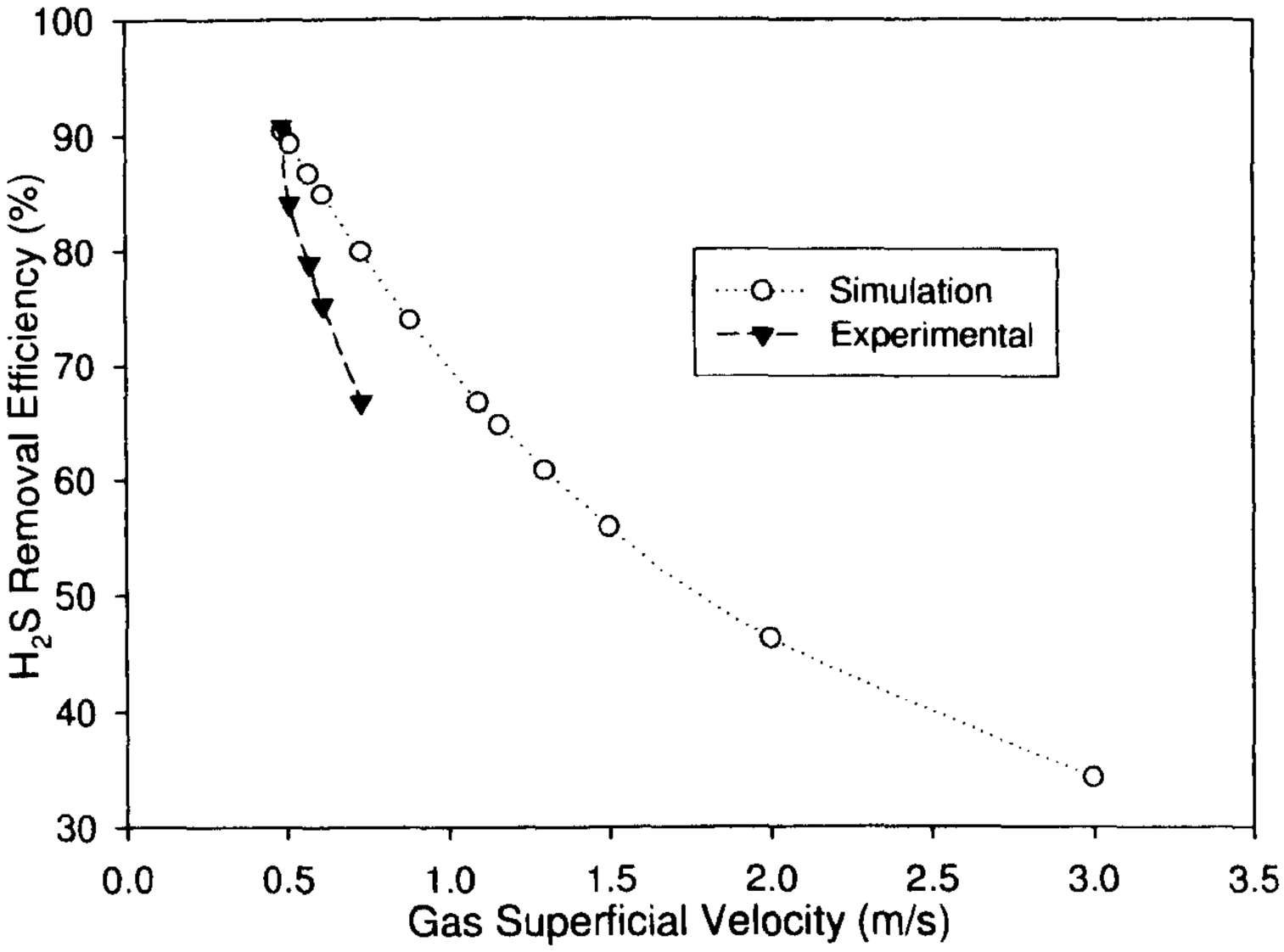

Figure 7.15: Comparison of predicted and measured η for different gas superficial velocity

7.2.4.5 Effect of Effective Specific Interfacial Area

Figure 7.16 shows the values of effective interfacial area in the packed column as a function of the liquid superficial velocity. The data obtained in this modelling work has been compared with the data reported by Neelakantan (1982) and Sahay (1973). The curve patterns of effective interfacial area obtained by using this system are found to be in reasonable agreement with those obtained with the use of other systems. Viscosity seems to influence the formation of effective interfacial area in two ways. On one hand, it favours the retention of liquid in the bed and the wettability of the packing, thus elevating the effective interfacial area. On the other hand, it tends to soften and reduce rippling, and the level of turbulence in the layer of liquid nearest the gas-liquid interface, as well as reducing the renewal of the liquid in the puddles; consequently, the effective interfacial area decreases. The strong dependence of the effective interfacial area on the liquid viscosity, as determined in this work, suggests that any model explaining the hydrodynamic and kinetic behaviour of a packed absorber must take into account the influence of this factor.

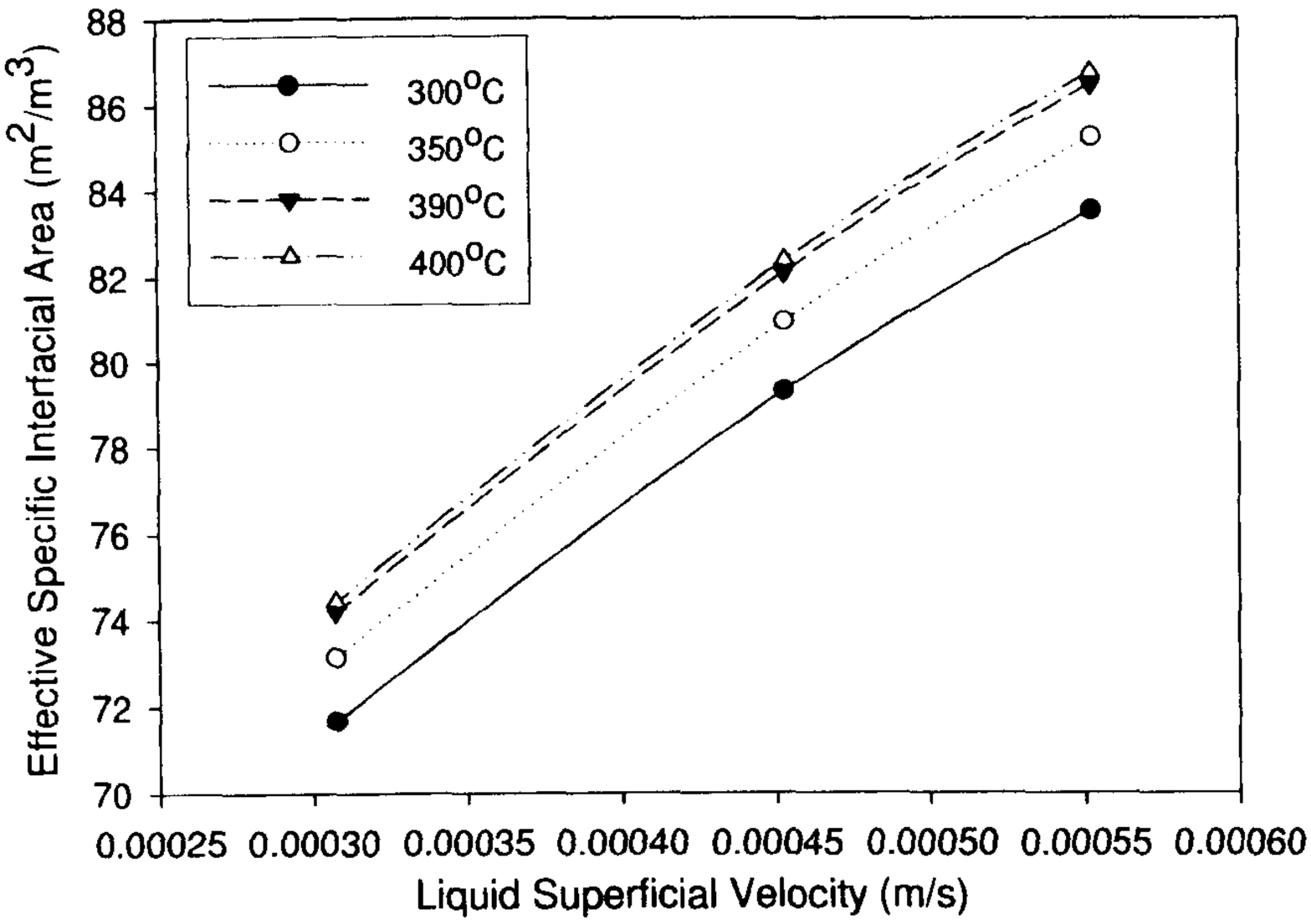

Figure 7.16: Effect of effective specific interfacial area with different liquid superficial velocity

7.3 Summary

7.3.1 Computational Fluid Dynamic – Particulate Cleaning

CFD modelling was performed to simulate particle removal in a packed-bed of spheres operating under hot gas conditions. Higher efficiencies were obtained for "*wall trap condition*" due to particle interaction with the instantaneous velocity fluctuations of the gas phase. Particle separation efficiency increased with particle size due to better capture by direct interception and inertial impaction mechanisms as well as increased randomness of particle trajectories from elastic collisions with the solid spheres. Efficiencies above 98% were predicted for particles 40 μm and larger. Particle separation improved with particle density due to the effects of greater inertia. Future CFD work should include other mechanisms of dust capture, i.e. presence of liquid tin droplets and also different systematic packing of spheres to investigate the effect of particle separation efficiency. The comparison of total efficiency is not carried out with experimental results as described in Chapter 6. This was due to the formation of agglomerates in the column. Nevertheless this simulation work is provided as basic information on how the mechanisms of particulate cleaning occurred in the packed-bed hot gas scrubber.

7.3.2 Reaction Rate - Desulphurisation

The mathematical model presented here combines chemical reactions and mass transfer in gas phases for the absorption of H_2S into liquid tin in a packed-bed hot gas scrubber. The model developed, in spite of the simple description of the mass transfer, is capable of predicting the transfer rates of absorption. The results of the mathematical simulations (using the removal efficiencies of the model presented) agreed fairly closely with the experimental data. The model should be useful for conservatively estimating scrubber performance at conditions similar to this study. The H_2S absorption is primarily affected by the operating temperature and gas superficial velocity. It is also affected by effective specific interfacial area and liquid viscosity. The range of reaction rate constants from this work is 0.011 to 0.019 m/s for various operating temperatures. These results are within the broad range of values as reported by Hedden (1986) as mentioned in sub-section 6.2.6. It should be stressed that analytical approximations are often over simplified and cannot be expected to predict the absorption rates for a wide range of conditions and therefore under practical conditions.

CHAPTER EIGHT

Overall Discussion on the Packed Bed Hot Gas Scrubber

Coal is currently a major source of fuel for power generation, industrial heat, and, on a smaller scale, manufacturing of coke and by-products such as coal tar. In the mid-to-long term, the anticipated increase in the cost of natural gas and petroleum relative to coal is expected to increase the incentive for expanded efforts to convert coal to ash-free, low-sulphur transportation fuels and, ultimately, gaseous fuels for domestic use. The current hot gas clean-up method centres on the use of metal oxide sorbents for sulphur removal and the utilisation of a ceramic barrier filter for particulate cleaning. This thesis presents a new approach to hot fuel gas cleaning technology incorporating molten tin as the scrubbing medium for the simultaneous removal of H_2S and solid particulates.

In the US and several countries across Europe, there has been a rapid introduction of hot gas cleaning systems. However, there is still of lot of research which can be done in the areas of chemical and technical developments to further improve these systems. In this study, the performance of packed bed hot gas scrubbers for particulate and desulphurisation were tested in an experimental packed-bed scrubber. Experimental investigation on this laboratory-scale plant provided detailed information on the performance of liquid tin as a scrubbing medium for both particulate and gas cleaning. Complementary to this, research on cleaning SnS using zinc powder for tin regeneration was also carried out. The small-scale furnace tests provided fundamental information on reaction between SnS and zinc powder. The scrubber was predicted earlier to be potentially better for solid removal efficiency. However, since there was a high temperature difference between the inlet particles and the scrubber, this increases the agglomeration of the particles coated by the liquid tin, and thus decreases the efficiency of the process. Therefore, future work on this topic is required. Nevertheless, results from the desulphurisation process were promising since high efficiencies can be achieved at larger scales (Changkook Ryu et al., 2007). Once the problem associated with the agglomeration has been solved, the assessment of both particulate cleaning and the desulphurisation process running simultaneously can be tested. Results from the small scale cleaning process have provided confirmation and evidence of the possibility to clean SnS using zinc under a gasification environment.

Therefore, if all three types of processes (particulate cleaning, desulphurisation and tin regeneration) were to be combined together, it would eliminate the production of wet slurry, doing away with costly wastewater treatment facilities and the corresponding additional hardware. Furthermore in HGCU, water consumption to run the system is significantly reduced, cutting down on operating costs.

Mathematical models were applied to both the particulate cleaning and desulphurisation process and this provided a deeper understanding of the cleaning process in the scrubber.

The high temperature product gas formed from the gasification process if combined with hot gas clean-up (HGCU) reduces the thermal efficiency losses associated with gas quenching and results in higher efficiency energy recovery for systems such as the integrated gasification combined cycle (IGCC). The gasification process offers the opportunity for integration with combined cycle turbines or reciprocating engines, converting fuel energy to electricity more efficiently (+40%). The lower volume of product gas from the gasification system also requires smaller and less expensive gas cleaning equipment compared to flue gas clean-up technology.

As mentioned in Chapter 2, the gasifier has the flexibility to handle a variety of feedstocks. In addition to coal, possible feedstocks include petroleum coke, refinery liquids, biomass, municipal solid waste, and sludge. These alternative feedstocks are typically low cost, sometimes even of negative expense. When a low-cost feed is used, the economics of gasification are enhanced and marketable products are created from a waste stream, avoiding disposal costs and environmental concerns. In this case, gasification fuel gas constituents other than sulphur removal are also worth investigating. The main gas components of interest are NH_3, HCl CO, H_2, CO_2 and H_2O (where steam gasification is employed).

Liquid tin is fairly reactive, and therefore other gas components in fuel gases may react with tin. Hedges (1960) reported that tin does not react directly with H_2, N_2, or NH_3. However, it reacts with H_2O, CO_2, and HCl. In particular, tin can be oxidised by steam to form solid oxides, which causes the loss of tin (Hedges, 1960); (Niesel and Sigurdardottir, 1993).

$$Sn(l) + 2H_2O(g) \leftrightarrow SnO_2(s) + 2H_2(g) \qquad (8.1)$$

This reaction depends on the H_2O/H_2 ratio and temperature. Temperatures above 500℃ are required to prevent SnO_2 dross formation for very wet fuel gases (Niesel and Sigurdardottir, 1993). HCl can react with the liquid tin to form chlorides, which are volatile (low melting and boiling points), and therefore will condense to aerosols when cooled in heat exchangers. However, coal typically has a low Cl content, and therefore high H_2/HCl ratios will suppress the reaction of tin with HCl. Tin reacts with CO_2 at high temperatures to form tin oxide (Hedges, 1960).

$$Sn(l) + 2CO_2(g) \leftrightarrow SnO_2(s) + 2CO(g) \qquad (8.2)$$

Niesel and Sigurdardottir (1993) reported that the forward reaction is favoured at temperatures of 350-500℃ with equal proportions of CO_2 and CO. However, fuel gases typically have higher CO concentration than CO_2, which would suppress the formation of SnO_2. From experimental investigation in a double-stirred reactor, Hedden et al. (1986) reported that gas components such as CO and CO_2 did not influence the degree of H_2S conversion to SnS, although the tested gas concentrations were not specified. The same study also reported that the reaction rate for COS at 500℃ was about 3 times smaller than that for H_2S.

The research carried out in this PhD also showed that employment of a gas lift system in the packed-bed hot gas scrubber using liquid tin could pose significant problems in the plant operation. As discovered from the desulphurisation experimental work, the gas lift may pose a problem during maintenance. It can be replaced by a centrifugal pump as reported by Warner (1959), which provides better control of the liquid tin flow rate. Magnets-hydrodynamic pumping is also a relevant technique.

This research work examines the performance of the packed bed hot gas scrubber for both particulate cleaning and desulphurisation processes. Although the test results especially from the desulphurisation and SnS cleaning work showed that the potential of this new system is very promising, further fundamental investigations are required on various aspects in order to obtain more information about fundamental mechanisms of the absorption process in the non-wetting packed bed scrubber. Development of reaction modelling for the scrubber is also crucial in any scale-up of the reactor. To sum up, hot gas cleaning will continue to play a major role in the development of coal-based combined cycle power generation systems in the foreseeable future.

An industrial pilot-scale unit was also studied along with this research. This section will present a simple analysis on how the scrubber can be integrated into an industrial process. Assuming that a scale-up counter-current flow packed bed scrubber is designed to have a capacity 150 tonnes/day (Masaki, 2002) throughput coal gasifier with inlet H_2S concentration is 1000ppm. The removal efficiency for the packed bed scrubber (scale-up) was estimated by using the results from the over-all gas phase transfer unit. Extrapolation of the results from Figure 6.20, at constant liquid flow rate (13900 kg/m^{2}hr) indicates that 5983 kg/m^{2}hr gas mass flow rates would give 2.84 meter of diameter column and 9.8 meter of packing depth respectively for the scrubber operation, with 99.9% of H_2S removal efficiency at the tested conditions. The designed packing depth was considered adequate to fulfil the gas turbine requirement, tolerable up to 20 ppmv H_2S entering the gas turbine (Haupt, 1997). Table 8 presents indicative information for the scrubber size and operating conditions for a typical industrial scale coal gasifier (Masaki, 2002). The hot gas packed bed scrubber can be design with staged packed beds with liquid distributors at the intermediate space between each packed bed. This will help to overcome the plugging problem and ensure that the packing is fully wetted by achieving uniform flow of liquid supply.

Table 8: Design conditions of the packed bed scrubber estimated for 150 tons/day (Masaki 2002) throughput coal gasifier.

	Based on Test Results	**Extrapolated Results**
Liquid mass flow rate (kg/m^{2}s)	3.86	3.86
Gas mass flow rate (kg/m^{2}s)	0.368	1.66
Height of transfer unit, H_{OG} (m)	0.181	1.36
Bed cross-sectional area (m^2)	26.65	6.32
Bed diameter (m)	5.83	2.84
Bed height (m)	2.14	9.80
η, estimated (%)	99.9	99.9
H_2S inlet/outlet concentrations (ppm)	1000/1	1000/1

CHAPTER NINE

Conclusions and Recommendations for Future Work

This chapter highlights the conclusions and study limitations during this research work. Areas where further developments are necessary are identified and suggestions are put forward for possible future work.

9.1 Conclusion

- All the design modifications and testing for the pilot plant unit of the liquid metal based scrubber were successfully completed. In this research work, the existing equipment has been modified in order to investigate the process of particulate cleaning. Various parts of the equipment have been modified such as packing support plate, gas heaters, air seal and gas lift. For particulate removal tests, an additional system was added to the original design i.e. particle feeder. It consisted of a screw feeder and a venturi system. An online filter was also added to the system to determine the total efficiency of particle removal. This modification work was considered to be a major contribution of this research work.

- This experimental work was carried out using nitrogen gas for tin circulation at high temperatures (350 - 400℃) and the glass particles inlet was kept at an ambient temperature of 15℃. The large temperature difference meant that the liquid (flowing downwards) solidified upon collision with the cool glass particles. This resulted in solid tin build-up on the surface of the glass particles, thus reducing the E_T. Also, on the exhaust side of the scrubber, liquid tin splashes were observed which were then identified in the filter paper.

- At the lower bed temperature (350℃), the agglomerates formed at early stages were very fragile and contained a grey Si-Sn mixture. The liquid tin solidified slowly, making it more adhesive and easily attached onto the surface of glass particles upon collision. At 400℃, the formed agglomerates were stronger and had a black colour. This is associated with liquid tin, which solidified even more rapidly during the filtration process. The liquid tin-irrigated packed bed scrubber demonstrated particulate removal performance with E_T ranging from 60 to 98%. The E_T decreased as the inlet dust loading increased.

- The results also showed that the temperature had a significant influence on the E_T. As the temperature increased from 350℃ and 400℃, the E_T decreased. The major reason for this is the large temperature difference between the inlet particles and the scrubber, which result in the formation of a thicker bed of agglomerates.

- The resulting grade efficiency curves were not able to demonstrate realistic results. This is because at corresponding liquid flow rates and inlet solid loading, the particles collected in the impinger were not representative of the total removal efficiency. From the particulate cleaning test, the results were unsatisfactory and the equipment operation had low efficiency for particulate cleaning. Nevertheless, the proposed objectives have been met and it is evident that with several important modifications, the equipment would be able to operate satisfactorily.

- The absorption behaviour of H_2S in a novel liquid tin irrigated hot gas scrubber was investigated for various operating parameters in a lab-scale packed bed. H_{OG} values ranged from 0.84 to 0.181 m for tested conditions at 1000 ppm of H_2S concentration, which meant that this system has very good potential for efficient desulphurisation. High liquid velocities increased the removal efficiency due to larger liquid holdup, creating a larger interfacial area. Increased gas velocities influenced the removal efficiency by altering the gas residence times, liquid holdup, and gas-phase mass transfer. The H_{OG} of an empty column was about 5 times higher at the tested conditions due to lack of contact between the two phases. The H_{OG} gradually reduced for increased H_2S concentrations or at lower operating temperatures.

- The cleaning of SnS was performed with and without the presence of zinc powder. Addition of zinc powder saw around 20% reduction of sulphur in the sample compared to without zinc. Observation from SnS cleaning without the addition of zinc powder gave a positive result. However, the sulphur reduction of ~13 % could not justify heating the sample to 400℃ for 6 hours.

- CFD modelling work was performed to simulate particle removal in a packed bed of spheres operating under hot gas conditions. The case study using a "*wall trap condition*" provided higher efficiency due to the particle interaction with the instantaneous velocity fluctuations of the gas phase.

Study showed that particle separation efficiency increased with particle size due to the mass and hence its inertia. It is also caused by larger particles colliding with the packing spheres. The elastic collisions increase the randomness of the particle trajectories hence improving the chances of particle entrapment by the walls and packing. Efficiencies above 98% were predicted for particles of 40 μm and larger. Particle separation improved with particle density due to the effect of greater interaction.

- The mathematical model presented here combines chemical reactions and mass transfer in gas phases for the absorption of H_2S into liquid tin in a packed-bed hot gas scrubber. The range of reaction rate constants from this work is 0.011 to 0.019 m/s for various operating temperatures, which are within the broad range of values as reported by Hedden (1986). The H_2S absorption is primarily affected by the operating temperature and gas superficial velocity. It is also affected by effective specific interfacial area and liquid viscosity.

9.2 Study Limitations

The following study limitations were identified in the investigation:

- The heat-up of the system was relatively slow, after 6 hours the bed temperature was only around 400℃ and this was not high enough for the most crucial part of gasification process. Therefore, an extra heater needs to be installed in order to provide sufficient heat and also to shorten the heat-up time.

- It was also not possible to clean the scrubber after every test run due to time constraints, especially for particulate cleaning experimental work. This is mainly because once the rig has been dismantled; it will take minimum of two days to re-assemble the rig. Since the experimental work dealt with liquid tin at a high temperature, another one-day of testing is needed in order to make sure there are no leakages at all joints.

- Even the main column was not clean after every test run, valves V4, V9 and V10 needed to be checked every time before new test runs. Solid tin had to be cleaned and removed from the valves to prevent blockage. Any blockage in one of the valves would tend to interrupt the test, especially when the tin starts to circulate inside the column.

- The tip of the nitrogen injector had to be checked regularly. During the experimental work, sometimes tin was not circulating due to a blockage of solid tin at the tip of the nitrogen injector. Since it was a closed system and it was not possible to visualise the actual situation inside the system, the only way to ensure smooth operation was to check all the possible sections that tended to give problems.

9.3 Recommendations for Future Work

- The temperatures of the particles need to be nearly the same as the temperature of the packed bed scrubber (≈ 400 ºC). An extra heater should be installed for the dust feeder and particles inlet line system for particulate cleaning experimental work. This would avoid any solidification of liquid tin upon colliding with cold particles. In this way, the total efficiency of particulate cleaning is expected to increase dramatically. This modification would also avoid any formation of agglomerated material inside the column.

- Extra semi-cylindrical ceramic radiant heaters are also needed to heat the main scrubber. This is necessary to provide sufficient heat to the scrubber and also to shorten the heat-up time.

- The capability of the scrubber for particle/tar removal should also be studied in order to fully exploit the potential of this technology.

- The test results presented here showed the excellent potential of this new desulphurisation system. However, further fundamental investigations are required on various aspects including wider ranges of test parameters such as gas and liquid flow rates, temperature, pressure, and test duration.

- This study touched on the mechanisms of SnS cleaning using Zinc powder. However, further work would be needed to create a better understanding of the fundamental mechanisms, which is essential for high H_2S removal efficiencies at high H_2/H_2S ratios. It is also anticipated that electromagnetic or mechanical pumps would be used to circulate the tin in an industrial environment.

- Further fundamental studies on the reaction chemistry between various gas species (H_2S, H_2O, HCl etc.), tin and its compounds (SnS, SnS_2 and Sn_2S_3) for various temperatures would identify the theoretical limits of this system.

- An economic analysis of the various aspects that involve the use of molten tin such as material recovery would provide valuable information to access the profitability of the hot flue gas cleaning.

- Further improvements to CFD work should include different expressions used for the kinetics of reactions in the case of the particle-liquid tin interaction. Improvement to CFD should be carried out in parallel with experimental work so that any development or improvement to the model can be simultaneously validated.

- Other aspects of the modelling work such as liquid film and effective specific interfacial area (a_e) correlations for non-wetting system for the desulphurisation process was outside the scope of the present study. However, full understanding of these topics is important in order to scale-up the system to industrial applications.

References

- Abbasian, J. & Slimane, R.B. (1998). "A regenerable copper-based sorbent for H_2S removal from coal gases". *Ind. Eng. Chem. Res.*, 37 (7), 2775-2782.

- Anderson, I.E., Gleeson, B. & Terpstra, R.L. (2003). *Development of metallic hot gas filters*. Oak Ridge National Laboratory. Available from: http://www.ornl.gov/sci/fossil/Publications/RECENT%20PUBS/AMES-3.pdf [Accessed: 15th December 2004].

- Androutsopoulos, G.P. & Hatzilyberis, K.S. (2001). "Electricity generation and atmospheric pollution: The role of solid fuels gasification". *Global Nest: The Int. Journal*, 3 (3), 171-178.

- ASM (1981). *Metal Handbook, Volume 4: Heat Treating. 9th Edition*. Ohio, American Society for Metals. Cited in: Chang, B. F. (2003)

- ASM (1984). *Metal Handbook, Volume 7: Power Metallurgy. 9th Edition*. Ohio, American Society for Metals. Cited in: Chang, B. F. (2003)

- Ayala, R.E. & Venkataramani, V.S. (1998). *Advanced sorbent development program: Development of sorbents for moving-bed and fluidized-bed applications (Volume I - Development of sorbents for moving-bed applications)*. GE Corporate Research and Development & U.S. Department of Energy, Morgantown, West Virginia. Report No. DE-AC21-94MC31089 -02.

- Bandosz, T.J. (1999). "Effect of pore structure and surface chemistry of virgin activated carbons on removal of hydrogen sulfide". *Carbon*, 37 (3), 483-491.

- Bonk, D.L., Freier, M.D., Buchanan, T.L., DeLallo, M.R., Goldstein, H.N. & White, J.S. (1996). "Asssessment of PFBC and gasification repowering". *Advanced Coal-Fired Power Systems '96 Review Meeting (July 16-18, 1996)*. Morgantown, West Virginia.

- Cal, M.P., Strickler, B.W. & Lizzio, A.A. (2000). "High temperature hydrogen sulfide adsorption on activated carbon I. Effects of gas composition and metal addition". *Carbon*, 38 (13), 1757-1765.

- Chang, B.F. (2003). *A non-wetting packed bed gas scrubber*. PhD. Thesis, Department of Chemical and Process Engineering, University of Sheffield, U.K.

- Chang, B.F., Sharifi, V.N., Swithenbank, J. & Warner, N. (2002). "Development of a liquid metal based fuel gas scrubbing system". *Proceedings of the 5th International Symposium on Gas Cleaning at High Temperature held at Morgantown, West Virginia*. U.S. DOE, Morgantown Energy Technology Center.

- Changkook Ryu, Ismail, M.H.S., Sharifi, V.N. & Swithenbank, J. (2007). "Liquid tin irrigated packed bed for hot fuel gas desulfurization". *Ind. Eng. Chem. Res.*, 46 (26), 9015-9021.

- ChevronChevron (2002). *Coal gasification for power generation. A New Role for Coal in Meeting the United Kingdom's Clean Energy Challenge.* ChevronChevron Texaco Worldwide Power & Gasification.

- Chilton, T.H. & Colburn, A.P. (1934). "Mass transfer (absorption) coefficient. Prediction from data on heat transfer and fluid friction". *Industrial and Engineering Chemistry Research*, 26 (11), 1183-1187.

- Christof, R. (2007). *Energy in perspective: BP statistical review of world energy 2007.* Available from: http://www.bp.com/home.do?categoryId=1&contentId=2006973 [Accessed: 21st November 2007]

- CIAB (2004). *International coal market & policy developments in 2003.* Coal Industry Advisory Board. Available from: http://www.iea.org/textbase/papers/2004/ciabmark_2003.pdf.

- Clift, R. (1997). "Inertial separators: Basic principles". In: Seville, J. P. K., Gas cleaning in demanding applications. London, Blackie Academic & Professional. p. 41-52.

- Colburn, A.P. (1939). "The simplified calculation of diffusional process, general consideration of two-film resistances". *Transactions of American Institute of Chemical Engineers*, 35, 211-231. Cited in: Chang, B. F. (2003).

- Coulson, J.M. & Richardson, J.F. (1990). *Chemical Engineering, Volume 2: Particle technology and separation processes. 4th Edition.* Butterworth Heinemann.

- Coury, R.C., Coury, J.R., Thambimuthu, K.V. & Clift, R. (1987). "Capture and rebound of dust in granular bag gas filtes". *Powder Technol*, 50, 253-265. Cited in: Chang, B. F. (2003).

- Danckwerts, P.V. (1951). "Significance of liquid-film coefficients in gas absorption". *Ind. Eng. Chem.*, 43 (6), 1460-1467.

- DEFRA (2006). *Climate Change The UK Programme 2006.* Department for Environment, Food and Rural Affairs. Report No. CM6764-SE/2006/43.

- DEFRA (2008). *INFORMATION BULLETIN: Statistical Release - UK Emissions of air pollutants - 2006 Results (13th March 2008).* London: Department for Environment, Food and Rural Affairs. Available from: http://www.defra.gov.uk/news/2008/080313a.htm [Accessed: 8th June 2008]

- DTI (2002). *Energy: Its impact on the environment and society.* Available from: http://www.berr.gov.uk/files/file32296.pdf [Accessed: 28th August 2007]

- EEA (2002). *Environmental signals 2002: Benchmarking the millennium (European environment agency regular indicator report).* European Environment Agency. Report No. TH-AG-02-001-EN-C.

- Elseviers, W.F. & Verelst, H. (1999). "Transition metal oxides for hot gas desulphurization". *Fuel*, 78 (5), 601-612.

- EPA (1996). *Draft technical support document for HWC MACT standards*. U.S. Environmental Protection Agency. Volume I - Description of source categories Report No. 68-D2-0164.

- EPA (2005). *Module 6: Air pollutants and control techniques*. U. S. Environmental Protection Agency. Available from: http://www.epa.gov/eogapti1/module6/matter/control/control.htm [Accessed: 23rd March 2005]

- EPA (2007a). *Design review of absorbers used for gaseous pollutants - Lesson 11*. Air Pollution Training Institute, U.S. Environmental Protection Agency. Available from: http://www.epa.gov/oar/oaqps/eog/ [Accessed: 28th April 2007]

- EPA (2007b). *Operating Principles of Scrubbers - Lesson 2*. Air Pollution Training Institute, U.S. Environmental Protection Agency. Available from: http://www.epa.gov/oar/oaqps/eog/ [Accessed: 18th February 2007]

- Fadel, T.M. (1984). "Selecting packed-column auxiliaries". *Chemical Engineering Science*, 91 (2), 71-76. Cited in: Chang, B. F. (2003)

- Gangwal, S.K. (1995). "Hot-gas-cleanup-sulfur recovery: Techanical, environmental, and economic issues". *Heat Recovery System and CHP*, 15 (2), 205-214.

- Gangwal, S.K., Portzer, J.W., Roberts, G.W. & Kozup, S.C. (1998). *Engineering evaluation of hot-gas desulfurization with sulfur recovery*. Research Triangle Institute. Research Triangle Park, NC. Report No. DEAC21-94MC31258.

- Gary, J.S. & Russell, C.M. (2001). "Gasification technologies: The path to clean, affordable energy in the 21st century". *Fuel Processing Technology*, 71 (1-3), 79-97.

- Grasa, G., Wellman, R.G., Kilgallon, P., Simms, N.J. & Oakey, J.E. (2004). *Novel hot gas cleaning/heat recovery system*. Power Generation Technology Centre, Cranfield University. Report No. COAL R269 DTI/Pub URN 04/1794.

- Graton, L.C. & Fraser, H.J. (1935). "J. Geol." *43, 785*, Cited in: Gray, W. A. (1968). "The packing of solid particles". London, Chapman & Hall Ltd.

- Gray, W.A. (1968). *The packing of solid particles*. London, Chapman & Hall Ltd. Cited in: Chang, B. F. (2003)

- Gupta, R.P. & Gangwal, S.K. (1993). *High temperature, high pressure testing of zinc titanate in a bench-scale fluidized bed reactor for 100 cycles*. Topical Report under U.S. Dept. of Energy Contract, Research Triangle Inst., Research Triangle Park. Report No. NC 27709-2194.

- Gupta, R.P., Turk, B.S. & Gangwal, S.K. (1996). "Bench-scale development of fluidized-bed spray-dried sorbents". *Proceedings of the Advanced Coal-Fired Power Systems '96 Review Meeting held at Morgantown, West Virginia*. U.S. DOE, Morgantown Energy Technology Center.

- Gupta, R.P., Turk, B.S. & Vierheilig, A.A. (1998). *Desulfurization sorbents for transport-bed applications.* Available from: http://www.netl.doe.gov/publications/proceedings/98/98ps/ps2a-2.pdf [Accessed: 5th November 2004]

- Haupt, G. (1997). *Erlangen, Germany, Siemen/KWU* London: IEA Coal Research. Cited in: Mitchell, S.C. (1998)

- Heath, B. (2004). *International coal market & policy developments in 2003.* Coal Industry Advisory Board (CIAB).

- Hedden, K., Rao, B.R. & Reitz, F. (1986). "Desulfurization of manufactured gases with liquid metals". *Proceedings of the 1986 International Gas Research Conference held at Toronto, Ont, Canada*, pp. 1124-1133. Government Inst Inc, Rockville, MD, USA.

- Hedges, E.S. (1960). *Tin and its alloys.* Edward Arnold Ltd.: London.

- Higbie, R. (1935). "The rate of absorption of pure gas into a still liquid during short periods of exposure". *Transactions of AIChE*, 31, 365. Cited in: Chang, B. F. (2003).

- Hrdlicka, T. & Swanson, W. (2003). *Demonstration of a full-scale retrofit of the advanced hybrid particulate collector technology.* Otter Tail Power Company, United States Department of Energy, National Energy Technology Laboratory. Report No. DE-FC26-02NT41420.

- Huque, Z., Mei, D. & Zhou, J. (1996). *Initial failure analysis of ceramic filters.* Advanced Coal-Fired Power Systems '96 Review Meeting, Morgantown, West Virginia.

- IEA (2003). *Control and minimisation of coal-fired power plant emissions: Zero emissions technologies for fossil fuels.* IEA, Clean Coal Centre. Available from: http://www.iea.org/textbase/papers/2003/Coal_Fired_Fossil_Fuels.pdf [Accessed: 14th June 2005]

- Jothimurugesan, K., Adeyiga, A.A. & Gangwal, S.K. (1986). "Advanced hot-gas desulfurization sorbents". *Proceedings of the Advanced Coal-Fired Power Systems '96, Review Meeting.* Morgantown Energy Technology Center, Morgantown, West Virginia.

- Jun, H.K., Lee, T.J., Ryu, S.O. & Kim, J.C. (2001). "A study of Zn-Ti-based H_2S removal sorbents promoted with cobalt oxides". *Ind. Eng. Chem. Res.*, 40 (16), 3547-3556.

- Kwon, K.C. (1998). *Investigation on durability and reactivity of promising metal oxide sorbents during sulphidation and regeneration.* U.S. Department of Energy, Morgantown, West Virginia, U.S. Report No. DE-FG21-94MC31206-13.

- Kwon, K.C. & Gangwal, S.K. (2004). *Kinetics of direct oxidation of H_2S in coal gas to elemental sulfur.* Tuskegee University, Tuskegee, Alabama and Research Triangle Institute. Report No. DE-FG26-00NT40835.

- Levenspiel, O. (1999). *Chemical reaction engineering.* John Wiley and Sons, New York.

- Lew, S., Jothimurugesan, K. & Flytzani-S, M. (1989). "High-temperature hydrogen sulfide removal from fuel gases by regenerable zinc oxide-titanium dioxide sorbents". *Ind. Eng. Chem. Res.*, 28 (5), 535-541.

- Lide, D.R. (2005). *CRC Handbook of Chemistry and Physics.* 86th edition. CRC Press: Boca Raton, FL.

- Linek, V., Petricek, P., Benes, P. & Braun, R.E. (1984). "Interfacial area and liquid side mass transfer coefficients in absorption columns packed with hydrophilised and untreated plastic packings". *Chem. Eng. Res. Des.*, 62 (13), Cited in: G. Q. Wang, X. G. Yuan and K. T. Yu. (2005). "Review of mass-transfer correlations for packed columns". Ind. Eng. Chem. Res., 44, 8715-8729.

- Lippert, T.E., Bruck, G.J., Sanjana, Z.N., Newby, R.A. & Bachovchin, D.M. (1996). "Westinghouse advanced particle filter system". *Advanced Coal-Fired Power Systems '96 Review Meeting.* Morgantown, West Virginia.

- Longwell, J.P., Rubin, E.S. & Wilson, J. (1995). "Coal: Energy for the future". *Progress in Energy and Combustion Science*, 21 (4), 269-360.

- Luke, C., Jin-Wei, L. & Chen-Lu, Y. (2002). "Absorption of NO_2 in a packed tower with Na_2S0_3 aqueous solution". *Environmental Progress*, 21 (4), 225-230.

- Mackey, P.J. & Warner, N.A. (1973). "Studies in the vaporisation of mercury in irrigated packed beds". *Chemical Engineering Science*, 28 (12), 2141-2154.

- Masaki, T. & Jun-Ichi, T. (2002). "Development status of the EAGLE gasification pilot plant". *Gasification Technologies 2002*, October 27-30, 2002. San Francisco, California.

- McCabe, W.L., Smith , J.C. & Harriott, P. (1993). *Unit operations of chemical engineering. 5th Edition.* New York, McGraw-Hill.

- McConville, A. (1997). *Emissions standards handbook.* IEACR/96. London: IEA Coal Research. Cited in: Chang, B. F. (2003)

- Meissner, H.P. (1976). *Removal of hydrogen sulfide from reducing gases.* Institute of Gas Technology, US Patent US3954938

- Meissner, H.P. & Shora, F.C. (1981). *High temperature pollutant removal from gas streams.* Institute of Gas Technology, US Patent US4308037

- Mersmann, A. & Deixler, A. (1986). "Packed columns". *Ger. Chem. Eng.*, 9 (265), Cited in: G. Q. Wang, X. G. Yuan and K. T. Yu. (2005). "Review of mass-transfer correlations for packed columns". Ind. Eng. Chem. Res., 44, 8715-8729.

- Minchener, A.J. (2005). "Coal gasification for advanced power generation". *Fuel*, 84 (17), 2222-2235.

- Mitchell, S.C. (1997). *Hot gas particulate filtration.* London. IEA Coal Research. Report No. IEACR/95.

- Mitchell, S.C. (1998). *Hot gas cleanup of sulphur, nitrogen, minor and trace elements.* CCC/12. London: IEA Coal Research.

- Mojtahedi, W., Salo, K. & Abbasian, J. (1994). "Desulfurization of hot coal gas in fluidized-bed with regenerable zinc titanate sorbents". *Fuel Processing Technology*, 37, 53-65.

- Neelakantan, K. & Gehlawat, J.K. (1982). "New chemical systems for the determination of liquid-side mass transfer coefficient and effective interfacial area in gas-liquid contactors". *The Chemical Engineering Journal*, 24, 1-6.

- Ness, H.M., Kim, S.S. & Ramezan, M. (1999). "Status of advanced coal-fired power generation technology development in the U.S". *13th U.S/Korea Joint Workshop on Energy and Environment.* Reno, Nevada.

- Neville, H.E. (2004). "Gasification process selection- Trade-offs and ironies". *Proceedings of the Gasification Technologies Conference 2004.* JW Marriott Hotel, Washington, DC.

- Nielsen, P.E.H. & Sigurdardottir, I.D. (1993). *Development and characterization of steam regenerable sorbents for hot gas desulphurization in coal gasification based combined cycle plant. In Gas Cleaning At High Temperatures; Clift, R., Seville, J. P. K., Eds.* Blackie Academic & Professional: Glasgow.

- Noll, C.G. & Peter Castle, G.S. (1995). "Electrostatics in gas cleaning: Contributions of Professor James R. Melcher". *Journal of Electrostatics*, 34 (2-3), 299-305.

- O'Brien, J.N., Blau, J. & Rose, M. (2004). *An analysis of the institutional challanges to commercialization and development of IGCC technology in the U.S. electric industry: Recommended policy, regulatory, executive and legislative Initiatives.* Global-Change Associstes. Available from: http://www.netl.doe.gov/energy-analyses/pubs/FinalReport2-20Vol1.pdf [Accessed: 24th February 2006]

- Oak-Ridge (2005). *Technology transfer: Ceramic filter is key to advanced coal technology.* Oak Ridge National Laboratory, Department of Energy. Available from: http://www.ornl.gov/info/ornlreview/rev28-4/text/tec.htm [Accessed: 24th March 2005]

- Oakey, J.E., Simms, N.J. & Kilgallon, P.J. (2004). "Gas turbines: Gas cleaning requirements for biomass-fired systems". *Materials Research*, 7 (1), 17-25.

- Oxford-Chemist (2006). *The physical and theoretical chemistry laboratory: Oxford University chemical and other safety information.* Oxford Chemist Dorothy Crowfoot Hodgkin, University of Oxford. Available from: http://www.pcl.ox.ac.uk/MSDS/ [Accessed: 22nd December 2006]

- Pahl, D. (1983). "EPA's program for establishing standards of performance for new stationary sources of air pollution". *J. Air Pollut. Control Assoc.*, 33 (5), 468-482.

- Parkinson, G. (2004). "Power Generation: OEMs getting ready for coal gasification". *Turbomachinery International*, (May/June 2004).

- Patrick, V., Gavalas, G.R., Flytzani-S, M. & Jothimurugesan, K. (1989). "High-temperature sulfidation-regeneration of copper(II) oxide-alumina sorbents". *Ind. Eng. Chem. Res.*, 28 (7), 931-940.

- Perry, R.H. & Green, D.W. (1997). *Chemical Engineers' Handbook. 7th Edition.* New York, McGraw-Hill.

- Pineda, M., Palacios, J.M., García, E., Cilleruelo, C. & Ibarra, J. (1997). "Modelling of performance of zinc ferrites as high-temperature desulfurizing sorbents in a fixed-bed reactor". *Fuel*, 76 (7), 567-573.

- Ratafia-Brown, J., Manfredo, L., Hoffmann, J. & Ramezan, M. (2002). *Major environmental aspects of gasification-based power generation technologies.* National Energy Technology Laboratory. Report No. DE-AT26-99FT20101.

- Reitz, F. (1985). *Selective desulfurization of hot reducing gases by liquid tin and lead.* Dr.-Ing. dissertation. University of Karlsruhe. Cited in: Hedden, K. (1986).

- Rhodes, K. (2006). *It's Academic: The case for coal gasification on campus.* Woolpert, Inc. Available from: http://www.woolpert.com/asp/articles/Its_Academic.asp [Accessed: 16th February 2008]

- Ron, Z. & Pia, K. (2004). *Control of pollutants in flue gases and fuel gases.* Finland: 3rd edition (ISBN: 951-22-5527-8). Helsinki University of Technology. Available from: http://web.abo.fi/~rzevenho/gasbook.html [Accessed: 24th November 2006]

- RS-Components (1996) Air process heaters. RS Components Ltd. Birchington Road, Corby, Northants, NN17 9RS, UK.

- Rutkowski, M.D., Klett, M.G. & Zaharchuk, R. (1996). "Assessment of hot gas contaminant control". *Advanced Coal-Fired Power Syatems '96 Review Meeting.* Morgantown, West Virginia.

- Sadownik, B., Nyboer, J., Murphy, R. & Laurin, A. (2004). *Potential impact of energy efficiency of electricity demand in Ontario: Appendix 4 - A comparison of combustion technologies for electricity generation.* The Pembina Institute, Ontario. Available from: http://www.pembina.org/publications.asp [Accessed: 18th November 2004]

- Sahay, B.N. & Sharma, M.M. (1973). "Effective interfacial area and liquid and gas side mass transfer coefficients in a packed column". *Chemical Engineering Science*, 28, 41-47.

- Samsanov, G.V. (1982). *The Oxide Handbook. 2nd Edition.* New York, Plenum Data Co. Cited in: Chang, B. F. (2003).

- Sanchez, J.M., Ruiz, E. & Otero, J. (2005). "Selective removal of hydrogen sulfide from gaseous streams using a zinc-based sorbent". *Ind. Eng. Chem. Res.*, 44 (2), 241-249.

- Sasaoka, E., Hatori, M., Yoshimura, H., Su, C. & Uddin, M.A. (2001). "Role of H_2O in oxidation of spent high-temperature desulfurization sorbent Fe_2O_3 and CuO in the presence of O_2". *Ind. Eng. Chem. Res.*, 40 (11), 2512-2517.

- Sasaoka, E., Hirano, S., Kasaoka, S. & Sakata, Y. (1994). "Stability of zinc oxide high-temperature desulfurization sorbents for reduction". *Energy and Fuels*, 8 (3), 763-769.

- Sasaoka, E., Ichio, T. & Kasaoka, S. (1992). "High-temperature H_2S removal from coal-derived gas by iron ore". *Energy and Fuels*, 6 (5), 603-608.

- Schürmann, B. (1984). "Untersuchungen üeber die Gasreinigung durch geschmolzene Stoffe und Entwicklung eines entsprechnenden Verfahrens (Studies of gas purification by molten materials and development of an appropriate method)". *Fortschritt-Berichte der VDI-Zeitschriften Reihe 3: Verfahrenstechnik*, 85, 231.

- Scott, D.H. (1997). *Improving existing power stations to comply with emerging emissions standards*. IEA Coal Research. Report No. IEACR/92.

- Seville, J.P.K. (1996). *Hot gas particulate clean-up: Curent technological and commercial status*. UK DTI's Coal Research and Development Programme. Harwell, Energy Technology Support Unit. Report No. COAL R092.

- Seville, J.P.K. (1997). *Rigid ceramic filters. In: Seville, J.P.K. (ed) Gas cleaning in demanding applications.* London: Blackie Academic & Professional.

- Shi, M.G. & Mersmann, A. (1985). "Effective interfacial area in packed columns". *Ger. Chem. Eng.*, 8 (87), Cited in: G. Q. Wang, X. G. Yuan and K. T. Yu. (2005). "Review of mass-transfer correlations for packed columns". Ind. Eng. Chem. Res., 44, 8715-8729.

- Shulman, H.L. & de Gouff, J.J. (1952). "Mass transfer coefficients and interfacial areas for 1-inch raschig rings". *Ind. Eng. Chem.*, 44, 1915, Cited in: G. Q. Wang, X. G. Yuan and K. T. Yu. (2005). "Review of mass-transfer correlations for packed columns". Ind. Eng. Chem. Res., 44, 8715-8729.

- Shulman, H.L., Ullrich, C.F., Proulx, A.Z. & Zimmerman, J.O. (1955). "Performance of packed column. 2. Wetted and effective interfacial area, Gas- and liquid-phase mass transfer rates". *American Institute of Chemical Engineers Journal, 1, 253*, Cited in: G. Q. Wang, X. G. Yuan and K. T. Yu. (2005). "Review of mass-transfer correlations for packed columns". Ind. Eng. Chem. Res., 44, 8715-8729

- Simms, N.J., Oakey, J.E., Stephenson, D.J., Smith, P.J. & Nicholls, J.R. (1995). "Erosion-corrosion modelling of gas turbine materials for coal-fired combined cycle power generation". *Wear*, 186-187, 247-255.

- Slimane, R.B. & Abbasian, J. (2000). "Copper-based sorbents for coal gas desulfurization at moderate temperatures". *Ind. Eng. Chem. Res.*, 39 (5), 1338-1344.

- Slimane, R.B. & Hepworth, M.T. (1994a). "Desulfurization of hot coal-derived fuel gases with manganese-based regenerable sorbents. 1. Loading (sulfidation) tests". *Energy and Fuels*, 8 (6), 1175-1183.

- Slimane, R.B. & Hepworth, M.T. (1994b). "Desulfurization of hot coal-derived fuel gases with manganese-based regenerable sorbents. 2. Regeneration and multicycle tests". *Energy and Fuels*, 8 (6), 1184-1191.

- Slimane, R.B. & Hepworth, M.T. (1995). "Desulfurization of hot coal-derived fuel gases with manganese-based regenerable sorbents. 3. Fixed-bed testing". *Energy and Fuels*, 9 (2), 372-378.

- Slimane, R.B. & Williams, B.E. (2002). "New ZnO-based regenerable sulfur sorbents for fluid-bed/transport reactor applications". *Ind. Eng. Chem. Res.*, 41 (23), 5676-5685.

- Smeers, Y., Bolle, L. & Squilbin, O. (2001). *Coal options: Evaluation of coal-based power generation in an uncertain context.* Federal Office for Scientific, Technical and Cultural Affairs. Report No. CG/DD/231 - G/DD/232.

- Standish, N. (1968). "Heat transfer in liquid metal irrigated packed beds countercurrent to gases". *Trans. Metall. Soc. AIME*, 242, 1733-1740.

- Standish, N. (1973). "On the flooding criteria for liquid metals". *Chemical Engineering Science*, 28 (10), 1906-1907.

- Stevens, D.J. (2001). *Hot gas conditioning: Recent progress with large-scale biomass gasification systems.* U.S. Department of Energy. Update and summary of recent progress Report No. NREL/SR-510-29952.

- Stiegel, G.J. (1999). *Integrated gasification combined cycle: Clean, affordable energy for tomorrow's world.* U.S. Department of Energy, Office of Fossil Energy, Pittsburgh. Available from: http://www.energy.gov/ [Accessed: 26th October 2005]

- Strigle, R.F. (1994). *Packed tower designs and applications. Random and structured packings. 2nd Edition.* Gulf Publishing Company: Houston.

- SugarUdyog (2005). *Controlling air pollution.* Haryana: SugarUdyog. Available from: http://www.sugarudyog.com/pollution.htm [Accessed: 30th March 2005]

- Svarovsky, L. (1981). *Solid-gas separation.* Amsterdam, Elsevier Scientific Publishing Company. Cited in: Chang, B. F. (2003).

- Tamhankar, S.S., Hasatani, M. & Wen, C.Y. (1981). "Kinetic studies on the reactions involved in the hot gas desulfurization using a regenerable iron oxide sorbent I: Reduction and sulfidation of iron oxide". *Chemical Engineering Science*, 36 (7), 1181-1191.

- Toor, H.L. & Marchello, J.M. (1958). "Film-penetration model for mass and heat transfer". *AIChE Journal*, 4 (1), 97-101.

- Turk, B.S., Merkel, T., Lopez-Ortiz, A., Gupta, R.P., Krishnan, G.N., Freeman, B.D. & Fleming, G.K. (2001). *Novel technologies for gaseous contaminants control.* U.S. Department of Energy. Report No. DE-AC26-99FT40675.

- UK-DTI (1998). *Technology status report-gasification of solid and liquid fuels for power generation.* UK DTI's Cleaner Coal Technology Programme. Department of Trade and Industry. Cited in: Chang, B. F. (2003)

- US-DOE (2004). *Gasification technology research and development.* Available from: http://www.fe.doe.gov/programs/powersystems/index.html [Accessed: 30th November 2004]

- Vogel, A.I. (1989). *Vogel's Textbook of Quantitative Chemical Analysis. 5th Edition.* Essex, Longman Scientific & Technical. Cited in: Chang, B. F. (2003).

- Wakker, J.P. & Gerritsen, A.W. (1993). "High temperature hydrogen sulfide and carbonyl sulfide removal with manganese oxide (MnO) and iron oxide (FeO) on .gamma.-alumina acceptors ". *Ind. Eng. Chem. Res.*, 32 (1), 139-149.

- Warner, N.A. (1959). "Liquid metal irrigation of a packed bed". *Chemical Engineering Science* 11 (3), 149-224.

- Warner, N.A. (1997). *Zinc-based clean technology for desulfurization in advanced power generation. COAR R127.* R127; UK DTI's Coal Research and Development Programme, Harwell, Energy Technology Support Unit.

- Warner, N.A. (2000). *Personal communication: Theoretical framework for liquid metal based coal gasification (Draft) - 23rd February 2000.* Cited in: Chang, B. F. (2003)

- Warner, N.A. (2001). *Personal communication: Theoretical framework for liquid metal based coal gasification (Draft) - 25th April 2001.* Cited in: Chang, B. F. (2003)

- WCI (2003). *Coal the role of as an energy source.* London: World Coal Institute. Available from: http://wci.rmid.co.uk/uploads/RoleofCoal.pdf [Accessed: 22nd July 2006]

- WCI (2006). *Coal facts 2006.* London: World Coal Institute. Available from: www.worldcoal.org [Accessed: 15th October 2006]

- Westmoreland, P.R., Gibson, J.B. & Harrison, D.P. (1977). "Comparative kinetics of high-temperature reaction between H_2S and selected metal oxides". *Environmental Science and Technology*, 11 (5), 488-491.

- White, A.M. (1935). "Pressure drop and loading velocities in packed towers". *Transactions American Institute of Chemical Engineers*, 31, 390-408. Cited in: Chang, B. F. (2003)

- Whitman, W.G. (1923). "The two-film theory of gas absorption". *Chemical and Metallurgical Engineering*, 29 (4), 146-148. Cited in: Various sources.

- Williams, B.C. & McMullan, J.T. (1998). *Hot gas chemical clean-up: Current commercial and technological status.* UK DTI's Coal Research and Development Programme, Harwell, Energy Technology Support Unit. Report No. COAL R319. Cited in: Chang, B. F. (2003)

- Zhu, Q. (2003). *Developments in particulate control (PF 03-04).* Available from: http://www.iea-coal.org.uk [Accessed: 21st December 2004]

APPENDIX

List of Journal Publication and Oral/Poster Presentations

- Changkook Ryu, **Mohd H. S. Ismail**, Vida N. Sharifi, and Jim Swithenbank, "***Liquid Tin Irrigated Packed Bed for Hot Fuel Gas Desulfurization***" *Ind. Eng. Chem. Res.* 2007, *46*, pp. 9015-9021.

- **Mohd H. S. Ismail**, Changkook Ryu, Vida N. Sharifi, and Jim Swithenbank, "***Hot Gas Clean-Up for Gasification Process***" Poster presented at CIWM 2006/5th International Symposium on Waste Treatment technologies, 13-15th June, 2006, Paignton, UK.

- **Mohd H. S. Ismail**, Changkook Ryu, Vida N. Sharifi, and Jim Swithenbank, "***Hot Gas Clean-Up for Gasification Process***" 24th Month Poster Presentation, Department of Chemical and Process Engineering, University of Sheffield. October 2006.

- **Mohd H. S. Ismail**, "***Development of Liquid Tin Irrigated Packed Bed for Hot Fuel Gas Desulphurisation***" Oral Presentation, Department of Chemical and Process Engineering, University of Sheffield. 25th April, 2007.

Liquid Tin Irrigated Packed Bed for Hot Fuel Gas Desulfurization

Changkook Ryu,* Mohd H. S. Ismail, Vida N. Sharifi, and Jim Swithenbank

Department of Chemical and Process Engineering, The University of Sheffield, Newcastle Street, Sheffield S1 3JD, U.K.

Hot fuel gas cleaning for gasification of coal can increase the energy efficiency by minimizing the loss of thermal energy. The current hot gas desulfurization studies focus on the development of various metal oxide sorbents. This paper presents a novel approach using liquid tin as a nonwetting scrubbing medium in a countercurrent packed bed. The H_2S removal efficiency of liquid tin was investigated in a 200 mm high reactor for various tin and gas flow rates, bed heights, and H_2S concentration at operating temperatures of 300−400 °C. For tested conditions, gas transfer unit heights of 0.084−0.181 m were obtained at H_2S concentration of 1000 ppm, which corresponded to an H_2S removal efficiency of up to 91% in the small test reactor. These results are promising since higher efficiencies can be achieved at larger scales. The effects of thermal equilibrium and interaction with other gases are also discussed. Further studies are required on various aspects including higher operating temperatures, larger flow rates, and the regeneration of tin using zinc.

1. Introduction

Gasification is a thermochemical process that converts carbon-containing fuels such as coal and biomass into a H_2- and CO-rich fuel gas and sensible heat using air, oxygen, and/or steam. The fuel gas contains pollutants such as H_2S, COS, NH_3, HCl, tar, and particulates. The levels of H_2S and COS for each of the gasification systems show considerable variation,[1,2] as shown in Table 1. Sulfur compounds can react with alkali species in the fuel gas to form alkali sulfates, which can cause high-temperature corrosion during the utilization of the fuel gas in energy conversion systems such as gas turbines, gas engines, and molten carbonate fuel cells.

Since the mid-1980s, significant research efforts have been directed toward the development of methods to clean the raw fuel gases from gasifiers. Hot fuel gas cleaning generally refers to the removal of fuel gas impurities at temperatures above 250 °C[3] before the gas stream enters a gas turbine, which can increase the thermal efficiency by 2−3%[4] and reduce the operating costs, especially with air gasifiers. The current industrial practice in fluidized bed gasifiers is to add disposable Ca-based sorbents such as limestone or dolomite that capture sulfur as CaS. However, a lower than desirable level of sulfur removal (80−90%) requires an additional desulfurization process.[5] The current hot gas desulfurization technologies focus on the development of regenerable metal oxide sorbents,[3,5,6] to be used in fixed, moving, or fluidized bed configurations. Metal oxides investigated in recent studies include Ca based,[7] Zn/Ti based,[8] and Zn and Cu based.[9] These sorbents can achieve a high desulfurization level at high temperatures (360−750 °C for Fe- or Zn-based sorbents and 800−1000 °C for Ca-based sorbents). For commercial application of these sorbents, however, there are still issues to be resolved regarding sorbent performance during long-term operation in different reactor systems. In particular, problems related to sorbent mechanical strength, attrition resistance in fluidized beds, long-term durability, and reactivity have yet to be fully resolved.

1.1. Desulfurization Using Liquid Metals. This study presents a novel approach for hot fuel gas desulfurization that employs liquid metals. The concept of using liquid metals for gas desulfurization dates back to the late 1970s, when Meissner[11] first patented the concept of removing sulfur from hot reducing gases using liquid lead. Since then, only a few studies have investigated the use of liquid metals for gas cleaning theoretically and experimentally.[12−17] Warner[16,17] identified three possible liquid metals: lead (Pb), bismuth−lead mixture (Bi−Pb), and tin (Sn). Lead (melting point 327 °C) is the most thermodynamically efficient, is relatively cheap, and is inert to oxidation by fuel gas. Its melting point can be lowered by adding Bi to form a 55.5% Bi−44.5% Pb eutectic with a melting point of 27 °C which could be less energy-intensive. However, the use of either Pb or Bi−Pb is discouraged due to health hazards associated with in-plant exposure as well as emissions to the environment.

1.2. Concept of Liquid Tin Irrigated Packed Bed Scrubber. This study investigated the use of liquid tin as scrubbing medium in a packed bed, as proposed by Warner.[17] In this process, sulfur removal occurs via absorption of hydrogen sulfide into liquid tin:

$$H_2S(g) + Sn(l) \leftrightarrow SnS(s) + H_2(g) \qquad (R1)$$

SnS(s) is soluble to tin. SnS has a melting point of 880 °C and a boiling point of 1210 °C. Tin-containing SnS can be regenerated externally by continuous treatment with liquid zinc to produce solid ZnS:[16]

$$Zn(l) + SnS(s) \leftrightarrow ZnS(s) + Sn(l) \qquad (R2)$$

The capability of tin for desulfurization has been theoretically and experimentally demonstrated.[13,14] Tin has a relatively low melting point (232 °C) and very low vapor pressure at high temperatures (boiling point 2620 °C). Tin also has a significantly high density and surface tension of 6980 kg/m^3 and 560 dyn/cm, respectively, at the melting point. Low vapor pressure is a major advantage compared to lead and zinc, which are easier to evaporate at high temperature causing massive metal loss. The vapor pressures of these metals are compared in Table 2, with tin being the least volatile and zinc the most volatile.[18] Liquid tin also has a low viscosity, for example, 1.41×10^{-3} Pa·s at 400 °C compared to that of water (1.13×10^{-3} Pa·s at 15 °C). With high surface tension, liquid tin exhibits nonwetting droplet and rivulet flow on the solid packing surface.

* To whom correspondence should be addressed. Tel.: +44 114 222 7523. Fax: +44 114 222 7501. E-mail: c.ryu@sheffield.ac.uk.

10.1021/ie0704804 CCC: $40.75 © xxxx American Chemical Society
Published on Web 11/28/2007 **PAGE EST: 6.6**

Table 1. Properties of Raw Fuel Gas from Different Gasification Systems for Bituminous Coals

gas species	Shell	Texaco	BGL	ABGC
CO (%)	61−63	39−43	53−57	16−18
CO_2 (%)	~1	12−14	1−2	9−10
H_2S (ppm)	1000−10 000	1000−9000	4500−14 000	300−2000
NH_3 (ppm)	1800−2000	1800−2000	5000	1000−1500

Table 2. Comparison of Vapor Pressure for Liquid Metals Considered

	temperature (°C)		
vapor pressure (Pa)	tin	lead	zinc
1	1224	705	337
10	1384	815	397
100	1582	956	477
1000	1834	1139	579
100 000	2620	1754	912

Compared to regenerable metal oxide sorbents, liquid tin has several potential advantages. Tin does not have any degree of reduction reactions which may cause a loss of the valuable fuel gases. The proposed regeneration of tin can produce saleable ZnS, while the regeneration of sulfidated metal oxides ($MS + 1.5O_2 \rightarrow MO + SO_2$) results in SO_2 that requires further treatment. In addition to desulfurization, the packed bed using liquid tin may also act as a secondary particle removal device due to high surface free energy providing good inertial capture of solid particulates.

For the proposed nonwetting flow scrubber, previous work by Chang[6,19] presented the results of cold tests using water conducted on nonwetting packed beds of polyethylene and waxed glass balls, and applied these data to the design of a lab-scale scrubber for liquid tin.

This paper presents the test results to evaluate the feasibility of hot fuel gas desulfurization in the liquid tin irrigated lab-scale packed bed. The effects of various parameters such as H_2S concentration, height of packing, and liquid and gas flow rates on the desulfurization were investigated to evaluate the desulfurization efficiency and the gas transfer unit height. Various aspects of this technology that require further investigation are also discussed.

2. Materials and Methods

2.1. Packed Bed Scrubber. 2.1.1. Scrubber Setup. Figure 1 shows the countercurrent packed bed scrubber used in this study. It was originally designed by Chang[6] and has gone through a series of modifications. The rig consisted essentially of an absorber column (height 23 cm, internal diameter 8 cm) placed in a semicylindrical heated compartment (ceramic radiant heaters) covered by insulation materials (Kaowool board and blankets). All parts of the system that contact the gas were made of stainless steel type 316 for good corrosion resistance. The packed bed of alumina spheres in the column was supported on a simple stainless steel plate with evenly spaced 5 mm perforations. The total fraction of the open area on the plate was about 0.48. To prevent the possible preferential wetting of liquid tin on the stainless steel wall compared to the alumina ceramic packing, an alumina tube was used to line the interior of the stainless steel column. The alumina tube allows an approximately 20 cm packed bed depth. High-purity alumina has excellent resistance to liquid metals and to reducing atmospheres at elevated temperatures. Details on the packing[6] are summarized in Table 3.

2.1.2. Liquid Tin. Liquid tin was introduced through a distributor with six holes (7.6 mm in diameter) at the top of the column. It disintegrates into discrete droplets and rivulets and flows downward by gravity, countercurrently to the upward gas flow. The countercurrent configuration can theoretically achieve higher efficiencies while having disadvantages of higher pressure drop and risk of flooding.

Liquid tin was irrigated by a simple nitrogen U-tube gas lift constructed from a 22 mm inner diameter stainless steel pipe. The submergence was 61 cm while the lift was 46 cm, giving a total height of just over 1 m. Preheated nitrogen (Tank 3 shown in Figure 1) was used as pumping agent to prevent oxidation of the tin.

The volume of liquid tin in the system was indicated by three level sensors installed at 20, 30, and 40 mm above the bottom of the column reservoir as shown in Figure 1. The sensors generate electric signals when the tip of the sensors contacts the tin, and can be monitored on the control panel.

The liquid tin flow rate was determined by measuring the time taken to fill the column (the packing support plate was completely sealed) of a known weight of tin (≈2 kg). The nitrogen gas was used to circulate the liquid tin at 400 °C (ρ_{tin} = 6878 kg/m^3) through the column. Since the column cross-sectional area is known and remains constant, the average velocity is an indication of the flow rate. For each nitrogen gas flow, the measurements were repeated three times to achieve a reliable rate of liquid tin flow per unit of time.

2.1.3. Simulated Syngas. In this study, the syngas was modeled as N_2 containing H_2S at various concentrations. As tin is fairly reactive, it can also react with other gas components in actual syngas. The effects of H_2 and other gases are discussed in section 3.5. As shown in Figure 1, the simulated syngas entered the column via an injector, which was made from an 11 mm internal diameter stainless steel pipe with four ports distributed at its side at one end. This end was capped, shielding

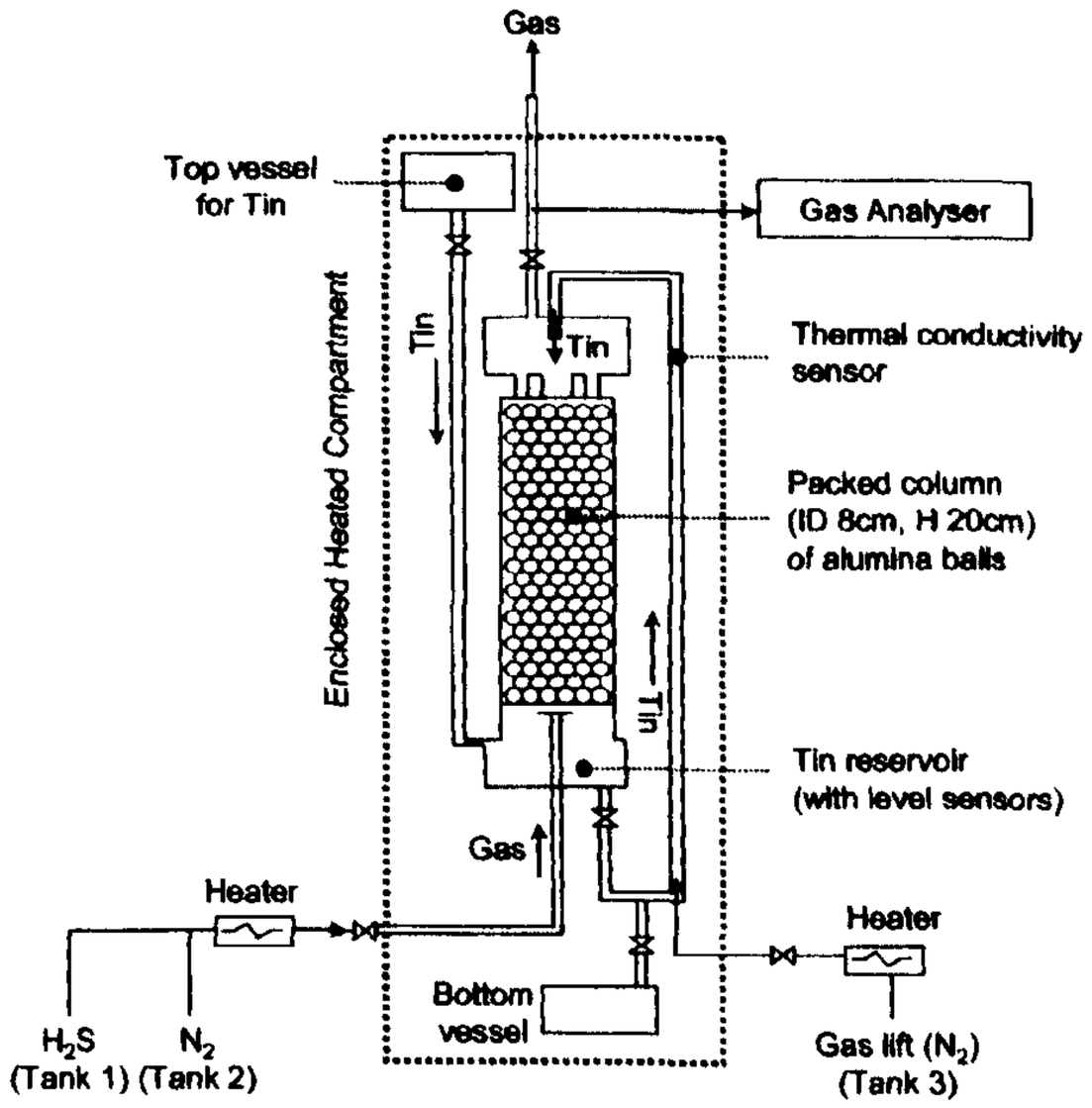

Figure 1. Laboratory-scale hot gas scrubbing system irrigated by liquid tin.

Table 3. Characteristics of the Alumina Packing Used

parameter	value
diameter, d (mm)	9.53
column to packing diameter ratio (m/m)	8.4
packing element specific surface area, $6/d$ (m^2/m^3)	630
packed bed porosity, ϵ (m^3/m^3)	0.45
packing specific surface area, $a_P = 6(1 - \epsilon)/d$ (m^2/m^3)	346
packing specific gravity (dimensionless)	4.0
liquid tin−alumina contact angle, θ (deg)	≈160−140 at 300−1130 °C[20]

Table 4. Test Conditions for Hot Gas Desulfurization in the Packed Bed Scrubber

test parameter	value
gas	
flow rate (kg/(m^2 s))	0.245−0.581
superficial velocity (m/s)	0.490−1.161
liquid tin	
flow rate (kg/(m^2 s))	2.15, 3.17, 3.86
superficial velocity (m/s)	3.07×10^{-4}, 4.53×10^{-4}, 5.52×10^{-4}
inlet H_2S concentration (ppm)	300−2000
height of packing (mm)	200, 100, 0 (empty column)
operating temperature (°C)	300, 350, 390, 400

the gas ports from the falling liquid stream. The gas was preheated by a series of three in-line gas heaters. K-type thermocouples with an Inconel sheath and magnesium oxide insulation were used for temperature measurement. H_2S in the outlet stream was analyzed using an on-line gas chromatograph (GC; ABB PGC2000) for every 5−10 min. The GC was calibrated using span gas with H_2S concentration of 4000 ppm ± 5%.

2.2. Test Conditions. The key test parameters in this study were gas flow rate, tin flow rate, inlet H_2S concentration, bed height, and temperature. The ranges of test conditions are summarized in Table 4. The gas flow rates ranged from 0.245 to 0.581 kg/(m^2 s) (gas superficial velocity of 0.490−1.161 m/s) with a liquid (tin) flow rate of 2.148, 3.165, or 3.860 kg/(m^2 s) (liquid superficial velocity of 3.07×10^{-4}, 4.53×10^{-4}, or 5.52×10^{-4} m/s). The inlet H_2S concentration in N_2 was varied from 300 to 2000 ppm (reference case 1000 ppm). The height of packing was also varied from 20 cm (reference case) to 10 and 0 cm (empty column). While the operating temperature was fixed at 400 °C as the reference condition for variation of other test parameters, its effect was assessed at 300, 350, and 390 °C.

2.3. Test Procedure. In each test, tin pellets (99.9% pure) of known weight (3 kg) were loaded into the top vessel and N_2 gas was fed into the system to purge air from the system. Then the radiant heaters were turned on while the N_2 gas flow was kept at a minimum to ensure an inert atmosphere within the scrubber to prevent tin oxidation. Once the temperature inside the column reached the desired value, sufficient time (5−10 min) was allowed for the tin from the top vessel to melt and fully drain into the reservoir and gas lift limbs. This was achieved when the tin level sensors showed constant readings. Preheated N_2 from tank 2 was introduced at the same flow rate as the target value of the N_2/H_2S mixture to be introduced later. After the inlet temperature of the main gas reached the desired value, N_2 flow from tank 3 was introduced to initiate the circulation of liquid tin through the packed column.

Once the inlet temperature of the gas lift reached the target value, N_2/H_2S mixture from tank 1 was introduced into the system and the gas sampling was initiated. Typically, 30−40 min was allowed for the system to acquire constant concentration readings on the GC. For the tests with different H_2S concentrations, N_2 from tank 2 was added to the N_2/H_2S mixture from tank 1.

Figure 2 shows the histories of H_2S concentration for selected test cases. In the graph, $t = 0$ min is when H_2S was introduced into the column. In the blank test (operation at 400 °C without tin circulation) at 983 ppm of inlet H_2S concentration, the outlet concentration (960 ppm) matched the inlet value within the accuracy of the GC (calibrated using standard gas at 4000 ppm ± 5%). It took 20 min to reach a steady concentration due to the time required for the gas to achieve complete mixing in the reactor and also for the gas retention time in the sampling line to the GC. The two tests for different test durations at 2000 ppm inlet H_2S concentration show that the tests were repeatable and the outlet H_2S concentration was not affected by the test duration up to 90 min. Although the removal efficiency will be affected by the test duration in the long term, the tin has sufficient sulfur capacity not to be affected by a few hours of tests. The sulfur concentration in the tin after 90 min of test was less than 1% by weight. Therefore, the concentrations at t = 30 min were used to evaluate the results.

2.4. Assessment of the Results. From the measured H_2S concentration at the outlet in each test, the desulfurization efficiency can be derived. It is defined as

$$\eta\ (\%) \equiv (1 - y_{out}/y_{in}) \times 100 \qquad (1)$$

Although this is the simplest way of evaluating the test results, it is case-dependent and does not provide insight into the absorption mechanism.

For a packed bed scrubber, the general equation for the scrubber is

$$-u_G\, dy = K_o(y - y_e)a_e\, dz \qquad (2)$$

where K_o is the overall mass transfer coefficient (m/s) incorporating the three rate-controlling mechanisms: the gas-phase

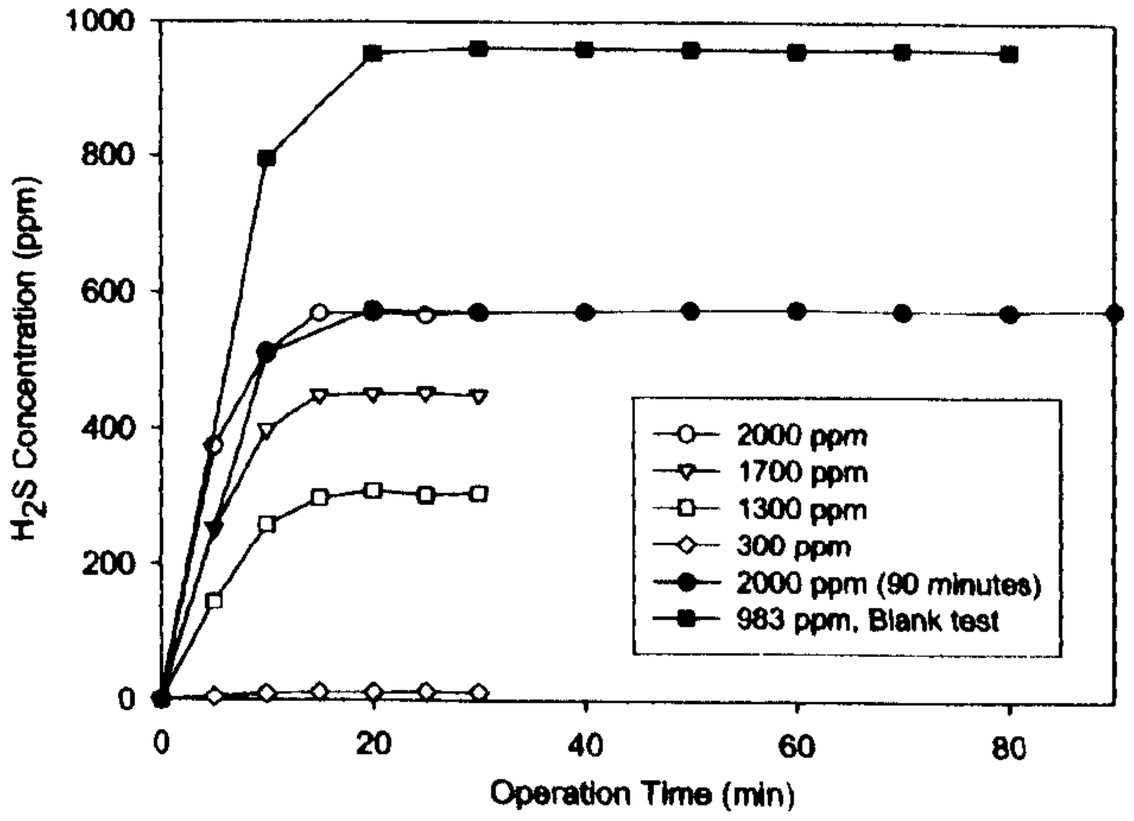

Figure 2. History of H_2S concentration for the test duration with various inlet H_2S concentrations (m_G = 0.258 kg/(m^2 s); m_L = 3.860 kg/(m^2 s) except for the blank test; T = 400 °C).

D

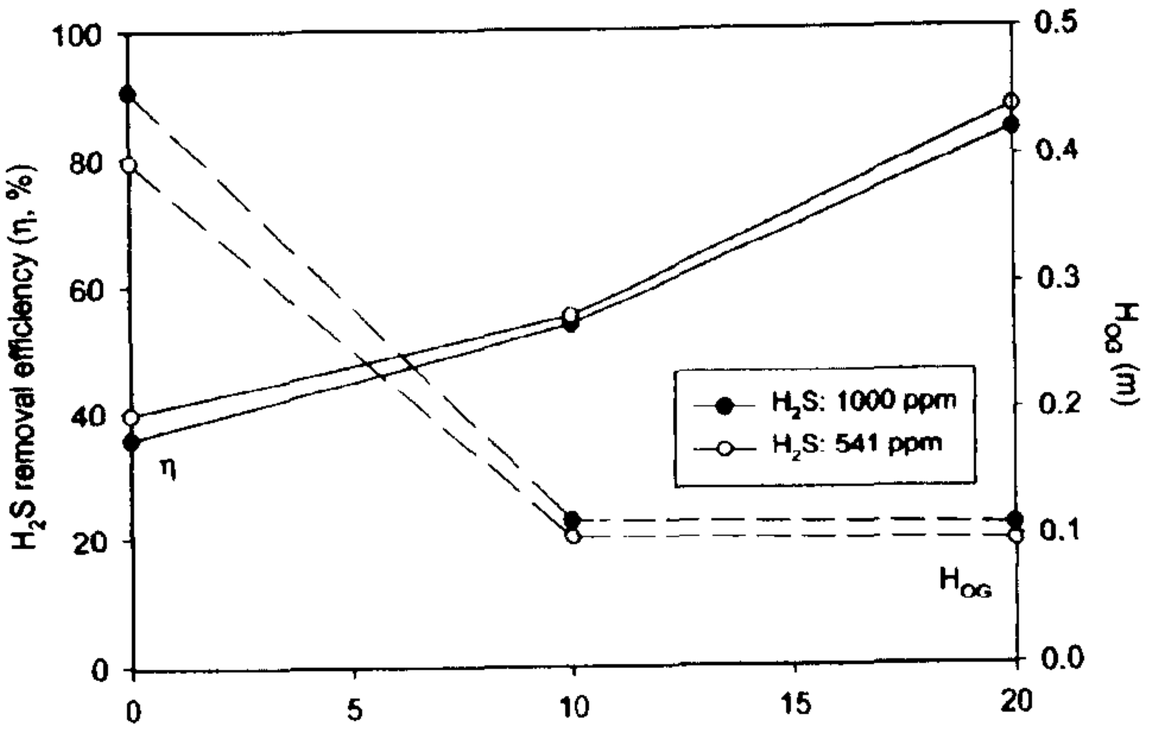

Figure 3. H_2S removal efficiency (η) and the gas transfer unit height (H_{OG}) for different packing heights (m_G = 0.258 kg/(m^2 s); m_L = 3.860 kg/(m^2 s); T = 400 °C).

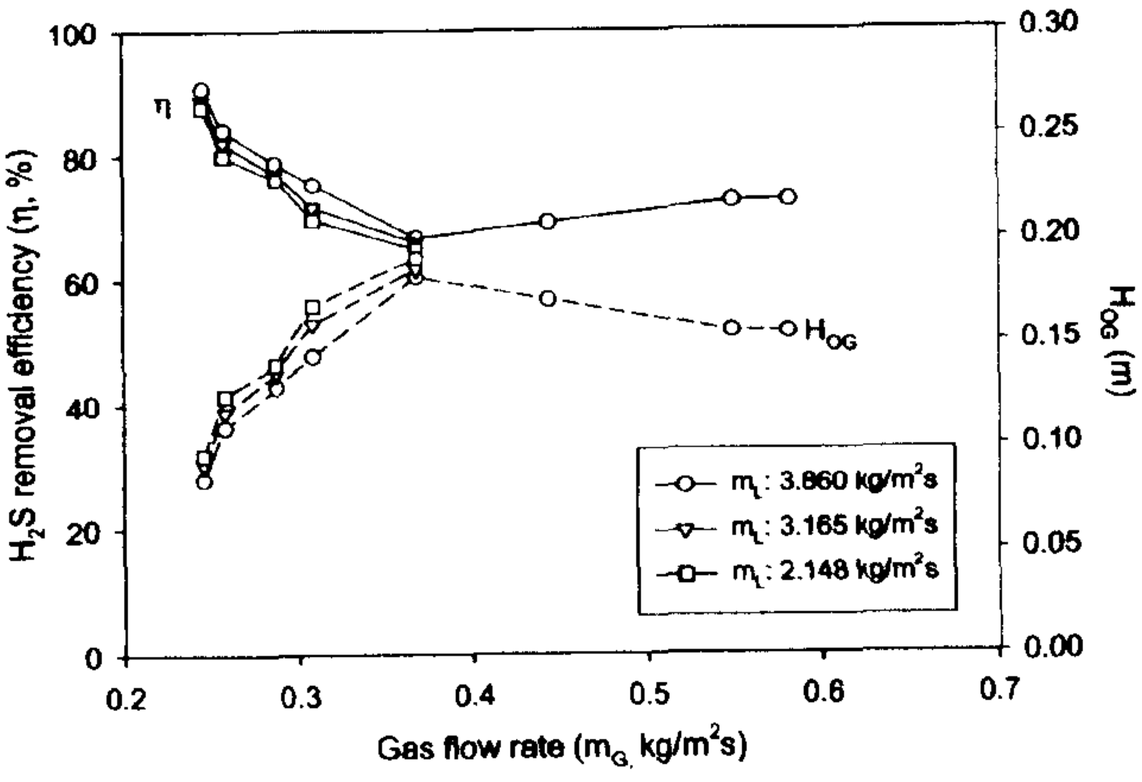

Figure 4. H_2S removal efficiency (η) and gas transfer unit height (H_{OG}) for various gas and liquid superficial velocities (inlet H_2S concentration = 1000 ppm; T = 400 °C).

mass transfer (k_G) of H_2S toward the liquid surface, the reaction kinetic effect at the interface (k_r), and the liquid-phase mass transfer (k_L) for SnS dissolving into tin. K_o can be expressed simply as

$$\frac{1}{K_o} = \frac{1}{k_G} + \frac{1}{k_r} + \frac{1}{k_L} \tag{3}$$

Rearranging eq 2 gives

$$-\frac{dy}{y - y_e} = \frac{K_o a_e}{u_G} dz \tag{4}$$

Integration of eq 4 yields

$$N_{OG} = \frac{\bar{K}_o a_e}{u_G} Z \tag{5}$$

where Z is the bed height, $\bar{K}_G$ is the overall mass transfer averaged along the bed height, and N_{OG} is the overall number of gas-phase transfer units defined as

$$N_{OG} \equiv \int_{y_{out}}^{y_{in}} \frac{dy}{y - y_e} \tag{6}$$

For a fast absorption process ($y \gg y_e$), N_{OG} can be simplified using only the inlet and outlet pollutant concentrations.

$$N_{OG} = \ln(y_{in}/y_{out}) \tag{7}$$

From eq 6, the removal efficiency of a packed bed scrubber can then be expressed in terms of the overall height of the gas-phase transfer unit (H_{OG}).[21]

$$H_{OG} \equiv Z/N_{OG} = \frac{u_G}{\bar{K}_o a_e} \tag{8}$$

H_{OG} represents the height (m) required to achieve a characteristic level of desulfurization (y_{in}/y_{out} = e or η = 63.2%). The smaller the value of H_{OG} is, the more efficient an absorption process is. As shown in the equations, H_{OG} is affected by the three reaction/mass transfer rates for K_o as well as the interfacial area (a_e) and gas velocity (u_G, or gas residence time in the column).

3. Results and Discussion

3.1. Effect of Scrubber Packing Height. Figure 3 shows η and H_{OG} acquired for three different bed heights (0, 100, and 200 mm) with two H_2S concentrations at the inlet (541 and 1000 ppm). The gas and tin flow rates were fixed at 0.258 and 3.860 kg/(m^2 s), respectively, with an operating temperature of 400 °C. The tests with an empty column had η of about 40% due to lack of interfacial contact area, which corresponded to H_{OG} values of 0.40 m. These H_{OG} values were then used to correct the results for the 100 mm high packing by removing the effect of the empty half of the column above the packing. Figure 3 shows that the increase in the bed height from 100 to 200 mm resulted in an increase in the removal efficiency from 66% to 84%. However, the H_{OG} was almost constant for both packing heights at both concentrations, which conforms to its definition.

3.2. Effect of Gas and Liquid Tin Flow Rates. Figure 4 shows the trends of the H_2S removal efficiency (η) and H_{OG} for different gas and liquid superficial velocities for an inlet H_2S concentration of 1000 ppm at 400 °C. η ranged from 67% to 91% in the test reactor, which resulted in H_{OG} values of 0.084−0.181 m. Increasing the liquid flow rate from 2.148 to 3.860 kg/(m^2 s) led to 2−4% higher values of η and, therefore, lower values of H_{OG} by 0.012−0.014 m. However, larger gas flow rates up to a certain point (0.443 kg/(m^2 s)) increased H_{OG} (reduced η) and then started to decrease the value. Recalling eq 8 for H_{OG}, these trends can be explained from the way the gas and liquid velocities affect the flow characteristics in the column such as the residence time, interfacial contact area, and mass transfer rate.

First, the gas velocity determines the residence time of the gas phase in the column, which represents the macro-opportunity for the gas to contact the liquid. For example, the gas residence time in the lab-scale scrubber decreased from 0.183 to 0.078 s based on the void volume of the dry column as the mass flow rate increased from 0.245 to 0.581 kg/(m^2 s). The actual values are lower than these due to the volume of the liquid retained in the bed, which is known as liquid holdup. The decrease in η from about 90% to about 66% for gas flow rates up to 0.443 kg/(m^2 s) is attributable to the reduced gas residence time.

Second, the gas and liquid velocities affect the liquid holdup in the bed. Higher liquid flow rates directly increase the liquid holdup. As more liquid is retained, it generally creates a larger interfacial contact area (a_e) between the two phases. This results in lower values of H_{OG} at higher liquid velocities. At a constant

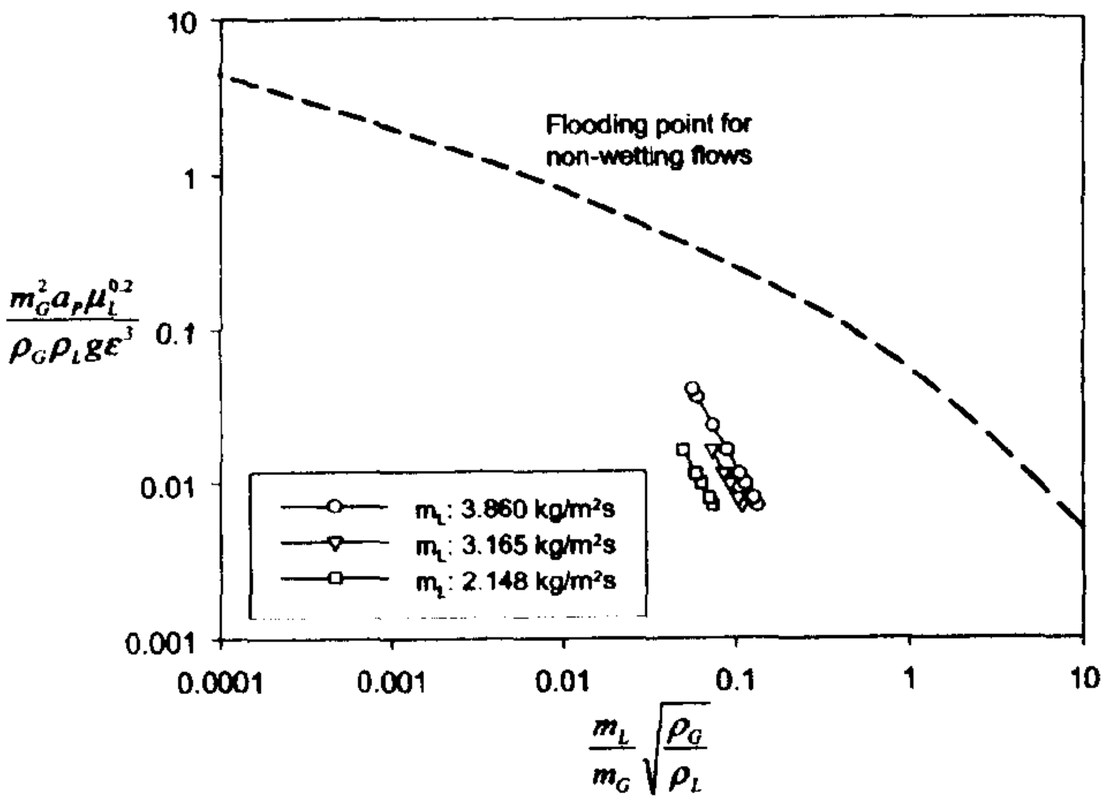

Figure 5. Comparison of test conditions to flooding capacity of nonwetting flows.

liquid flow rate, the liquid holdup is not noticeably affected by low gas velocities. When the gas velocity or momentum is sufficiently high to interfere with the liquid droplets, the dynamic liquid holdup begins to increase. Chang[19] derived the correlation for the liquid holdup of a nonwetting flow below the flooding point from the cold flow tests to be proportional to $u_G^{0.178} u_L^{0.580}$. This suggests that the liquid velocity exerts a stronger influence on the liquid holdup.

Third, increased velocities also result in higher mass transfer coefficients of the gas phase (k_G) due to increase in turbulence and interaction between the two phases. Strigle[22] reported k_G to be proportional to $m_L^{0.22} m_G^{0.79}$. The decrease in H_{OG} at high gas velocities (>0.443 kg/(m² s)) in Figure 4 suggests that the enhancement of desulfurization by increased liquid holdup and gas-phase mass transfer became more significant at high gas velocities than the adverse effect of reduced gas residence times.

One thing to note is that increased liquid holdup does not always lead to larger interfacial area. High gas and liquid flow rates increase liquid holdup and connect more droplets with each other to change the flow pattern into rivulets. Standish[23] and Mackey and Warner[24] reported that the interfacial area for the rivulet flow pattern is lower than that of droplet flow.

Flooding of the liquid sets the upper operational limits for gas and liquid flow rates. Figure 5 compares the test conditions to the flooding line for nonwetting flows proposed by Standish and Drinkwater.[25] The liquid and gas flow rates were well below the flooding line. Therefore, the gas and liquid flow rates can be further increased in order to intensify the desulfurization reactions, reducing the volume of the scrubber required to process fuel gases.

3.3. Effect of H_2S Concentration. The desulfurization efficiencies for various H_2S concentrations at the inlet are shown in Figure 6. The gas and tin flow rates were fixed at 0.258 and 3.860 kg/(m² s), respectively, at 400 °C. The increase in the inlet concentration of H_2S from 300 to 2000 ppm gradually reduced the removal efficiency from 95.9% to 71.5%. Recalling eq 8, this is due to the change in K_o while the gas velocity and interfacial surface area are identical. K_o is determined by k_G, k_r, and k_L. k_G is constant in this set of tests and is expected to be faster than the other rates. Hedden[14] postulated from the tests in a double-stirred reactor that the reaction of H_2S with Sn is of first order with k_r of 0.012−0.020 m/s at 500 °C. If the reaction is of first order, then H_{OG} is determined mostly by k_L, i.e., limited mass transfer rate of SnS in tin. In other words, how quickly the liquid surface can be refreshed by dissolving

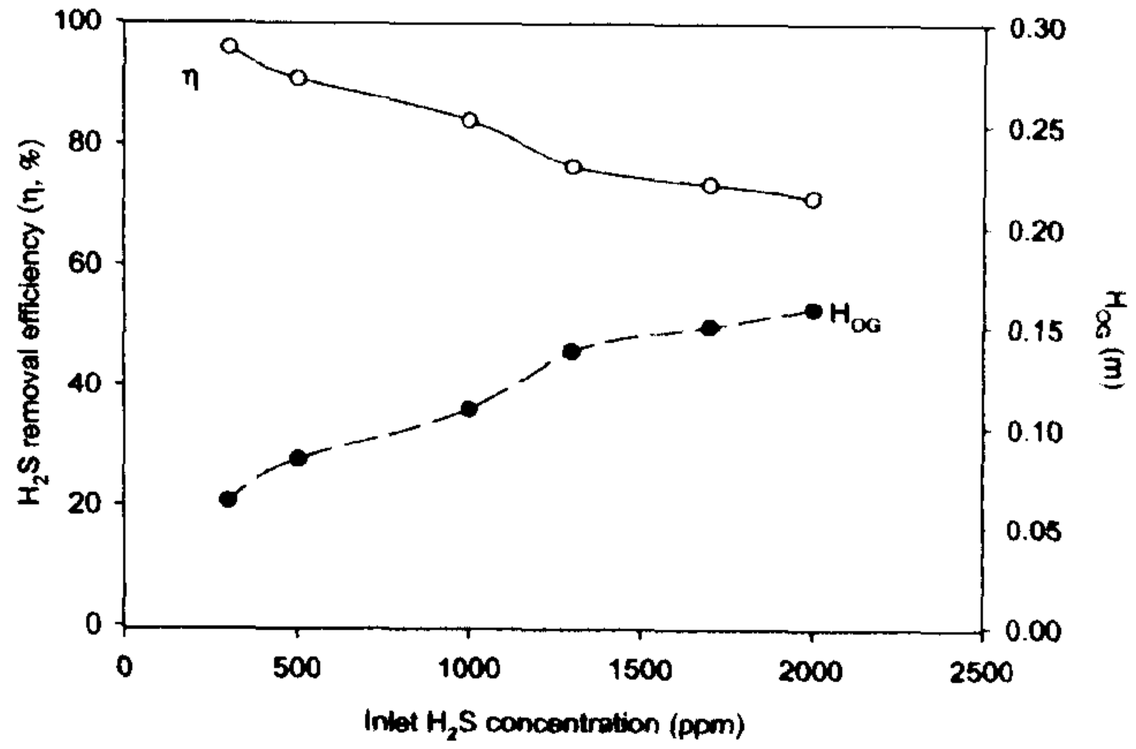

Figure 6. H_2S removal efficiency (η) and gas transfer unit height (H_{OG}) for different inlet H_2S concentrations (m_G = 0.258 kg/(m² s); m_L = 3.860 kg/(m² s); T = 400 °C).

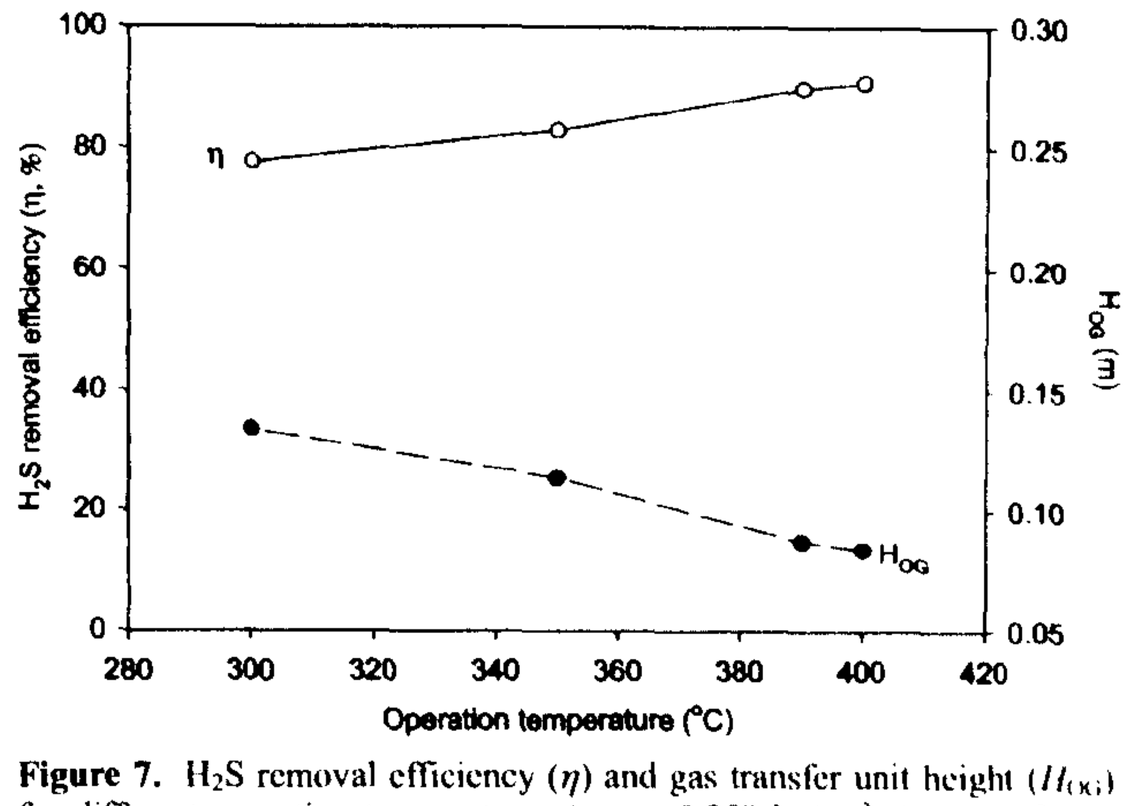

Figure 7. H_2S removal efficiency (η) and gas transfer unit height (H_{OG}) for different operation temperatures (m_G = 0.258 kg/(m² s); m_L = 3.860 kg/(m² s)).

SnS into tin becomes an important rate-controlling factor for an increased amount of S (SnS) due to higher H_2S concentrations.

3.4. Effect of Operating Temperature. Figure 7 shows the effect of operating temperature ranging from 300 to 400 °C. The gas and tin flow rates were fixed at 0.258 and 3.860 kg/(m² s), respectively, with an inlet H_2S concentration of 1000 ppm. H_{OG} decreased from 0.133 at 300 °C to 0.084 at 400 °C. The desulfurization became efficient at high temperatures because the increase in the mass transfer and reaction rates is larger than the increase in the gas velocity. However, the effect of thermal equilibrium becomes significant at higher temperatures with high H_2/H_2S ratios, as discussed in the next section.

3.5. Discussion on Further Investigations. 3.5.1. Theoretical limits of Desulfurization Efficiency and Tin Regeneration. Higher temperatures are expected to increase the mass transfer and reaction rate of H_2S while reducing the viscosity of liquid tin. It does not cause a problem with the volatility of liquid tin, but the desulfurization efficiency at high temperatures would be limited by thermal equilibrium. Figure 8 shows the variation of Gibbs free energy for the desulfurization reaction (reaction R1: $H_2S(g) + Sn(l) \leftrightarrow SnS(s) + H_2(g)$), based on Schürmann's study.[13] Negative Gibbs free energy favors the forward reaction, and vice versa. This suggests that higher temperatures and a higher partial pressure ratio of H_2/H_2S shifts the reaction toward H_2S formation. Especially at high H_2/H_2S ratios or higher desulfurization efficiencies, the dependence on temperature becomes very significant. At a typical H_2 concentration of 30%,

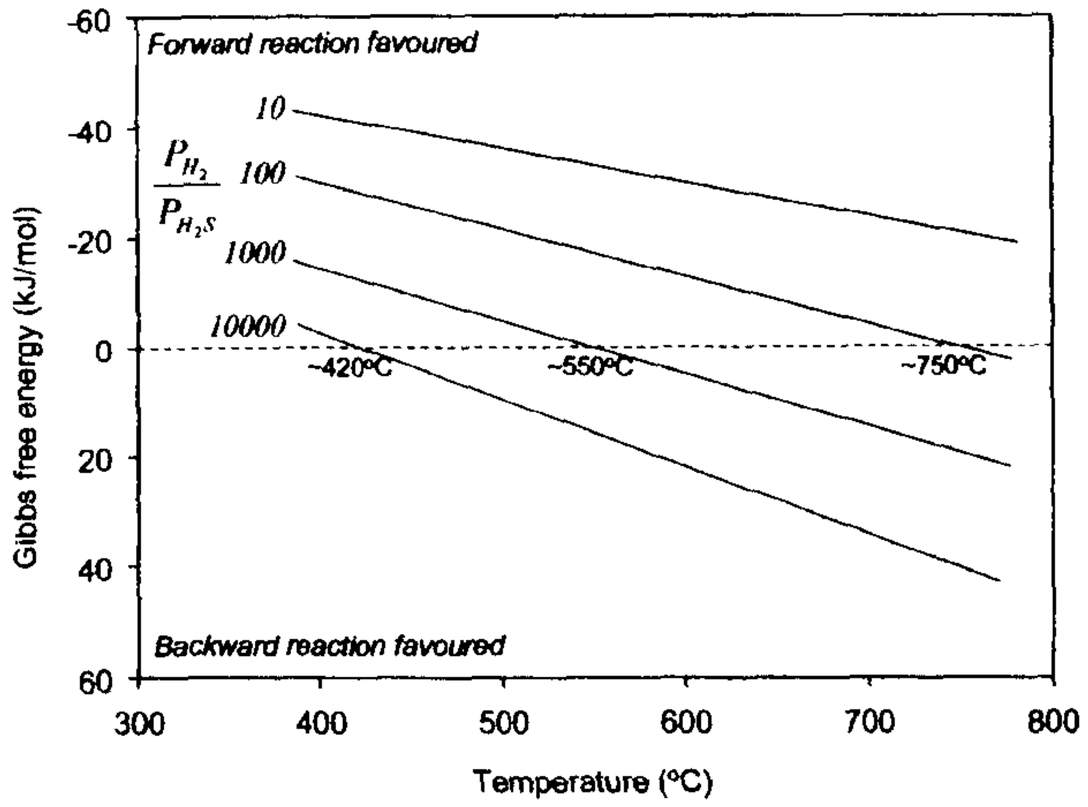

Figure 8. Variation of Gibbs free energy for the desulfurization reaction of tin by H_2/H_2S ratio and temperature.

for example, temperatures below 550 °C can reduce the H_2S concentration theoretically to 30 ppm ($P_{H_2}/P_{H_2S} = 1000$) if the SnS concentration is sufficient in the liquid tin. Therefore, it is essential to suppress the backward reaction by removing SnS in the tin introduced at the top of the counterflow reactor. The dissolved level of SnS can be minimized through the regeneration process using zinc presented in reaction R2. Warner[16] proposed an external regeneration in a fluidized bed where coarse granular ZnS can be grown on seeds of fine ZnS. The coarse ZnS can be readily separated from the liquid tin. Investigations are required on the theoretical limits and the tin regeneration process.

3.5.2. Interaction with Other Gas Species. Liquid tin is fairly reactive, and therefore other gas components in fuel gases may react with tin. Hedges[26] reported that tin does not react directly with H_2, N_2, or NH_3. However, it reacts with H_2O, CO_2, and HCl. First, tin can be oxidized by steam to form solid oxides, which causes the loss of tin.[26,27]

$$Sn(l) + 2H_2O(g) \leftrightarrow SnO_2(s) + 2H_2(g)$$

This reaction depends on the H_2O/H_2 ratio and temperature. Temperatures above 500 °C are required to prevent SnO_2 dross formation for very wet fuel gases.[27]

HCl can react with the liquid tin to form chlorides which are volatile (low melting and boiling points) and therefore will condense to aerosols when cooled in heat exchangers. However, coal typically has a low Cl content, and therefore high H_2/HCl ratios will suppress the reaction of tin with HCl.

Tin reacts with CO_2 at high temperatures to form tin oxide.[26]

$$Sn(l) + 2CO_2(g) \leftrightarrow SnO_2(s) + 2CO(g)$$

Niesel and Sigurdardottir[26] reported that the forward reaction is favored at temperatures of 350−500 °C with equal proportions of CO_2 and CO. However, fuel gases typically have higher CO concentration than CO_2, which would suppress the formation of SnO_2. From experimental investigation in a double-stirred reactor, Hedden et al.[14] reported that the gas components such as CO and CO_2 did not influence the degree of H_2S conversion to SnS, although tested gas concentrations were not specified. The same study also reported that the reaction rate for COS at 500 °C was about 3 times smaller than that for H_2S.

From the current experimental investigation, a very thin film of shiny yellow SnS_2 was identified on part of the liquid surface from tin collected after the scrubber was cooled down, while tin containing SnS lost its shine and became dull. The formation of SnS_2 is presumably with the following surface reaction of SnS with H_2S:

$$H_2S(g) + SnS(s) \leftrightarrow SnS_2(s) + H_2(g)$$

3.5.3. Further Investigations. The test results presented here show the good potential of this new desulfurization system. However, further fundamental investigations are required on various aspects including wider ranges of test parameters including gas and liquid flow rates, temperature, pressure, and test duration. The capability for particle/tar removal should be also studied in order to fully exploit the potential of this technology. Our initial trials with glass powders showed that heavy dust loading may clog the bottom of the reactor where the dust is introduced and then mix with the liquid tin. Therefore, this scrubber should be employed after a primary particle removal device.

4. Conclusions

The absorption behavior of H_2S in a novel liquid tin irrigated hot gas scrubber was investigated for various operation parameters in a lab-scale packed bed. H_{OG} values ranged from 0.84 to 0.181 m for tested conditions at 1000 ppm H_2S concentration, which showed the good potential of this system for efficient desulfurization. High liquid velocities increased the removal efficiency due to larger liquid holdup creating larger interfacial area. Increased gas velocities influenced the removal efficiency by altering the gas residence times, liquid holdup, and gas-phase mass transfer. The H_{OG} of an empty column was about 5 times higher at the tested conditions due to lack of contact between the two phases. The H_{OG} gradually reduced for increased H_2S concentrations or at lower operating temperatures. Further fundamental studies are required on various aspects of this scrubber, especially for higher gas and liquid velocities and operating temperatures. Regeneration of tin should be also investigated, which is essential for high H_2S removal efficiencies at high H_2/H_2S ratios. It is also anticipated that electromagnetic or mechanical pumps would be used to circulate the tin in an industrial environment.

Acknowledgment

The authors wish to acknowledge the financial support for this research program from the United Kingdom Engineering and Physical Sciences Research Council (EPSRC) and the Malaysian Government.

Nomenclature

N_{OG} = number of transfer units
H_{OG} = height of the gas-phase transfer unit, m
Z = total column height, m
K_o = overall mass transfer coefficient, m/s
a_e = effective specific interfacial area, m^2/m^3
a_P = packing specific surface area (see Table 3), m^2/m^3
k = reaction or mass transfer rate, m/s
g = gravitational acceleration, m/s^2
m = mass flow rate, kg/m^2 s
u = velocity, m/s
y = H_2S concentration, $kmol/m^3$
z = coordinate along the vertical direction, m

Greek Symbols

ϵ = porosity, m^3/m^3
η = H_2S removal efficiency, %
μ = dynamic viscosity, kg/m s
ρ = density, kg/m^3

Subscripts

G = gas phase
L = liquid phase
e = equilibrium
in = inlet
r = reaction
out = outlet

Literature Cited

(1) William, B. C.; McMullan, J. T. *Hot gas chemical clean-up: current commercial and technological status*; R139; UK DTI's Coal Research and Development Programme; Harwell Energy Technology Support Unit, 1998.

(2) ETSU. *Hot gas chemical cleanup*; TSR 006; Harwell, Energy Technology Support Unit, 1998.

(3) Mitchell, S. C. *Hot gas cleanup of sulfur, nitrogen, minor and trace elements*; CCC/12; IEA Coal Research, London, 1998.

(4) DOE (Department of Energy). *Texaco gasifier IGCC base cases*; Report No. PED-IGCC-98-001 (rev 1), issued by Office of Systems Engineering and Analysis, U.S., 1998.

(5) Gangwal, S. K.; Gupta, G.; McMichael, W. J. Hot-gas cleanup—sulfur recovery technical, environmental and economic issues. *Heat Recovery Syst. CHP* **1995**, *15*, 205−214.

(6) Chang, B. F. A non-wetting packed bed gas scrubber. Ph.D. Thesis, University of Sheffield, U.K., 2003.

(7) Adánez, J.; Abad, A.; García-Labiano, F.; de Diego, L. F.; Gayán, P. H_2S retention with Ca-based sorbents in a pressurized fixed-bed reactor: application to moving-bed design. *Fuel* **2005**, *84*, 533−542.

(8) Bu, X.; Ying, Y.; Ji, X.; Zhang, C.; Peng, W. New development of zinc-based sorbents for hot gas desulfurization. *Fuel Process. Technol.* **2007**, *88*, 143−147.

(9) Park, N.; Lee, D.; Jun, J.; Lee, J.; Ryu, S. O.; Lee, T. J.; Kim, J.; Chang, C. H. Two-stage desulfurization process for hot gas ultra cleanup in IGCC. *Fuel* **2006**, *85*, 227−234.

(10) Turk, B. S.; Merkel, T.; Lopez-Ortiz, A.; Gupta, R. P.; Portzer, J. W.; Krishnan, G. N.; Freeman, B. D.; Fleming, G. K. *Novel technologies for gaseous contaminants control*; DOE Contract No. DE-AC26-99FT40675; DOE, U.S., 2001.

(11) Meissner, H. P. (Institute of Gas Technology). Removal of hydrogen sulfide from reducing gases. U.S. Patent 3,954,938, 1976.

(12) Meissner, H. P.; Shora, F. C. (Institute of Gas Technology). High temperature pollutant removal from gas streams. U.S. Patent 4,308,037, 1981.

(13) Schürmann, B. Studies of gas purification by liquid materials and development of an appropriate method. *Fortschr.-Ber. VDI Z., Reihe 3: Verfahrenstech.* **1984**, No. 85.

(14) Hedden, K.; Rao, B. R. Desulfurization of manufactured gases with liquid metals. In *Proceedings of the 1986 International Gas Research Conference*, Toronto, Ontario, Canada, 1986.

(15) Warner, N. A. *Zinc-based clean technology for desulfurization in advanced power generation*; R127; UK DTI's Coal Research and Development Programme, Harwell, Energy Technology Support Unit, 1997.

(16) Warner, N. A. Personal communication: theoretical framework for liquid metal based coal gasification (draft)—Feb 23, 2000; cited in ref 6.

(17) Warner, N. A. Personal communication: theoretical framework for liquid metal based coal gasification (draft)—April 25 2001; cited in ref 6.

(18) *CRC Handbook of Chemistry and Physics*, 86th ed.; Lide, D. R., Ed.; CRC Press: Boca Raton, FL, 2005; p 6-15.

(19) Chang, B. F.; Sharifi, V. N.; Swithenbank, J.; Warner, N. Development of a liquid metal based fuel gas scrubbing system. In *Proceedings of the 5th International Symposium on Gas Cleaning at High Temperature*, Sept 17−20, 2002, Morgantown, WV.

(20) Nogi, K. Wettability of solid oxides by liquid pure metals. *J. Jpn. Inst. Met.* **1988**, *52*, 72−78.

(21) Calvert, S.; Goldschmid, J.; Leith, D.; Mehta, D. *Wet Scrubber System Study. Vol. I. Scrubber Handbook*; EPA-R2-72-118a; U.S. Environmental Protection Agency, 1972.

(22) Strigle, R. F. *Packed tower designs and applications − random and structured packings*, 2nd ed.; Gulf Publishing Company: Houston, 1994.

(23) Standish, N. Heat transfer in liquid metal irrigated packed beds countercurrent to gases. *Trans. Metall. Soc. AIME* **1968**, *242*, 1733−1740.

(24) Mackey, P. J.; Warner, N. A. Studies in the vaporisation of mercury in irrigated packed beds. *Chem. Eng. Sci.* **1973**, *28* (12), 2141−2154.

(25) Standish, N. On the flooding criteria for liquid metals. *Chem. Eng. Sci.* **1973**, *28* (10), 1906−1907.

(26) *Tin and its alloys*; Hedges, E. S., Ed.; Edward Arnold Ltd.: London, 1960.

(27) Nielsen, P. E. H.; Sigurdardottir, I. D. Development and characterization of steam regenerable sorbents for hot gas desulphurization in coal gasification based combined cycle plant. In *Gas Cleaning At High Temperatures*; Clift, R., Seville, J. P. K., Eds.; Blackie Academic & Professional: Glasgow, 1993.

Received for review April 3, 2007
Revised manuscript received August 17, 2007
Accepted October 4, 2007

IE0704804

Hot Gas Clean-Up for Gasification Process

Mohd Halim Shah Ismail, Changkook Ryu, Vida N Sharifi and Jim Swithenbank

Sheffield University Waste Incineration Centre (SUWIC), Sheffield University

Introduction

- Gas cleaning systems for gasification-based power generation are needed to remove dust, S-species, N-species (e.g. ammonia, cyanides, etc), halides and trace metals from the gasifier fuel gases prior to their passage through the gas turbine and their subsequent release.
- Hot fuel gas cleaning generally refers to the removal of fuel gas impurities at temperatures above 250°C (Mitchell 1998) before the gas stream enters the gas turbine. The integration of hot gas clean-up (HGCU) technology to remove pollutants from coal-derived fuel gas offers the prospect of increasing thermal efficiency whilst simultaneously reducing the capital and operating cost of IGCC systems without compromising the environmental performance.
- Why Hot Gas Cleaning
  - Avoid the high capital cost, energy losses & complexity of totally cooling the hot raw syngas.
  - Avoids waste water & black/gray water slurry processing.
  - Increases IGCC efficiency & capacity by increasing the mass flow & sensible energy into the gas turbine.
- Objective: To investigate a novel hot flue clean-up system using molten tin as the scrubbing medium for the removal of solid particulates and H_2S.

Hot Fuel Gas Cleaning

- **Hot Fuel Gas Cleaning (HGCU) vs Cold Fuel Gas Cleaning (CGCU)**
  - HGCU increases the overall energy efficiency (by 2-3%) by reducing heat loss as latent heat
- **Fuel Gas Cleaning versus Flue Gas Cleaning**
  - Better control system, low capital and operating costs
- **Gas Turbine Protection**
  - Particulate Matter: Fly Ash, trace components and metals
  - Particulates: 2 ppmw (< 10 mm)
  - Sulphur (H2S, COS, CS2): 20 ppmw

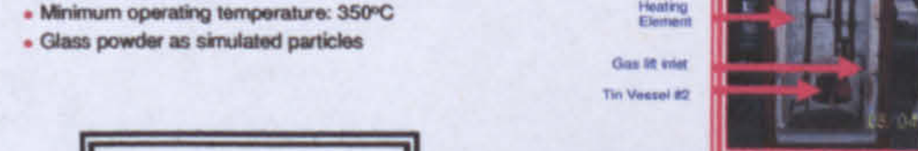

Hot Gas Scrubber – Using Molten Tin

- **Tin (Sn) - Melting Point: 232°C**
  - Not pose a health impact
  - Low viscosity 1.41 cP at 400°C
  - Non wetting, easy dispersion into small droplets on the packing surface
  - Molten tin as the scrubbing medium for the removal of H_2S and solid particulates.

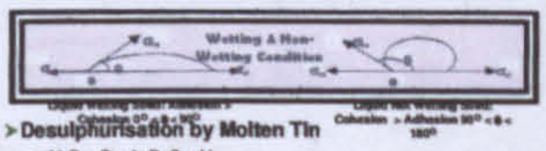

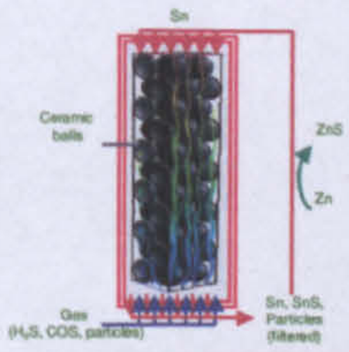

- **Desulphurisation by Molten Tin**
  - $H_2S + Sn \rightarrow SnS + H_2$
  - $COS + Sn \rightarrow SnS + CO$
  - Recovery of Tin: $Zn + SnS \rightarrow ZnS + Sn$

- **Particle Removal by Molten Tin**
  - Discrete molten tin droplets and rivulets on the packing surface act as solid particulate collectors.

- **Lab-scale Packed Bed Scrubber**
  - Size of packed bed: 8 cm - internal diameter and 23 cm - length
  - Ceramic balls: 9.53 mm high-purity ceramic alumina spheres
  - 316 Stainless Steel for resistance to corrosion.
  - Countercurrent flows of tin and gas.
  - Minimum operating temperature: 350°C
  - Glass powder as simulated particles

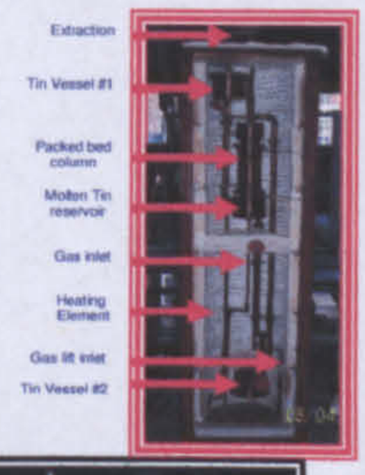

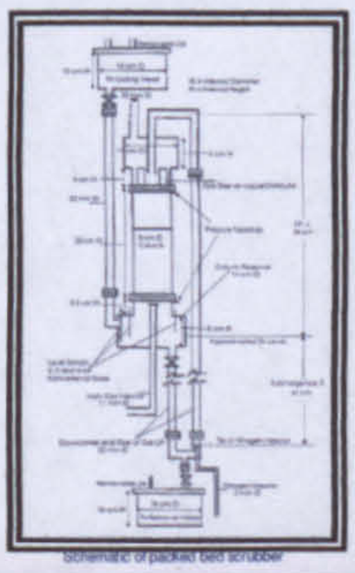

Schematic of packed bed scrubber

Setup for particle removal tests

Experiments: Particulate Removal & Desulphurisation

- **Key parameters: Dust loading, flow rates of H_2S, N_2 and tin, and bed temperature**
- **Particle removal tests**
  - The low capture of particles were due to the limitations of lab-scale scrubbers such as low temperature of particles at the inlet causing Si (glass powder)-Sn agglomeration.

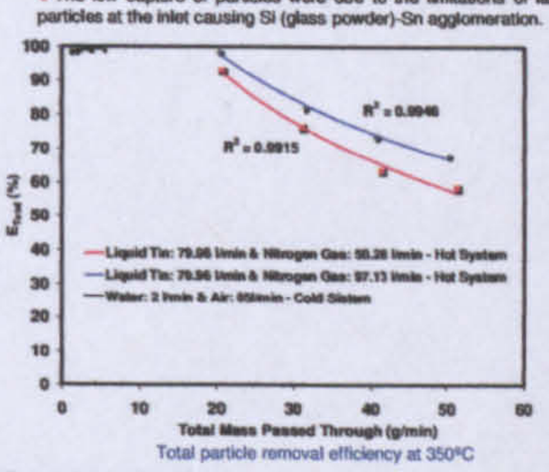

Total particle removal efficiency at 350°C

Accumulation of particles and tin

- **Desulphurisation Tests**
  - Absorption in the scrubbing solution (molten tin) was rapid as indicated by the high removal rate

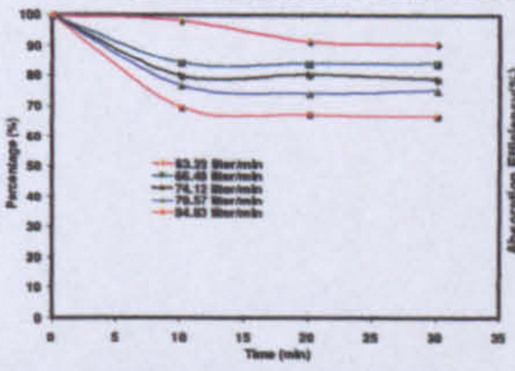

Absorption of H_2S with inlet concentration of 1000 ppm

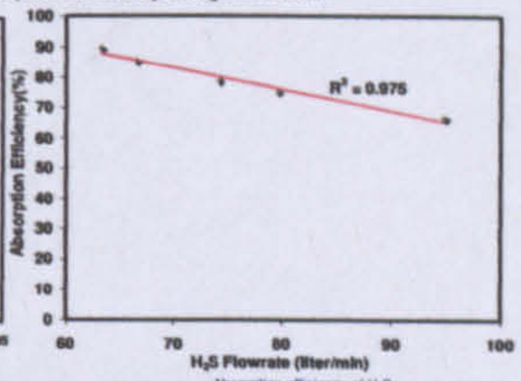

Absorption efficiency of H_2S

Computational Fluid Dynamics – Particle Removal

- FLUENT code used for simulation of particle removal
  - No tin flow: sphere balls as particle trap

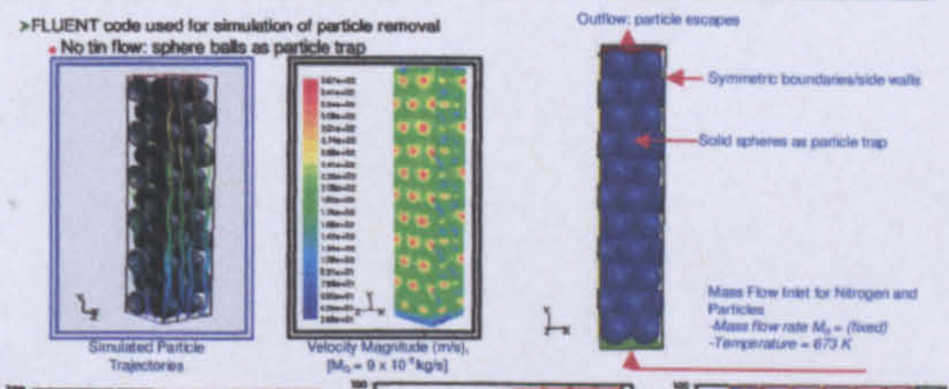

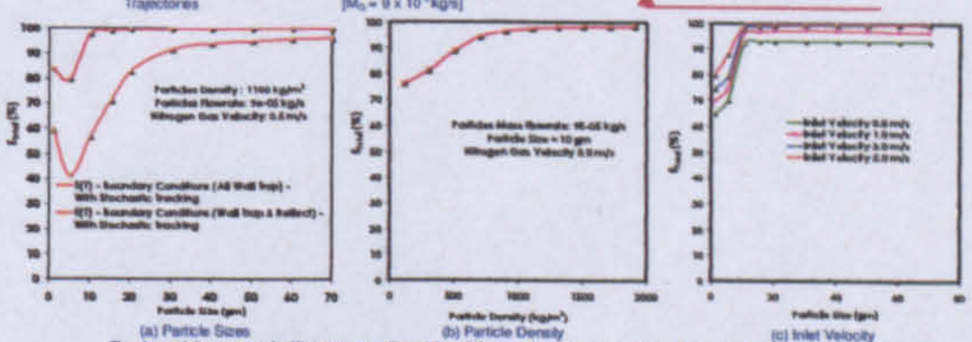

Total particle removal efficiency predicted for different particle sizes, particle density and inlet velocity

Conclusions and Future Work

- Total separation efficiencies were obtained, ranging from 60 to 95 % for particle removal.
- An increase in the H_2S gas flowrate will decrease the efficiency of the gas absorption.
- Desulphurisation efficiencies ranging from 67 – 95 % for H_2S cleaning
- Future Work
  - Investigation H_2S removal by molten tin.
  - Investigate the reactivity of the molten tin with others chemicals.
  - Further CFD modelling work incorporating chemical reactions of H_2S in the packed bed.
  - Validate the model using experimental data.

Acknowledgement

- UK Engineering and Physical Sciences Research Council (EPSRC)
- Malaysian Government

More Information on SUWIC can be found at our websites: http://www.kvtg.group.shef.ac.uk/

Contact: Professor V N Sharifi,
Dept. of Chemical & Process Engineering, Sheffield University
Mappin Street, Sheffield S1 3JD, UK
Tel: +44-114-222 7519 E-mail: v.n.sharifi@sheffield.ac.uk